Role of Keratin 8 Phosphorylation in Neoplastic Progression of Squamous Cell Carcinoma

By
Richa Tiwari
[LIFE09201004011]

TATA MEMORIAL CENTRE,

MUMBAI

A thesis submitted to the
Board of Studies in Life Sciences
In partial fulfillment of requirements

For the Degree of
DOCTOR OF PHILOSOPHY
Of
HOMI BHABHA NATIONAL INSTITUTE

August 2017

Homi Bhabha National Institute

Recommendations of the Viva Voce Committee

1. As members of the Viva Voce Committee, we certify that we have read the dissertation prepared by Ms Richa Tiwari entitled **"Role of keratin 8 phosphorylation in neoplastic progression of squamous cell carcinoma"** and recommend that it may be accepted as fulfilling the thesis requirement for the award of Degree of Doctor of Philosophy.

Chairman – Dr. Sorab N. Dalal S.N. Dalal Date: 10/8/17

Guide/Convener – Dr. Milind M. Vaidya M M Vaidya Date: 10/8/17

External Examiner – Dr. Mahesh J Kulkarni Date: 10/8/2017

Member 1 – Dr. Sanjay Gupta Date: 10/8/17

Member-2 – Dr. Abhijit De Date: 10/8/17

Final approval and acceptance of this thesis is contingent upon the candidate's submission of the final copies of the thesis to HBNI.

I hereby certify that I have read this thesis prepared under my direction and recommend that it may be accepted as fulfilling the thesis requirement.

Date: 10-08-17
Place: Navi Mumbai

M M Vaidya
Dr. Milind M Vaidya
Guide

STATEMENT BY AUTHOR

This dissertation has been submitted in partial fulfillment of requirements for an advanced degree at Homi Bhabha National Institute (HBNI) and is deposited in the Library to be made available to borrowers under rules of the HBNI. Brief quotations from this dissertation are allowable without special permission, provided that accurate acknowledgement of source is made. Requests for permission for extended quotation from or reproduction of this manuscript in whole or in part may be granted by the Competent Authority of HBNI when in his or her judgment the proposed use of the material is in the interests of scholarship. In all other instances, however, permission must be obtained from the author.

Richa Tiwari

DECLARATION

I, hereby declare that the investigation presented in the thesis has been carried out by me. The work is original and has not been submitted earlier as a whole or in part for a degree /diploma at this or any other Institution / University.

Richa Tiwari

List of Publications arising from the thesis

Journal:

R. Tiwari, I. Sahu, B. L. Soni, G. J. Sathe, K. K. Datta, P. Thapa, S. Sinha, C. K. Vadivel, B. Dhaka, H. Gowda, M. M. Vaidya, Quantitative phosphoproteomic analysis reveals system-wide signaling pathways regulated by site-specific phosphorylation of Keratin-8 in skin squamous cell carcinoma derived cell line. *Proteomics* 2017, 17, 1600254.

Chapters in books and lectures notes: Nill

Conferences attended:

1. Attended an International Conference "1st Global Cancer Genomics Consortium-Tata Memorial Centre Symposium" **(GCGC-2011**) on 10th to 12th November 2011 at ACTREC-TMC, Navi Mumbai.
2. Attended an International Conference "31st Annual Convention of Indian Association of Cancer Research (**IACR-2012)** and International Symposium of Cancer Genomics and its impact in the clinics" on 26th to 29th January 2012 at ACTREC-TMC, Navi Mumbai.
3. Attended an "International Symposium on Stem Cell Biology-2012" on 30th January 2012 at ACTREC-TMC, Navi Mumbai.
4. Attended an International Conference "2nd Global Cancer Genomics Consortium-Tata Memorial Centre Symposium" **(GCGC-2012**) on 19th to 20th November 2012 at ACTREC-TMC, Navi Mumbai.

5. Attended a meeting "International Conference on Radiation Biology and 11th Biennial Meeting of Indian Society for Radiation Biology **(ICRB-2012**)" on 22nd to 24th November 2012 at ACTREC-TMC, Navi Mumbai.

6. **Won Best Poster Presentation Award** at an International Conference "The XXXVII All India Cell Biology Conference on Cell Dynamics and Cell Fate **(AICBC-2013)",** conducted by Indian Society for Cell Biology on 22nd to 24th December 2013 at Indian Institute of Science, Bangalore, India.

7. **Presented Poster** at an International Conference "American Society of Cell Biology **(ASCB)/** International Federation for Cell Biology (IFCB) **Meeting-2014**" held on 6th -10th December 2014 at Philadelphia, PA, US.

8. Presented Poster at an International Conference "Carcinogenesis-2015", organized by Carcinogenesis foundation, USA and ACTREC-TMC, India on 11-13 February 2015 at Advanced Centre for Treatment Research and Education in Cancer, Navi Mumbai, India.

Others: Nill

Signature

Richa Tiwari

This Thesis is dedicated to my parents
for their love, endless support
and encouragement

ACKNOWLEDGEMENT

I would like to take the opportunity to convey my heartiest regards to those who have contributed, supported and guided me throughout the entire duration of my PhD research.

Foremost, I would like to thank my guide Dr. Milind M Vaidya for his constant support and encouragement during good and bad times of my PhD tenure. Under his able guidance, I have got an extensive understanding about the concepts of research. He has also fostered in making me a better person. I thank him for extending compassion and flexibility when I needed it. I am deeply indebted to him for allowing me to put forth my suggestions and always expressing faith in my ideas and abilities. The pleasant lab environment was appreciable since we could work without restraints. Had he not encouraged me I would not have been able to surpass the obstacles I faced. "Things will work out, don't worry!"- His approach towards tackling difficult situations with patience and optimism but being realistic at the same time inspires me. His humble, warm and caring nature has earned him the admiration that he deserves. He is truly an inspiration to each of us.

I take this opportunity to record my sincere thanks to Vinita ma'am for being the pillar of strength for each of us at Vaidya Lab. Her efforts are motivational and irreplaceable. Most importantly we can acquire the trait of being forever dedicated to our work from her.

I would like to express my sincerest gratitude to the Director of ACTREC Dr. Shubhada V. Chiplunkar and Deputy Director Dr. Sudeep Gupta for providing such a wonderful infrastructure and facilities to work with. I am also thankful to Dr. Rajiv Sarin (Ex-Director, ACTREC) and Dr. Surekha Zingde (Ex-Deputy Director, ACTREC) for giving me such a great opportunity to pursue my PhD degree in this institute. I am honor-bound to ACTREC-DAE, India for my PhD fellowship and DBT for funding the project. I acknowledge the Sam-Mistry travel fund and HBNI international travel fund for supporting my visit for international conferences.

I thank profusely my DC members- Dr. Sorab Dalal, Dr. Sanjay Gupta, Dr. Abhijit De. I was unaware about the fundamentals like designing the experiment, analysing the data, critically analysing a research paper which I learnt from Dr. Sorab, from the time I was assigned the course-work. I am very thankful to all my DC members for their indispensable advice, guidance and being supportive about my viewpoint when everyone else thought otherwise. I would like to thank Dr. Girish Maru, my former DC Chairperson for his notable contribution towards the progress of my work.

I would like to acknowledge late Dr. Kalraiya, Dr. Sorab, Dr. Bhattacharya, and Dr. Prasanna for their help in terms of protocols, apparatus and reagents for the experiments. I would like to thank Dr. Prasanna particularly for her cooperation and providing access to the resources from her lab.

I am deeply indebted to Dr. Subeer Majumdar (Director, NIAB, Hyderabad) and Dr. Nirmalya Ganguly (Scientist, NIAB, Hyderabad) for collaborating with us and making it possible to generate Transgenic Mice by electroporation. I am thankful for their steadfast rebuttal and critical suggestions at the time of need. I am under obligation to also thank our other collaborator- Dr. Harsha Gowda (IOB, Bengaluru), and his students, Dr. Gajanan Sathe, Keshava Dutta- for performing the Quantitative proteomics experiment and helping me with the analysis. Apart from them, I would like to thank Ankit Jain and Kiran Kumar for their help and cooperation during the data analysis. It is the critical contribution of my collaborators which made achievable all the things that seemed far-fetched.

It is my privilege to thank the members of Vaidya Lab. I am deeply obliged to Dr. Hunain Alam, my senior, for his expert advice and supervision during the early phase of my PhD. He was a disciplinarian and his accomplishments set a paradigm for us at Vaidya Lab. He has a pivotal role in giving structure to my work. He inculcated the virtues of dedication towards science and work-ethics in me. I thank my super senior, Deepak for all his standardised protocols and procedures which are still being used in the lab. I can't thank Sapna enough for being the dear friend that she is. She was one of the most calm and humble people I have ever met. She was always there to protect us from all the adverse situations. I am thankful to Biharlilal Soni for all his help and support. He was the most jovial person in our lab. I dedicate special thanks to Crismita for the multiple roles of batchmate, roommate, labmate and friend. She justified all these with ease. All I can say is her scientific inputs, constant motivation, being straight forward and being positive even when dealing with criticism have been benchmarks for our friendship. I thank Saumya Di for her valuable suggestions in both personal and professional front which have helped me time and again. She is tender- hearted and gentle. I am amazed by her ability to manage her work and family giving equal importance to both. Pratik was the youngest amongst us and the target for all the leg-pulling and teasing. He doesn't have the realization of his contribution as a stress-buster. His "Pravachans" are always a topic for discussion. His impromptu ideas have always worked wonders for me. I thank Harsh for his technical and scientific inputs which have helped me time and again. Apart from Harsh, I share a special bond with Neha, Archana, Anagha, Cyrus and Ankur. I am thankful to them being amiable and comforting. Ankur has been the most affable person and with his antics given me reasons to laugh. Zinia was a cute and likable person. She, Sunita, Silvania, Rashmi, Yashvi and Chetan made the lab environment pleasurable to work in. I thank Vaishali, our lab scientific assistant for teaching nuances of cell culture techniques in early days of my PhD. Our lab would have not been organised and we would have lost track of time in arranging reagents and other requisites for our experiments had it not been for Rajesh, Shridhar, Ram, Kishor, Naresh. I thank them for the same. I thank Prema Ma'am, Maya, Yashwant Sir, Aruna, Anil, Alka, Sharvari and Kamala Ma'am for their generous help with all the laboratory and official formalities.

I owe a profound sense of gratitude to my trainees, each one of them has made contributions towards the completion of my project. I thank Sajada and Apurva as they were efficient, sincere and hardworking. All the experiments were performed by them with ease. I thank Pankaj, he was not only a trainee but also a precious friend. I have learnt from him as much as he has learnt from me. He is empathetic and has always been there to check on me. He made sure I had a good laugh everytime he was around. I thank Pavan as he always completed the work well in time without complaining. I admire his sincerity and patience. I am thankful to Shruti. She has always been a call away. She is positive, good-humoured and quick-witted. She works systematically which makes her trustworthy and dependable. Also, her endless jabber made me wonder how anyone could talk so much. I thank Krishna. He is sharp-witted, dependable, dedicated and hard-working. He has worked with me for the longest time and his efforts cannot be paralleled. I would like to thank Shweta. I truly appreciate the professionalism and focus with which she handles everything. She has always been keen to learn new things and is a quick learner. Her approach is thoughtful, organised and responsible. She, along with Krishna and Shruti, took initiatives in the right direction for my projects even during tough times. I thank Swapnil as he is skilled and diligent in his work. I also want to thank Anamika, Nancy, Radha and Bhagyashree for they have come to aid when I was in need. I thank all of you for bearing with me.

I would like to give special note of thanks to Batch of 2010. I have had some wonderful times with my batchmates and I will forever cherish the moments. Though each one was different from the other, yet on any account everyone was willing to help without any apprehensions. Today, each of them is successful in his/her respective fields. I thank Abira, Shyam, Prasad, Rushikesh, Aditi, Poonam, Saikat, Asif and Raja. They have been the greatest support system in gritty situations. I thank Indrajit. He has ushered me to believe in myself. He acquainted me with the concepts of science and

was available whenever I wanted to substantiate my experiments. He has been a tower of strength and a well-wisher who has always been there to ward off my glitches. The contributions he made are indispensable. The clichés- competitor, critic, philosopher and guide would still not suffice what I want to thank him for.

I am grateful for the resources and facilities available at ACTREC. I thank Mr. Dandekar for the systematic organization and timely maintenance of the instruments enabling us to carry out our experiments without any hindrance. I thank Vaishali, Tanuja and Jairaj who have always aided in confocal, inverted and upright microscopy. I thank Shashi, Prashant and Savita for their help in Mass Spectrometry. I am thankful to Ravi for his assistance with FACS.

I would like extend my heartfelt thanks to the ACTREC Animal house facility. I thank Dr. Ingle for allowing me to work in the animal house and for all his help. I am grateful to Dr. Thorat for being considerate and helping us selflessly. His technical and scientific guidance made my work in the animal house possible. I thank Sada and Tushar for taking care of the animals.

I am filled with gratitude for my roommate and dance partner Sudeshna. We share the same level of craziness be it singing songs at midnight with cold-coffee by our side or just roaming around aimlessly. Basically, she has been the perfect Jerry to my Tom. She is benevolent, vivacious and mischievous. She has been the reason for my happiness invariably.

I extend my thanks to ACTREC student community and for all sort of scientific help. I would like to acknowledge Prasanna, Sonali, Rahul, Rasika, Bhawik, Gopal, Rai, Shalaka, Pravin, Mukund and Shreosi for their help and support in my good and bad times. I thank all my seniors from whom I have learnt a lot.

My joy knows no bounds in expressing my gratitude for my family. My father has been a stalwart in motivating me to be self-sufficient. It is his belief that knowledge and wisdom surpasses everything else. Irrespective of the social impediments he has been supportive for my aspirations. My mother has made a paramount contribution for me to accomplish my dreams. She has been firm and enduring whenever I have approached her with my problems and has been equally joyous at every little success. I thank my siblings Rashmi, Divya and Manas as they have been taking care of my parents whenever I am not around. They have ineffably stood by me in tough times, likewise in happy times.

Richa Tiwari

Table of Content

Synopsis

Synopsis

Homi Bhabha National Institute

Ph. D. PROGRAMME

1. **Name of the Student:** Richa Tiwari
2. **Name of the Constituent Institution:** TMC-ACTREC
3. **Enrolment No.:** LIFE09201004011
4. **Title of the Thesis:** "Role of keratin 8 phosphorylation in neoplastic progression of squamous cell carcinoma".
5. **Board of Studies:** Life Sciences

Synopsis

"Role of keratin 8 phosphorylation in neoplastic progression of squamous cell carcinoma".

Introduction

Keratins are the largest subgroup of intermediate filament (IF) proteins expressed in a tissue specific and differentiation dependent manner. They are stable as 10 nm obligate hetero-polymeric filaments of a Type-I (K9–K28, K31–K40) and Type-II (K1–K8, K71–K86) keratins each [1]. Keratin 8/18 (K8/18), the simple epithelia specific keratin-pair is known to execute only mechanical functions however, growing evidence has established its role in various regulatory functions too [2]. They share a common prototype structure comprising of a central coiled coil alpha helical rod domain flanked by two non-helical head and tail domains. Apart from providing heterogeneity to all the keratins, the head and tail domains harbor sites for various post translational modifications (PTM), including phosphorylation. The three major

physiological phosphorylation sites known to regulate K8 functions are Ser23, Ser73 in the head domain and Ser431 in the tail domain [1,3]. Among these, Ser-23 is a highly conserved site across all type II keratins, rendering some common functions to them, whereas phosphorylation at Ser431 increases during mitosis and upon exposure to epidermal growth factor in association with filament reorganization [3]. Contrary to this, K8 Ser73 gets phosphorylated during a variety of cellular stresses, including heat and drug exposure, whereas under normal conditions, it remains dephosphorylated [3]. Kinases like JNK, p38-MAPK, PKC δ, are known to phosphorylate K8 at ser 73 position in specific conditions whereas K8 phosphorylation at Ser431 is mediated by Cdc2 and MAPK [1,3]. K8/18 phosphorylation regulates several keratin functions in a site-specific fashion, including solubility, binding to other proteins like 14-3-3 sigma, modulation of cell cycle progression, keratin filament organization and affecting keratin protein turnover by ubiquitination or during apoptosis. They protect the cells from injury by serving as a "phosphate sponge" for stress-activated kinase [1,3].

Keratin 8/18 pair is often aberrantly expressed in squamous cell carcinomas (SCC) where its expression is correlated with increased invasion and poor prognosis [4]. Apart from being used as a diagnostic tumor marker, K8/18 pair has also been reported to modulate different signaling pathways involved in tumor progression [5, 6, 7]. Previous report from our laboratory has shown that forced expression of K8/18 leads to increased invasiveness and tumorigenic potential of FBM cells, which is also supported by transgenic mouse studies [8, 9]. Further, our laboratory has shown that depletion of keratin 8/18 (K8/18) in an oral squamous cell carcinoma derived AW13516 cell line leads to decreased tumorigenic potential by deregulating alpha6 beta 4 integrin pathway together with the changes in fascin mediated actin organization [10]. These results suggest that aberrant expression of K8/18 could contribute to neoplastic progression of oral SCC. Similarly, phosphorylation is associated with many diverse physiological functions of

K8, but the reports related to its role in the neoplastic progression of different carcinomas and the associated mechanisms are largely unknown. An earlier report by Mizuuchi et al. has demonstrated correlation of PRL-3 dependent K8 dephosphorylation at Serine^{73} and Serine^{431} with increased cell motility in colorectal cancer derived-cells [11]. In addition, our laboratory has shown that when the K8 phosphomutants were expressed in K8 knockdown AW13516 cells, it resulted in increased tumorigenic and motile phenotype. Further, loss of K8 phosphorylation was also observed in human OSCC tissues which significantly correlated with size, lymph node metastasis and stage of the tumor [12]. Contrary to this, a recent report demonstrated that, reduced K8 ser73 phosphorylation via P38 MAPK pathway upon sec 8 down-regulation resulted in decreased cell migration [13].

Non-melanoma skin cancers (NMSC), one of the most common neoplasms known to cause serious morbidity and mortality, are curable at early stages, but delayed diagnosis leads to metastasis [14]. Although, K8/18 pair is known to be aberrantly expressed in skin cancers [9], till now, to our knowledge there are no reports about the mechanism associated with the involvement of K8 in neoplastic progression of skin SCCs [15]. Similarly, phosphorylation is associated with many diverse physiological functions of K8, but the reports related to its role in the neoplastic progression of different carcinomas and the underlying mechanisms are inconsistent. Hence further studies are required to elucidate K8 and its phosphorylation function in neoplastic progression of skin squamous cell carcinomas and mechanisms underlying the same. Deciphering the role of K8 and its phosphorylation in tumorigenic potential of skin epidermoid carcinoma cells and associated signaling will give us a better in sight towards its role in oncogenic progression of skin SCC. Development of a tissue specific transgenic mouse model expressing K8 wild type and phosphomutants followed by DMBA/TPA mediated skin

carcinogenesis will be useful to strengthen and signify the role of K8 phosphorylation in neoplastic progression of SCC.

Aims and Objectives:

Part 1:

Aim: To study the role of K8 phosphorylation in neoplastic progression of SCC using transgenic mouse model.

Objectives:

a) To generate a tissue specific transgenic mouse model expressing wild type K8 and phosphomutants.

b) To use DMBA-TPA mediated skin carcinogenesis in order to study the role of K8 phosphorylation in neoplastic progression.

Part 2:

Aim: To investigate role of K8 phosphorylation in squamous epithelium derived cell lines at phenotypic and molecular level so as to understand whether these effects are cell line specific and further to understand mechanism underlying the same.

Objectives:

a) To express K8 phosphomutants and wild type in the cells with K8 null background.

b) To study the phenotypic and molecular changes on expressing K8 phosphomutants in cells with K8 null background compared to WT.

Materials and methods:

Ethics statement: All protocols for animal studies were approved by the ‘‘Institutional Animal Ethics Committee (IAEC)’’ (Approval ID: 5/2015). A Committee formed under the guidelines of the Committee for the Purpose of Control and Supervision of Experiments on Animals (CPCSEA), Government of India.

Cell lines and their maintenance: Human epidermoid carcinoma derived A431 cells and HEK293-FT cells were maintained in DMEM supplemented with 10% FBS as well as 1% antibiotic solution, and grown at 37^0C in 5% CO2 atmosphere. K8-knockdown stable clones were maintained in 500ng/ml of puromycin whereas all K8 overexpressing stable clones were maintained in 500ng/ml of puromycin and 600ng/ml of G418 sulphate containing complete DMEM.

Plasmids and retroviral constructs: pTU6 puro vector containing the shRNA 8.2, [10], (Generated earlier in the lab) was used to generate K8 knock down clones in A431 cells. The shRNA-resistant pLNCX2-Flag-K8-WT-GFP, phosphodead mutants (pLNCX2-3XFlag-K8-73A-GFP/pLNCX2-3XFlag-K8-431A-GFP) and Phosphomimetic mutants (pLNCX2-3XFlag-K8-S73D-GFP/pLNCX2-3XFlag-K8-S431D-GFP) were generated as described earlier. For the generation of tissue specific transgenic mice, K8 wild type and phosphomutants were first cloned in pCCL K14 GFP vector. The wild type K8 was sub-cloned in pCCL-K14- GFP vector by replacing GFP with K8 WT GFP from pEGFP N3 vector backbone. The pCCL-K14-K8 WT GFP was then used to generate the phosphomutants by Site Directed Mutagenesis (SDM) with the same primers used earlier. High-titer retroviral particles for all the constructs were generated as described earlier [12].

Semi-Quantitative reverse transcriptase PCR (RT-PCR): RT-PCR was performed as described previously [11].

Western blotting and Immunofluorescence analysis: For western blotting, whole cell lysates were prepared in SDS lysis buffer whereas lysates from skin tissue samples were prepared in RIPA buffer as described previously. Immunofluorescence staining was performed as described previously [10,11].

In-vitro and in vivo tumorigenicity assay: Scratch wound healing, transwell migration, invasion, Cell proliferation, clonogenic, soft agar and in vivo tumorigenicity assays for the respective cell lines were carried out as described previously [8,10,11].

Differential quantitative total and phosphoproteomics: Mammalian cell lysis, Protein digestion, TMT labelling, b-RPLC, Phosphopeptides enrichment using TiO2 Chromatography followed by LC-MS/MS were carried out for all the clones in collaboration with "Institute of Bioinformatics", Bangalore, as described earlier [17]. Total proteins or phosphoproteins differentially expressed with a cut off ≥1.5 folds were subjected to further bioinformatics analysis as described earlier [18]

Generation of transgenic mice and genotyping: Transgenic mice were generated in collaboration with Dr. Subeer Majumdar, NII Delhi using "transgenesis via spermatogonia mediated *in vivo* approach" [19]. The genomic DNA isolation followed by PCR based genotyping was performed to screen transgene integration positive mice followed by southern blotting as described earlier [19].

Tissue immunofluorescence: Skin tissue samples were collected from respective mice and IF was carried out to screen the mice expressing transgene as described previously [18].

Statistical analysis: Statistical analysis was carried out as described previously [17, 18]. A *p* value of less than 0.05 was considered statistically significant.

Results:

Part 1:

Aim: To study the role of K8 phosphorylation in neoplastic progression of SCC using transgenic mouse model.

Objective 1: Generation of tissue specific transgenic mice: In order to understand the role of keratin 8 phosphorylation in neoplastic progression of SCC *in vivo*, transgenic mouse model

expressing K8 WT as well as phosphomutants for both the sites Serine^{73} and Serine^{431} were generated using spermatogonia mediated *in vivo* approach. The expression cassette (K14-K8-GFP WT/73A/431A) for all the transgenes with a DNA concentration of 1µg/µl was then sent to NII, Delhi for electroporation in the testis of FVB/j male mice. Further, the electroporated male mice were allowed to mate with the females and the first litter was analyzed for the integration of the transgene. Tail genomic DNA PCR as well as southern blot data showed the integration of the transgene for K14-K8 WT GFP, K14-K8 S73A GFP as well as K14-K8 S431A GFP. Mice positive for transgene integration were further kept for inbreeding (in the ACTREC animal house facility) in order to generate pure line. We carried out the in breeding of positive mice till F4 generation and few of them were validated for transgene expression at protein level by tissue immunofluorescence as well as western blotting.

Objective 2: DMBA-TPA two stage skin carcinogenesis protocol: Transgene positive mice were subjected to DMBA-TPA two stage skin carcinogenesis protocol. 157 µl of DMBA (0.32 µg/µl of acetone) was applied to each of the mice thrice a week followed by 2.5 µg/200 µl of TPA application twice a week. The sequential changes from initiation to progression are being studied. Our preliminary observations have shown early tumor initiation in case of K8 WT transgenic mice compared to K8 S73A or K8 S431A transgenic mice. Further replication of the data is under process.

Part 2:

Aim: To investigate role of K8 phosphorylation in squamous epithelium derived cell lines at phenotypic and molecular level.

Objective 1: Effect of K8 knockdown on tumourigenic potential of A431 cells: In order to understand the role of keratin 8 in tumourigenic potential of A431 cells, shRNA based stable clones for K8 knockdown were generated using pTU6 puro vector containing the shRNA 8.2

(Generated earlier in the lab). K8 knockdown led to a significant reduction in the tumorigenic potential (migration, anchorage independent cell growth, invasion, proliferation, tumor formation in nude mice) of A431 cells compared to vector control cells. After K8 knockdown, its binding partner K18 also showed a decrease at protein level whereas its RNA levels were unaffected. We also observed a significant upregulation of K7 at protein level which is a probable binding partner of K18 in the absence of K8. Immunofluorescence imaging for K18 showed a loss of normal filament architecture suggesting that up regulated K7 might be stabilizing K18 at proto-filament stage but is not able to form a complete filament assembly after K8 knockdown.

Molecular alterations associated with downregulation of K8 in A431 cells: After establishing K8 knockdown clones as well as vector control cells, they were subjected to TMT based quantitative protein profiling in order to understand the global proteomic changes taking place after keratin 8 knockdown. The IPA analysis of the data showed, most of the differentially regulated proteins to be involved in cancer associated signalling pathways like cell movement, apoptosis, cell death and survival, cell proliferation etc., which correlated with our phenotypic data. Few such proteins including TMS1, RANBP1, 14-3-3 gamma, MARCKSL1, K17, K15 and CDK6 which showed a significant level of differential expression with a ≥1.5 folds cut off were further validated at protein level which correlated well with our MS/MS data. TMS1 is known regulate apoptosis through NF-κB [21]. We observed a decreased NF-κB activity in case of K8 knockdown clones compared to vector control cells together with increased IkB α stability after K8 downregulation. Further, we identified and JNK to be the main effectors of this pathway. There were significant changes in total Pkcδ, IKKα, and JNK phosphorylation levels a probable regulator of NF-κB activity and thereby K8 mediated tumorigenic potential of A431 cells [22]. In addition, another important intermediate filament protein, K17 which is known to undergo caspase mediated degradation upon apoptotic stimuli, was found to be stabilised upon

pan caspase inhibition in K8 knockdown cells. A caspase 3 specific inhibitor also resulted in the accumulation of K17, but the changes were not to the same extent as pan caspase inhibitor, indicating involvement of other caspases, most probably caspase 6, 7 or 9 [23]. Annexin V-PI staining showed an increased sensitivity of A431 cells upon K8 knockdown towards the apoptotic stimuli. Altogether these results suggest that K8 may be providing resistance to apoptotic stimuli and thereby increased tumorigenic potential to the A431 cells upon aberrant expression. In addition, MARCK-SL1 an actin organisation associated protein [24] also showed significant upregulation in TMT based quantitative proteomics analysis. Therefore, we performed actin phalloidin staining, which showed a significant difference in the lamellipodial architecture between the vector control and knockdown cells. Further, the probable downstream effectors like Cofilin/pCofilin, Paxilin/pPaxilin, FAK/pFAK and RAC activity showed significant alterations suggesting a probable mechanism for K8 mediated regulation of migratory phenotype of A431 cells.

Role of K8 phosphorylation in tumorigenic potential of A431 Cells

Phosphorylation is established as a potent modulator of keratin 8 conventional functions, but its role in malignant transformation and the mechanism involved to bring about the same is still uncertain. To study the effect of keratin 8 phosphorylation on tumorigenic potential of A431 cells; clones expressing the shRNA resistant wild type K8, phosphodead mutants (K8S73A and K8S431A) together with phosphomimetic mutants (K8S73D and K8S431D) were first subjected to a TMT based quantitative phosphoproteomics for total phosphoproteome profiling and quantification. We quantified total 5839 unique phospho-peptides corresponding to 2145 phospho-proteins including many known and novel phosphopeptides in all the datasets together. Comparative data analysis using various analysis software tools allowed us to identify number of differentially regulated signaling pathways associated with biological functions like cell

proliferation, migration, invasion and metastasis. We further validated few of the kinases and phosphoproteins associated with cancer phenotype [25,26,27] which included, $CDK1^{T14,Y15}$, $MAPK1^{Y187}$, $EIF4EBP1^{T37/T46}$, $AKTS1^{T246}$, $EIF4B^{S422}$, $CTTN^{Y421}$, and $cJUN^{S243}$ using western blot analysis. This correlated well with the MS/MS data. Further, phenotypic analysis like scratch wound healing, Boyden chamber cell migration, proliferation and invasion assays showed K8 phosphorylation to provide more aggressive phenotype to the A431 cells in concordance with our mass spectrometric data [18]. Altogether, our western blot analysis followed by phenotypic validation substantiated their role in Keratin 8 phosphorylation mediated oncogenic pathways.

Summary and conclusion:

To understand the role of K8 phosphorylation in neoplastic progression of SCC in vivo, tissue specific transgenic mouse models for K8 WT as well as the two phosphodead mutants K8 S73A and K8 S431A were generated. Preliminary observation of DMBA-TPA mediated skin carcinogenesis showed an early tumor initiation in case of K8 WT expressing mice compared to the two phosphodead mutant expressing mice.

Keratin 8 downregulation in A431 cells led to decreased tumourigenicity of these cells as shown by various in vitro and in vivo tumorigenicity assays. Quantitative proteomics revealed few significant links between the K8 and associated phenotypic changes. These included molecules like TMS1, RANBP1, 14-3-3 gamma, CDK6 and MARCKSL1. Further analysis demonstrated decreased NF-κB activity (through deregulation of PKCδ, phospho IIKα, IkBα and phospho JNK levels) upon K8 downregulation as well as caspase mediated K17 degradation suggesting increased sensitization of these cells for apoptotic stimuli. Cell motility associated changes correlated with altered RAC GTPase activity and differential phosphorylation of actin associated

proteins like paxillin, cofillin etc. Altogether, this study provides new connecting links between K8 and different cancer related signaling pathways.

Quantitative phosphoproteomic analysis identified differential phosphorylation of many known and novel phosphosites of proteins, which are well established key players in cancer biology and are associated with cell migration, proliferation and apoptosis. Further protein phosphorylation level validation followed by phenotypic analysis correlated well with our phosphoproteomic data. Hence, this study is an addition to the existing knowledge about the role of K8 phosphorylation in modulating different signaling mechanisms and thereby cancer progression.

In conclusion, our *in vitro* as well as in vivo data emphasizes the role of K8 and its phosphorylation in neoplastic progression of skin SCC. Our study also has given many new leads related to the possible mechanisms underlying this phenomenon.

Bibliography:

1. Coulombe, P. A., Omary, M. B., 'Hard' and 'soft' principles defining the structure, function and regulation of keratin intermediate filaments. *Curr Opin Cell Biol* 2002, 14, 110-122.
2. Owens, D. W., Lane, E. B., The quest for the function of simple epithelial keratins. *Bioessays* 2003, 25, 748-758.
3. Omary, M. B., Ku, N. O., Tao, G. Z., Toivola, D. M., Liao, J., "Heads and tails" of intermediate filament phosphorylation: multiple sites and functional insights. *Trends Biochem Sci* 2006, 31, 383-394.
4. Fillies, T., Werkmeister, R., Packeisen, J., Brandt, B., et al., Cytokeratin 8/18 expression indicates a poor prognosis in squamous cell carcinomas of the oral cavity. *BMC Cancer* 2006, 6, 10.
5. Chu, Y. W., Runyan, R. B., Oshima, R. G. and Hendrix, M. J. Expression of complete keratin filaments in mouse L cells augments cell migration and invasion. *Proc. Natl. Acad. Sci. USA* 1993 90, 4261-4265.
6. Chu, Y. W., Seftor, E. A., Romer, L. H. and Hendrix, M. J. Experimental coexpression of vimentin and keratin intermediate filaments in human melanoma cells augments motility. *Am. J. Pathol.* 1996, 148, 63-69.
7. Hendrix, M. J., Seftor, E. A., Chu, Y. W., Seftor, R. E., Nagle, R. B., McDaniel, K. M., Leong, S. P., Yohem, K. H., Leibovitz, A. M., Meyskens, F. L., Jr et al. Coexpression of vimentin and keratins by human melanoma tumor cells: correlation with invasive and metastatic potential. *J. Natl. Cancer Inst.* 1992, 84, 165-174.

8. Raul, U., Sawant, S., Dange, P., Kalraiya, R., Ingle, A. and Vaidya, M. Implications of cytokeratin 8/18 filament formation in stratified epithelial cells: induction of transformed phenotype. *Int. J. Cancer* 2004, 111, 662-668.
9. Casanova, M. L., Bravo, A., Martinez-Palacio, J., Fernandez-Acenero, M. J., Villanueva, C., Larcher, F., Conti, C. J. and Jorcano, J. L. Epidermal abnormalities and increased malignancy of skin tumors in human epidermal keratin 8-expressing transgenic mice. *FASEB J.* 2004, 18, 1556-1558.
10. Alam, H., Kundu, S. T., Dalal, S. N., Vaidya, M. M., Loss of keratins 8 and 18 leads to alterations in alpha6beta4-integrin-mediated signalling and decreased neoplastic progression in an oral-tumour-derived cell line. *J Cell Sci* 2011, 124, 2096-2106.
11. Dmello C , Sawant S , Alam H et.al, Vimentin-mediated regulation of cell motility through modulation of beta4 integrin protein levels in oral tumor derived cells. *The International Journal of Biochemistry & Cell Biology* 2016, 70:161-172.
12. Mizuuchi, E., Semba, S., Kodama, Y., Yokozaki, H., Down-modulation of keratin 8 phosphorylation levels by PRL-3 contributes to colorectal carcinoma progression. *Int J Cancer* 2009, 124, 1802-1810.
13. Alam, H., Gangadaran, P., Bhate, A. V., Chaukar, D. A., et al., Loss of keratin 8 phosphorylation leads to increased tumor progression and correlates with clinico-pathological parameters of OSCC patients. *PLoS One* 2011, 6, e27767.
14. Tanaka, T., Iino, M., Sec8 regulates cytokeratin8 phosphorylation and cell migration by controlling the ERK and p38 MAPK signalling pathways. *Cell Signal* 2015, 27, 1110-1119.
15. Chinembiri, T. N., du Plessis, L. H., Gerber, M., Hamman, J. H., du Plessis, J., Review of natural compounds for potential skin cancer treatment. *Molecules* 2014, 19, 11679-11721.
16. Darwiche, N., Ryscavage, A., Perez-Lorenzo, R., Wright, L., et al., Expression profile of skin papillomas with high cancer risk displays a unique genetic signature that clusters with squamous cell carcinomas and predicts risk for malignant conversion. *Oncogene* 2007, 26, 6885-6895.
17. Wisniewski, J. R., Zougman, A., Nagaraj, N., Mann, M., Universal sample preparation method for proteome analysis. *Nat Methods* 2009, 6, 359-362.
18. Tiwari R, Sahu I, Soni B, Sathe G.J, Datta K.K, Thapa P, Dhaka B, Sinha S, Gowda H, and Vaidya M.M. Quantitative phosphoproteomic analysis reveals system-wide signaling pathways regulated by site-specific phosphorylation on Keratin-8 in skin squamous cell carcinoma derived cell-line. *Proteomics* 2017, 10.1002/pmic.201600254.
19. Majumdar SS, Usmani A, Bhattacharya I, Sarda K, Gautam M, Sharma D, Basu S, Dhup S: A method for rapid generation of transgenic animals to evaluate testis genes during sexual maturation. *J Reprod Immunol* 2009, 83(1-2):36-39.
20. Sehgal L, Thorat R, Khapare N, Mukhopadhaya A, Sawant M, Dalal SN: Lentiviral mediated transgenesis by in vivo manipulation of spermatogonial stem cells. *PLoS One* 2011, 6(7):e21975.

21. Stehlik C, Fiorentino L, Dorfleutner A, Bruey JM, Ariza EM, Sagara J, Reed JC: The PAAD/PYRIN-family protein ASC is a dual regulator of a conserved step in nuclear factor kappaB activation pathways. *J Exp Med* 2002, 196(12):1605-1615.
22. Basu A, Pal D: Two faces of protein kinase Cdelta: the contrasting roles of PKCdelta in cell survival and cell death. *ScientificWorldJournal* 2010, 10:2272-2284.
23. Badock V, Steinhusen U, Bommert K, Wittmann-Liebold B, Otto A: Apoptosis-induced cleavage of keratin 15 and keratin 17 in a human breast epithelial cell line. Cell Death Differ 2001, 8(3):308-315.
24. Li J, Zhu Z, Bao Z: Role of MacMARCKS in integrin-dependent macrophage spreading and tyrosine phosphorylation of paxillin. *J Biol Chem* 1996, 271(22):12985-12990.
25. Choo AY, Yoon SO, Kim SG, Roux PP, Blenis J: Rapamycin differentially inhibits S6Ks and 4E-BP1 to mediate cell-type-specific repression of mRNA translation. *Proc Natl Acad Sci U S A* 2008, 105(45):17414-17419.
26. Livingstone M, Bidinosti M: Rapamycin-insensitive mTORC1 activity controls eIF4E:4E-BP1 binding. *F1000Res* 2012, 1:4.
27. Martinez-Quiles, N., Ho, H. Y., Kirschner, M. W., Ramesh, N., Geha, R. S., Erk/Src phosphorylation of cortactin acts as a switch on-switch off mechanism that controls its ability to activate N-WASP. *Mol Cell Biol* 2004, 24, 5269-5280.

Publications in Refereed Journal:

a) Accepted:

Tiwari R, Sahu I, Soni B, Sathe G.J, Datta K.K, Thapa P, Dhaka B, Sinha S, Gowda H, and Vaidya M.M. Quantitative phosphoproteomic analysis reveals system-wide signaling pathways regulated by site-specific phosphorylation on Keratin-8 in skin squamous cell carcinoma derived cell-line. *Proteomics*, February- 2017, 10.1002/pmic.201600254.

b) Other Publications:

1. Crismita Dmello, Sharada Sawant, Hunain Alam, Prakash Gangadaran, **Richa Tiwari**, Harsh Dongre, Neha Rana, Sai Barve, Daniela Elena Coste, Davendra Chaukar, Shubhada Kanee, Harish Pant, Milind Vaidya. Vimentin mediated regulation of cell motility through modulation of beta4 integrin protein levels in oral tumor derived cells. *The International Journal of Biochemistry & Cell Biology*. Volume 70, January 2016, Pages 161–172.

2. Hunain Alam, Prakash Gangadaran, Amruta V. Bhate, Devendra A. Chaukar, Sharada S. Sawant, **Richa Tiwari**, Jyoti Bobade, Sadhana Kannan, Anil K. D'cruz, Shubhada Kane, Milind M. Vaidya. Loss of Keratin 8 Phosphorylation Leads to Increased Tumor Progression and Correlates with Clinico-Pathological Parameters of OSCC Patients. *PLoS One* 2011, 6, e27767.

Award for the poster / oral presentation if any:

1. **Won Best Poster Presentation Award** at an International Conference "The XXXVII All India Cell Biology Conference on Cell Dynamics and Cell Fate (AICBC-2013)", conducted by Indian Society for Cell Biology on 22nd to 24th December 2013 at Indian Institute of Science, Bangalore, India.
2. **Presented Poster** at an International Conference "American Society of Cell Biology (ASCB)/ International Federation for Cell Biology (IFCB) Meeting-2014" held on 6th -10th December 2014 at Philadelphia, PA, US.
3. **Presented Poster** at an International Conference "Crcinogenesis-2015", organized by Carcinogenesis foundation, USA and ACTREC-TMC, India on 11-13 February 2015 at Advanced Centre for Treatment Research and Education in Cancer, Navi Mumbai, India.

Signature of Student:

Date: 16/2/17

Doctoral Committee

S. No.	Name	Designation	Signature	Date
1.	Dr. Sorab N. Dalal	Chairman		16/2/17
2.	Dr. Milind M. Vaidya	Guide & Convener		16/2/17
4.	Dr. Sanjay Gupta	Member		16/2/17
5.	Dr. Abhijit De	Member		16/2/17

Forwarded Through:

21/2/17

Dr. S.V. Chiplunkar
Director, ACTREC
Chairperson,
Academic & training Program, ACTREC

Dr. S. V. Chiplunkar
Director
Advanced Centre for Treatment, Research & Education in Cancer (ACTREC)
Tata Memorial Centre
Kharghar, Navi Mumbai - 410 210.

Prof. K. Sharma
Director, Academics
T.M.C.

Prof. K. S. Sharma
DIRECTOR - ACADEMICS, TMC
Mumbai - 400 012.

List of Illustrations

List of Figures

List of Tables

List of Abbreviations

AAK1	: Adaptor-associated kinase 1
ACN	: Acetonitrile
ACS	: Apoptosis-associated speck-like protein containing a CARD
AMPK	: 5' adenosine monophosphate-activated protein kinase
ATM	: Ataxia-telangiectasia mutated
BCA	: Bicinchoninic acid assay
BCC	: Besal cell carcinomas
BCL2L12	: Bcl-2-like protein 12
bRPLC	: Basic reversed-phase liquid chromatography
BSA	: Bovine serum albumin
BUB1B	: Budding uninhibited by benzimidazoles 1 homolog beta
CAFs	: Cancer-associated fibroblasts
cAMP	: Cyclic Adenosine Monophosphate
CARHSP1	: Calcium Regulated Heat Stable Protein 1
CASP1	: Caspase-1
CAV1	: Caveolin-1
CDC42	: Cell division control protein 42
CDK6	: Cyclin Dependent Kinase 6
cDNA	: Complementary Deoxyribonucleic acid
CHX	: Cycloheximide
CRC	: Colorectal Cancer
CTC	: Copper Tartarate Carbonate
CTTN	: Cortactin
DAPI	: 4, 6-diamidino-2-phenylindole
DEPC	: Diethyl pyrocarbonate
DMBA	:7,12-Dimethylbenz[a]anthracene
DMEM	: Dulbecco’s Modified Eagle’s medium
DMSO	: Dimethyl sulfoxide
DNA	: Deoxyribonucleic acid
dNTP	: Deoxynucleotide

DSP	: Desmoplakin
DTT	: Dithiothreitol
EBS	: Epidermolysis bullosa simplex
ECL	: Enhanced chemiluminescence
EDTA	: Ethylenediaminetetraacetic acid
EEF1D	: Elongation factor 1-delta
EF1	: Elongation Factor 1
EGF	: Epidermal growth factor
EGTA	: Ethylene glycol tetra acetic acid
EIF3	: Eukaryotic Initiation Factor 3
eIF4	: Eukaryotic initiation factors
EIF4EBP1	: Eukaryotic translation initiation factor 4E-binding protein 1
EIF6	: Eukaryotic Initiation Factor 3
ELISA	: Enzyme-linked immunosorbent assay
ERK	: Extracellular signal–regulated kinases
ERK	: Extracellular signal-regulated kinase
FACS	: Fluorescence-activated cell sorting
FAK	: Focal Adhesion Kinase
FASP	: Filtered sample preparation
FBS	: Fetal bovine serum
FITC	: Fluorescein isothiocyanate
GAPDH	: Glyceraldehyde 3-phosphate dehydrogenase
gDNA	: Genomic Deoxyribonucleic acid
GEMMs	: Genetically modified mouse models
GFP	: Green Fluorescence Protein
GFP	: Green fluorescent protein
GNRH	: Gonadotropin-releasing hormone
GSK3	: Glycogen synthase kinase 3
GSK3β	: Glycogen synthase kinase-3β
HEK	: Human embryonic kidney
HEPES	: (N-[2-Hydroxyethyl] piperazine-N’-[2-ethanesulfonicacid]) sodium salt

HEPES	: 4-(2-hydroxyethyl)-1-piperazineethanesulfonic acid
Hh	: Hedgehog
HNRNPK	: Heterogeneous nuclear ribonucleoprotein K
HSP70	: Heat Shock Proteins 70
IF	: Immunofluorescence
IkB	: Inhibitor of NF-kB
IKK	: Inhibitor of NF-kB kinase
IMDM	: Iscove's Modified Dulbecco's Medium
IPA	: Ingenuity Pathway analysis
JNK	: c-Jun N-terminal kinase
KD	: Knockdown
KF	: Keratin Filament
LAMTOR	: Late endosomal/lysosomal adaptor and MAPK and MTOR activator 1
LARP1	: La-related protein 1
LC-MS/MS	: Liquid chromatography tandem mass spectrometry
LMNA	: Lamin A/C
MAPK	: Mitogen activated protein kinase
mRNA	: Messenger Ribonucleic Acid
mTOR	: Mammalian Target of Rapamycin
MTT	: 3-(4, 5-Dimethylthiazol-2-yl)-2, 5-Diphenyltetrazolium Bromide
NFkB	: Nuclear Factor kappa-light-chain-enhancer of activated B cells
NLS	: Nuclear localization signals
NMSC	: Non-melanoma skin cancers
NOD-SCID	: Nonobese diabetic-Severe combined immunodeficiency
OSCC	: Oral Squamous cell carcinoma
PAGE	: Polyacrylamide gel electrophoresis
PBS	: Phosphate Buffered Saline
PCR	: Polymerase chain reaction
pERK	: Phospho-Extracellular signal–regulated kinases
PFA	: Paraformaldehyde
pJNK	: Phospho-c-Jun N-terminal kinase

PKA	: Protein kinase A
PKC	: Protein Kinase C
PKP3	: Plakophilin-3
PNN	: Pinin
PP2A	: Protein Phosphatase 2A
PPI	: Protein-Protein Interaction
ppm	: parts per million
pRAS	: Proline-rich Akt substrate
PRL3	: Phosphatase of Regenerating Liver 3
PSM	: Peptide-spectrum match
PVDF	: Polyvinylidene difluoride
qRT-PCR	: Quantitative reverse transcriptase PCR
RAC1	: Ras-related C3 botulinum toxin substrate1
Raf	: Rapidly accelerated fibrosarcoma
RANBP1	: Ran-specific binding protein 1
RAS	: Renin–angiotensin system
Rho GDI2	: RHO protein Guanosine-diphosphate dissociation inhibitor
RIPA	: Radioimmunoprecipitation assay
RNA	: Ribonucleic Acid
SCC	: Squamous cell carcinoma
SCC	: Squamous cell carcinoma
SCRIB	: Scribbled Planar Cell Polarity Protein
SDS	: Sodium dodecyl sulphate
SEM	: Standard error of the mean
shRNA	: Short hairpin RNA
SPC	: Statistical Process Control
SRRM2	: Serine/arginine repetitive matrix protein 2
STAT3	: Signal transducer and activator of transcription 3
STK10	: Serine/threonine-protein kinase 10
SUMO	: Small Ubiquitin-like Modifiers
TBS	: Tris-buffered saline

TBST	: Tris-buffered saline-Tween 20
TFA	: Trifluoroacetic acid
TJP2	: Tight junction protein ZO-2
TMT	: Tandem mass tags
TNF	: Tumor necrosis factor
TNF-a	: Tumour Necrosis Factor alpha
TNFR	: Tumour Necrosis Factor Receptor
TPA	: 12-O-tetradecanoyl phorbol-13-acetate)
TPA	: 12-O-tetradecanoylphorbol-13-acetate
TPCK	: Tosyl phenylalanyl chloromethyl ketone
TRADD	: TNFR-1 associated death domain
TSC1	: Tuburous Sclerosis 1
ULF	: Unit Length Fragment
UVC	: Ultraviolet-C
WASP	: Wiskott-Aldrich syndrome protein
WT	: Wild type
ZYX	: Zyxin

Chapter-I

Introduction

INTRODUCTION:

The cytoskeleton of epithelial cells is a network of three major classes of filamentous biopolymers: microfilaments, microtubules and intermediate filaments [1, 2]. Intermediate filaments are composed of a large family of cell-specific proteins that organize to form 10 nm filaments sharing sequence homology and structural features [3, 4]. 'Keratins' is the largest subgroup of intermediate filament (IF) proteins which are known to be expressed in tissue specific and differentiation state specific manner [3, 5] . They are subdivided into type I (relatively acidic keratins with low molecular weight, K9–K28, K31–K40) and type II (relatively basic keratins with high molecular weight K1–K8, K71–K86) keratins [5, 6] on the basis of their biochemical properties like molecular weight and isoelectric point. They exist as obligatory hetero-polymers of one type I and one type II keratin each, assembled in 1:1 molar ratio [3, 4]. Epithelial tissues express different pairs of keratins depending on the cell type e.g. Simple epithelia express K8/18, K7/19, and K20 whereas stratified epithelia express K1/10, K5/K14, K6/17 *etc.* [7, 8]. Keratins share a common prototype structure of all cytoplasmic IF proteins. All keratin filaments have a highly conserved central coil-coil α-helical 'rod' domain flanked by a non-α-helical N terminal 'head' and C-terminal 'tail' domains of various lengths [9, 10]. The head and tail domains are known to harbor specific sites for various posttranslational modifications like phosphorylation, glycosylation, ubiquitination and sumoylation. Amongst these phosphorylation is considered to be the major regulator of keratin functions [11, 12].

Being cytoskeletal protein, the widely accepted function of keratins was to only provide mechanical stability and integrity to the epithelial tissue and protect them from various cellular stresses by forming structural scaffolds. The integrity of these filaments is critical to provide mechanical support to tissue architecture and for the maintenance of cell viability [13-15].

Recent reports confirmed that apart from their cryo-protective functions, they also perform some important regulatory functions by modulating certain signaling pathways [16, 17]. Most of these functions include, modulation of protein localization, targeting, trafficking and synthesis [7, 18, 19], protecting cells from apoptotic stress [20], cell motility [21], apico-basal polarity[22], modulation of Rho-dependent actin organization and dynamics [21], modulation of the cell adhesion, size, cell-cycle progression [18, 23-25]. The simple epithelia express K8/18 as their predominant keratin pair and most of the above mentioned functions are studied on and attributed to keratin pair of 8 and 18. Majority of such mechanical or non-mechanical functions of keratin 8/18 are regulated by its posttranslational modifications, most importantly phosphorylation [26]. Phosphorylation mediated functions of keratin8/18 include, filament organization, solubility, turnover, binding to other proteins, protecting cells from stress and apoptosis by acting as a phosphate sponge for stress activated kinases *etc*. [27]. K8 contains three major physiological phosphorylation sites, Serine^{23}, Serine^{73} in head-domain and Serine^{431} in tail-domain. Phosphorylation at Serine^{23} is highly conserved among all type-II keratins, rendering some common functions to them, whereas Serine^{73} and Serine^{431} are unique to K8 [11, 28-30]. Keratin 8 serves as a substrate for many kinases and phosphatases, involved in various signaling cascades, like c-Jun N terminal kinase (JNK) and p38 kinases, which phosphorylate at Serine^{73} residue during cellular stresses and mitogen-activated protein kinase (MAPK), which phosphorylates at Serine^{431} after stimulation of cells by epidermal growth factor where as PP2A and PRL3 are two phosphatase known to dephosphorylate keratin 8 at specific residues [31, 32].

Keratin 8/18, is often aberrantly expressed in squamous cell carcinomas where its expression is correlated with increased invasion and poor prognosis. Apart from being used as a diagnostic tumor marker, K8/18 is also reported to modulate different signaling pathways involved in tumor

progression [4, 24, 33, 34]. Previous report from our laboratory has shown that forced expression of K8/18 leads to increased invasiveness and tumorigenic potential of FBM cell-line [35]. Further, in this direction, our laboratory has shown that depletion of keratin 8/18 in an oral squamous carcinoma derived AW13516 cell line leads to decreased tumorigenic potential by deregulating α6β4 integrin pathway together with the changes in fascin mediated actin organization [36, 37]. These results suggest that aberrant expression of K8/18 could contribute to neoplastic progression of oral SCC.

Apart from aberrant expression, deregulation of K8 phosphorylation has been also associated with cancer progression. In case of simple epithelia derived cancers, perinuclear reorganization of keratin 8 by SPC has been shown to increase migratory potential of these cells assisted by MEK–ERK pathway which putatively targets K8 Serine^{431} residue [38]. Another report, indirectly demonstrated the concurrent de-phosphorylation of keratin 8 at Serine^{73} and Serine^{431} position at the invasive front of colorectal carcinoma derived tumor samples upon aberrant expression of phosphatase of regenerating liver 3 with supportive cell line based studies [39]. Mutational studies from our laboratory substantiated a potential role of K8 phosphorylation in augmenting migration and tumorigenicity of oral squamous cell carcinoma derived cell line AW13516 which showed a significant correlation with clinico-pathological parameters of OSCC patients, a finding which was not reported earlier [40] . In case of oral squamous cell carcinomas a recent report demonstrated reduced K8 Serine^{73} phosphorylation via P38 MAPK pathway upon sec 8 down-regulation which resulted in decreased cell migration [41].

Non-melanoma skin cancers (NMSC), one of the most common neoplasms known to causes serious morbidity and mortality, are curable at early stages, but delayed diagnosis leads to metastasis [42]. Although K8/18 pair is known to be aberrantly expressed in skin cancers [9], till

now, to our knowledge there are no reports about the mechanism associated with the involvement of K8 in neoplastic progression of basal SCCs [43]. Similarly, phosphorylation is associated with many diverse physiological functions of K8 but the reports related to its role in the neoplastic progression of different carcinomas and the underlying mechanisms are inconsistent. Hence further studies are required to elucidate K8 and its phosphorylation function in neoplastic progression of skin squamous cell carcinomas and mechanisms underlying the same; *in vitro* as well as *in vivo*. Deciphering the role of K8 and its phosphorylation in tumourigenic potential of skin epidermoid carcinoma cell line A431 and associated signaling will give us a better in sight towards its role in oncogenic progression of skin SCC. Development of a tissue specific transgenic mouse model expressing K8 wild type and phosphomutants followed by DMBA/TPA mediated skin carcinogenesis will be useful to strengthen and signify role of K8 phosphorylation in neoplastic progression of SCC.

1.1 Aims and Objectives:

1.1.1 Part 1:

Aim: To study the role of K8 phosphorylation in neoplastic progression of SCC using transgenic mouse model.

Objectives:

a) To generate a tissue specific transgenic mouse model expressing wild type K8 and phosphomutants.

b) To use DMBA-TPA mediated skin carcinogenesis in order to study the role of K8 phosphorylation in neoplastic progression.

1.1.2 Part 2:

Aim: To investigate role of K8 phosphorylation in squamous epithelium derived cell lines at phenotypic and molecular level so as to understand whether these effects are cell line specific and further to understand mechanism underlying the same.

Objectives:

a) To express K8 phosphomutants and wild type in the cells with K8 null background.

b) To study the phenotypic and molecular changes on expressing K8 phosphomutants in cells with K8 null background compared to WT.

Chapter-II

Review of Literature

2.1 Intermediate filaments

Intermediate filaments (IF) are flexible, rod-shaped fibers averaging 10nm in diameter, a size that is 'intermediate' between microfilaments (MF; 7-8nm) and microtubules (MT; 25nm) [1]. Out of these, IFs are the most diverse and are encoded by approximately 70 IF genes in the human genome. IFs are classified into six major families and are expressed in cell-type, tissue-type, differentiation and developmental state specific manner. Families I–IV and VI are localized to the cell cytoplasm whereas the type V, nuclear lamins are important organizers of the nuclear envelope and karyoplasm. The integrated network formed by these filament systems is responsible for the mechanical integrity of the cell and is critical for cellular processes like cell division, motility and plasticity[2]. Unlike MTs and MFs, IFs are highly insoluble structures and are resistant to detergent action as well as high and low ionic salt concentration. IFs can self-assemble into the characteristic 10-12nm wide filaments and they have been found to be highly dynamic in spite of their insoluble nature. IFs are flexible intracellular fibrous polymers that provide resilience to the cells in which they are expressed. They are mostly involved in the maintenance of cell shape, positioning of cell organelles, locomotion, intracellular organization, cell division and transport [23].

2.1.1 IF Structure

In 1982, Geisler and Weber discovered that IF family members with distinct primary sequences share a common tripartite structure made up of a central a-helical coiled-coil rod domain flanked by flexible, little secondary structure containing and highly variable N- and C-termini that lead to exceptional structural diversity among IFs.

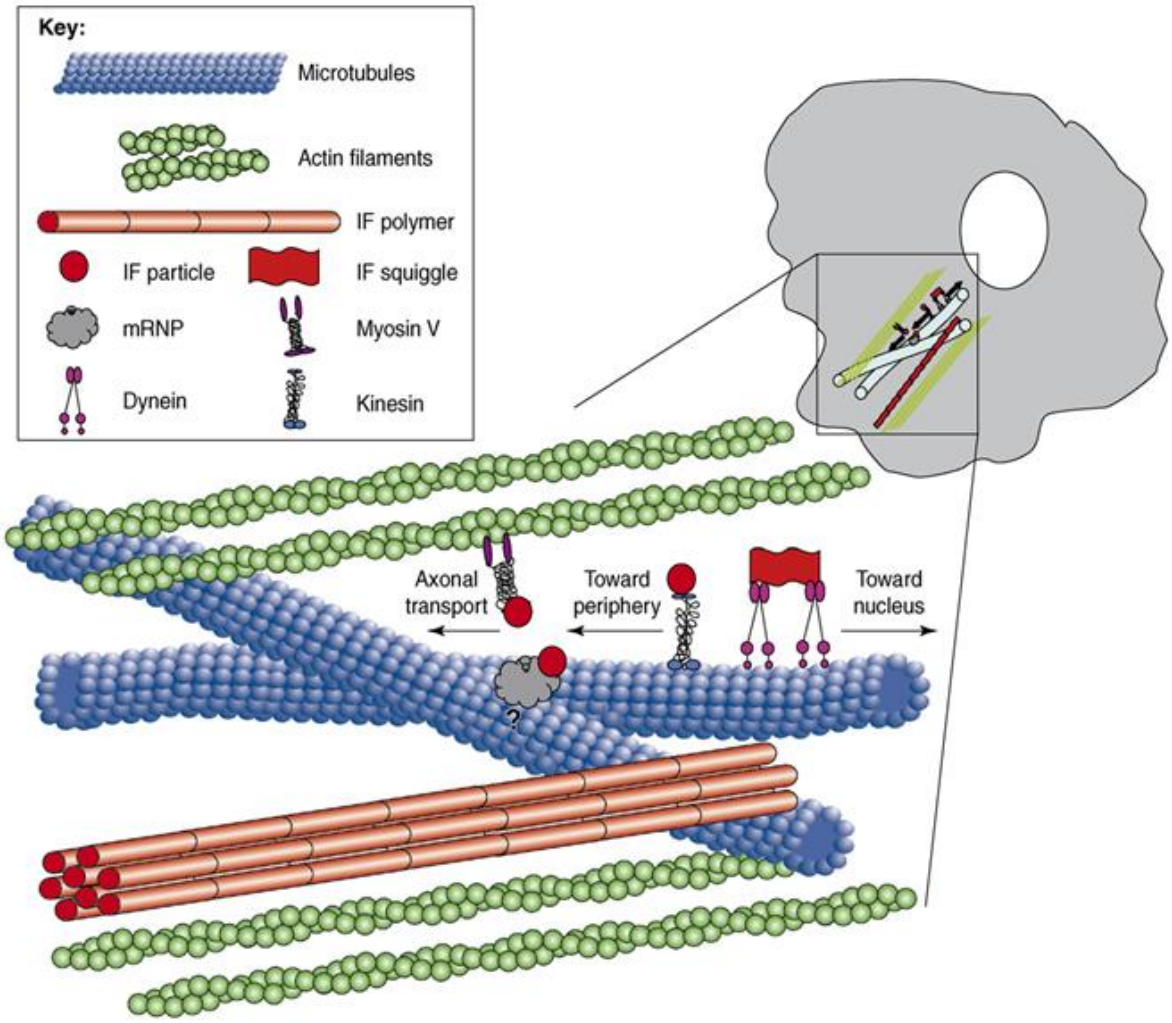

Figure 2.1.1.1 Schematic representation of the interaction of IF precursors with microtubule and actin-associated motor complexes (Adapted from [1]).

This diversity brings about the cell type specific functions to IF networks unlike the broadly conserved functions of MT and MF. The interaction of IF precursors with microtubule and actin-associated motor complexes is shown in **Figure 2.1.1.1**. A centrally located rod domain of fixed length (either ~310 or ~352 residues) is subdivided into α-helical segments featuring long-range heptad repeats of hydrophobic/apolar residues (subdomains 1A, 1B, 2A and 2B), which are interrupted by non- α -helical 8–17 amino acid linker (L) stretches, L1, L12, and L2. Rod domain boundaries consist of highly conserved 15- to 20-amino-acid regions that are crucial for

polymerization and are frequently mutated in human diseases. A coil consists of two or more α-helices wound around each other in a 'superhelix', and comprises of widespread structural motifs in proteins. This structure is formed mainly due to the seven residue periodicity in the distribution of apolar residues. The coiled-coil structure determines the overall elongated shape of IF dimers. The central rod domain is highly conserved among all IFs whereas the head and the tail domains are variable in Sequences as well as length. It is due to the variability of the end domains that IFs proteins exhibit different molecular sizes, charge and antigenicity. The non-helical end domains (head and tail domains) are also divided into subdomains based on homologous (H), variable (V) or end (E) sequences. The structure of intermediate filament is depicted in **Figure 2.1.1.2**. The flanking head and tail domains contain all the known post-translational modifications like O-GlcNAcylation, phosphorylation, ubiquitination, sumoylation *etc.* [3, 44-47].

2.1.2 IF Classification

On the basis of Genomic structure and nucleotide sequence homology throughout the rod domain, IFs are classified into six major types (I-VI). At the protein level, polymerization properties define four assembly groups (A-D). Type I and type II IF genes encode the 'acidic' and 'basic' keratins, respectively, which copolymerize in obligatory manner (assembly group A) to give rise to the IFs present in the cytoplasm of all epithelial cells. Assembly group B includes proteins encoded by type III, type IV and type VI IF genes, which encode cytoplasmic proteins. The prototypic type III gene, vimentin, is expressed in non-epithelial cell types, and its product can homopolymerize to form 10nm filaments. Many of the type III and type VI genes are expressed in muscle cells. Apart from Vimentin, Desmin, Glial Fibrillary Acidic Proteins (GFAPs) and peripherin are grouped in Type III, Neurofilaments and Nestin are grouped into Type IV, the nuclear lamins as type V and Phakinin, Filensin as orphans (8, 42). Pattern of IF proteins expression in different tissues is shown

in the **Table 2.1.2**. Type IV sequences, which consist of the neurofilament triplet proteins (NF-Light, NF-Medium and HF-Heavy) and α- internexin, are expressed in neurons. In common with keratins, neurofilaments are also obligatory heteropolymers of L, M and H subunits interacting with a 5:3:1 molar ratio [10, 46, 48].

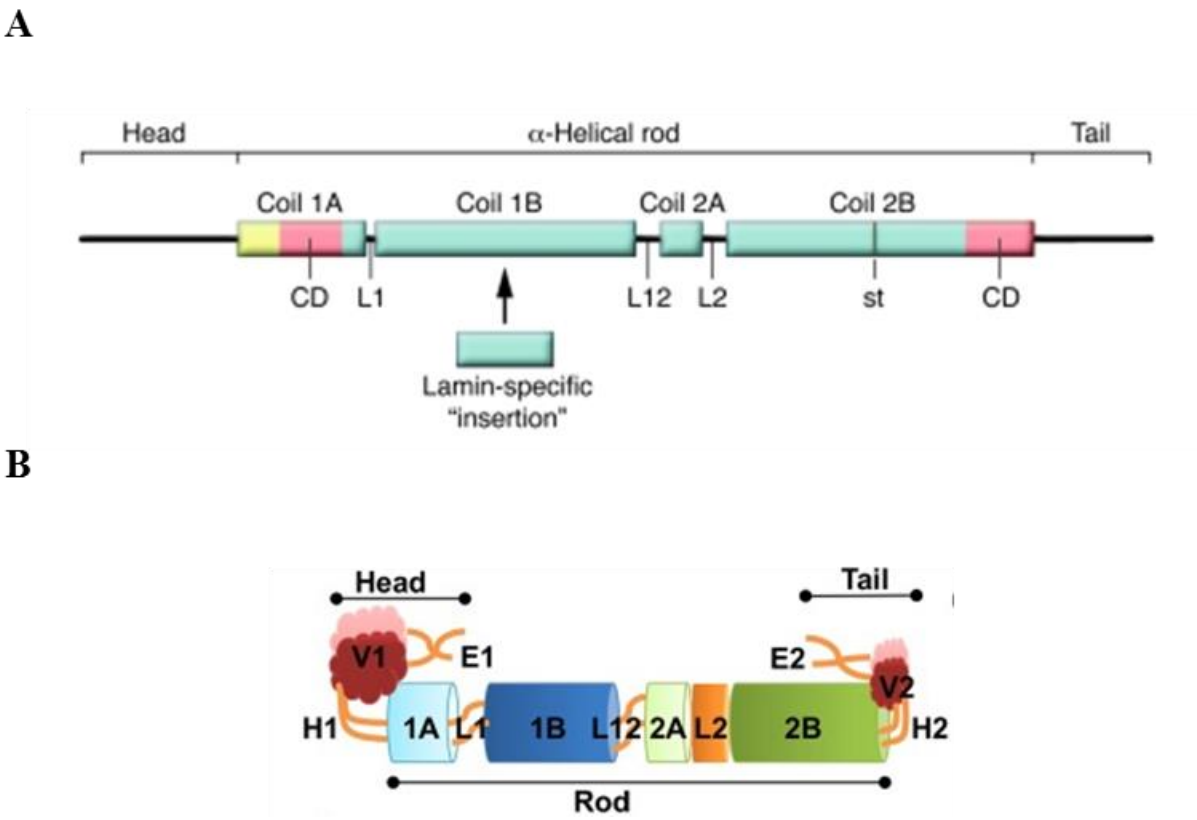

Figure 2.1.1.2 Schematic depictions of the common structure of intermediate filament*:* A) In the representative IF structure, blue boxes correspond to different segments; orange boxes correspond to IF-consensus motifs (CD); and the yellow box represents an α-helical pre-coil domain (specific to vimentin-like IF proteins). L1, L12, and L2 are linker segments. "Head" and "tail" represent non–α-helical domains. The stutter (st) indicates a discontinuity in the heptad repeat pattern of coil 2B. The blue box designated lamin-specific "insertion" highlights a position in which an additional α-helical segment is found in lamins. B) Schematic of the domain structure of the keratin dimer [44, 45].

Table 2.1.2 Intermediate filament classification and their tissue distribution (Adapted from [48]).

Location and Name	Type	Size	Chromosome with Associated Gene	Cell or Tissue Distribution	Comments
		kD			
Cytoplasmic					
Keratins	I	40–64	17	Epithelium (keratins 9–20); hair (keratins Ha1–Ha8)	Form obligate 1:1 heteropolymers with type II; protect from mechanical and nonmechanical forms of stress
	II	52–68	12	Epithelium (keratins 1–8); hair (keratins Hb1–Hb6)	Form obligate 1:1 heteropolymers with type I; protect from mechanical and nonmechanical forms of stress
Vimentin	III	55	10	Mesenchyme	Involved in vascular tuning and wound repair in mice
Desmin	III	53	2	All muscle	May be important for mitochondrial positioning and integrity
Glial fibrillary acidic protein	III	52	17	Astrocytes	Also found in hepatic stellate cells
Peripherin	III	54	12	Peripheral neurons	Found in enteric neurons; may be required for development of a subset of sensory neurons
Syncoilin	III	54	1	Muscle (mainly skeletal and cardiac)	Interacts with α-dystrobrevin
Neurofilaments (light, medium, and heavy chains)	IV	61 (light), 90 (medium), 110 (heavy)	8 (light), 8 (medium), 22 (heavy)	Central nervous system	Form obligate 5:3:1 (light:medium:heavy) heteropolymers
α-Internexin	IV	61	10	Central nervous system	May partially compensate for peripherin in peripherin-null mice
Nestin	IV	240	1	Neuroepithelial	Is also an early developmental marker, as found in the pancreas
Synemin	IV	180 (α) and 150 (β) (two splice variants)	15	All muscle (β isoform mainly in striated muscle)	Found at lower levels than desmin; also found in astrocytes; probably identical to desmuslin
Nuclear					
Lamins A and C	V	62–78	1	Nuclear lamina	Arise from a single, differentially spliced gene
Lamins B1 and B2	V	62–78	5, 19	Nuclear lamina	Arise from two different genes
Other					
Phakinin (CP49)	Orphan	46	3	Lens	Forms beaded filaments; deletion in mice causes lens defects
Filensin (CP115)	Orphan	83	20	Lens	Forms beaded filaments; deletion in mice causes lens defects

2.1.3 IF assembly

The soluble subunit for creating intermediate filaments is a tetramer. The tetramer is created from monomers in a stepwise fashion. First, two monomers associate via their central domains to form parallel helical coils around each other. This parallel dimer then associates with another parallel dimer in an antiparallel arrangement to form a staggered tetramer. The lateral association of eight tetramers results in the formation of a unit-length filaments (ULF). Two ULFs are able to anneal

longitudinally to form a thick filament, approximately 16nm in diameter. Further end-to-end annealing of ULFs results in filament elongation, which is followed by radial compaction resulting in the final intermediate filament diameter [1, 49, 50]. **Figure 2.1.3** shows the schematic model of filament formation from dimer to mature filament.

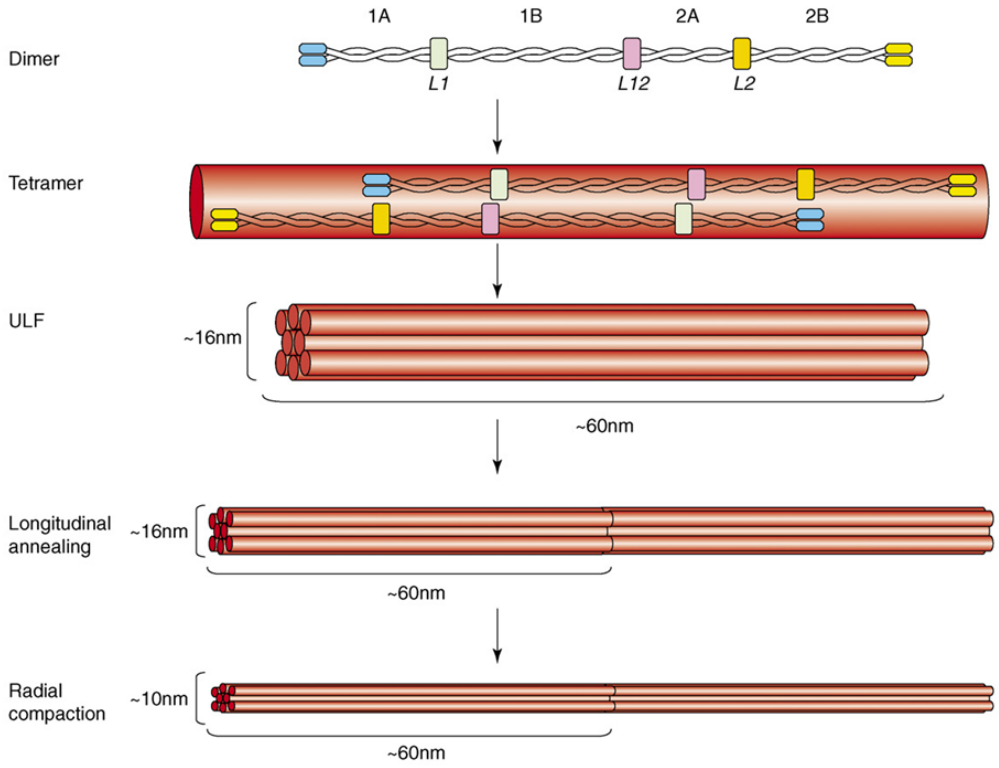

Figure 2.1.3 Schematic model of filament formation from dimer to mature filament, based on in vitro assembly data (Adapted from [1]).

2.2 Keratins

The most diverse and abundant cytoskeletal components of epithelial cells are keratin intermediate filaments. There are >50 keratin isotopes expressed in epithelia and account for the majority of IF genes in the human genome as shown in **Figure 2.2**. They are expressed in all types of epithelial cells. Like other IFs, keratins also form a cytoplasmic network like of 10-12nm wide filaments [5].

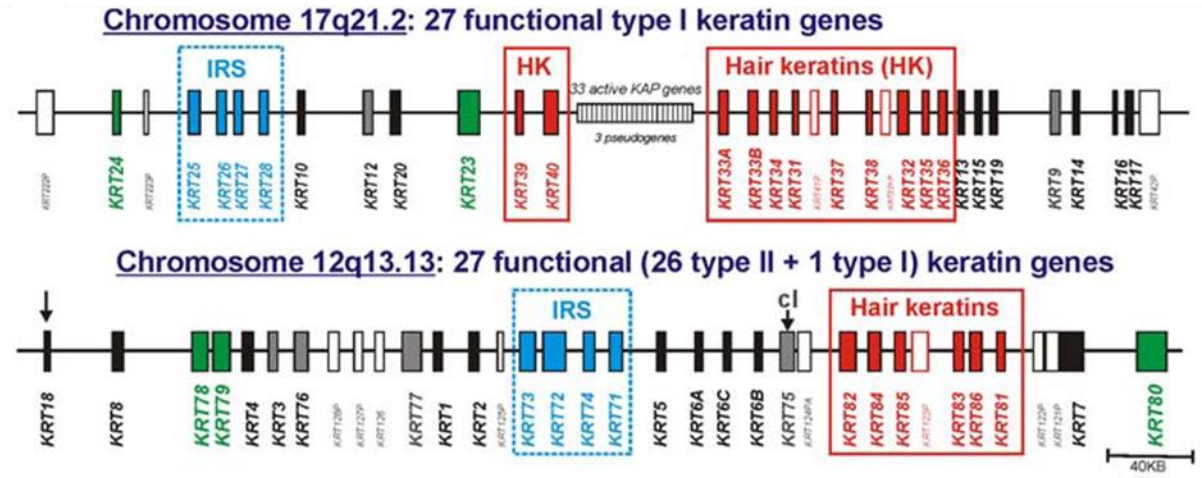

Figure 2.2 Organization of the human keratin genes in the genome. The type I and type II keratin gene subdomains are located on chromosomes 17 and 12, respectively (Adapted from [5]).

Keratins share a wide range of common properties to IFs as they are highly insoluble and are known to provide structural integrity to the cells. Surprisingly, despite their resistant nature, like other IFs, keratin filaments are highly dynamic and are involved in different mechano-transduction pathways too. Mutations in most of them are now associated with specific diseases. Dynamic nature of the keratins is regulated by their posttranslational modifications such as phosphorylation and glycosylation [3].

2.2.1 Classification of keratins

Keratins are encoded by a large multigene family of more than 60 individual members which are identified from the human genome sequence analysis. 53 of them are found to be functional genes. Expression of 37 different polypeptides of keratins has been reported in different human epithelial tissues [4, 5].

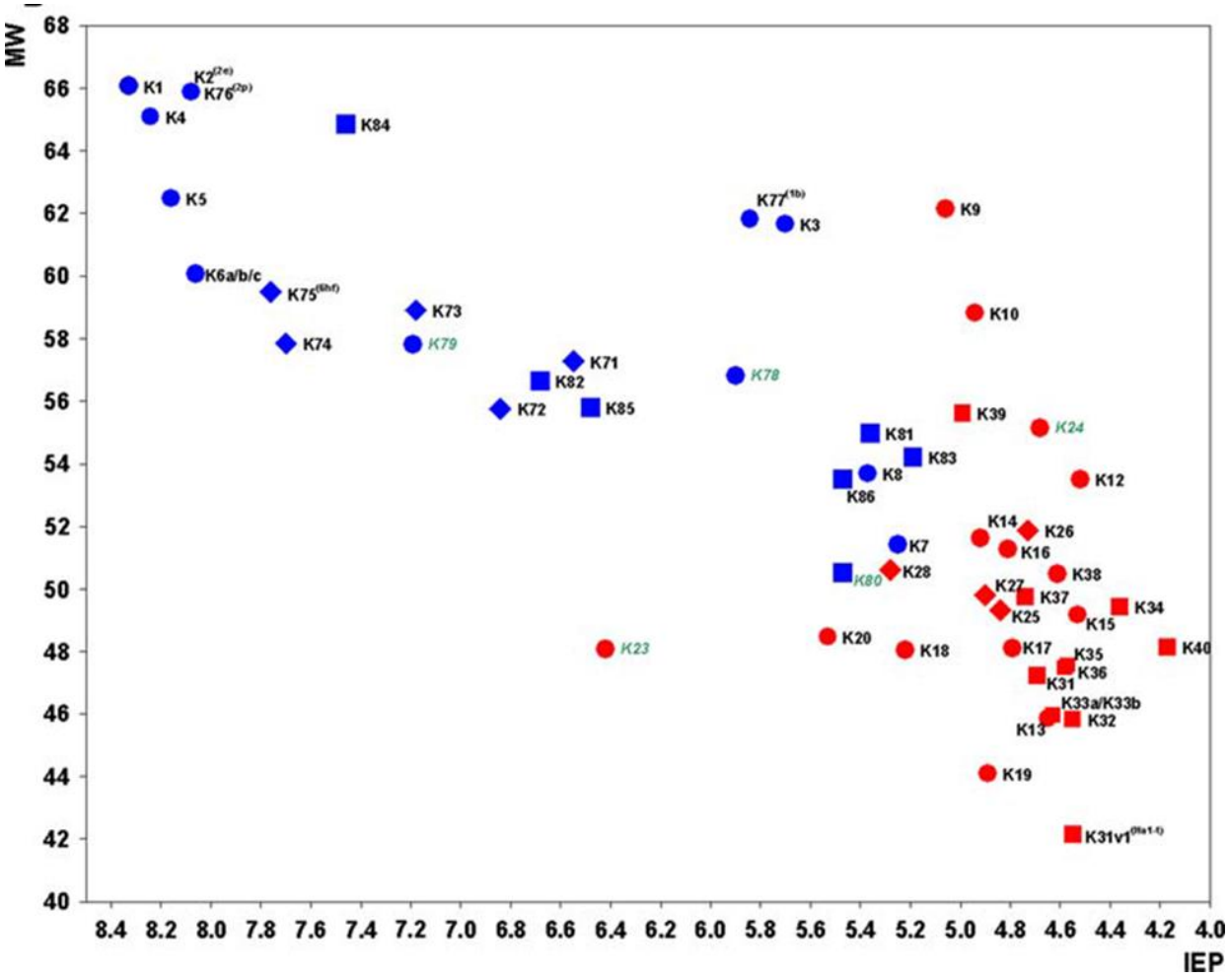

Figure 2.2.1 Two-dimensional catalogue of the human keratins based on molecular weights (MW) and isoelectric points (IEP) calculated from amino acid sequences (Adapted from [5]).

Keratins are subdivided on the basis of different classification systems like, Primary keratins and Secondary keratins on the basis of pattern of synthesis or on the basis of distribution, Soft keratins and Hard keratins *etc*. [6].

Table 2.2.1 Keratin classification and expression pattern (Adapted from [32]).

Keratin	Epithelial tissue	Partner
Type I		
Simple		
K18	Simple epithelia (e.g. liver, pancreas, colon, lung)	K8, K7
K20	Simple epithelia, especially gastrointestinal	K8, (K7)
Barrier		
K9	Stratified cornifying epithelia; palm, sole	(K1)
K10	Stratified cornifying epithelia; suprabasal	K1
K12	Stratified epithelia; cornea	K3
K13	Stratified epithelia; non-cornifying; suprabasal	K4
K14	Stratified and complex epithelia; basal	K5
K15	Stratified epithelia	(K5)
K16	Stratified epithelia; induced during stress, fast turn over; suprabasal	K6a
K17	Stratified epithelia; induced during stress, fast turn over	K6b
K19	Simple and stratified epithelia	K8
K23, K24	Epithelia	
Structural		
K25, K26, K27, K28	Stratified epithelia; hair follicle sheath	
K31, K32, K33a, K33b, K34, K35, K36, K37, K38, K39, K40	Stratified epithelia; hair, hard structure	
Type II		
Simple		
K7, K8	Simple epithelia	K18
Barrier		
K1	Stratified cornifying epithelia; suprabasal	K10
K2	Stratified cornifying epithelia; late suprabasal	(K10)
K3	Stratified epithelia, cornea	K12
K4	Stratified epithelia; non-cornifying; suprabasal	K13
K5	Stratified and complex epithelia; basal cells	K14, (K15)
K6a	Stratified epithelia; induced during stress, fast turn over	K16
K6b	Stratified epithelia; induced during stress, fast turn over	K17
K6c	Epithelia	
K76	Stratified cornifying epithelia, oral, suprabasal	(K10)
K78, K79, K80	Epithelia	
Structural		
K75	Stratified epithelia; hair follicle	
K71, K72, K73, K74	Stratified epithelia; hair follicle sheath	
K81, K82, K83, K84, K85, K86	Stratified epithelia; hair, hard structure	

*Modified from Haines and Lanes, and Loschke (Haines and Lane, 2012; Loschke *et al.*, 2015).

But the most accepted classification was on the basis of biochemical properties like molecular weight and isoelectric point, as depicted in **Figure 2.2.1**, was further renewed on amino acid sequence; Type I and Type II keratins (relatively acidic and basic respectively) as shown in **Table 2.2.1**. According to recent classification, the type II keratins comprise of 20 different proteins (K1-K8, K71-K86, K6b, K6c) and the type I keratins include 17 different proteins (K9-K28, K31-K40) [5, 32].

2.2.2 The keratin cycle:

The first step in the keratin cycle is nucleation where soluble keratin oligomers assemble into particles in the cell periphery in proximity to focal adhesion sites. This is followed by elongation where these particles grow and move toward the cell center in an actin-dependent process (transport). Subsequently, integration occurs where elongated Keratin filament particles are incorporated into the peripheral keratin network. Next to this, transport takes place in which filament bundling occurs during further centripetal translocation toward the nucleus. Soluble oligomers dissociate which is disassembly followed by diffusion throughout the cytoplasm, and are reutilized for another cycle of Keratin filament formation in the cell periphery. Alternatively, maturation occurs in which bundled filaments are further stabilized forming the stable peri-nuclear cage [51, 52]. The Keratin cycle has been depicted in **Figure 2.2.2**.

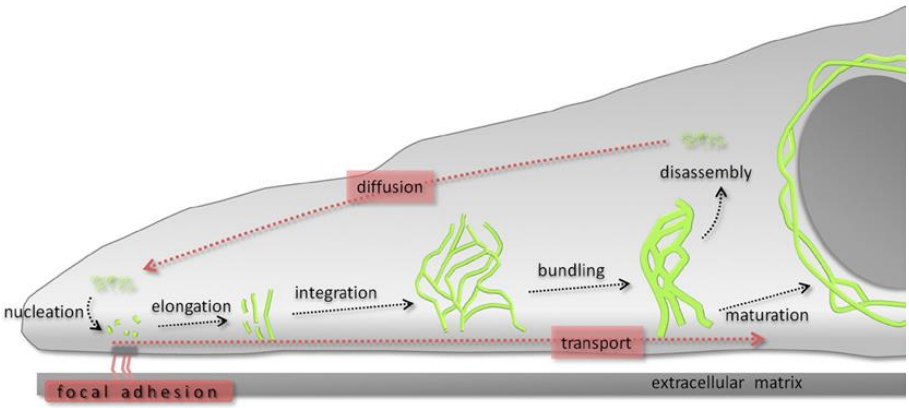

Figure2.2.2 The keratin cycle (Adapted from [52]).

2.2.3 Keratins Expression

Keratins are expressed in all epithelial cells; from the single-layered epithelia of most internal organs (simple epithelia) to the complex multi-layered epithelium (stratified epithelium) of the epidermis**.** They are expressed in a highly tissue/ cell type specific and differentiation state specific

manner. They are stable as a heterodimers made up of one Type I and one Type II keratin each coming together in 1:1 molar ratio. Simple epithelia of internal parenchymatous organs where comparatively less mechanical stress is experienced, express only a few keratin family members, which form keratin network of scant and loosely distributed filaments in the cytoplasm. On the other side majority of the keratins are being expressed and form densely bundled tono-filaments in case of squamous epithelia and cornified stratified epithelia such as in the epidermis lining the outer body surfaces. The loose filaments in the former case are composed of "simple-epithelial keratins" like K8/K18 (and K19), while the bundled filaments (tonofilaments) in the latter case are built up from keratins such as K5/K14 in the basal layer , K1/K10 in the suprabasal layers and K2/K10 in the uppermost layers. Differentiating cells express K1/10 in skin, K4/13 in internal stratified epithelia such as esophagus and K3/K12 in corneal cells. In breast epithelium the basal/myoepithelial cells (proliferation compartment) express K5 and K14, while the luminal cells (differentiation compartment) express K8 and K18. The strictly regulated tissue and differentiation specific pattern of expression is suggestive of the fact that the keratins may have tissue specific functions [5, 53-56].

2.2.4 Posttranslational modifications of keratins:

Like other IFs majority of the keratin functions are regulated by their post translational modifications as shown in **Table 2.2.4**, including glycosylation, phosphorylation, sumoylation, acetylation, proteolysis and transglutamination [12]. Six major posttranslational modifications of keratins are as follows:

2.2.4.1 Glycosylation:

Various Keratins have been identified to undergo glycosylation, like K13, K8 and K18. This dynamic post translational modification is shown to be partly governed by the adjacent site specific phosphorylation mediated crosstalk. Keratin solubility properties together with their filament organization/reorganization are some of the known functions to be governed by glycosylation, in a site dependent manner. The other functions of this modification are largely unknown and remain to be investigated [12, 57, 58].

2.2.4.2 Transglutamination/Transamidation:

Transamidation, the formation of amide bonds between the ε-N group of Lysine and the γ-C group of Glutamine is catalyzed by The activity of transglutaminase 2 (TGase 2) — an inducible acyltransferase and in turn regulates IF function under various physiological and pathological conditions. This modification is identified in both epidermal as well as simple epithelial keratins and the first transamidation site was recently identified on K8 as Glutamine^{70} in the head domain. Transamidation, appears to provide a keratin associated barrier function through the attachment of several epidermal type II keratins to the cornified envelope of the skin. In the physiological context, the role of this modification is clear in terms of providing a compact protective structure. In the different pathological conditions like certain chronic liver diseases, K8 in hepatocytes becomes cross-linked by TGase2 which results in the formation of K8/18 aggregates termed Mallory–Denk bodies (MDBs) [12].

Table 2.2.4 IF protein Post Translational Modifications and the modifying enzymes (Adapted from [31]).

PTM	IFs	PTM enzyme (on)	PTM enzyme (off)
Extensively studied			
Phosphorylation	Most IFs*	SAPKs, AKT1, PKC, CDK1, CDK5 and others	PP1, PP2A and PTP1B
Farnesylation	Lamins	Farnesyltransferase	ZMPSTE24 (through proteolysis)
Ubiquitylation	Most IFs‡	CHIP, UBC3, UBCH5, SIAH1 and TRIM32	Not known
Accumulating data			
Sumoylation	Lamins, keratins and vimentin	UBC9	Not known
Glycosylation	Keratins, neurofilaments and vimentin	OGT	*O*-GlcNAcase
Acetylation	Keratins	Not known	SIRT2
Limited data			
Transamidation	Keratins	Transglutaminases	Not known
ADP ribosylation	Desmin and vimentin	ADP-ribosyl transferase SpyA	Not known

2.2.4.3 Sumoylation:

IFs are modified in a covalent and reversible manner by a modification analogous to Ubiquitylation but which involves addition of SUMOs (small ubiquitin-like modifiers). Conjugation of SUMO (SUMO1, SUMO2 and SUMO3) to mammalian proteins involves Lysine residues. Sumoylation of cytoplasmic and nuclear IFs regulates their filament formation and solubility. Disease causing alteration in sumoylation affects these properties of IFs e.g. especially during stress and extensive tissue injury K8/K18/K19 get hypersumoylated, which retains keratins in an insoluble compartment, thereby limiting their cytoprotective function [31, 59].

2.2.4.4 Ubiquitylation:

Ubiquitylation of IF proteins is a normal physiological process which is involved in its turnover. The obligatory heterodimeric nature of keratins suggests that one of the keratin monomer might be degraded by the ubiquitin–proteasome system in the absence of its partner, which usually provides a stabilizing function. Accumulation of ubiquitylated IF proteins occurs in the context of cellular dysfunction, which is accompanied by proteasome inhibition [31, 60].

2.2.4.5 Proteolysis:

Apoptosis associated caspase mediated Proteolysis of K18 and K19 generates stable keratin fragments that are highly enriched within the cytoskeletal compartment. It is likely that this apoptosis-associated degradation involves all type I keratins [12].

2.2.4.6 Acetylation:

IF proteins are among ~1,000–1,700 acetylation targets and this Lysine acetylation is known to modulate IF properties in response to metabolic changes. A conserved Lysine residue (Lysine ^{207}) in the rod domain of K8 was identified as a putative acetylation site. Basal acetylation at Lysine ^{207} reduces K8 solubility and promotes the formation of a dense perinuclear K8 filament network whereas increased K8 acetylation is observed during hyperglycemia which is accompanied with changes in K8 biochemical and filament properties. The dynamics of this process are regulated by specific enzymes carrying out lysine acetylation and deacetylation. Keratin acetylation provides a new mechanism to regulate keratin filaments, possibly via modulating keratin phosphorylation [61].

2.2.4.7 Phosphorylation:

Phosphorylation is one of the best-studied, highly dynamic and multifunctional posttranslational modifications of keratins. In general, the Serine/Threonine phosphorylation which is modulated by numerous kinases and phosphatases, facilitates IF reorganization and maintains filament structural dynamics. This is achieved by 'dynamic subunit exchange', where new IF subunits can be incorporated anywhere along the length of IF structures [12].

Phosphorylation also regulates keratin binding to other proteins (e.g. 14-3-3) and in-turn their role in mechano-transduction. Head and the tail domains of keratins are known to harbor most of the phosphorylation sites (mainly distinct Serine and Threonine residue) identified so far. **Table 2.2.4.7** contains the list of kinases and their corresponding phosphorylation sites on keratins. The 'head' and 'tail' domains impart most of the structural heterogeneity, and hence tissue specific expression and functions to keratins [11]. This suggests that phosphorylation plays an important role in regulating tissue specific keratin functions. These Serine phosphorylation sites are targets for several protein kinases, including members of the MAP kinases, p38, ERK, PKC, cAMP, JNK and phosphatases including PRL3 and PP2A regulating keratin functions under specific physiological conditions [32]. Several Serine/Threonine phosphorylation sites and some of the relevant kinases have been characterized in case of K1, K8 and K18. Tyrosine phosphorylation is rare but has been identified on K8 and K19. Other associated functions with keratin phosphorylation include protection against cell stress, cell signaling, apoptosis, and cell compartment-specific roles [11, 62]. Hyperphosphorylation of K8/18 is observed under conditions of tissue injury and stress. It can be either protective or can also increase tissue damage. Serine^{23}, Serine^{73} and Serine^{431} are the three phosphorylation sites of K8. Serine^{431} is apparently specific to K8 and in particular is phosphorylated in response to epidermal growth factor (EGF) stimulation.

Serine[73] is also specific to K8 and is phosphorylated in response to various types of cellular stresses. In the case of K18, two phosphorylation sites Serine[33] and Serine[52] have so far been demonstrated [11, 62]. K8 phosphorylation at a highly conserved residue in the rod domain (Tyrosine[267]), promotes keratin insolubility and proper filament formation, whereas the effects of Tyrosine phosphorylation on other IF proteins is poorly understood.

Table 2.2.4.7 List of kinases and their corresponding phosphorylation sites on keratins (Adapted from [32]).

Keratins	Phosphorylated residues	Kinases involved
K8	Ser-8	PKA, PKC_{ε}
	Ser-12	PKA
	Ser-23	PKA, PKC_{ε}
	Ser-33	PKA
	Ser-36	PKA
	Ser-42	PKA
	Ser-50	PKA
	Ser-73	JNK, PKC_{δ}, MK2*
	Ser-416	PKA
	Ser-423	PKA
	Ser-425	PKA
	Ser-431	ERK, JNK
	Not determined	AKT, AMPK, CAMK II, CK-Iα,
K17	Ser-44	RSK1
	Not determined	US3
K18	Ser-33	PKC_{ζ}
	Ser-52	MK2
	Not determined	AMPK
K19	Ser-35	Not determined
	Tyr-391	Src kinase
K20	Ser-13	MK2, PKC*

2.2.5 Functions of keratins

2.2.5.1 Mechanical functions of keratins

The most accepted function of keratins is to provide mechanical integrity and maintenance of cell shape and viability [13]. *In vitro* suspensions of keratin IFs are shown to harbor remarkable

micromechanical properties that are distinct from those of F-actin and microtubules. Keratin mediated structural support is particularly important in tissues mostly exposed to physical stress conditions, such as the surface epithelia (skin, oral mucosa, cornea) and muscle. Loss of these functions due to single point mutations in keratin gene are reported are responsible for many keratin-associated human disorders. Such disease-causing mutations markedly weaken the strength and stiffness of keratin IF in suspensions as shown in **Figure 2.2.5.1**. The single dominating frame shift mutations in keratin genes can cause Sevier keratinopathies, including epidermolysis bullosa simplex (mutations in K5/14 genes), epidermolytic hyperkeratosis (mutations in K1/10 genes) and epidermolytic palmoplantar keratoderma (mutations in the K9 gene) [16]. Keratin cytoskeleton is also required for the maintenance of cell shape in epithelial cells which retain the distinct morphologies of various surface-lining tissues.

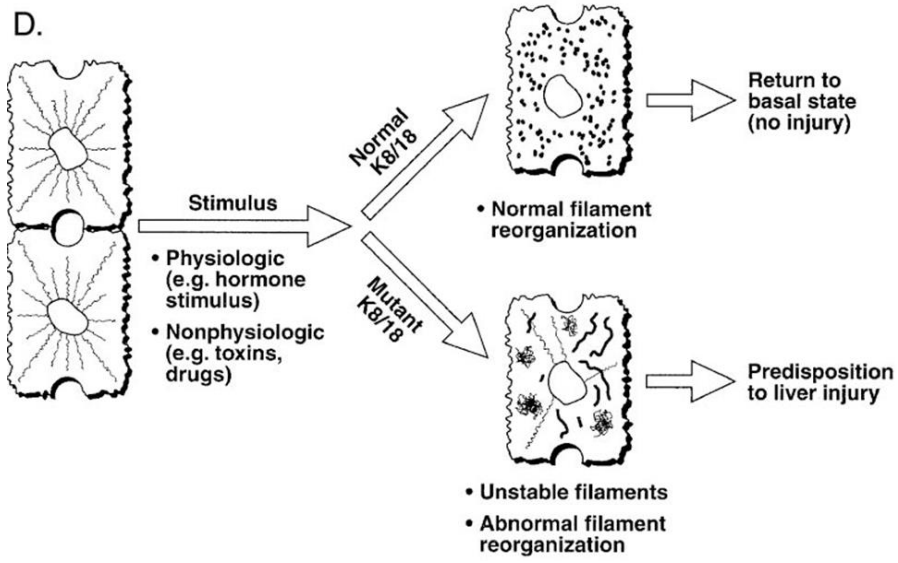

Figure 2.2.5.1 Cells with mutant keratin are unable to withstand mechanical stress (Adapted from [63])

K8 null mice showed significantly reduced microvilli together with a redistribution of microtubules. Interaction of keratin filaments with constituents of the microtubule organizing

center is involved in the apicobasal orientation of microtubules, which maintains the cell polarity of enterocytes. **Table 2.2.5.1** is the compilation of mouse keratins null mutations.

Similar phenotypes were also observed in case of other transgenic and knock out studies confirming that keratins are organized into a network architecture, which in turn is important for cellular micromechanics. It is also noticeable that keratins are functionally redundant, hence they can assemble in various combinations to form keratin filaments (e.g. in the epidermis K1/K10, K1/K9, K2/K9 or K2/ K10), and some keratins can be replaced by each other's without a loss of functionality of the keratin filaments [10, 64].

Table 2.2.5.1 Compilation of mouse keratins null mutations (Adapted from [7]).

Keratin	Mouse model	Phenotype
K7	None described	–
K8	Knockout (in C57Bl/6)	Liver hemorrhage with embryo lethality
K8	Knockout (in FVB/n)	Colorectal hyperplasia; colitis and mild hepatitis
K8	Mouse WT overexpression	Spontaneous MDB formation; chronic pancreatitis only when expression levels are very high
K8	Human WT with high overexpression	Chronic pancreatitis
K8	Human G62C (a human-related genetic variant)	Predisposition to liver injury and apoptosis; inhibition of K8 S74 phosphorylation by stress kinases
K8	Human S74A (prevents S74 phosphorylation)	Predisposition to liver injury and apoptosis
K8	Human R341H (a human-related genetic variant)	Predisposition to liver injury
K18	Knockout	Spontaneous MDB formation, mild hepatitis, and increased hepatocyte fragility
K18	Human WT overexpression	Resistant to MDB formation, otherwise normal
K18	Human R90C overexpression (mutation hot spot in other keratins)	Mild hepatitis; hepatocyte fragility; marked predisposition to liver injury; liver and pancreas keratin filament disruption
K18	Human S34A overexpression (prevents S34 phosphorylation and 14-3-3 binding)	Abnormal mitotic bodies after partial hepatectomy; persistent 14-3-3 nuclear localization
K18	Human S53A overexpression (prevents S53 phosphorylation)	Predisposition to liver injury
K19	Knockout	Compensatory K18 and K20 overexpression in gallbladder; mild myopathy
K19	Human WT overexpression	None
K20	Human WT overexpression	Lack of K20 distribution in pancreas and stomach (related to the genomic transgene used)
K20	Human R80H overexpression	Disruption of keratin filaments in small intestine enterocytes
K8, K19	Double knockout	Degeneration of placenta with embryo lethality
K18, K19	Double knockout	Fragility of trophoblast giant cells with embryo lethality
K18, K19	Mixed K19 knockout and K18 dominant negative	Lethal at E10.5 when K18 is null on one copy and mutant R90C on the other, which is rescued when the null K18 is replaced with a WT copy

2.2.5.2 Regulatory functions of keratins

Keratins were thought to perform only structural or mechanical functions, which do not describe their diverse tissue- and differentiation-specific expression patterns. None the less, recent evolving evidence suggests that IF are not mere structural proteins but they also act as an important framework for the modulation and control of essential cell processes, mainly signal transduction events [16]. In addition to their widely accepted role as protectors of epithelial cell integrity under a variety of stressful conditions, keratins are also considered to be important regulators of diverse cellular functions, such as, protein translation control, organelle positioning and membrane protein targeting, regulation of stress and apoptosis, proliferation, cell cycle, osmolarity, *etc*. by modulating different signal transduction pathways [17, 19, 20]. Other regulatory functions of keratins such as their role in cell differentiation and transformation are still emerging. Some of the major known functions of keratins are described below

2.2.5.2.1 Keratins and the stress response

Involvement of Keratins in providing resistance towards multiple kinds of stress conditions has been well accepted. It has been shown that persistent keratin cytoskeleton helps a cell to maintain its tissue position even during osmotic swelling or shrinkage and provide a stress-resistant framework upon which to recover its structure and shape after regulatory volume recovery. There is evidence that cells devoid of intermediate filaments are less resistant to osmotic stress. It has been suggested that intermediate filaments may have evolved to preserve tissue structure during osmotic shock, because both the actin and tubulin filament systems of the cell are transiently disrupted at this time. Toxic insults to cells may also result in osmotic imbalance which slows a cell's metabolism and in turn shutting down the membrane ion pumps. It is possible that osmotic

protection is the key feature of the chemo-protective effect of keratin filaments in liver. In colon carcinoma-derived HT29 and Caco cells, phosphorylation of K8, K18, K19 and K20 is individually altered in the presence of osmotic stress [65].

Involvement of Keratins in providing resistance towards multiple kinds of stress conditions is best reported in the studies using transgenic mouse model with K8 G61C mutation. It is the most common keratin mutation in humans, associated with progression of cirrhosis and fibrosis in hepatocytes. These mice showed an increased susceptibility to stress-induced hepatotoxic injury and apoptosis by inhibiting stress activated protein kinases such as p38, JNK and p42 mediated K8 Serine^{73} phosphorylation. Similar susceptibility to stress was also observed in the K8 S73A mutant mice. Based on these observations, authors suggested that keratins during stress act as a "phosphate sponge" absorbing the stress-activated phosphate kinases, thereby reducing their untoward effects and hence protect the cells from injury [66]. K18 has also been documented to play similar functions in response to stress stimuli. K18 interacts with Raf-1 kinase under basal conditions. During oxidative stress or other toxin exposure, Raf1 activation disrupts the keratin-Raf-1 association in a phosphorylation dependent manner. Thereby, keratins can regulate Raf-1 kinase signaling potential by kinase sequestration, activation, inactivation or compartmentalization. Furthermore, in the absence of a normal K18 gene, expression of the dominant negative mutant K18 R89C caused embryo lethality in mice that was rescued by K18 or K19 allele. The injury model of lung alveolar epithelial cells also suggests the protective role of keratin cytoskeleton in the presence of different kind of stress in a phosphorylation dependent manner [67]. Similar functions of other keratins in response to stress stimuli are emerging.

2.2.5.2.2 Keratins and Apoptosis

Keratins are known to be involved in both upstream and downstream events of apoptosis signaling pathways. They have been shown to provide resistance to apoptosis before commitment. They are also involved in activation of the caspase cascade which results in ordered cellular dismantlement [20, 68]. The K8/18 pair can desensitize cells to pro-apoptotic signaling mediated by tumor necrosis factor-α (TNF-α) or by Fas ligand, by either binding to their receptors or downstream effectors. The disruption of K8/18 filaments is accompanied by an increase of JNK- and NFκB-protein levels, both being downstream targets of the TNF signaling pathway [20, 68, 69].

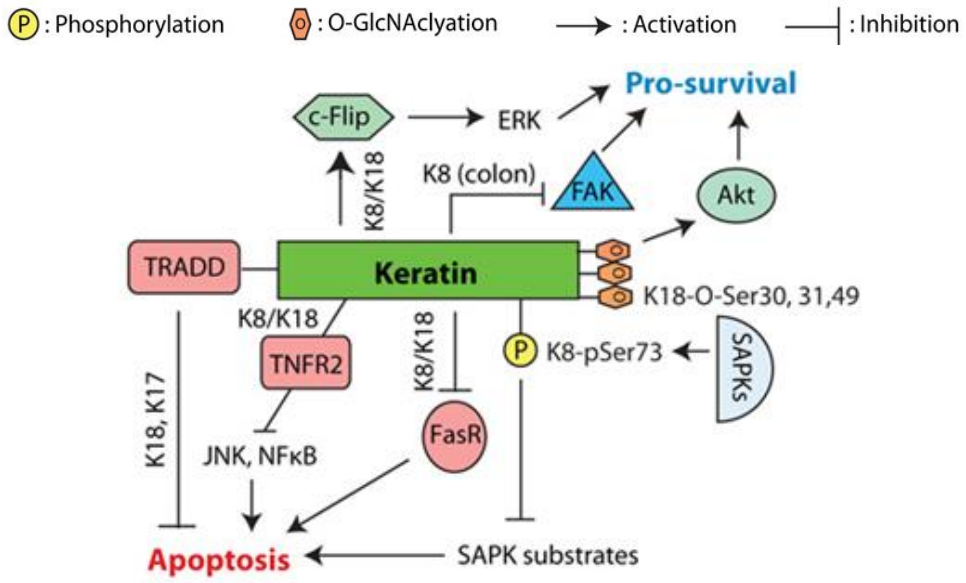

Figure 2.2.5.2.2 Keratins and apoptosis (Adapted from [69]).

Recent reports suggest that the type I keratin such as K14 and K18 bind to downstream TNFR effector, TNFR1-associated death domain (TRADD) in stratified and simple epithelia respectively. These keratins seemed to sequester TRADD, thereby modulating TNFR1-mediated apoptosis signaling [20]. Sequestration of signaling components by binding them to the cytoplasmic keratin network could interrupt the signaling cascade, as has also been shown for Fas receptor mediated

apoptosis. K8/18 dependent resistance to Fas mediated apoptosis occurs through a regulation of Fas density at the surface together with a c-Flip-induced upregulation of pro-apoptotic caspases and downregulation of anti-apoptotic ERK 1/2 signaling [70, 71]. A similar role for K17 in modulating hair follicle cycling has been suggested by its association with TRADD [72], although the mechanism underlying the genetic interaction for TNF-α and K17 has not been identified. The association of keratins post translational modification such as phosphorylation with apoptosis has also been demonstrated. The hyperphosphorylation of K8 Serine^{73}, Serine^{431} and K18 Serine^{52} occurs during apoptosis [29]. These studies suggest that phosphorylation may have protective role during apoptosis. **Figure 2.2.5.2.2** is the representative image of the links between Keratin and Apoptosis.

2.2.5.2.3 Keratins and Autophagy:

Autophagy is an important homeostatic cellular recycling mechanism which is responsible for degrading unnecessary cellular organelles and proteins in all living cells. Autophagy is particularly active during metabolic stress. In the cancer cells it is shown to perform a dual role harboring tumor-promoting and tumor-suppressing properties. Various reports suggest that autophagy modulates keratin-containing inclusion formation and apoptosis in cell culture in a context-dependent fashion. It has been shown that many proteasome inhibitors induce Mallory–Denk body-like inclusions composed of K8/K18, ubiquitin, HSP70 and p62 *etc*. [73]. It is also speculated that the intermediate filament-related inclusion formation and organelle reorganization might be linked to the role for intermediate filaments in organelle positioning and function. Further, inclusion mediated effects have been associated to keratin sequestration into the inclusions, which is supported by changes in mitochondrial function, size and location in hepatocytes of K8-null mice. Similar inclusion-associated changes have been described in non-epithelial contexts,

including changes in Golgi and lysosome distribution in huntingtin expressing cells and in α-synuclein inclusion-containing cells. There are indirect reports where an increased level of K8, K19 and K17 are associated with decreased autophagy suggesting an important role of these keratins in autophagy, which can be further investigated [74].

2.2.5.2.4 Keratins, protein synthesis and epithelial cell growth

Unexpected function of keratins in protein synthesis and epithelial growth was shown by K17 knockout studies. K17-null keratinocytes were similar to wild-type controls in their ability to attach to the substratum and go through the cell cycle, but showed 18-20% decreased protein synthesis. The reduced protein synthesis correlated with decrease in activation of Akt and mTOR kinases. K17 was specifically shown to bind adaptor 14-3-3s in a phosphorylation-dependent fashion, and which was wound-inducible in skin. Further, it has been shown that K17/14-3-3s interaction plays an important role in protein synthesis and cell growth by regulating the distribution /localization of 14-3-3s in cytoplasm and nucleus [19]. Similar role for K10 and K18 has been shown in cell growth in association with 14-3-3 proteins [75].

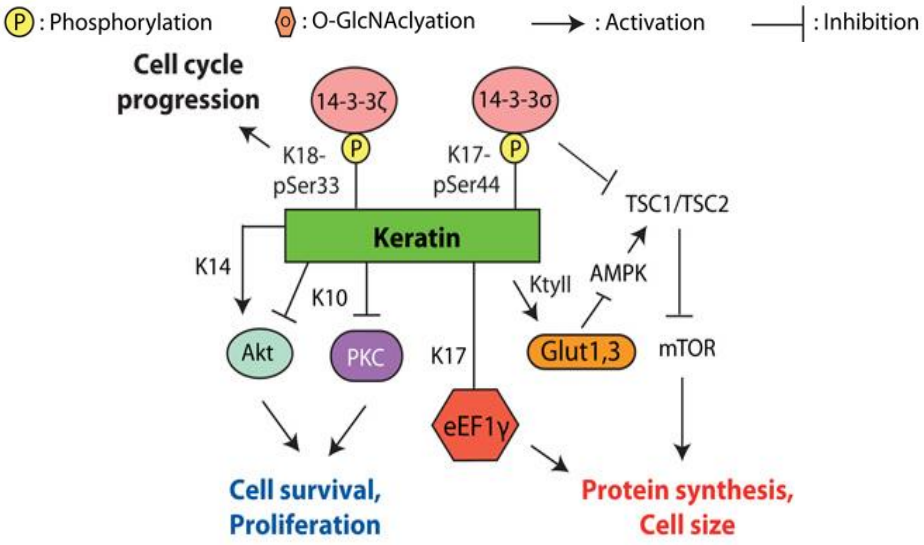

Figure 2.2.5.2.4 Keratin, proteins synthesis and cell growth (Adapted from [69]).

It is possible that keratins may regulate protein synthesis and cell growth also by their interaction with additional components of the translational machinery including EF1g, EIF3, TSC1 and even ribosomes [69]. **Figure 2.2.5.2.4** is the representative image of role of Keratins in cell growth and protein synthesis.

2.2.5.2.5 Keratin-dependent cell migration and wound healing

During the cell migration and wound healing, alterations are observed in the keratin filament (KF) system that are induced by and coordinated with altered cell polarity and differentiation. These alterations appeared to be one of the determinants of the altered migratory behavior of the cell [16, 76]. The recent reports indicate the link between KF formation and focal adhesions in lamellipodia and subcellular localization of KF in migratory cells [77].

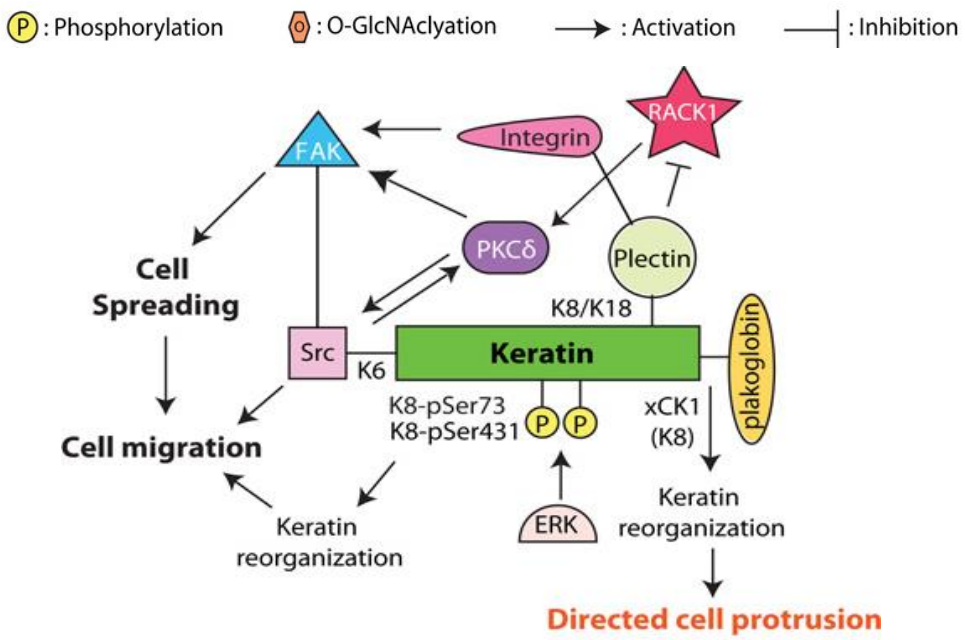

Figure 2.2.5.2.5 Keratin and cell motility (Adapted from [69]).

A similar association is suggested by delayed FAK autophosphorylation possibly via integrin signaling in K8- deficient hepatocytes [78]. The knockdown/knockout experiments revealed that

the reduction of the focal adhesion component talin led to inhibition of KF precursor formation, resulting into reduced focal adhesion size, decreased adhesion and impaired migration [69, 77]. Similarly, loss of K17 compromised wound healing in mouse embryos and loss of K6a led to delayed re-epithelialization upon skin wounding [79]. Role of aberrantly expressed K8/18 in cell migration has also been documented in different cell types [80]. Overexpression of K8/18 in human melanoma and carcinoma cells leads to increased migration and invasion of the cells [80, 81]. The mouse fibroblasts expressing complete K8/18 filaments also have a higher migratory and invasive ability [82]. Recently, the association between keratin phosphorylation and tumor cell migration has been shown in colorectal cancer (CRC).

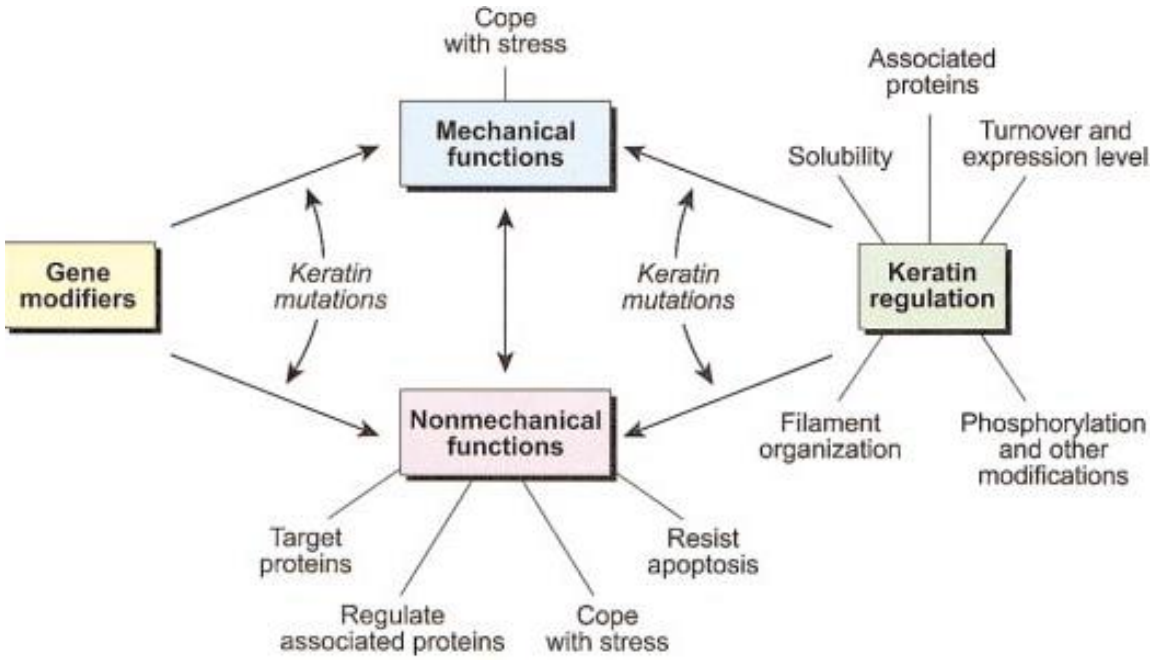

Figure 2.2.5 Summation of Keratin mechanical and regulatory functions.

PRL-3 (phosphatase of regenerating liver-3) was found to be upregulated in metastatic tumors of CRC and was correlated with decreased phosphorylation of K8 at residue Serine^{73} and Serine^{431}. In this study, authors have concluded that, PRL-3 may play an important role to promote cell

migration and metastatic potential of CRC through K8 dephosphorylation [39]. However the significance of K8 dephosphorylation in tumor cell migration and metastasis is still largely unknown. The role of Keratins in cell migration and wound-healing has been shown in **Figure 2.2.5.2.5**. Further, a concise depiction of the structural and regulatory functions of Keratins has been done in **Figure 2.2.5**.

2.2.5.3 Keratins in Cancer:

Keratins are among the earliest markers of epithelial tumors and are used as diagnostic markers of different types of carcinomas. **Table 2.2.5.8** lists the Keratins used as diagnostic markers in different tumor pathology. Beyond their well-established role as diagnostic markers in cancer, keratins have also been recognized as prognostic indicators in a variety of epithelial malignancies [4, 53]. In colorectal cancer, reduced expression of K8 and K20 has been associated with epithelial-to-mesenchymal cancer cell transition, which is generally indicative of higher tumor aggressiveness, and decreased patient survival [83]. Squamous cell carcinomas, independently of their site of origin, are characterized by the expression of the stratified epithelial keratins K5, K14 and K17 and the hyperproliferative keratinocyte-type keratins K6 and K16. K1/K10 may also be focally expressed, and K4 and K13 to a lesser extent. Interestingly, in poorly differentiated squamous cell carcinomas, co-expression of the simple epithelial keratins which are not normally found in these tissues; K8, K18 and K19 is often observed [5, 24]. At present, the exact role of these keratins in tumorigenesis is not completely understood and needs further investigation Although most keratin Knock out and transgenic mice do not have any apparent tumor phenotype [84], K8 deficiency (in the FVB background) resulted in colorectal hyperplasia and inflammation, and also shortens the latency, but not the incidence or the morphological features in mammary adenocarcinomas [85, 86] . Human K8 overexpression results in early neoplastic-like alterations

in the pancreas, including loss of acinar architecture, dysplasia and increased cell proliferation [87]. This correlates with the extent of spontaneous pancreatic injury [88]. Furthermore, Ectopic expression of K8 in the skin causes epidermal hyperplasia in young mice, epidermal atypia and pre-neoplastic changes in aging mice, and malignant progression of benign skin tumors induced by chemical skin carcinogenesis assays [87]. Based on transgenic mice studies and overexpression in cultured cells, K10 was anticipated to block cell cycle progression in a retinoblastoma protein dependent manner through sequestration of Akt and PKCζ [25]. These K10 null mice showed an increased turnover of skin cells in situ and showed decrease in papillomas formation compared to wild type [16]. Another report where, Chen et al. expressed chimeric keratin that contained the K14 rod flanked by the K10 head and tail domains in basal keratinocytes using K14 promoter. The turnover of basal keratinocytes in these mice was unaffected but accelerated papilloma formation was observed in these mice after the chemical skin carcinogenesis protocol, most likely due to suppression of apoptosis [89]. Furthermore, it has also been reported that K17 promotes cell proliferation and tumor growth by polarizing immune response in skin and establish an immunomodulatory role for K17 in Hedgehog (Hh) signaling driven basaloid skin tumors [90].

2.2.5.3.1 Keratin 8/18 and Cancer

It was demonstrated that simple epithelial keratins, K8/18 are aberrantly expressed in majority of the squamous cell carcinomas including OSCC [4, 34]. Further, their aberrant expression has been correlated with aggressiveness of the tumor and poor prognosis [33, 91]. K8/18 along with vimentin has also been associated with drug resistance, metastatic and invasive properties of some carcinomas and melanomas [80]. Transgenic mice expressing human K8 in the epidermis have a dramatic increase in the progression of papilloma towards malignancy [92]. Previous work in our laboratory has shown that K8 overexpression leads to neoplastic transformation and increased

invasive and metastatic potential in stratified epithelial cell line derived from human fetal buccal mucosa [35]. It has also been reported that K8/18 expression indicates a poor prognosis in squamous cell carcinomas of the oral cavity [93]. Our laboratory has also shown that loss of keratins 8 and 18 leads to alterations in α6β4-integrin-mediated signalling and decreased neoplastic progression in an oral-tumor-derived cell line [36]. These observations together raise the possibility that apart from being used for diagnosis and prognosis of cancers, keratins 8 and 18 may also be potential targets for SCC therapies. Hence, the molecular mechanism of the K8/18 mediated neoplastic transformation needs to be investigated.

Cancer site and subtype	Keratin expression
Biliary duct	K7, K8, K18–20
Bladder, transitional cell	K5[a], K7, K8, K18, K19, K20[a]
Breast	K5[a,b], K6[a,b], K7, K8, K14[a,b], K17[a,b], K18, K19
Cervix	K4–8, K10, K13–19
Colon	K7[a], K8, K18–20
Kidney, clear cell	K8, K18, K19[a]
Papillary	K7, K8, K18, K19
Chromophobe	K7, K8, K18, K19[a]
Liver	K7[a], K8, K18, K19[a], K20[a]
Lung, adenocarcinoma	K7, K8, K18, K19
Small cell	K8, K18, K19[a]
Ovary, adenocarcinoma[c]	K7, K8, K18, K19
Pancreas	K5[a], K7, K8, K18, K19, K20[a]
Pleura (mesothelioma)	K5, K7[a], K8, K18, K19
Prostate	K8, K18, K19
Skin, squamous	K1, K4–6, K8[d], K10, K13–17, K18[d], K19[d]
Merkel cell	K8, K18, K20
Stomach	K7[a], K8, K18, K19, K20[a]
Uterus	K5[a], K7, K8, K18, K19

Table 2.2.5.3 Keratins as diagnostic markers in different tumor pathology, where ***a*** indicates Focal/heterogeneous staining in some, but not all, cases. ***b*** indicates Focal or extended staining in basal-like tumor. ***c*** indicates Non-mucinous. ***d*** indicates poorly differentiated cases. **(Adapted from [24]).**

2.2.5.3.2 Keratin 8 phosphorylation and Cancer

Phosphorylation is established as a potent modulator of keratin 8 conventional functions, although its role in malignant transformation and the mechanism involved to bring about the same is still ambiguous. Recently it has been shown that, phosphatase of regenerating liver 3; PRL3 may play an important role in cell migration, invasion and metastatic potential of colorectal cancer through direct K8 dephosphorylation at Serine^{73}and Serine^{431} positions. They have also shown increased PRL3 expression levels and concurrent dephosphorylation of K8 Serine^{73}/ Serine^{431} at invasive front in CRC tumour samples [39]. This was supported by data from our laboratory where overexpression of K8 phosphomutants in an oral SCC derived cell line (AW13516) resulted in increased cell migration and tumorigenic potential of the cells compared with the cells expressing K8 wild type. Further the loss of K8 phosphorylation was observed in human OSCC tissues which significantly correlated with size, lymph node metastasis and stage of the tumour [40]. Contrary to this, a recent report demonstrated reduced K8 Serine^{73} phosphorylation via P38 MAPK pathway upon sec 8 down-regulation, resulting in decreased cell migration in case of oral SCC derived cell line [41]. Altogether, these reports suggest a context dependent role of K8 phosphorylation in different cancers, although, the associated mechanism is still to be investigated. Moreover, an *in-vivo* transgenic study could be helpful to better understand and clarify the exact role of K8 phosphorylation in SCC.

Keratin mutations are associated with several skin, oral, esophageal, ocular, hair, and liver diseases and more than expression their mutations are deleterious. For example, livers of K8- or K18-null mice or mice that express K18 A89C (an EBS-like mutation) manifest a remarkable predisposition

to injury and apoptosis [94]. K18 R89C and K14 R125 residues and their surrounding amino acids are highly conserved, and K14 R125 mutations cause the severest form of EBS and are the most common in keratin-related skin diseases [95, 96]. Abrogation of K18 Serine^{52} phosphorylation by Alanine mutation did not affect filament organization after partial hepatectomy nor the ability of mouse livers to regenerate. However, exposure of K18 S52A expressing mice to the hepatotoxins, griseofulvin or microcystin, resulted in more dramatic hepatotoxic injury compared to WT K18-expressing mice [97]. This suggests a physiologic role of K18 in protecting hepatocytes from stress-induced liver injury. As stated earlier, K8 S73A expressing transgenic mice, mimic the susceptibility of K8 G61C mice to injury, and provide a link between K8 phosphorylation and disease-associated mutation. Upon apoptotic stimulation, G61C and S73A hepatocytes showed increased non-keratin pro-apoptotic substrate phosphorylation by stress-activated kinases, compared with wild-type hepatocytes. This was followed by Fas or MLR administration mediated significant lethality and the G61C mice were markedly more susceptible to lethal liver injury as compared with non-transgenic and K8 WT mice. Further, the inhibition of K8 Serine^{73} phosphorylation (K8 S73A mutation) increases susceptibility to Fas-mediated liver injury, which was confirmed by the marked lethality of S73A, as compared with WT K8 and non-transgenic mice. The increased lethality of K8 S73A mice is likely attributable to increased hemorrhage and apoptosis [66]. Further, the role of these important physiological sites and their respective PTM in cancer is still to be explored.

Chapter-III

Materials and Methods

3.1 Plasmids and Cloning:

3.1.1 For the generation of tissue specific transgenic mice, K8 wild type and phosphomutants were first cloned in pCCL K14 GFP vector [98]. The K8 wild type was PCR amplified from pEGFP-N3 vector with the help of forward and reverse primers containing 5' AgeI and kozak sequence and 3' NotI-SalI enzyme sites respectively. Further AgeI and SalI enzymes were used to replace GFP of pCCL-K14 GFP vector with K8 wild type GFP cassette. pCCL-K14-K8 WT GFP was then used to generate the phosphomutants by SDM with the same primers used earlier [40].

3.1.2 pTU6 puro vector containing the shRNA 8.2 (Generated earlier in the laboratory [36]) was used to knock down K8 in A431 cells .

3.1.3 To generate stable clone expressing K8 WT and phosphomutants in a K8 knockdown background, retroviral constructs (pLNCX2) containing shRNA-resistant K8 WT and phosphomutants were prepared. For this initially, shRNA-resistant K8 wild type GFP from pEGFP N3 vector backbone was subcloned into pCMV 3X-Flag vector with EcoRV and BsrG1 enzymes. The whole cassette containing shRNA-resistant Flag-K8 WT GFP was then excised from pCMV vector and further cloned in pLNCX2 retroviral vector to generate pLNCX2-Flag-K8 WT GFP construct. Further, shRNA-resistant Phosphodead mutants (pLNCX2-3XFlag-K8 S73A GFP and pLNCX2-3XFlag-K8 S431A GFP) and Phosphomimetic mutants (pLNCX2-3XFlag-K8 S73D GFP and pLNCX2-3XFlag-K8 S431D GFP) were generated by site-directed mutagenesis of the pLNCX2-3XFlag-K8 WT GFP using Quick change site directed mutagenesis kit (Stratagen). The Oligonucleotides were designed according to manufacturer's protocol (**Table 3.1.3**).

Table 3.1.3 List of the primers used for K8 site directed mutagenesis

S/No	Primers for Site directed mutagenesis	Sequences of the primers (5'-3')
1	K8 S73A FWD	CCAGAGCCTGCTGGCACCCCTTGTCCTGG
2	K8 S73A REV	CCAGGACAAGGGGTGCCAGCAGGCTCTGG
3	K8 S431A FWD	GGGCCTCACAGCCCCCGGCCTC
4	K8 S431A REV	GAGGCCGGGGGCTGTGAGGCCC
5	K8 S73D FWD	CCAGAGCCTGCTGGACCCCCTTGTCCTGG
6	K8 S73D REV	CCAGGACAAGGGGGTCCAGCAGGCTCTGG
7	K8 S431D FWD	GGGCCTCACAGACCCCGGCCTC
8	K8 S431D REV	GAGGCCGGGGTCTGTGAGGCCC

3.2 Virus Production

3.2.1 To generate high titer Lentiviral particles of K8 wild type and phosphomutants, the K8 GFP wild type (pCCL-K14-K8 WT GFP) and phosphodead mutants (pCCL-K14-K8 S73A GFP/ pCCL-K14-K8 S431A GFP) together with the Virapower packaging mix (Sigma) were transfected in HEK293-FT cells (at 70-80% confluency) by X-tremeGENE™ HP DNA Transfection Reagent (Roche) according to manufacturer's protocol. After 48h supernatant was collected and ultracentrifugation was carried out at 25000G for 90min each. The pellet was further resuspended in 100µl of incomplete DMEM and stored at -80°C. 48h post-transduction, the titer of the viral particles was analyzed on A431 cells by immunofluorescence and FACS.

3.2.2 To generate high titer retroviral particles, the shRNA resistant K8 wild type (pLNCX2 3XFlag-K8 WT GFP), phosphodead mutants (pLNCX2-3XFlag-K8 S73A GFP /pLNCX2-3XFlag-K8 S431A GFP) and phosphomimetic mutants (pLNCX2-3XFlag-K8 S73D GFP and pLNCX2-3XFlag-K8 S431D GFP) together with the packaging plasmids (pCL-Eco

and pMD2.G) were transfected in HEK293-FT cells (at 70-80% confluency) by X-tremeGENE™ HP DNA Transfection Reagent (Roche) according to manufacturer's protocol. After 48h supernatant was collected and then ultracentrifugation was carried out at 25000G for 90mins each. The pellet was further re-suspended in 100µl of incomplete DMEM and stored at -80°C. 48h post-transduction, the titer of the viral particles was analyzed on A431 cells by immunofluorescence and FACS.

3.3 List of reagents: The reagents used are listed in the **Table 3.3**

Table 3.3 List of reagents

Reagents	Catalogue	Company	Country
CHX	C 7698	Sigma-Aldrich	USA
DAPI	D 9542	Sigma-Aldrich	USA
Dulbecco's modified eagle's medium (DMEM)	12800-017	Life technologies	Carlsbad, CA, USA
EGF	E9644	Sigma-Aldrich	USA
E64D	E8640	Sigma-Aldrich	USA
Fetal bovine serum	SH30071.03	Hyclone, Thermo Scientific	Lafayette, CO
FITC-conjugated Phalloidin	P5282	Sigma Aldrich	USA
G418	A1720	Sigma-Aldrich	USA
Matrigel	354234	BD Biosciences	Franklin lakes, NJ, USA
MG-132	474790	Calbiochem	San Diego, CA, USA

Protease inhibitor Cocktail	539131	Calbiochem	San Diego, CA, USA
Puromycin	P8833	Sigma-Aldrich	USA
PVDF membrane	RPN303F	GE Healthcare	UK
Revert Aid First Strand cDNA synthesis Kit	K1622	Thermo Fischer Scientific	USA
TNF-α	T 6674	Sigma-Aldrich	USA
TRI reagent	93289- 100ml	Sigma-Aldrich	USA
Vectashield mounting Medium	H-1000	Vector Laboratories	CA, USA
X-tremeGENE™ HP DNA Transfection Reagent	Cat. No. 06 366 244 001	Sigma-Aldrich	USA

3.4 Maintenance of cell lines:

3.4.1 Reagents:

- Dulbecco's Modified Eagle's medium: DMEM was procured from GIBCO and the powdered medium was dissolved in 1l of water (3.7g of sodium bicarbonate per liter was added and the pH of medium was adjusted to 7.4). The medium was filtered using Tarson's assembly – 0.45µM Membrane filter (Whatman). 1ml of the filtered medium was added to the sterility test medium and kept at room temperature for 6 days under observation to ensure the sterility.
- Sterility test medium: 14.9g of Fluid- Thioglycolate was dissolved in approximately 250 ml of water. The volume was made up to 500ml in measuring flask and boiled.

After aliquoting, 6ml of the medium in glass tubes a pinch of calcium carbonate was added to each tube and autoclaved.

- Complete medium was prepared by adding 10% FBS, 10% of HEPES (100mM) and 1% antibiotic solution (GIBCO).
- Phosphate Buffered Saline (PBS) : 150mM NaCl, 2mM KCl, 8 mM Na2HPO4, 1mM KH2PO4.
- Trypsin-EDTA solution: 0.025% Trypsin, 0.2mM EDTA, 5mM D-glucose, 5mM KCL, 0.1M NaCl, 6mM NaHCO3 and autoclaved deionized water was prepared and filtered using Millipore assembly – 0.45μM Membrane before use.
- Erythrocin B staining solution:0.4% Erythrocin B in 1X PBS.
- Freezing medium: 90% Fetal Bovine Serum, 10% DMSO.

Majority of the experiments were performed using A431 (a human epidermoid carcinoma derived cell line) and HEK 293-FT cell lines. The cell-lines were maintained in DMEM supplemented with 10% FBS, 1% antibiotic concoction and grown in 5% CO2 atmosphere at 37^0C. For the routine maintenance of the cell lines following protocols were used.

3.4.2 Protocols:

3.4.2.1 Revival of cells: A vial was taken out from liquid nitrogen cylinder and placed into a 37ºC water bath for quick thawing. The thawed cell suspension was mixed gently and transferred into a sterile test tube. 5ml of complete medium was added drop wise with gentle shaking. The thawed cells with medium were further mixed smoothly using glass pipette. The cell suspension obtained was centrifuged for 10min at 1500 rpm at RT. The supernatant was discarded and the pellet was dislodged by finger tapping. 3ml of complete medium was added

drop wise to the test tube with continuous shaking followed by centrifugation at 1000rpm for 10min at RT. The supernatant was discarded and the pellet was dislodged by tapping and re-suspended in 1ml of complete medium**.** Total cell count and the percent viability were calculated by dye exclusion method using Erythrocin B dye on a haemocytometer under an inverted microscope. The medium was mixed by pipetting and the 100mm petri plates were seeded with 1 X 10^6 cells. The cells were incubated in a humidified CO2 (5%) incubator at 37ºC and their growth was observed each day under inverted microscope.

3.4.2.2 Subculture/Trypsinization and transfer of cells: The cells were washed with 1X PBS twice and trypsin-EDTA was added to the culture plate. Excess trypsin-EDTA was discarded and the plate was incubated till the cells were partially detached. Complete medium was added to inhibit the trypsin activity into plate containing detached cells. The resulting cell suspension was mixed by pipette to make a single cell suspension**.** Total cell count was taken and appropriate amount of cells depending upon cell type were seeded in culture plates. The plates were incubated in humidified CO2 incubator at 37ºC.

3.4.2.3 Freezing and cryopreservation of cells: Log phase cells were trypsinized and single cell suspension was obtained. After noting the total cell count, the cell suspension was spun at 1500rpm for 10min at RT. The supernatant was discarded and the pellet was dislodged by tapping. One ml of freezing medium was added drop wise into the tube and mixed gently by pipette. The cells suspension was then transferred to freezing vials. The freezing vials were then placed in bio-freezer with 3 rings. First ring was removed after 90min, the second ring was removed after 120min and third ring was removed after 150min. The vials were then kept in liquid nitrogen freeze boxes at -196ºC for long term storage.

3.5 Generation of stable cell-lines:

To generate pTU6 puro vector control and K8 knockdown clones, A431 cells were transfected with pTU6 puro empty vector and pTU6 shRNA 8.2 with the help of X-tremeGENE™ HP DNA Transfection Reagent (Roche) according to manufacturer's protocol, respectively. The stable clones with significant K8 down-regulation were then selected and maintained in 500ng/ml of puromycin and were validated with different biochemical techniques. Two of the K8 knockdown clones thus generated (KD2/KD8) were further transduced with the respective viral particles: the shRNA resistant K8 wild type (pLNCX2-3XFlag K8 WT GFP), phosphodead mutants (pLNCX2-3XFlag-K8 S73A GFP /pLNCX2-3XFlag-K8 S431A GFP) and phosphomimetic mutants (pLNCX2-3XFlag-K8 S73D GFP and pLNCX2-3XFlag-K8 S431D GFP). Stable clones were then selected and maintained in 500ng/ml of puromycin and 600ng/ml of G418 sulphate.

3.6 Generation of transgenic mice:

For the lentiviral mediated transgenesis Swiss mice Crl:CFW (SW) were bred and maintained in the laboratory animal facility of ACTREC. For the generation of transgenic mice using electroporation, the purified Expression cassette was sent to Dr. Majumdar's laboratory, NII Delhi. Mice (FVB/J), bred at the small animal facility of National Institute of Immunology, were used for the study. All protocols for animal studies were reviewed and approved by the Institutional Animal Ethics committee constituted under the guidelines of the CPCSEA, Government of India, (Project number 05/2015). All animals were kept at 24 ± 2°C under 14h light and 10h dark cycles and used as per the National Guidelines provided by the Committee for the Purpose of Control and Supervision of the Experiments on Animals (CPCSEA). The animals were received an autoclaved balanced diet prepared in-house as per the standard formula and sterile water adlibitum. Mice were

housed in the Individually Ventilated Cage (IVC) system (M/S Citizen, India) provided with autoclaved rice husk bedding material available locally.

3.6.1 Lentiviral Mediated Transgenesis by *In vivo* Manipulation of Spermatogonial Stem Cells [99]: 28 day old Crl:CFW (SW) male mice were anesthetized by intraperitoneal injection of Avertin (Sigma) (2,2 tribromo-ethanol and t-amyl alcohol at the rate of 0.015ml/g body weight). Hair was removed from the inguinal area of mice and the surgical site was cleaned using betadine. Anterior to the penis, a single midline cutaneous incision of approx. 1–1.5cm length was made using sterile surgical scissors under aseptic conditions. After making the incision in the muscles, the testes were removed from the scrotal sac with curved sterile forceps through the incision by gently pulling the dorsal fat pad associated with the testis. A solution of lentiviral particles for each of the constructs (pCCL-K14-K8 WT/ S73A/ S431A GFP) re-suspended in incomplete media and injected slowly into the inter-tubular space of both the testis of male mice using a 30-gauge needle. The animals were kept on thermal plate until they recovered from the surgery to avoid hypothermia. The profounder male mice were co-habituated with wild-type females 35 days post-transduction and the pups generated were analyzed for the presence of transgene. The pre-founder male mice were mated with wild-type females (ratio 1:2). The progeny obtained was screened for the respective transgene integration by gDNA PCR for further use.

3.6.2 Generation of transgenic mice with non-surgical *in vivo* injection and electroporation of mice testis [100] :

The protocol was performed at NII, Delhi as a collaborative work with Dr. Subeer Majumdar. Briefly, about 30 days old male mice (FVB/J) were anesthetized for short duration by intraperitonial injection (100µl) of ketamine hydrochloride (45mg/kg) and xylazine hydrochloride (8mg/kg). After removing hair from lower abdominal and scrotal region, area was cleaned with

betadine (povidone-iodine) solution. Subsequently, sterile water was spread on scrotal area to remove excess betadine. The respective K8 WT GFP and phosphomutant expression cassette having K14 promoter with 0.04% Trypan blue, which was used to monitor the accuracy of the injection, was injected slowly into the testis using the 10µl Hamilton syringe (701N; Hamilton Bonaduz AG, Switzerland) from two different, diagonally opposite sites. DNA was delivered through one injection site at a time. A small (0.5-inch-long) 26-gauge sterile needle (usually supplied with tuberculin syringe) was slowly inserted up to middle of the testis and withdrawn to generate path for introducing the needle of a Hamilton syringe. For standardization, about 20µl–25µl of sterile water containing respective plasmid DNA (concentration ranging from 0.5µg/µl–1.2µg/µl) was delivered unilaterally into a testis. Mild square electric pulses ranging from 50V to 90V were delivered to testis injected with DNA using tweezer type electrode and an electric pulse generator (Electroporator ECM2001, BTX Instrument Division, Harvard Apparatus, Inc., Holliston, Massachusetts, USA). Sterile normal saline was spread occasionally on scrotum to keep the skin moist for uniform electrical conductance during the procedure.

3.7 Genomic DNA extraction from mouse tail snips:

For genotyping and screening of transgenic mice, tail snips of ~2 mm size were collected and used immediately (or stored at -80^{0}C) for the genomic DNA extraction. Proteinase K, 20mg/ml and TNES buffer (1M Tris-HCl pH 7.4, 0.5M EDTA pH 8, 5M NaCl, 10% SDS, sterile water) were thawed at 55°C until the solutions are clear. 500µl TNES buffer followed by 12.5µl Proteinase K was added to each tube with tail in it. The preparation was then incubated at 55^{0}C water bath overnight. After the digestion was completed, tubes were shortly centrifuged to spin down the remaining tissue along with the drops in the cap. 150µl 6M saturated NaCl was added to each tube

and vigorously shaken for at least 1 minute. The solution was spun down at full speed (13,000rpm) for 5min to pellet protein and tissue remnants. Supernatant was removed and transferred into fresh tubes. 500µl 100% Ethanol was added to each tube and mixed by inverting. A white thread like material was visible which was pelleted by spinning down at full speed (13,000rpm) for 5min. The supernatant was decanted and tubes were monitored for the presence of pellet. Pellets were washed with 500µl 70% Ethanol. Supernatant was removed and pellet was air dried at room temperature for about 10min. 100µl autoclaved water was added to each of the tubes and kept for dissolution overnight at 4^0C or at 65^0C for 20min. Concentration of the isolated DNA was measured using nanodrop Spectrophotometer before performing PCR.

3.8 Genotyping by PCR:

To screen the transgene positive mice, PCR was performed and the gDNA isolated from mouse tail snips was used as a template. Primers specific to GFP were used for the screening and for Patch gene were used as internal control. The primers used are described in **Table 3.8**. Amplified PCR products were analyzed in 2% agarose gels containing 0.5g/ml ethidium bromide.

Table 3.8 List of primers for genotyping

S/NO.	Primer name	Sequence of primers	Annealing temperature (°C)	Cycles
1.	GFP Forward	5’ GTGAGCAAGGGCGAGGAG 3’	52	34
2.	GFP Reverse	5’ GCAGGACCATGTGATCG 3’	52	34
3.	Ptch Forward	5’ CTGCGGCAAGTTTTTGGTTG 3’	58	30
4.	Ptch Reverse	5’ AGGGCTTCTCGTTGGCTACAAG 3’	58	30

3.9 Slot blot analysis

The results of PCR were further confirmed by Slot blot analysis (T A Brown) of few PCR-positive animals. Transgene specific probe (for EGFP region) was generated with αP^{32}dCTP using High Prime DNA labeling kit (Roche Diagnostic GmbH, Mannheim, Germany). About 1 µg of gDNA was blotted on membrane and hybridized with transgene specific probe for detection of transgene in the progeny.

3.10 Tissue immunofluorescence:

Skin tissue samples were collected from respective mice and IF was carried out to screen the mice expressing transgene. Formalin-fixed, paraffin-embedded, 5µm thick mice tissue sections were mounted on poly-l-lysine coated glass slides. Sections were de-paraffinized with xylene and incubated with 3% hydrogen peroxide in methanol for 30min in dark to quench the endogenous peroxidase activity of the tissues. After blocking with horse serum for 1h at 37°C in humidified chamber, sections were incubated with respective primary antibodies overnight at 4°C. The sections were washed thrice with 1X PBS for 10min each followed by incubation with anti-mouse (Alexa Fluor 488) or anti-rabbit (Alexa Fluor 568) conjugated secondary antibody for 1h. DAPI was used to stain the nucleus and sections were then mounted using antiquenching agent (Vectashield) and sealed. Confocal images were obtained using a LSM 780 Carl Zeiss Confocal system.

3.11 DMBA-TPA mediated skin carcinogenesis:

Mouse skin was shaved at Postnatal day 22 and then Briefly, mice were treated 3 times (at post-natal day 23, 25 and 27) with DMBA (9,10-dimethyl-1,2-benzanthracene) (50µg; 195nmol) and

then treated twice weekly with TPA (12-O-tetradecanoyl phorbol-13-acetate) (2.5µg; 4nmol) until their sacrifice. DMBA stock solution was prepared by dissolving 15mg DMBA in powder form in 4.68ml acetone (1500µg /4680µl acetone i.e. 3.2µg/µl of acetone). This was Diluted 10 fold (1ml main stock to 9ml of acetone) to make a working solution of 0.32µg/µl of acetone. A final concentration of 50µg/animal (156.25µl) was used at the time of application. For TPA, stock solution of 1mg/ml in acetone i.e. 1000µg/1000µl was prepared. 2.5µg of TPA animal, i.e. 2.5µl of main stock/animal is required for each application. For this TPA was diluted by adding 25µl of main stock (1mg/ml) in 1975µl of acetone at the time of application (2.5µg/ 200µl).

3.12 Preparation of whole cell lysates

The cells grown up to 70-80% confluency were scraped and suspended in SDS lysis buffer {5mM EGTA, 5mM EDTA, 0.4% SDS and protease inhibitor cocktail (Calbiochem, 1X solution contains 500µM AEBSF, 500µM EDTA, 1µM E-64, 1µM Leupeptin and 1µg/ml Aprotinin, Cat no. 539131) in 25mM Tris HCl pH 7.2}. The cell suspension was then boiled in a boiling water bath for 5-10min followed by centrifugation at 13000 rpm for 15min to remove cell debris. The supernatant was then aliquoted and stored at -80°C for further use.

3.13 Preparation of Mouse tissue lysates:

To generate skin tissue lysates, mice were first sacrificed, shaved and the skin was excised (2"× 2" approximately). The excised skin tissue was kept in Trypsin-EDTA (1X), epidermis facing the bottom, at 4^0C overnight. The dermis was separated from epidermis the next day using two sterile forceps. Further mouse skin tissue lysate was prepared by homogenization followed by sonication in modified RIPA buffer (50mM Tris-HCl, pH 7.4, 1% Triton X-100, 0.2% sodium deoxycholate,

0.2% sodium dodecyl sulfate (SDS), 1mM sodium ethylene diamine tetra acetate, 1mM phenyl methyl sulfonyl fluoride, 5µg/ml of aprotinin, 5µg/ml of leupeptin). The lysates for different organs were prepared by first homogenizing in liquid nitrogen and then process in the same way using RIPA buffer. Cell debris was removed by centrifugation (13000rpm, 4°C, 15min). The supernatant was then aliquoted and stored at -80°C for further use.

3.14 Protein estimation by modified Lowry's method [101]

Standards were prepared of BSA concentration gradient. 1ml of 5 to 25µg/ml BSA was taken in test tubes in duplicates as standard along with blank. 3µl of whole cell lysates were added in test tubes in duplicates and the volume was made up to 1ml by distilled water. 1ml of Copper Tartarate Carbonate (CTC) solution (0.1 % copper sulphate (w/v), 0.2 % potassium tartarate (w/v), 10 % Sodium carbonate (w/v), Solution A (Equal volumes of CTC solution, 10 % SDS (w/v), 0.8N NaOH (w/v) and distilled water (1: 1: 1: 1 proportion)) was added to each test tube and the tubes were vortexed followed by incubation at RT for 10min. 500µl diluted FC reagent (1 part of FC reagent and 5 parts of distilled water) was added to each tube. The tubes were vortexed and incubated at RT for 30min in dark and absorbance was read at 750nm using a spectrophotometer. First the standard curve was plotted which was further used to determine protein concentrations of respective samples.

3.15 SDS PAGE [102]

The samples were dissolved in PAGE sample buffer (62.5mM Tris HCl pH 6.8, 25% Glycerol w/v, 2% SDS, 0.5% Bromophenol blue) and were separated on 10-15% SDS PAGE depending on the molecular weight of the proteins being analyzed with 5% stacking gel.

3.16 Western blotting[103]

After SDS-PAGE, the gel with resolved proteins and the activated PVDF membrane were placed in form of the sandwich and wet electro-blotting using transfer buffer (190mM Glycine, 20% methanol, 0.05% SDS, 25mM Tris base) was carried out at 100 V for 1h. Transfer of proteins was visualized using Ponceau-S staining (0.2% ponceau stain in 5% acetic acid). The blot was incubated in blocking solution (3% BSA in TBS or 5% Milk in 1X TBS) for 1h at RT on a rocker. After blocking the blot was incubated with diluted primary antibody for 1h at RT on the rocker. The list of primary antibodies used is given in the **Table 3.16.1.1**. The blot was then washed thrice with TBST (0.1% TWEEN 20 (v/v), 150mM NaCl, 10mM Tris HCl pH 8.0) followed by incubation with horseradish peroxidase (HRPO) conjugated secondary antibody for 1h at RT on the rocker. The list of secondary antibodies used is given in the **Table 3.16.1.2**. The secondary antibody was removed and the blot was washed thrice with TBST. Blots were developed using ECL prime- chemiluminescence reagent according to the manufacturer's protocol.

Table 3.16.1.1: List of primary antibodies used in western blotting and Immunofluorescence

S/No	**Name of antibody**	**Catalog No**	**Western blotting dilutions**	
			Primary	Secondary
1	Keratin 8	Sigma(#C5301)	1:8000(WB)	1:4000 (anti mouse)
2	Anti-Flag	Sigma (#3165)	1:8000(WB)	1:4000 (anti mouse)
3	β-actin	Sigma(#A5316)	1:8000 (WB)	1:4000 (anti mouse)
4	Keratin8-pSer73	Sigma (#SAB4503768)	1:1000(WB)	1:2000 (anti Rabbit)
5	Keratin8-pSer431	Abcam(#ab59434)	1:1000(WB)	1:2000 (anti Rabbit)

6	Keratin14	Serotec(#MCA890)	1:8000(WB)	1:4000 (anti mouse)
7	Keratin5	Novacastra(#NCL-CK5)	1:1000(WB) 1:200(IF)	1:4000 (anti mouse)
8	Keratin18	Sigma (#C8541)	1:4000(WB) 1:200(IF)	1:4000 (anti mouse)
9	ERK1/2	Abcam(#Ab36991)	1:2000(WB)	1:4000 (anti mouse)
10	Phospho ERK1/2 pThr185/Thr202	Abcam(#Ab4819)	1:1000(WB)	1:2000 (anti Rabbit)
11	JNK/SAPK	Cell signaling technologies (#9252)	1:1000(WB)	1:2000 (anti Rabbit)
12	Phospho JNK/SAPK pThr183/Tyr18	Cell signaling technologies (#9251)	1:1000(WB)	1:2000 (anti Rabbit)
13	FAK	Cell signaling technologies (#3285)	1:1000(WB)	1:2000 (anti Rabbit)
14	Phospho FAK pTyr397	Cell signaling technologies (#3283)	1:1000(WB)	1:2000 (anti Rabbit)
15	Shc	Cell signaling technologies (#2432)	1:1000(WB)	1:2000 (anti Rabbit)
16	Phospho Shc pTyr317	Cell signaling technologies (#2431)	1:1000(WB)	1:2000 (anti Rabbit)

17	Phospho-Shc pTyr239/240	Cell signaling technologies (#2434)	1:1000(WB)	1:2000 (anti Rabbit)
18	Fascin	Abcam(#Ab49815)	1:1000(WB)	1:4000 (anti mouse)
19	Phospho Fascin pSer39	Abcam(#Ab90618)	1:1000(WB)	1:2000 (anti Rabbit)
20	Beta 4 Integrin	Millipore (#MAB1964)	1:1000(WB)	1:4000 (anti mouse)
21	AKT	Cell signaling technologies(#9272)	1:1000(WB)	1:2000 (anti Rabbit)
22	Phospho AKT	Abcam(#Ab27773)	1:1000(WB)	1:4000 (anti mouse)
23	p21	Santacruz(sc-471)	1:1000(WB)	1:2000 (anti Rabbit)
24	p27	Santacruz(sc-528)	1:1000(WB)	1:2000 (anti Rabbit)
25	E-cadherin	Abcam(#Ab1416)	1:1000(WB)	1:4000 (anti mouse)
26	TMSI	Cell signaling technologies (#13833)	1:1000(WB)	1:2000 (anti Rabbit)
27	PKCδ	Santacruz(sc-213)	1:1000(WB)	1:2000 (anti Rabbit)
28	RANBP1	Cell signaling technologies(#8780)	1:1000(WB)	1:2000 (anti Rabbit)
29	14-3-3γ	Cell signaling technologies(#9637)	1:6000(WB)	1:4000 (anti Rabbit)
30	RhoGDI	Cell signaling technologies(#2564)	1:1000(WB)	1:2000 (anti Rabbit)

31	IκBα	Cell signaling technologies(#4812)	1:1000(WB)	1:2000 (anti Rabbit)
32	Phospho IκBα pSer32/36	Cell signaling technologies(#9246)	1:1000(WB)	1:4000 (anti mouse)
33	Ikk*β*	Cell signaling technologies(#2684)	1:1000(WB)	1:2000 (anti Rabbit)
34	Phospho Ikkα/*β* pSer170/180	Cell signaling technologies(#2697)	1:1000(WB)	1:2000 (anti Rabbit)
35	CDK6	Cell signaling technologies(#3136)	1:2000(WB)	1:4000 (anti mouse)
36	SHIP1	Cell signaling technologies(#2725)	1:1000(WB)	1:2000 (anti Rabbit)
37	Paxilin	Cell signaling technologies(#2542)	1:1000(WB)	1:2000 (anti Rabbit)
38	Phospho Paxilin pTyr118	Cell signaling technologies(#2541)	1:1000(WB)	1:2000 (anti Rabbit)
39	Cofilin	Cell signaling technologies(#3318)	1:1000(WB)	1:2000 (anti Rabbit)
40	Phospho Cofilin pSer3	Cell signaling technologies(#3313)	1:1000(WB)	1:2000 (anti Rabbit)
41	MARCKSL1	Cell signaling technologies (#59568)	1:1000(WB)	1:2000 (anti Rabbit)

42	NFκβ	Abcam(#Ab7970)	1:1000(WB)	1:2000 (anti Rabbit)
43	Cdc2	Cell signaling technologies (#9116)	1:1000 (WB)	1:4000 (anti mouse)
44	Cdc2 pThr14	Cell signaling technologies (# 2543)	1:1000 (WB)	1:2000 (anti Rabbit)
44	Cdc2 pTyr15	Cell signaling technologies(#9111)	1:1000(WB)	1:2000 (anti Rabbit)
45	MAPK (ERK1/2)	Cell signaling technologies(#9102)	1:1000(WB)	1:2000 (anti Rabbit)
46	MAPK (ERK1)-pTyr204/187	Cell signaling technologies(#5726)	1:1000(WB)	1:4000 (anti mouse)
47	PRAS40	Cell signaling technologies(#2691)	1:1000(WB)	1:2000 (anti Rabbit)
48	PRAS40 pThr246	Cell signaling technologies(#2997)	1:1000(WB)	1:2000 (anti Rabbit)
49	c-JUN	Cell signaling technologies(#9165)	1:1000(WB)	1:2000 (anti Rabbit)
50	c-JUN pSer243	Cell signaling technologies(#2994)	1:1000(WB)	1:2000 (anti Rabbit)
51	eIF4B	Cell signaling technologies(#3592)	1:1000(WB)	1:2000 (anti Rabbit)

52	eIF4B pSer422	Cell signaling technologies(#3591)	1:1000(WB)	1:2000 (anti Rabbit)
53	4EBP1	Cell signaling technologies(#9542)	1:1000(WB)	1:2000 (anti Rabbit)
54	4EBP1 pThr37/46	Cell signaling technologies(#3929)	1:1000(WB)	1:2000 (anti Rabbit)
55	Cortactin	Cell signaling technologies(#3503)	1:1000(WB)	1:2000 (anti Rabbit)
56	Cortactin pTyr421	Cell signaling technologies(#4569)	1:1000(WB)	1:2000 (anti Rabbit)

Table 3.16.1.2 List of secondary antibodies used in western blotting and Immunofluorescence

S/No	Name of antibody	Catalog No	Dilution
1	Anti-Mouse HRPO	GE healthcare(#NA931)	1:8000 (WB)
2	Anti-Rabbit HRPO	GE healthcare(#NA934)	1:2000 (WB)
3	Anti-Mouse Alexafluor 488	Invitrogen (#2465)	1:200(IF)
4	Anti-Rabbit Alexafluor 568	Invitrogen (#)	1:200(IF)
5	Anti-Mouse Alexafluor 568	Invitrogen (#A10011)	1:200(IF)

3.17 Quantitative total and phosphoproteomics:

3.17.1 Cell lysis, Protein digestion and TMT labelling:

For total proteomics, cell lysates were prepared from A431 vector control and K8 knockdown cells in TEABC lysis buffer (2% SDS, 5mM sodium fluoride, 1mM β-glycerophosphate, 1mM sodium orthovanadate in 50mM Triethyl ammonium bicarbonate). The cell lysates were sonicated and centrifuged at 12,000rpm for 10min. The protein concentration was estimated using Bicinchoninic acid assay (BCA) (Pierce, Waltham, MA). 8mg of protein from each cell type was reduced (using DTT at a final concentration of 5mM at 60˚C for 20min) and alkylated using 10mM iodoacetamide for 10min at room temperature in the dark. We employed filtered sample preparation (FASP) protocol as described earlier [104] to remove SDS. After SDS removal again protein estimation was carried out. 1.4mg of protein from each cell types were subjected to digestion using TPCK treated trypsin (1:20, Promega, cat. No. V542A) at 37°C for 12-16h. Peptides equivalent to 1.4mg of protein from each cell type was labelled using TMT labelling method as per manufacturer's instruction in two different channels (700µg of protein was labelled per channel). Peptides derived from vector control were tagged with TMT tag 128C/128n, K8 knockdown clone KD8 with 129N/C and K8 knockdown clone KD8 with 130C/131. For phosphoproteomics of K8 wild type and phosphomutants, the lysates were prepared and processed as above. Peptides derived from wild type (KD-8WT) were labelled with TMT tag 126 and 127C, KD8-S73A with TMT tag 127N and 128C, KD8-S431A with TMT tag 128N and 129C, KD8-S73D with TMT tag 129N, and 130C and KD8-S431D with TMT tag 130N and 131 (**Table 3.17.1**). After labelling, all the peptides were pooled and subjected to basic reverse phase liquid chromatography.

Table 3.17.1 Table depicting the TMT tags used for differential quantitative proteomics and phosphoproteomics

		m/z
VC	128N, 128C	128.12, 128.13
KD8	129N, 129C	129.13, 129.14
KD2	130C, 131	130.14, 131.14

		m/z
WT	126, 127C	**126.13, 127.13**
K8-73A	127N, 128C	**127.12, 128.13**
K8-431A	128N, 129C	128.12, 129.14
K8-73D	129N, 130C	**129.13, 130.14**
K8-431D	130N, 131	130.13, 131.14

3.17.2 Basic reversed-phase liquid chromatography (bRPLC)

Pooled labelled peptides were subjected to bRPLC fractionation generating 96 fractions, as described earlier [105]. The fractions were concatenated into 12 fractions.

3.17.3 Phosphopeptides enrichment using TiO2 Chromatography (for phosphoproteomics):

Each fraction was subjected to TiO_2-based phosphopeptide enrichment. The TiO_2-beads (Titansphere, GL Sciences Inc.) were incubated with DHB solution (80% ACN, 1% TFA and 3% 2,5-dihydroxybenzoic acid) for 1h at room temperature. Each fraction was resuspended in 3% DHB solution and incubated with TiO_2beads at 1:1 ratio for 30min at room temperature. Phosphopeptide-bound TiO_2beads were washed three times with DHB solution and twice with 40% ACN. Phosphopeptides were eluted three times with 40µL of 2% ammonia solution into tubes containing 10µL of 20% TFA on ice. The phosphopeptides were dried and resuspended in 30µL of 0.1% TFA and desalted using C_{18} Stage Tips. The eluted phosphopeptides were subjected to LC-MS/MS analysis.

3.17.4 LC-MS/MS analysis

The enriched phosphopeptides were analyzed on Orbitrap Fusion™ Tribrid™ Mass Spectrometer (Thermo Electron, Bremen, Germany) interfaced with Easy-nLC 1000 liquid chromatography system (Thermo Scientific, Odense, Denmark). The peptide digests were reconstituted in 0.1% formic acid and loaded onto trap column (75µm x 2cm) packed in-house with Magic C_{18} AQ (Michrom Bioresources, Inc., Auburn, CA, USA). Peptides were resolved on an analytical column (75µm x 20cm) at a flow rate of 350nl/min using a linear gradient of 10-35% solvent B (0.1% formic acid in 95% acetonitrile) over 80min. Data dependent acquisition with full scans in 350-1700 m/z range was carried out using an Orbitrap mass analyzer at a mass resolution of 120,000 at 400 m/z. Fifteen most intense precursor ions from a survey scan were selected for MS/MS which were fragmented using HCD fragmentation with 32% normalized collision energy and detected at a mass resolution of 30,000 at 400 m/z. Dynamic exclusion was set for 30sec with a 10ppm mass window. Internal calibration was carried out using lock mass option (m/z 445.1200025) from ambient air.

3.18 RNA extraction

The RNA from cell lines was isolated by Tri reagent as per the manufacturer's instructions. Briefly, the cells were grown to a confluency of 80% in a 100mm dish. The medium was removed and cells were lysed by adding 1ml/100 cm^2 plate of Tri-reagent. The lysate was transferred into a 1.5ml tube and 100µl of chloroform was added and incubated for 2min at RT. The phase was separated by centrifugation at 12000rpm and supernatant was transferred to a new tube. RNA was precipitated by adding isopropanol and spun at 12000rpm. The pellet was washed by 75%ethanol;

air dried and dissolved in 50µl of DEPC treated water. The purity and content of RNA was determined using NanoDrop TM Spectrophotometer.

3.19 Reverse transcriptase based cDNA synthesis:

cDNA synthesis was carried out as per the manufacturer's protocol (MBI fermantas). Briefly, 3-4µg of total RNA and 0.2µg (100pmol of random hexamer/oligo(dT) in a volume of 12µl were incubated at 70ºC for 5min and chilled on ice and centrifuged. Reaction buffer, RiboLock™ RNase Inhibitor, dNTP Mix was added to obtain final concentration of 1X, 1unit/µl and 1mM each respectively and incubated at 25°C for 5min. RevertAid™ H Minus M-MuLV Reverse Transcriptase (200 units) was added and the reaction mixture was incubated at 25°C for 10min followed by 42°C for 1h. The reaction was terminated by heating at 70°C for 10min.

3.20 Semi Quantitative PCR

To determine mRNA levels of different genes, semi-quantitative PCR amplification method was used. cDNA synthesis was carried out as per the manufacturer's protocol (MBI fermantas). Briefly, 1µg of total RNA and 0.2µg (100pmol of random hexamer/oligo(dT) in a volume of 12µl were incubated at 70ºC for 5min and chilled on ice and centrifuged. Reaction buffer, RiboLock™ RNase Inhibitor, dNTP Mix was added to obtain final concentration of 1X, 1unit/µl and 1mM each respectively and incubated at 25ºC for 5min. RevertAid™ H Minus M-MuLV Reverse Transcriptase (200 units) was added and the reaction mixture was incubated at 25ºC for 10min followed by 42ºC for 1h. The reaction was terminated by heating at 70ºC for 10min. PCR products were run on agarose gel electrophoresis to compare RNA levels. The PCR conditions and primers

used are described in the table 3.20. Amplified PCR products were analyzed in 2% agarose gels containing 0.5g/ml ethidium bromide.

Table 3.20 RT-PCR details of target genes (Primer sequence and PCR Condition)

S/No.	Gene	Sequence (5'-3')	Annealing temperature (°C)	PCR cycles
1	GAPDH F	ATCGTGGAAGGACTCATGACC	52	27
2	GAPDH R	AGGGATGATGTTCTGGAGAGC	52	27
3	Keratin 8 F	AGATGAACCGGAACATCAGC	54	30
4	Keratin 8 R	TCCAGCAGCTTCCTGTAGGT	54	30
5	Keratin 18 F	TGAGACGTACAGTCCAGTCCTT	56	30
6	Keratin 18 R	GCTCCATCTGTAGGGCGTAG	56	30
7	Keratin 17 F	GGAGCTGGCCTACCTGAAGAAG	52	28
8	Keratin 17 R	GCGGTTCTTCTCTGCCATCTTC	52	28
9	Keratin 5 F	GAGGCCAAGGTTGATGCACTG	58	30
10	Keratin 5 R	GTCCAGGTTGCGGTTGTTGTC	58	30

F: Forward primer, R: Reverse primer

3.21 Immunofluorescence:

Cells were grown on glass cover slips for 48h till they reached a confluency of 60-70%. Adhered cells were directly fixed either with chilled 100% methanol in -20°C or 4% paraformaldehyde at RT for 10min and 15min respectively. After fixation, coverslips were washed thrice with 1X PBS for 10min each. The cells were then permeablized using 0.3%Triton X-100 for 90sec in case of methanol fixation and 10min in 0.7% Triton X-100 when cells were fixed with paraformaldehyde. The coverslips were again washed thrice with 1X PBS for 5min each. They were then placed in a

small humidified chamber and 5% BSA was layered over the cells for blocking and incubated for 1h. BSA was drained and the cells were layered with 50µl of primary antibody diluted in 5% BSA and incubated for 1h. The coverslips were washed thrice with 1X PBS for 10min each followed by incubation with 100µl of anti-mouse (Alexa Fluor 488) or anti-rabbit (Alexa Fluor 568) conjugated secondary antibody for 1h and later washed with 1X PBS thrice for 10min each. DAPI was used to stain the nucleus. Coverslips were then mounted using antiquenching agent (vectashield) and sealed. Confocal images were obtained using a LSM 780 Carl Zeiss Confocal system. Scatter Plots were generated and Pearson's correlation coefficient(R) for colocalization were calculated using Carl Zeiss (zen 2012 SPI black edition, 64 bit) software. List of the primary and secondary antibodies used are given in the **Table 3.16.1.1 and 3.16.1.2.**

3.22 Luciferase Reporter assay:

A431 vector control and K8 knockdown cells were co-transfected with ConA luc control or 3x κB ConA luc, pBIND-Renilla-Luc and other relevant vectors by calcium phosphate method. After 48h, cells were lysed and 10µg lysate was used for the assay. Luciferase assay was performed in 96 well white plate using Dual Luciferase Assay System (Promega) as per the manufacturer's protocol. Luciferase activity was measured using the 96-well luminescence plate reader. Renilla luciferase was used for transfection normalization.

3.23 Rac Activity assay: Rac activity assay was performed as per manufacture protocol (RhoA / Rac1 / Cdc42 Activation Assay Combo Biochem Kit (bead pull-down format) (Cat. # BK030) Cytoskeleton, inc.

3.24 Mass Spectrometry data analysis:

The mass spectrometry derived data was searched against "Human RefSeq protein database" (Version 65, containing 36211 protein entries with common contaminants added) using "SEQUEST" and "Mascot" search algorithms through "Proteome Discoverer" platform (version 1.4.1.14, Thermo Scientific,) as described in earlier report [105, 106]. The search parameters for both algorithms included: carbamidomethylation of cysteine and TMT 10-plex (C229.163) modification at N-terminus of peptide and lysine as fixed modifications; N-terminal acetylation, oxidation of methionine, phosphorylation at Serine, Threonine and Tyrosine (+79.966 Da) as variable modifications. MS/MS spectra were searched with a precursor mass tolerance of 10 ppm and fragment mass tolerance of 0.05Da. Trypsin was specified as protease and a maximum of two missed cleavages were allowed. The data were searched against decoy database and the false discovery rate was set to 1% at the PSM level. The probability of phosphosite localization for each Serine/Threonine site on each protein was calculated by the phosphoRS 3.1 node in the Proteome Discoverer (version 1.4, Thermo Scientific). Phosphopeptides with > 75% localization probability were considered. The phosphorylation sites that were identified with >75% localization probability were assigned to different sites by the search algorithm and were manually corrected based on the phosphoRS localization probability for a given residue. Peptide with ratio ≥1.5-fold cut-off were considered for differential phosphosites.

3.25 Bioinformatics analysis

The mass spectrometry-derived data was searched against "HPRD" (Version 65, containing 36211 protein entries with common contaminants added) using "SEQUEST" and "Mascot" search algorithms through "Proteome Discoverer" platform (version 1.4.1.14, Thermo Scientific,) as

described in earlier report [105, 106]. Phosphopeptides with a fold change of ≥1.5 (up/downregulated) were considered for further bioinformatics analysis. "PhosphoELM" [107], "PhosphoSitePlus" and "Uniprot" database were referred to determine the known and novel phosphosites identified in our Mass-spectrometry data. To determine the orthogonal or overlapping phosphoproteomic profile amongst all the datasets, "Venny2.1 tool" was used. "STRING analysis tool" was used for protein-protein interaction analysis of different Phosphoproteins. All quantified phosphopeptides were analyzed using "Ingenuity Pathway Analysis" (IPA, Ingenuity systems, Qiagen, used in collaboration with IOB, Bangalore) by core analysis. The over represented "Biological processes", "Molecular functions" and "Canonical pathways" were generated based on information contained in the Ingenuity Pathways Knowledge Base. The significance of the association between the dataset and the canonical pathway was measured in 2 ways: (1) A ratio of the number of molecules from the dataset that map to the pathway divided by the total number of molecules that map to the canonical pathway is displayed. (2) Fisher's exact test was used to calculate a p-value determining the probability that the association between the genes in the dataset and the "Canonical pathways" is explained by chance alone. "Enrichr tool" [108] was used to analyze "PPI hub proteins" of the set of phosphoproteins showed significant reversal in phosphorylation levels. "PANTHER GO-functional annotation" [109] was used to determine "Protein class" within the datasets showing significant reversal in phosphorylation levels. Xcalibur version-3.0 was used to determine the quantitative spectra for phosphopeptides.

3.26 *In vitro* wound healing assay for migration:

The cells were grown in 35mm plates to 95% confluency. Cells were replaced with fresh medium containing 20µg/ml mitomycin C for 3h. After incubation medium was discarded and wounds were scratched with the help of sterile 2µl pipette tip. The cells were fed with fresh medium without serum and observed under an Axiovert 200 M Inverted Carl Zeiss microscope fitted with a stage maintained at 37ºC and 5% CO2. Cells were observed by time lapse microscopy, and images were taken every 20min for 20h using an AxioCam MRm camera with a 103 phase 1 objective. Migration was measured using Axiovision software version 4.5 (Zeiss).

3.27 Boyden chamber cell invasion and migration assay:

The invasiveness of the cells was determined by the Boyden chamber invasion assay. 40µl Matrigel (1mg/ml) with 140µl incomplete DMEM was applied to 8µm-pore-size polycarbonate membrane filters and the bottom chamber was filled with 0.6ml of complete DMEM. 2 x 10^5 cells were seeded in the chamber in serum-free medium, and then incubated for 16h at 37°C. At the 15^{th}h, the cells on the upper surface were carefully removed with a cotton swab. The membranes containing invaded cells were fixed with 4% PFA and stained with DAPI. The invasiveness was quantified by counting 25 random fields under an upright microscope. Results obtained from three independent experiments each in triplicate were represented as mean values using ±SEM obtained from software Graphpad prism 5. For Boyden chamber migration assay, same protocol was followed without adding matrigel to the 8µm-pore-size polycarbonate membrane filters.

3.28 Cell proliferation/MTT (3-(4, 5-Dimethylthiazol-2-yl)-2, 5-Diphenyltetrazolium Bromide) viability assay [110]

2000 cells/100µl were seeded per well, in a 96-well microtitre plate. Proliferation was studied every 24h up to a period of 4 days. At the desired time points, 100µl of the medium was replenished from the designated wells and 20µl MTT solution (5mg/ml MTT in 1X PBS) was added to each well. Plate was incubated at 37°C in a CO2 incubator for 4h, then 100µl of acidified SDS (10%SDS in 0.01N HCl) was added to each well and incubated overnight at 37°C. Next day, the absorbance was measured on an ELISA plate reader at 540nm against a reference wavelength of 690nm. Growth curve was plotted from three independent experiments.

3.29 Colony-forming assay

200 cells were plated in 60mm tissue culture plates in triplicates. Cells were grown in complete medium for 14 days, with medium changes every 2–3 days. Cells were first fixed with methanol for 5min at RT and then washed twice with 1X PBS. They were later stained with crystal violet solution (0.5% crystal violet in 20% methanol) for 5min at RT. After washes with distilled water, the images of stained cells were captured using high-resolution Nikon camera. The colonies were counted with Metamorph software.

3.30 Soft agar colony forming assay

The assay was performed in a 35mm Petri plates. As a first step, 1ml of the basal layer was made by adding equal volumes of 2X complete IMDM/DMEM and 2% low melting agarose. 1000 cells in complete medium containing 0.4% low melting agarose were seeded over the basal layer. Plates were fed with complete medium on every alternate day and incubated at 37°C in a 5% CO2

incubator for 15 days. Opaque and dense colonies were observed and counted microscopically on day 15. The assay was carried out in triplicates.

3.31 *In vivo* tumorigenicity assay:

The tumorigenic potential of K8 knockdown/vector control was determined by subcutaneous injection in NOD-SCID mice. The cells were suspended in plain medium without serum and 1 x 10^6 cells were injected sub-cutaneously in the dorsal flank of 6-8 weeks old mice. 6 mice were injected per clone and were observed for tumor formation over a period of approximately 2 weeks. Tumor volume was determined using a digital vernier caliper and its calculation was carried out by the modified ellipsoidal formula, [Tumor volume = 1/2(length x width2)]. All protocols for animal studies were approved by the ‘‘Institutional Animal Ethics Committee (IAEC)’’ (Approval ID: 5/2015). A Committee formed under the guidelines of the Committee for the Purpose of Control and Supervision of Experiments on Animals (CPCSEA), Government of India.

3.32 Statistical analysis:

Two groups of data were statistically analyzed by t *test* using Graph-pad Prism5 Software. A *p* value less than 0.05 was considered statistically significant.

Chapter-IV
Results

4.1 To generate Keratin 8-WT and phosphomutant expressing tissue specific Transgenic mouse.

Our cell line based studies together with other reports have shown that K8 phosphorylation regulates neoplastic progression of different carcinomas in a context dependent manner. To understand the exact function of K8 phosphorylation in neoplastic progression, we wanted to generate transgenic mouse model expressing K8 wild type and phosphomutants (K8 S73A and K8 S431A). Earlier reports have shown that, K8 S73A expressing mice (under a ubiquitous CMV promoter) died due to hepatotoxic injuries under stress conditions. Therefore, we chose to generate transgenic mouse model which would express K8 phosphomutants and wild type specifically in basal cells of stratified epithelia with the help of K14 promoter.

4.1.1 Lentiviral Mediated Transgenesis:

4.1.1.1 Generation of lentiviral particles and determination of titer: The lentiviral particles for all three constructs (pCCL-K14-K8 WT/S73A/S431A GFP) were generated as shown in the **Figure 4.1.1.1.1 A, B**. The constructs were validated by restriction digestion with XhoI and BamHI resulting in the release of K14 promoter (2.1kb) and K8 (1.5kb). The gel image is shown in the **Figure 4.1.1.1.1 C**. All the three constructs were further sequence verified using CNV forward and GFP reverse primers respectively (**Figure 4.1.1.1.2 A, B)**. In addition the complete expression cassette was sequenced using overlapping primers **(Figure 4.1.1.1.2 C)**. Further high titer lentiviral particles were produces as described in **Figure 4.1.1.1.3** using vira power packaging mix. The transduction efficiency was assessed by transducing each of these viral particles with a dilution of 1:100 and 1:1000 to the HEK 293 cells. 36h post transduction, these cells were collected and the GFP positive cells were analyzed by FACS which confirmed titer to be 10^9TU/µl

for all the three constructs in case of both the dilutions suggesting that a high titer viral particles could be prepared for further use **(Figure 4.1.1.1.4 A, B, C).**

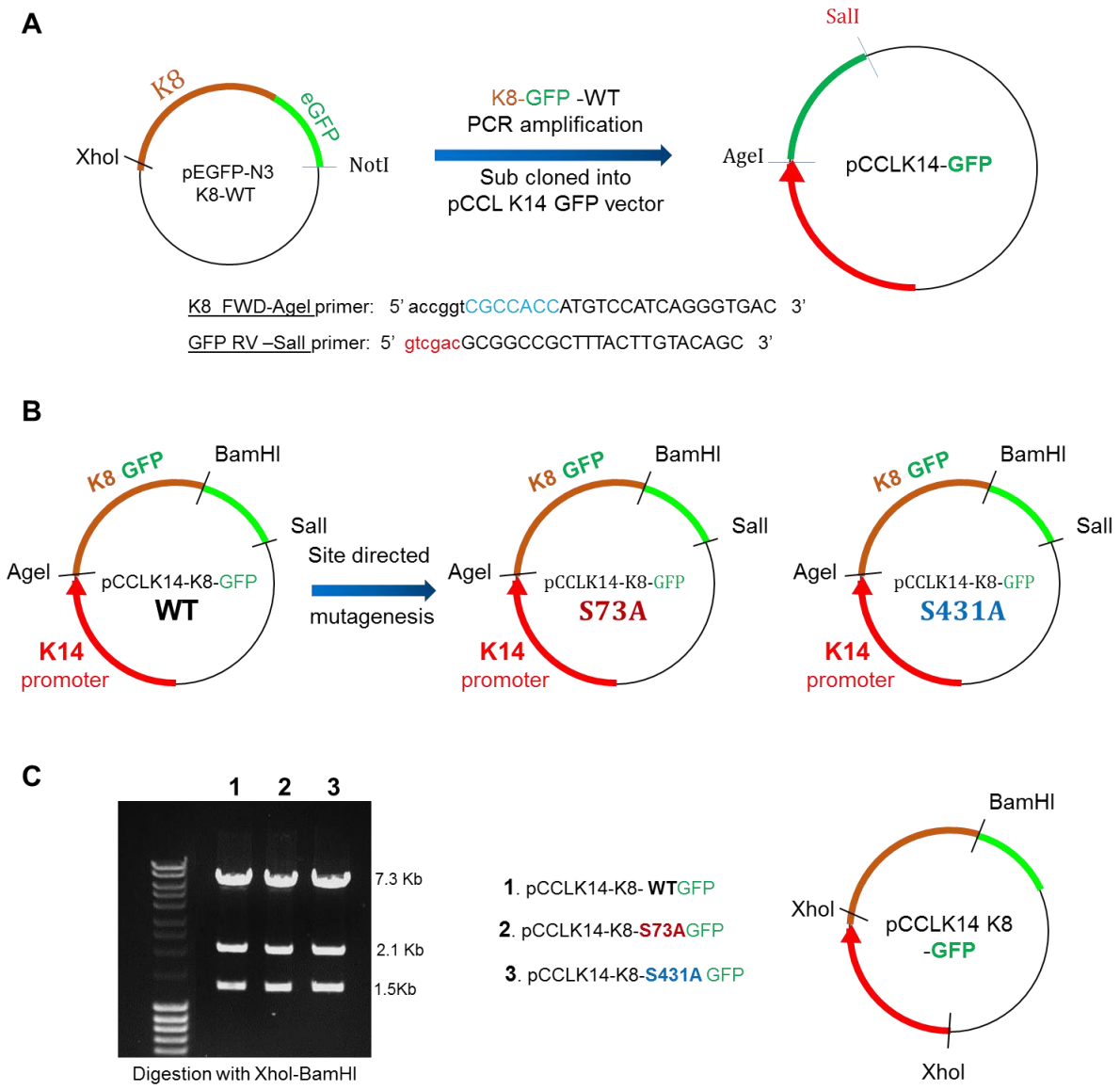

Figure 4.1.1.1.1: Generation and validation of K8 WT and phosphodead mutant constructs: A) The schematic depicting the strategy used to generate pCCLK14-K8 WT GFP construct using AgeI-SalI enzymes in pCCL-K14 GFP lentiviral vector backbone. B) Cartoon demonstrating the generation of phosphodead mutant constructs (pCCL-K14-K8 S73A/ S431A GFP) by SDM of pCCLK14-K8 WT GFP. C) Representative gel pictures showing positive clones for K8 WT GFP, K8 S73A GFP and K8 S431A GFP in pCCL –K14 vector backbone.

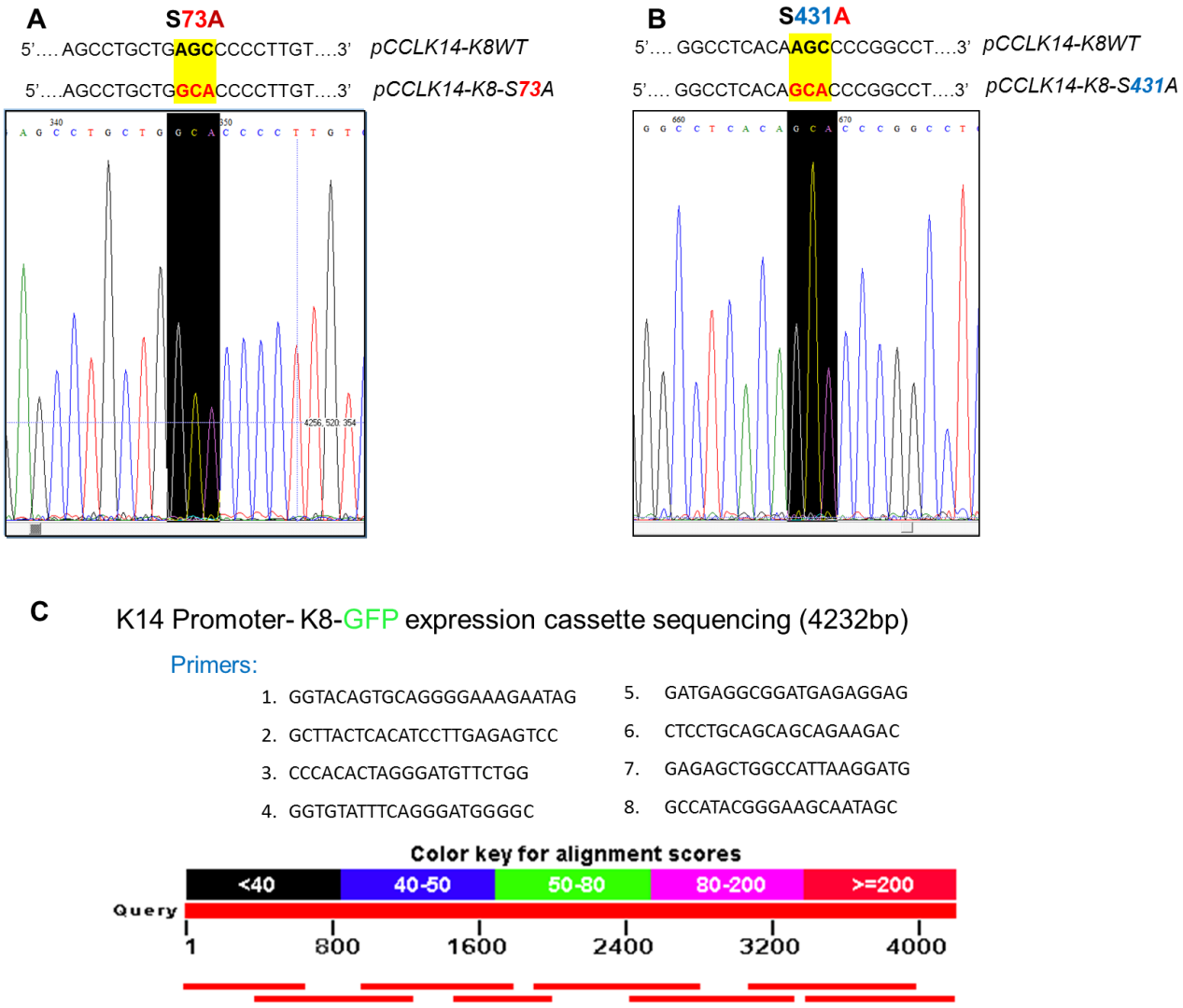

***Figure 4.1.1.1.2**: **Sequence analysis of the respective lentiviral constructs**:* Representative images of sequencing for the validation of insertion of the respective mutation in the phosphodead mutant constructs, pCCL-K14-K8 S73A (A) and K8 S431A GFP (B) using CMV forward and GFP reverse primers respectively. (C) Representative image of full length expression cassette "K14-K8 GFP" sequenced using overlapping primers. (Respective primers are shown in the figure).

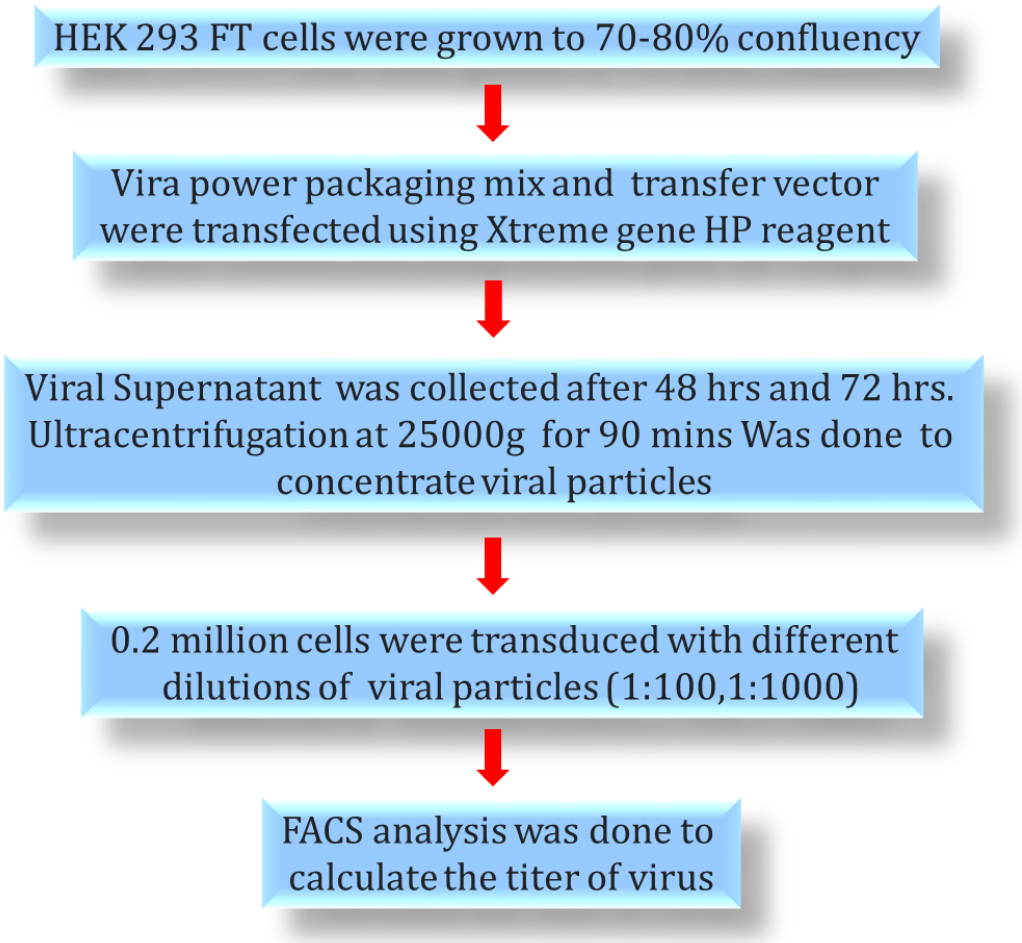

Figure 4.1.1.1.3: Preparation of high titer lentiviral particles for generation of transgenic mice: Schematic of the protocol used to generate the high titer lentiviral particles for all the three constructs.

4.1.1.2 Validation of viral particles: HEK 293 cells were transduced with each of the K8 wild type and phosphomutant viral particles and incubated for 48h. Further the expression of K8 wild type GFP together with phosphomutants was analyzed by immunofluorescence western blotting and semi-quantitative PCR. The immunofluorescence images show proper filamentous architecture of K8 WT and phosphomutants in the HEK293 cells post 48h of transfection **(Figure 4.1.1.2 A**). Further the 82kD high molecular band in the western blot corresponds to K8 GFP whereas a 52kD band represents endogenous K8. The appearance of a higher molecular weight band (82kD) validated the integration as well as expression of respective exogenous K8 GFP for

all three constructs at protein level **(Figure 4.1.1.2 B)**. Semi-quantitative PCR with GFP specific primers further confirmed our results **(Figure 4.1.1.2 C).**

A

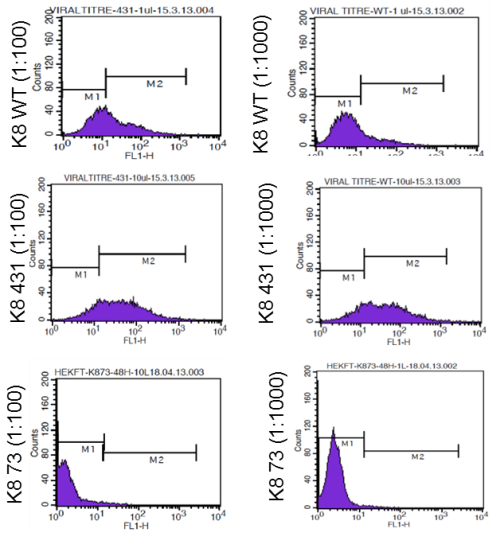

B

Sample ID and dilution	% positive cells	MFI
pCCL K14 K8 WT 1ul	14.63%	40.36
pCCL K14 K8 WT 10ul	46.85%	81.36.
pCCL K14 K8S431A , 1ul	35.0%	48.52
pCCL K14 K8 S431A, 10ul	52.44 %	80.02
pCCL K14 K8 S73A 10ul	1.47 %	24
pCCL K14 K8 S73A 1ul	0.66 %	22

C **Titer calculation**

$$T = (P \times N)/(D \times V)$$

T = titer (TU/ml)
P = % GFP+ cells (ie: N = 0.2 for 20% GFP+ cells)
N = number of cells at the time of transduction
D = dilution factor (ie: 10-3 = 0.001)
V = volume of viral inoculum (0.2 ml)

S/N	Name of Construct	%positive	TU/ml
1.	K8 WT 1ul	14.63	10^9
2.	K8 WT 10ul	46.85	10^9
3.	K8 431 1ul	35.0	10^9
4.	K8 431 10ul	52.44	10^9
5.	K8 73 1ul	0.66	10^7
6.	K8 73 10 ul	1.47	10^7

Figure 4.1.1.1.4: Preparation of high titer lentiviral particles for generation of transgenic mice: A) Representative image showing the FACS analysis of HEK 293 cells post 48h of transduction of pCCL K14-K8 WT GFP, pCCL K14-K8 S73A GFP and pCCL K14-K8 S431A GFP viral particles, respectively. For titer calculations 1:100 and 1:1000 dilutions of concentrated viral particles were used. B) Table shows the percent GFP positive cells and mean fluorescent intensity of HEK 293 cells post 48h of transduction of pCCL K14-K8 WT GFP, pCCL K14-K8 S73A GFP and pCCL K14-K8 S431A GFP viral particles, respectively. C) Table shows the titer calculated according to the formula given in the figure for viral particle of each of the constructs.

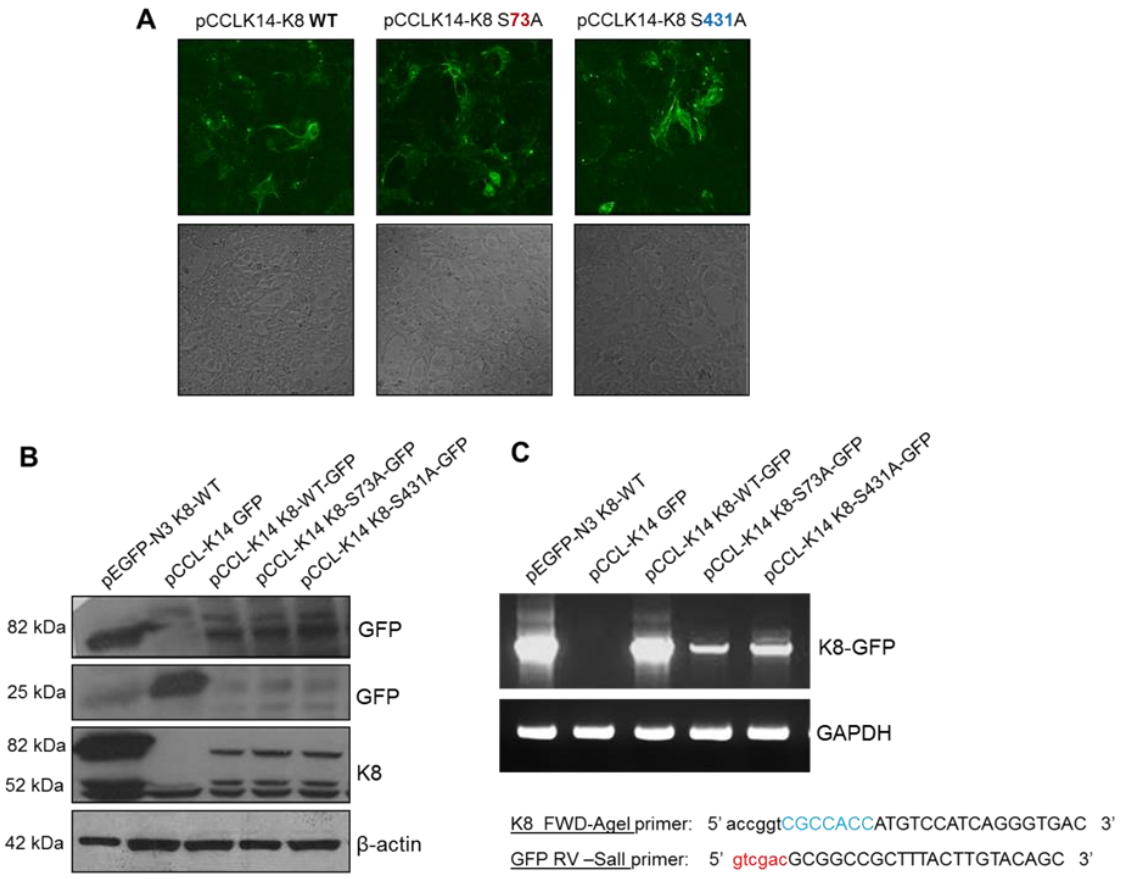

Figure 4.1.1.2: Validation of lentiviral particle: A) Immunofluorescence images of HEK 293 FT after 48h of transfection with K8 WT and phospodead mutants. GFP positive cells (Green) were observed using confocal microscopy for all the three constructs. Nucleus is counterstained with DAPI (blue) (Scale bar 20µm) B) Western blot analysis of HEK 293 FT cells post 48h of transfection with respective K8 WT or phosphodead mutant constructs. Appearance of an 82kD band corresponds to K8 GFP. C) Representative image of semi-quantitative PCR of full length K8 GFP (2.3kbp) for all the three K8 WT and phosphodead mutant constructs.

4.1.2 Generation of transgenic mice by lentiviral mediated *in vivo* Manipulation of Spermatogonial Stem cells: To generate tissue specific transgenic mouse model, *in vivo* Manipulation of spermatogonial Stem Cells by high titer lentiviral particles was carried out. For this 5-10µl of recombinant viral particles (10^9TU/µl) expressing K8 wild type as well as phosphomutants were injected into the intertubular spaces of the testis of 3 weeks old Swiss mice Crl:CFW (SW) targeting undifferentiated spermatogonia present in the seminiferous tubules.

Injection into the intertubular space allows the lentivirus to infect undifferentiated spermatogonial cells located at the basement of the seminiferous tubules. These male mice, referred to as pre-founder mice, were mated with wild type females of the same strain (Swiss) 35 days post infection (**Figure 4.1.2.1, 4.1.2.2 and 4.1.2.3**). To determine whether the progeny from these crosses carried the transgene, genotyping by tail gDNA PCR was performed. For this genomic DNA was isolated from the tail snips of all the pups. The integrity of the genomic DNA was verified by 0.8% agarose gel electrophoresis (**Figure 4.1.2.4 A**). Further, to screen transgene positive pups PCR using EGFP specific primers was performed. None of the mice showed integration of transgene in the respective progeny for all the three clones. An amplification for the patch gene served as an internal control, the gDNA from untransduced mice of the same strain served as a negative control and the gDNA isolated from the cells transduced with the same viral particles served as a positive control (**Figure 4.1.2.4 B**).

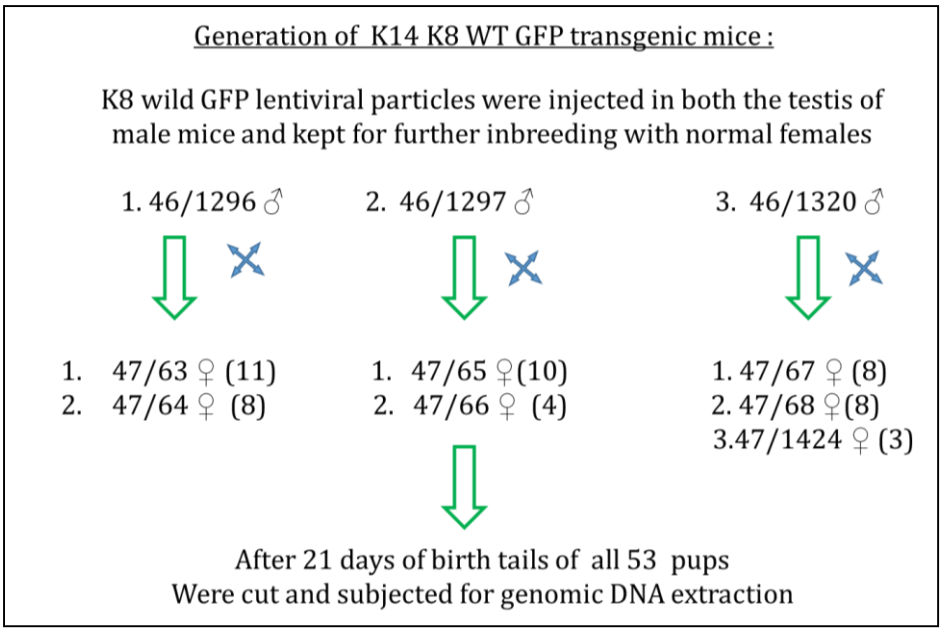

Figure 4.1.2.1: Schematic representation of inbreeding post 35 days of testicular injection of K14-K8 WT GFP lentiviral particles into 3 FVB/j male mice. Identification numbers of respective male and female mice are depicted in the figure together with number of pups obtained in the F1 generation post mating.

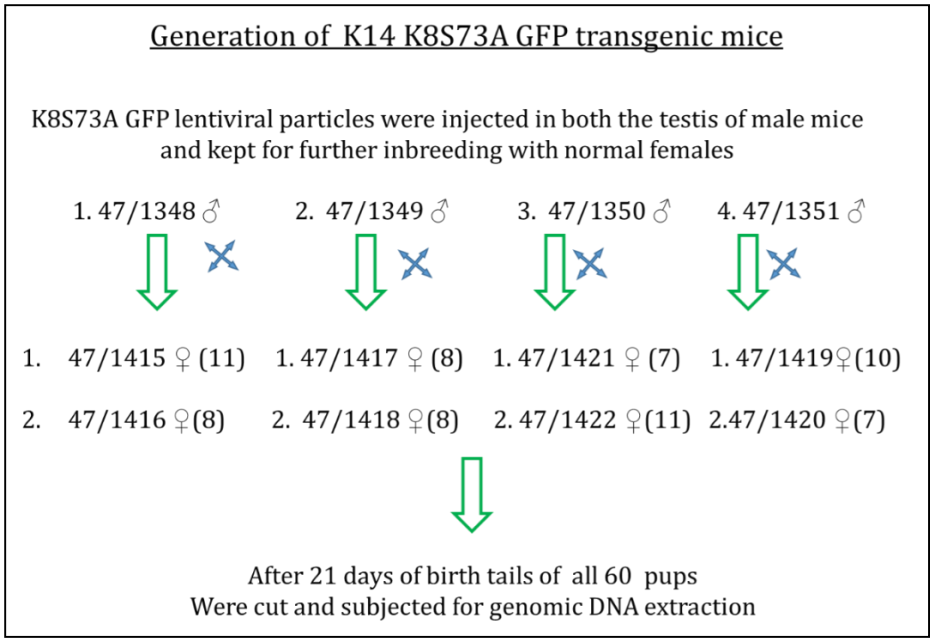

Figure 4.1.2.2: Schematic representation of inbreeding post 35 days of testicular injection of K14-K8 S73AGFP lentiviral particles into 4 FVB/j male mice. Identification numbers of respective male and female mice are depicted in the figure together with number of pups obtained in the F1 generation post mating.

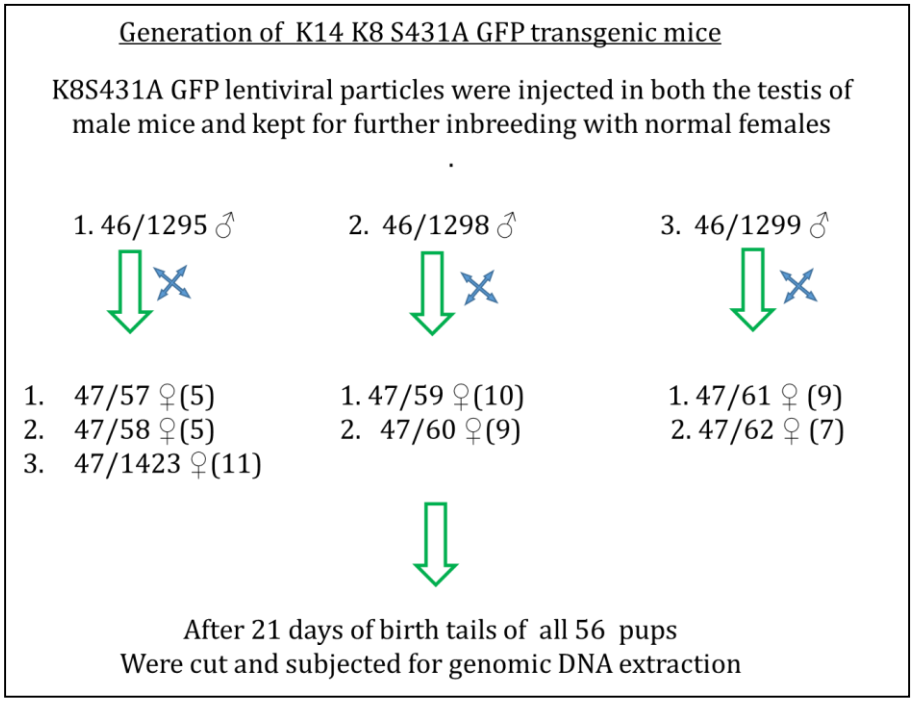

Figure 4.1.2.3: Schematic representation of inbreeding post 35 days of testicular injection of K14-K8 S431A GFP lentiviral particles into 4 FVB/j male mice. Identification numbers of respective male and female mice are depicted in the figure together with number of pups obtained in the F1 generation post mating.

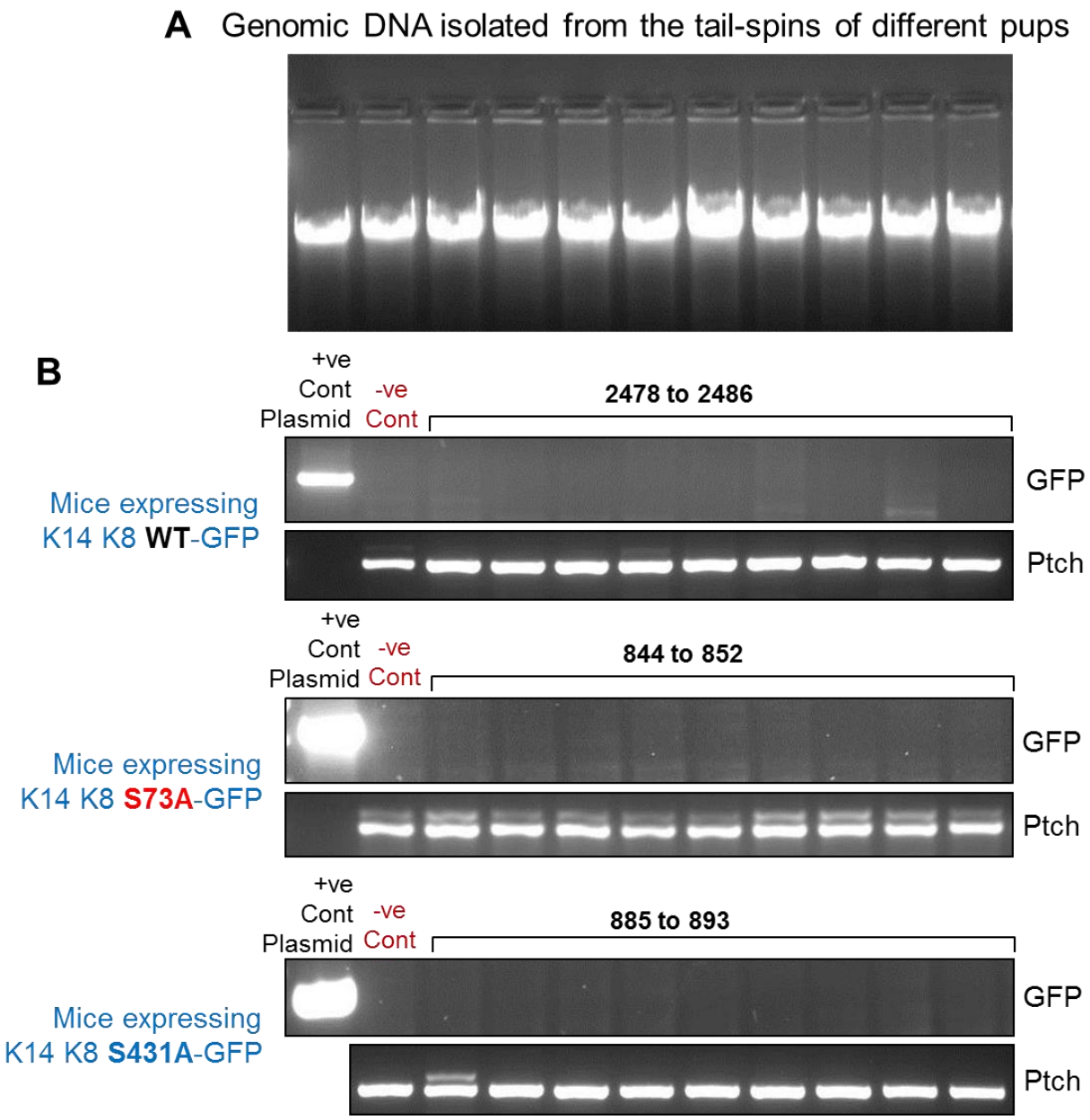

Figure 4.1.2.4: Screening of the transgene positive pups: (**A**) Representative gel picture of tail genomic DNA isolated from tail snips of mice for screening of transgene integration. Representative gel image of gDNA PCR with Ptch primers as an internal control. (**B**) Representative gel images of gDNA PCR using GFP specific primers to screen the transgene positive mice for all three K8 WT GFP and phosphomutant constructs. The genomic DNA from a cell line transduced with the K14-K8 WT GFP was used as a positive control. Note: None of the pups were positive for the transgene integration.

4.1.3 Transgenesis by electroporation:

4.1.3.1 Preparation of expression cassette for electroporation:

As an alternative strategy for generation of tissue specific transgenic mouse model, the electroporation of the expression cassette to the male germ cells was carried out. For this purpose, the expression cassettes were excised from pCCL K14-K8 wild type GFP and phosphomutant constructs with the help of HpaI and NdeI restriction enzymes. The gel picture shows the 5.2kbp blunt end linearized expression cassette containing K14-K8 GFP wild type as well as phosphomutants (**Figure 4.1.3.1 A, B)**. After digestion the expression cassette was eluted out from the gel and a final concentration of 200µg/200 µl was obtained after gel extraction. The integrity and purity of expression cassette was further analyzed on agarose gel as shown in the gel picture (**Figure 4.1.3.1 C)**. The schematic representation of electroporation of expression cassette into the testis of male mice is shown in the **Figure 4.1.3.1 D**.

4.1.3.2 Electroporation of the expression cassette and screening of transgene positive pups:

The electroporation of the expression cassettes was carried out at NII, New Delhi in collaboration with Dr. Majumdar. For this, the testicular germ cells of 3 weeks old FVB/j male mice were electroporated with K14-K8 GFP constructs for wild type and phosphomutants (K14-K8 S73A GFP/ K14-K8 S431A GFP) respectively. These fore-founders were allowed to mate with the normal females of the same strain (FVB/j). Further, transmission of transgene from electroporated mice (fore-founder) to several of their progeny was discerned by tail genomic DNA PCR analysis. We could obtain few transgene positive pups for all the three constructs as shown in the gDNA PCR analysis with GFP specific primers in the third attempt.

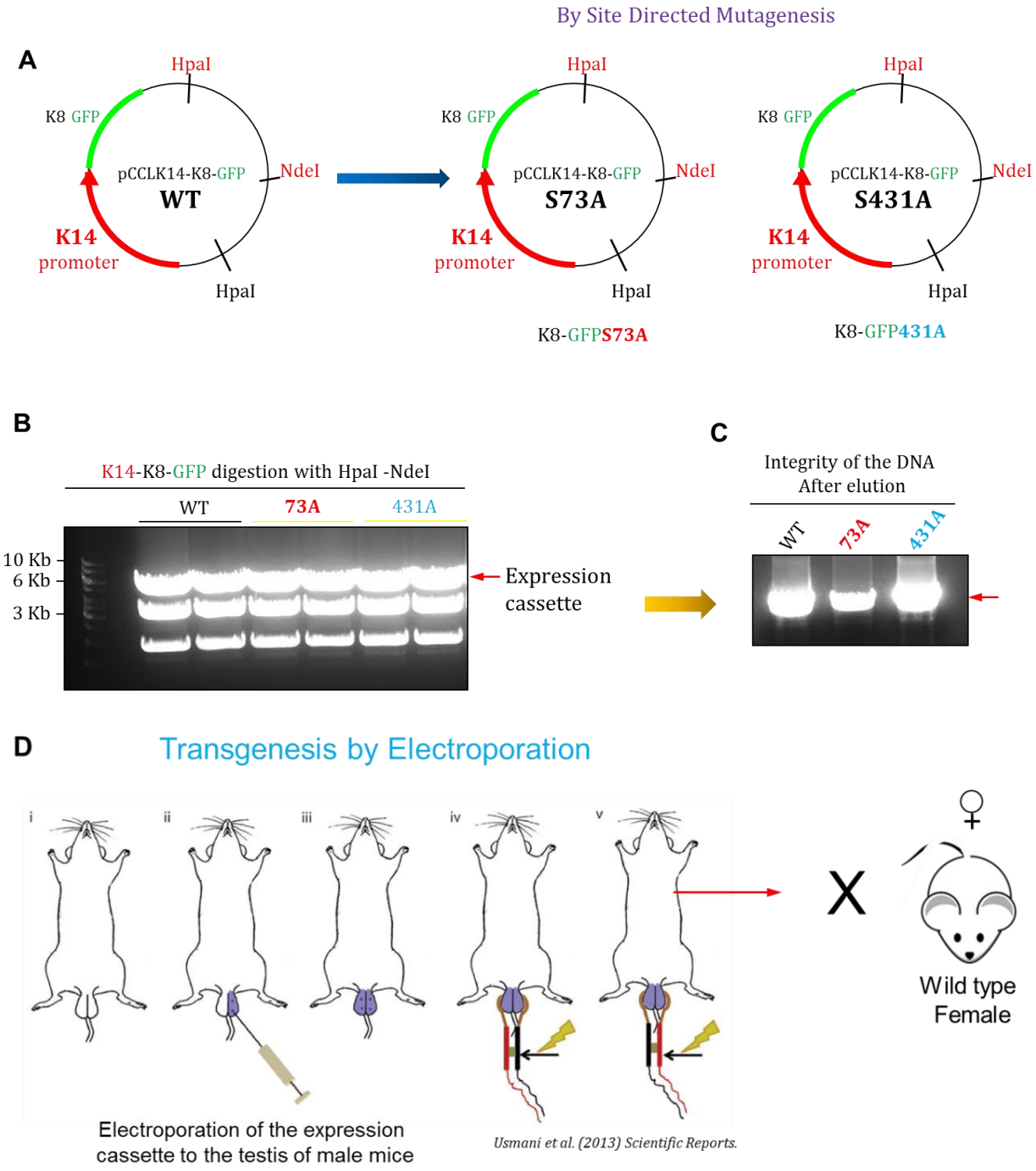

Figure 4.1.3.1**: **Preparation of expression cassette for generation of transgenic mice by electroporation: (**A**) Schematic of the constructs used to generate the transgenic mice (pCCL K14-K8 WT GFP, pCCL K14 K8 S73A GFP and pCCL K14-K8 S431A GFP respectively) by electroporation. Two main restriction sites (HpaI-NdeI) used to cleave the respective expression cassettes are highlighted in the vector map. (**B**) Gel picture showing 5.2kbs expression cassettes cleaved off from the vector backbone for all the three constructs (Right panel). (**C**) Gel picture showing intact and purified expression cassettes for K8 WT

and phosphodead mutants to generate transgenic mice by electroporation. (**D**) Schematic representation of the protocol for electroporation of expression cassette to generate transgenic mice.

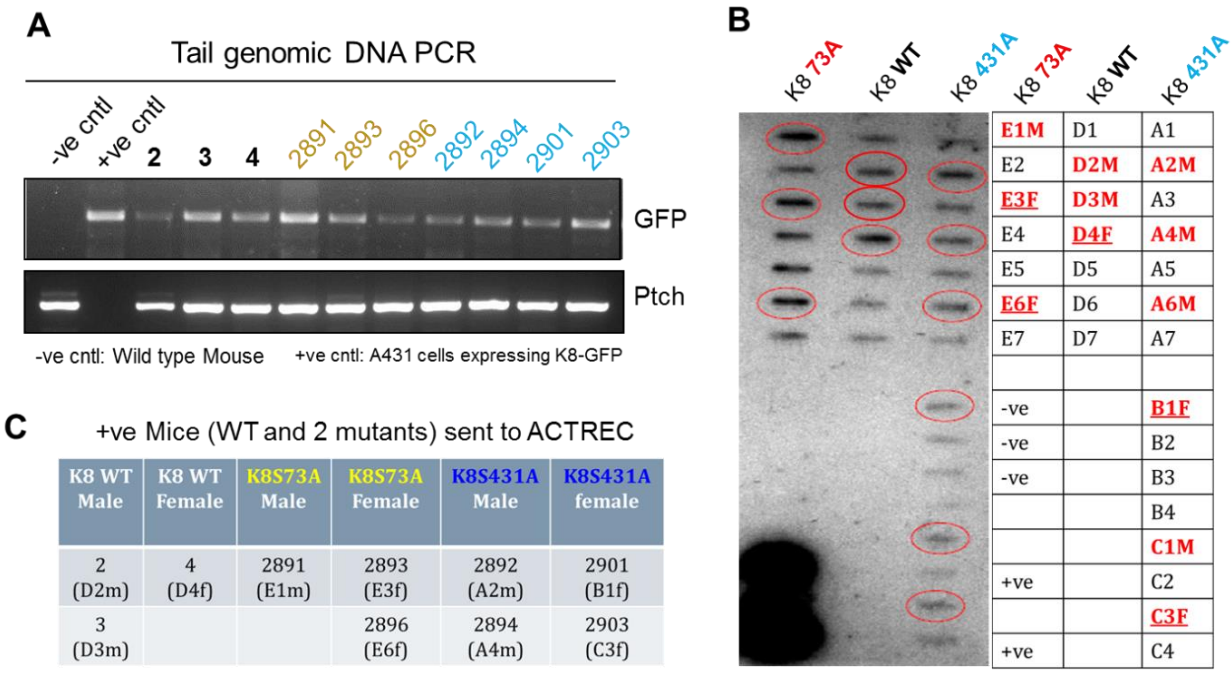

C

+ve Mice (WT and 2 mutants) sent to ACTREC

K8 WT Male	K8 WT Female	K8S73A Male	K8S73A Female	K8S431A Male	K8S431A female
2 (D2m)	4 (D4f)	2891 (E1m)	2893 (E3f)	2892 (A2m)	2901 (B1f)
3 (D3m)			2896 (E6f)	2894 (A4m)	2903 (C3f)

Figure 4.1.3.2.1: Screening of the transgene positive mice: (**A**) Gel image for tail genomic DNA PCR based validation of transgene positive pups, selected for inbreeding and generation of different lines of mice for all the three constructs (K14-K8 WT GFP, K14-K8 S73A GFP and K14-K8 S431A GFP). Primers specific to EGFP were used for genotyping whereas Ptch primers were used as an internal control. The genomic DNA from a cell line transduced with the K14-K8 WT GFP was used as a positive control. The tail genomic DNA of normal mice (non-transgenic) of the same strain (FVB/j) was used as negative control. Specific identification numbers of mice are depicted in the figure. (**B**) Slot blot analysis demonstrating the transgene positive pups for K14-K8 WT GFP, K14-K8 S73A GFP and K14-K8 S431A GFP constructs. Corresponding panels for all the three are depicted in the figure, respectively. The red circles highlight transgene positive mice selected for further experiments. (**C**) The table shows list of transgene positive pups selected for further inbreeding and generation of different lines of mice for all the three constructs (K14-K8 WT GFP, K14-K8 S73A GFP and K14-K8 S431A GFP).

Here amplification for the patch gene served as an internal control, the gDNA from normal mice of the same strain served as a negative control and the gDNA isolated from the cells transduced with the same viral particles served as a positive control **(Figure 4.1.3.2.1 A, B).** These results

were further confirmed by slot-blot analysis where GFP region of the transgene was detected with αP^{32} labelled probe **(Figure 4.1.3.2.1 C).** The positive male and female mice (data shown in table) for respective clones were brought to ACTREC animal house facility and were subjected to further in breeding to generate pure line of mice after validating all the results. Further in breeding for the transgenic mice from all the three groups was carried out and the representative pedigree analysis is shown in the **(Figure 4.1.3.2.2 A, B, 4.1.3.2.3 A, B, 4.1.3.2.4 A, B).**

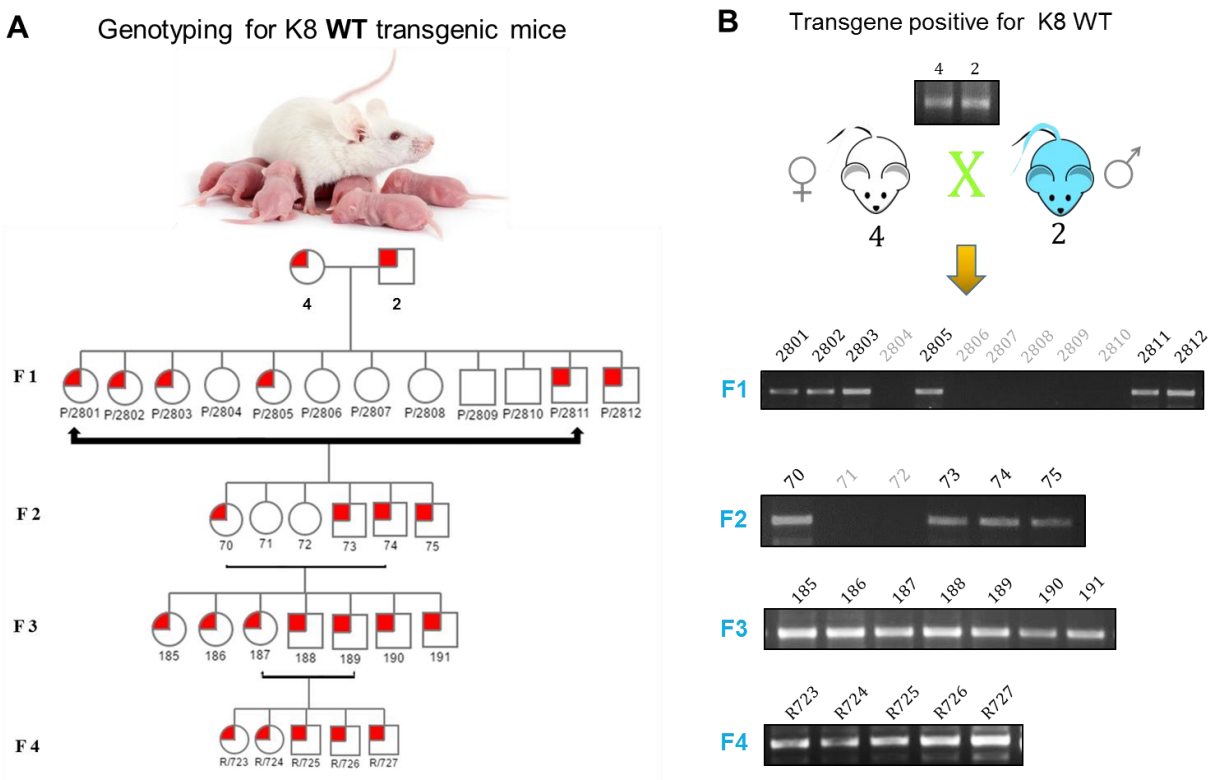

Figure 4.1.3.2.2: Inbreeding and genotyping of K14-K8 WT GFP expressing transgenic mice: (**A**) Pedigree analysis for pre-founder mice 4 (female) and 2 (male) showing germ-line transmission of the transgene. Individual mice were assigned numbers for further experiments. (**B**) Genomic DNA amplification using primers for EGFP is shown in the gel picture whereas Ptch is used as an internal control.

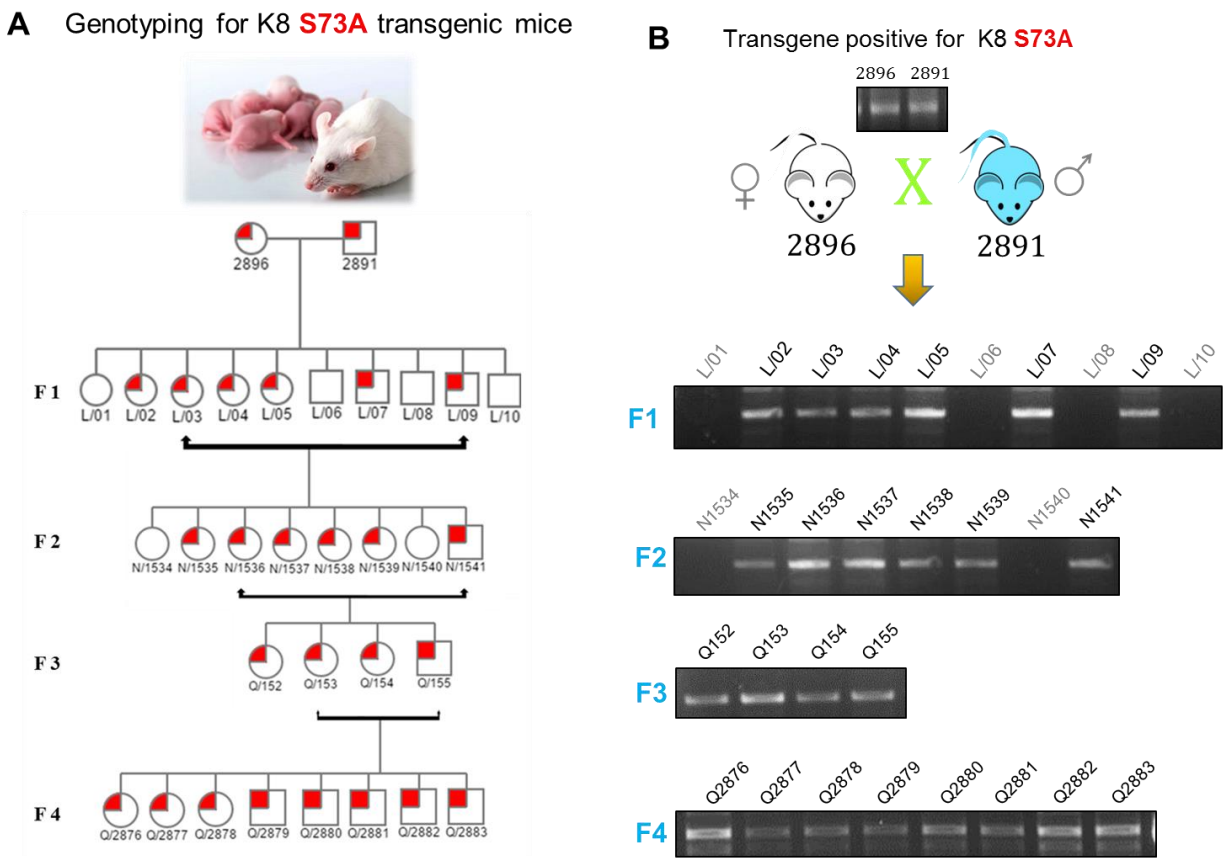

Figure 4.1.3.2.3: Inbreeding and genotyping K14-K8 S73A GFP expressing transgenic mice: (**A**) Pedigree analysis for pre-founder mice 2896 (female) and 2891 (male) showing germ-line transmission of the transgene. Individual mice were assigned numbers for further experiments (**B**) Genomic DNA amplification using primers for EGFP is shown in the gel picture whereas Ptch is used as an internal control.

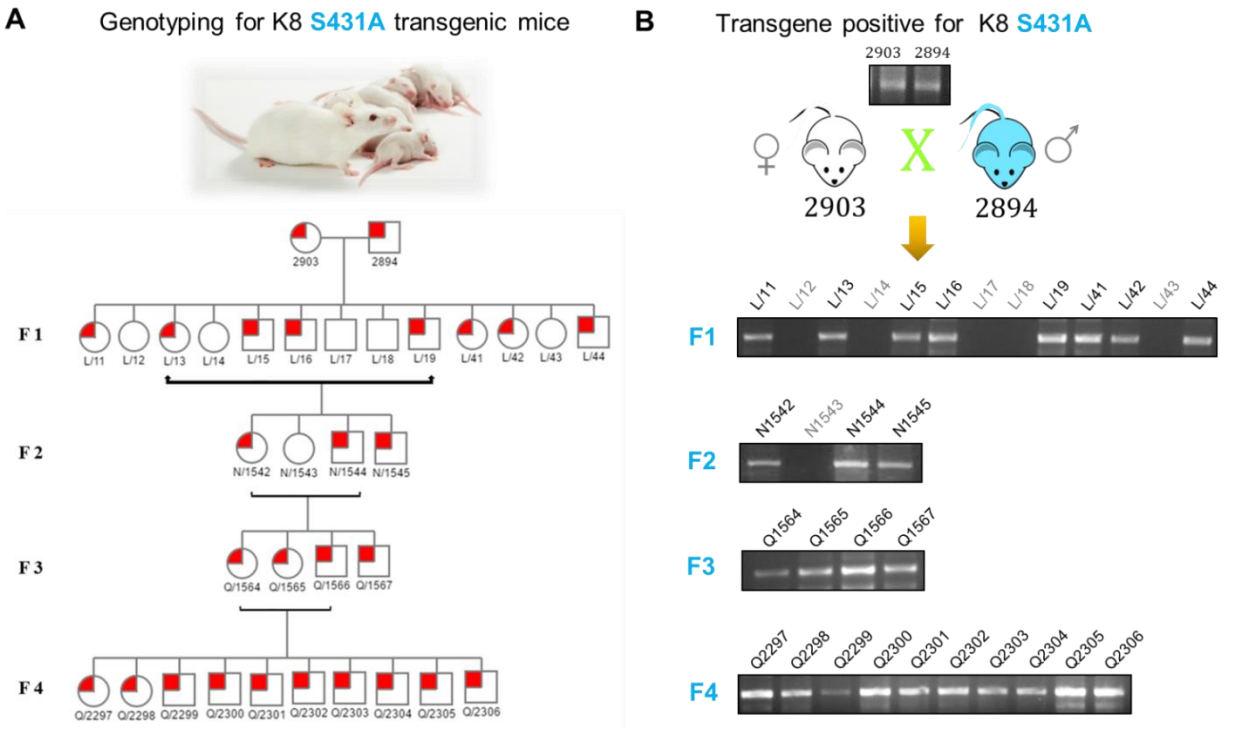

Figure 4.1.3.2.4: Inbreeding and genotyping of K14-K8 S431A GFP expressing transgenic mice: (**A**) Pedigree analysis for pre-founder mice 2903 (female) and 2894 (male) showing germ-line transmission of the transgene. Individual mice were assigned numbers for further experiments. (**B**) Genomic DNA amplification using primers for EGFP is shown in the gel picture whereas Ptch is used as an internal control.

4.1.3.3 Validation of transgene expression at protein level: To validate the expression of the transgene in case of K8 wild type and phosphomutant transgenic mice, few of the transgene positive mice were sacrificed and the skin was collected. The lysates from these tissue samples were prepared in RIPA buffer after separating epidermis from dermis as mentioned in material methods. This was followed by western blotting. Our western blotting data showed an 82kD high molecular weight band for transgene whereas negative control (the tissue samples from normal mice) did not show any signal at the same position. This further confirmed that the PCR positive mice are able to express the transgene at protein level (**Figure 4.1.3.3 A, B, C**). In addition, the tail snips were taken and paraffin embedded blocks were prepared for all the PCR positive pups.

The transverse sections of the tail snips were further used to perform tissue immunofluorescence with keratin 8 and GFP antibody. Nucleus was counter stained with DAPI. The tail sections of the normal FVB/j mice were used as a negative control. The immunofluorescence images show both GFP as well as K8 expression in the different layers of skin epithelia of PCR positive pups whereas negative control showed a faint signal mostly at the stromal region (**Figure 4.1.3.3 D, E, F, G)**.

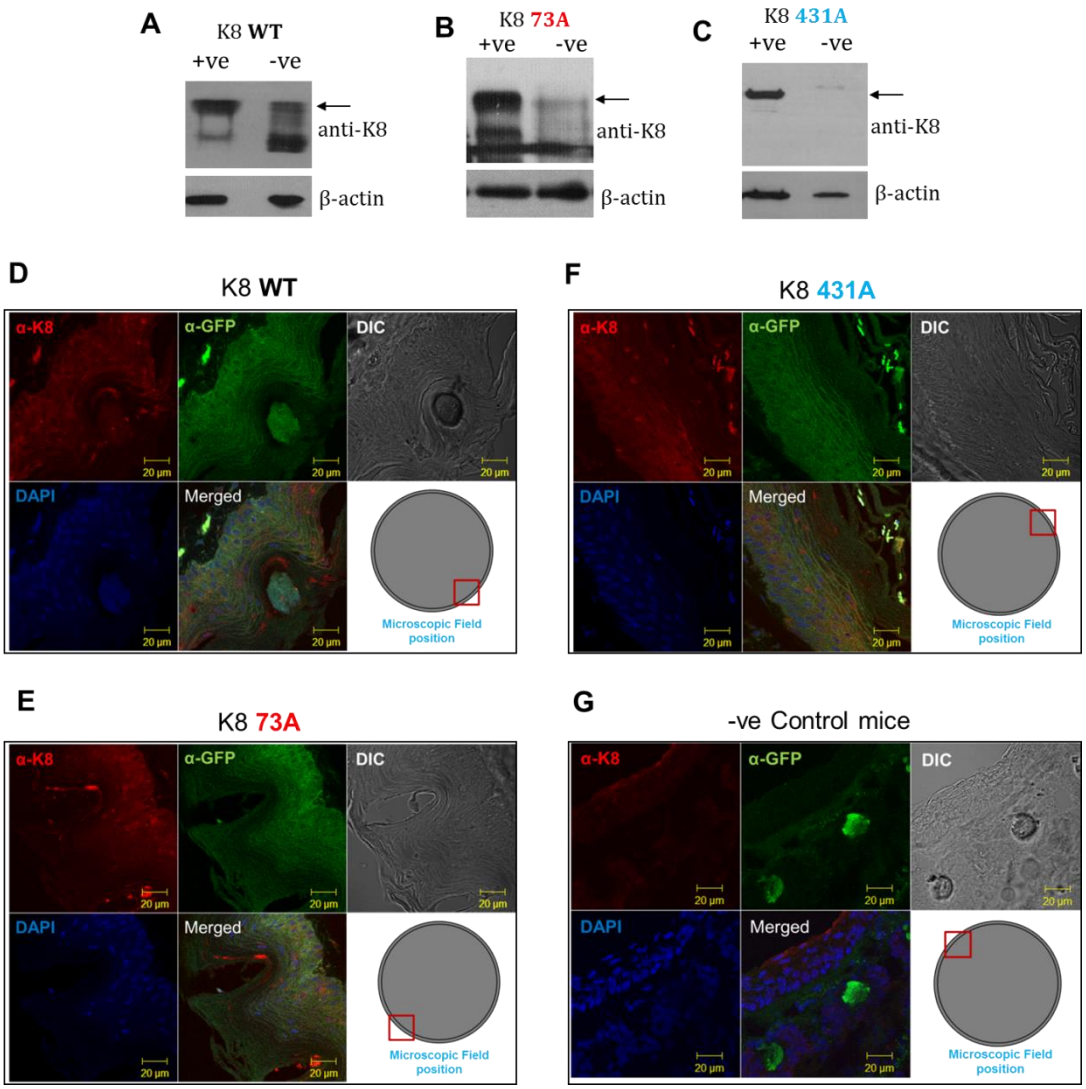

Figure 4.1.3.3: Biochemical and histological validation of K8-GFP expression in respective transgenic mice: (**A-C**) Representative western blot images of K8 GFP expression in the skin epidermal tissue lysates of transgene positive mice for K8 WT GFP (**A**), K8 S73A GFP (**B**), K8 S431A GFP (**C**).

Antibody against human K8 was used for the validation of K8 GFP resulting in an 82kD high molecular weight band. *β*-actin was used as a loading control. The skin tissue lysates of a non-transgenic normal (FVB/j) mice was used as a negative control. (**D, E, F, G**) Immunofluorescence analysis of mice for K8 GFP expression. Paraffin embedded skin tissue sections for all the three constructs were stained with the antibodies against GFP (green, Alexa flour 488) and K8 (red, Alexa flour 568). Nucleus was counterstained with DAPI (blue) in all the cases. Skin sections of non-transgenic mice were used as a negative control.

4.2 DMBA TPA mediated skin carcinogenesis to understand the role of K8 phosphorylation in neoplastic progression of skin SCC:

To determine the exact role of site specific K8 phosphorylation in neoplastic progression of skin SCC *in vivo*, DMBA TPA mediated skin carcinogenesis was performed. To begin with, minimum of three transgene positive pups, for all the three constructs (pCCL-K14-K8 WT/ S73A/ S431A GFP) were subjected to DMBA TPA mediated skin carcinogenesis protocol. For this 3-4 weeks old transgene positive pups were first subjected to DMBA treatment thrice for one week. Post DMBA treatment TPA was applied to the skin of these mice twice a week till the formation of tumor. In the present study, we followed the tumor progression in the stepwise manner mice till 35^{th} week for all the three groups of transgenic mice. In the K8 WT GFP group two of the mice showed an earlier onset of tumors after one week of TPA application which further progressed towards a full grown tumor of ~12-14mm by 6^{th} week. One of the K8 WT GFP mice showed regression of the tumor after 4^{th} week of TPA application possibly because of metastasis. The TPA treatment for this mouse is still ongoing. Furthermore, both K8 phosphodead (K8 S73A and K8 S431A) expressing mice showed delayed onset of tumor after 15^{th} and 9^{th} week of TPA application, respectively. In addition, the K8 S431A expressing mice progressed towards full grown tumors by 16^{th} week of TPA application. Altogether, in concordance with our *in vitro* data (as presented in this thesis in the next part results 4.3), this preliminary observations suggest that K8 phosphorylation may provide an increased aggressiveness to the tumors during neoplastic

progression of skin SCC. Besides this, on the basis of this pilot experiment, minimum 18 mice from each group (K8 WT/ S73A/ S431A GFP) are being treated with DMBA/TPA mediated skin carcinogenesis to further strengthen our hypothesis. This will also overcome the effects of genetic heterogeneity and environment and will allow us to better extrapolate the results **(Figure 4.2.1 and 4.2.2).**

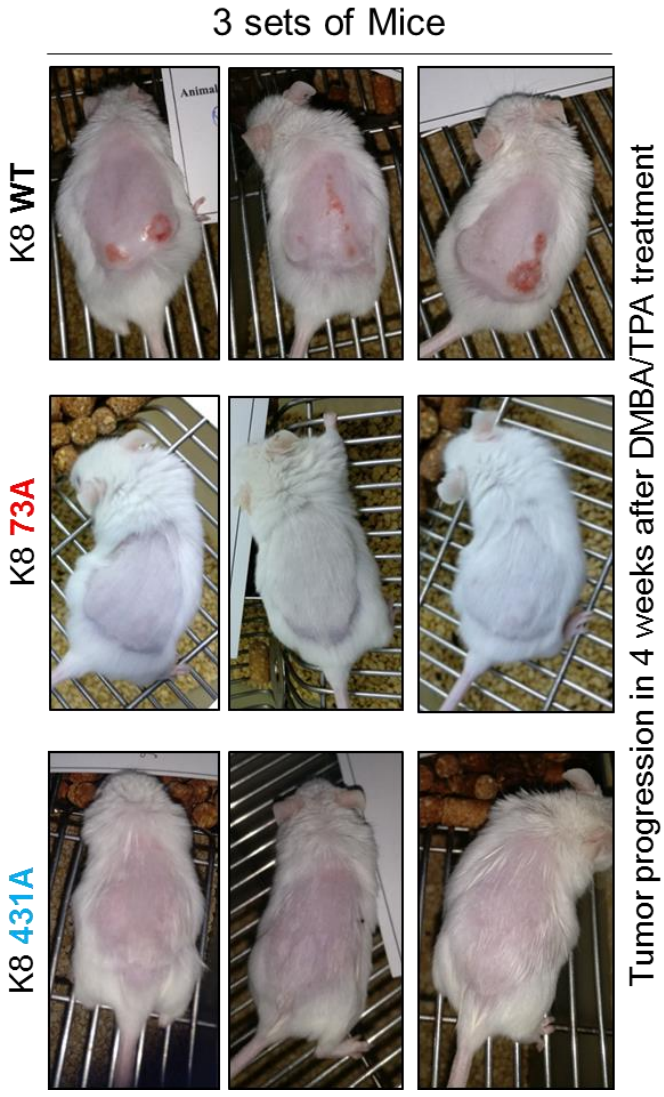

Figure 4.2.1: DMBA –TPA mediated skin carcinogenesis of transgenic mice: Tumor progression after 4 weeks of DMBA-TPA application in three sets of mice; K8 WT GFP, K8 S73A GFP and K8 S431A GFP (n= 3) in a pilot experiment.

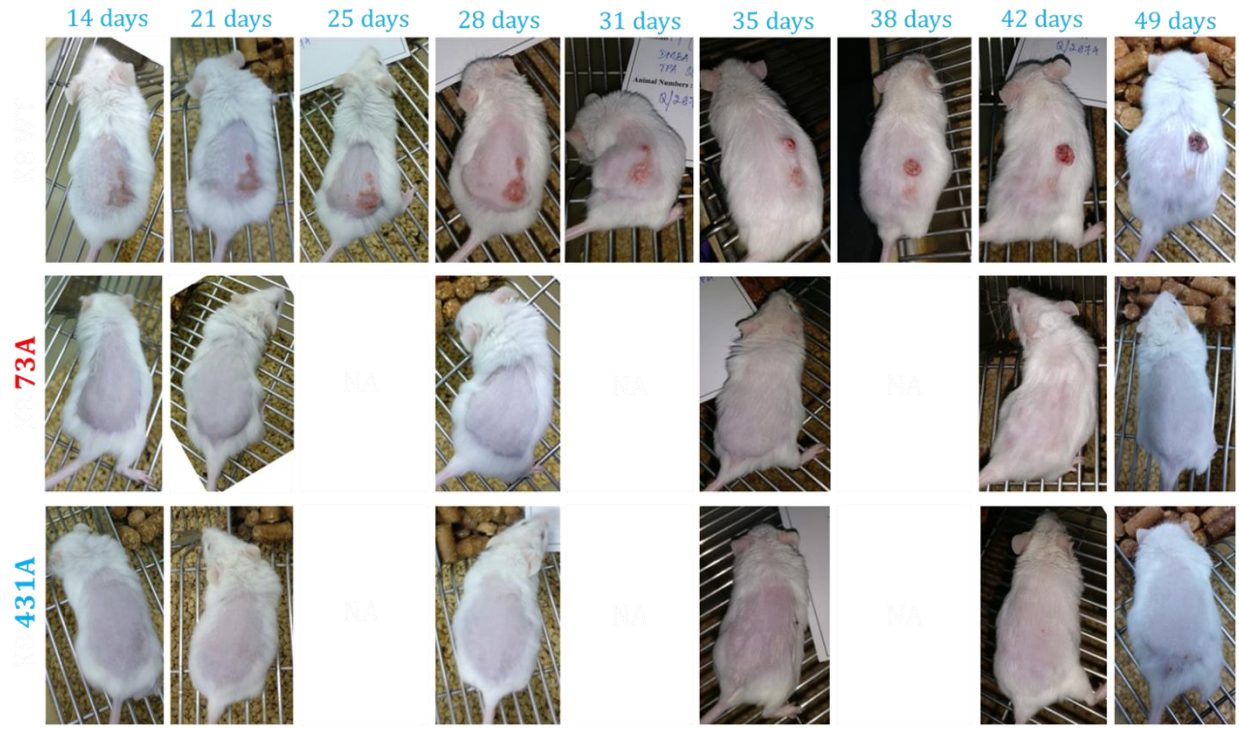

Figure 4.2.2: Sequential changes after DMBA –TPA mediated skin carcinogenesis of transgenic mice: The representative images of all the three sets of mice during DMBA-TPA application. Images were taken initially once a week and then every 3rd day for all the mice till 49th day of TPA application.

4.3 To investigate the role of K8 in neoplastic progression of Skin SCC derived A431 cells:

4.3.1 Generation of stable clones:

In order to generate stable K8 knockdown and vector control clones, the shRNA construct, shRNA-K8.2 or the empty vector control (pTU6 puro) were transfected into the skin SCC derived A431 cell line. K8 knockdown clones showed a significant reduction in K8 protein as well as RNA levels upto 80% (**Figure 4.3.1A & B**). The immunofluorescence imaging showed a substantial reduction in K8 filament formation with K18 (the preferential binding partner) (**Figure 4.3.1 C**). There was no change in mRNA levels of K18 indicating that the reduction in K18 was due to the decreased stability of the protein in absence of its type II binding partner (**Figure 4.3.1 B**). We

also observed a significant upregulation of K7 at protein level, which is a probable binding partner of K18 in the absence of K8 (**Figure 4.3.1 A**). Immunofluorescence imaging for K18 showed a significant reduction in their protein level together with the loss of normal filament architecture suggesting that K7/18 might be forming proto-filaments rather than complete filaments after K8 knockdown (**Figure 4.3.1 C**).

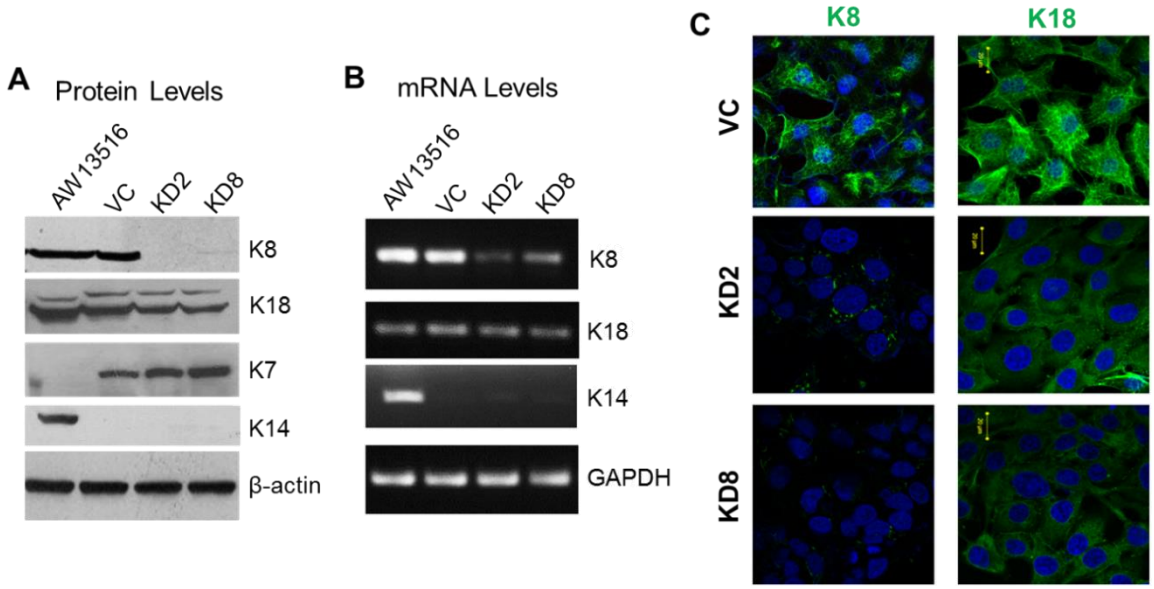

Figure 4.3.1 Establishment of K8 knockdown clones in A431 cells: (**A**) Western blot analysis of pTU6 vector control (VC) and knockdown clones (KD2/KD8) derived from A431 cells with antibodies to K8, K18, K7, respectively. *β*-actin was used as a loading control. Cell lysate from AW13516 cell line was used as a positive control. (**B**) RT-PCR analysis of K8 and K18 in pTU6 vector control (VC) and stable K8 knockdown clones (KD2/KD8). GAPDH was used as internal control. cDNA from AW13516 cell line was used as a positive control (**C)** Immunofluorescence analysis of K8 and K18. Note: Significant decrease in K8 levels and defective filament architecture in K8 knockdown clones compared to vector control cells. Keratin 8 was stained with alexa flour 488 (Green) whereas the nucleus is counter stained with the DAPI (Blue), (Scale bars: 10μm).

4.3.2 K8 knockdown leads to a reduction in the tumorigenic potential of A431 cells both *in vitro* and *in vivo*:

4.3.2.1 Reduction in cell motility and Invasion: To assess the effect of K8 knockdown on migratory potential of A431 cells, scratch-wound healing assay was performed. K8 knockdown

cells (KD2 and KD8) showed a significant reduction (by ~50-60%) in cell motility compared to vector control cells ($p < 0.0001$) (**Figure 4.3.2.1 A**). Further, invasive potential of K8 knockdown cells compared to vector control cells was determined by Boyeden chamber matrigel invasion assay. K8 knockdown cells (KD2 and KD8) showed a significant decrease ($p < 0.001$ and 0.0005 respectively) in the invasive potential compared to vector control cells (by ~60-70%) (**Figure 4.3.2.1 B**).

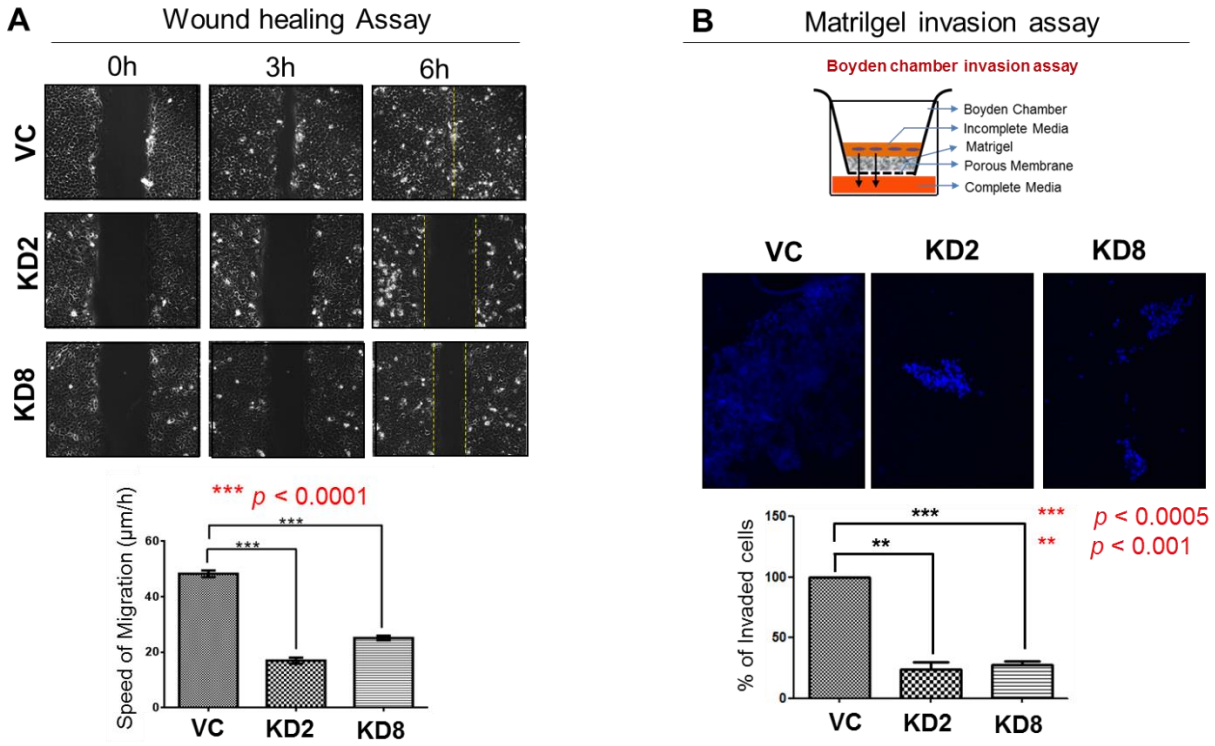

Figure 4.3.2.1 K8 knockdown resulted in reduced cell migration and invasion: (**A**) Scratch wound healing assay of pTU6 vector control (VC) and K8 knockdown clones (KD2/KD8). Phase contrast images (10X) of wound closure at 0, 3 and 6h are shown (upper panel) (Scale bar: 100µm). Migration rate was calculated by AxioVision software. The data shown is the average from three independent experiments with the mean and standard deviation ($p < 0.0001$) as shown in the bar graph (lower panel). (**B**) Boyden chamber invasion assay of pTU6 vector control (VC) and K8 knockdown clones (KD2/KD8). Membrane filter inserts were coated with Matrigel and cells were seeded in the upper chamber. After 12h of incubation, the cells that invaded through the membrane were stained with DAPI and images were captured using upright microscopy. A representative field for each clone has been shown in the figure. (Magnification- 20X) (Upper panel). Cell invasion was quantified by counting cells in all the fields using Metamorph software.

The data shown is the average from three independent experiments with the mean and standard deviation ($p < 0.001$ and 0.0005 for KD2 and KD8 respectively) (Lower panel).

4.3.2.2 Soft Agar Assay showed reduction in colony formation:

In order to find out the effects of K8 down-regulation on tumorigenic potential of A431 cells, soft agar assay was performed on the K8 knockdown (KD2/KD8) and vector control cells. A significant reduction was observed in size (by ~60-70%; $p < 0.0005$) and number of colonies formed (by ~50-60%; $p < 0.0005$ and $p < 0.001$) of K8 knockdown cells in soft agar colony formation assay compared with vector control cells (**Figure 4.3.2.2 A**).

4.3.2.3 Reduction in Cell proliferation and clonogenic potential of A431 cells:

To evaluate the effect of K8 knockdown on proliferative potential of A431 cells, MTT cell viability and clonogenic assays were performed. K8 knockdown clones showed a significant reduction in proliferation compared to vector control cells in MTT cell viability assay (**Figure 4.3.2.2 B**). In correlation with this clonogenic assay demonstrated a significant reduction in number of colonies (by ~70-80%) in K8 knockdown clones compared to vector control clone ($p < 0.0005$ and $p < 0.001$) (**Figure 4.3.2.2 C**). Together with this, there was a visible decrease in colony size in K8 knockdown clones compared to vector control clone.

4.3.2.4 *In vivo* tumorigenicity assay:

Further, *in vivo* tumorigenicity potential of K8 knockdown clones and vector control clone was assessed by sub-cutaneous injection in NOD SCID mice. The representative pictures of mice injected for each of the clones is given in the **Figure 4.3.2.4 A**. There was a delayed onset of tumor formation in K8 knockdown cells i.e. 2 weeks post subcutaneous injection whereas, the vector control cells formed tumors within 1 week.

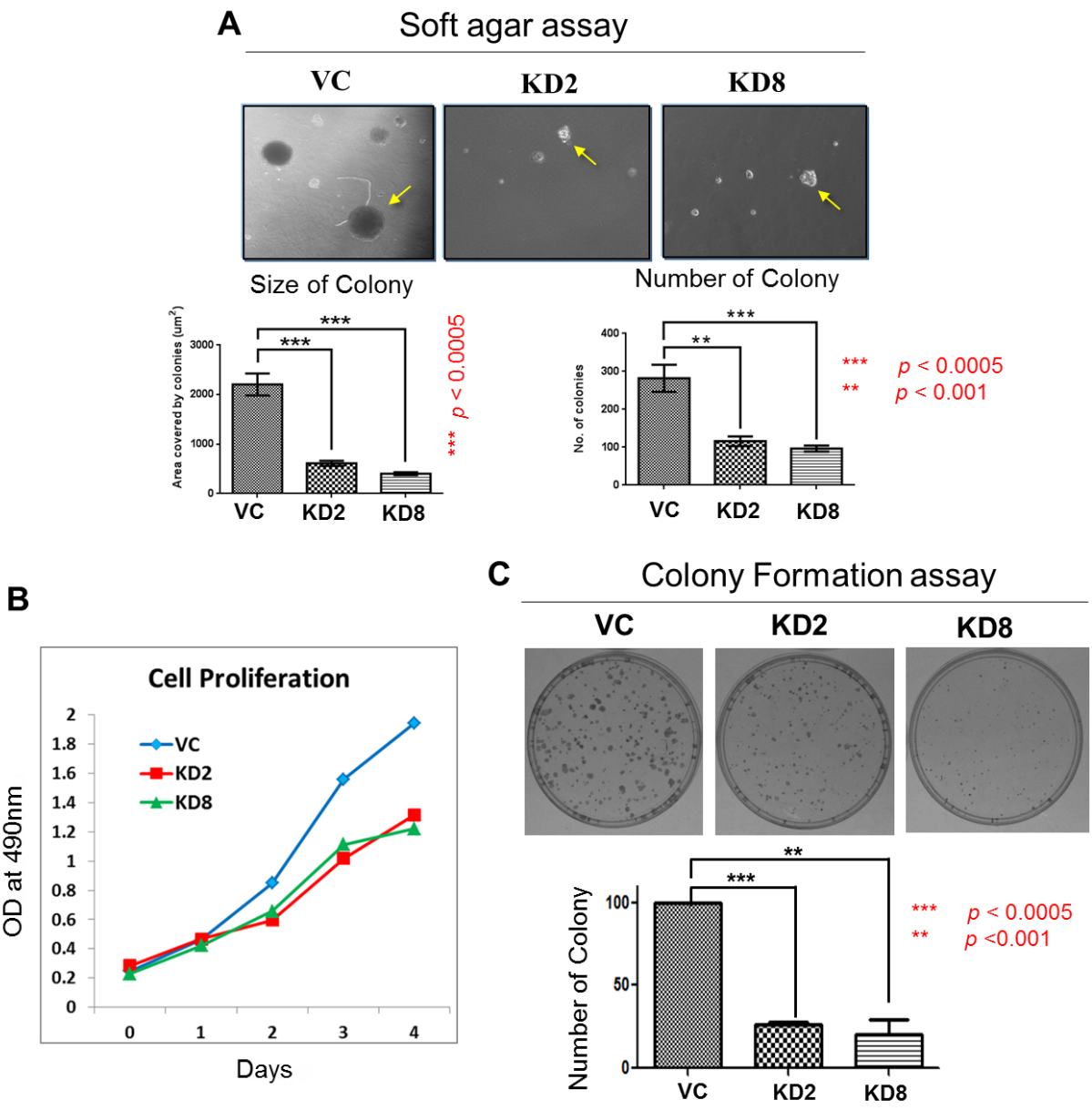

Figure 4.3.2.2: K8 knockdown resulted in reduced soft agar colony formation and proliferative potential of A431 cells: (**A**) Representative phase contrast (10X) images of soft agar colonies of the pTU6 vector control (VC) or K8 knockdown clones (KD2/KD8) after 14 days (Upper panel). Bar graph shows the total number of colonies formed per plate by the respective clones. Mean and standard deviation of 3 independent experiments is plotted for size (p<0.0005) and number of colonies (p< 0.001 and 0.0005) formed, (Lower panel). (**B**) Cell proliferation curve of pTU6 vector control and K8 knockdown (KD2/KD8) cells using MTT assay. Fifteen hundred cells were plated per well in 96 well plates; medium was changed every 2 days. The cell number was determined at the times indicated using MTT assay. Each point represents the mean and the standard errors of three independent experiments done in triplicate. (**C**) Representative images of Colony-forming assay of pTU6 vector control and K8 knockdown (KD2/KD8) cells

after staining with crystal violet (Upper panel). Bar graph shows the total number of colonies formed per plate by the respective clones. Mean and standard deviation of 3 independent experiments is plotted for the number of colonies ($p < 0.001$ and $p < 0.0005$) formed (Lower panel).

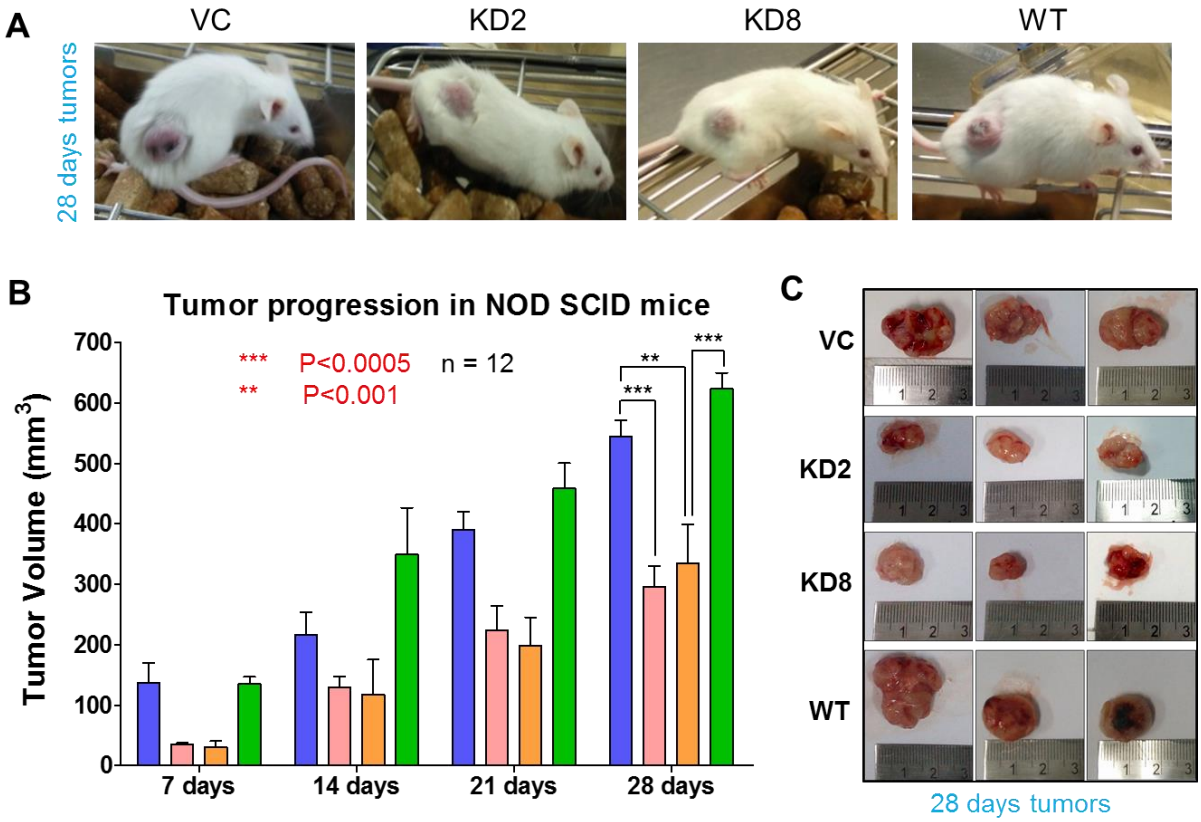

Figure 4.3.2.4: K8 knockdown resulted in reduced tumorigenicity: (**A**) Representative images of NOD/SCID mice bearing tumors of pTU6 vector control (VC), K8 knockdown (KD2/KD8) and K8 WT clones after 28 days of the injection. (**B**) Tumor growth was plotted against time interval of 3 independent experiments done in triplicate (Total 12 animals were injected for each clone). **Note**: Decreased tumorigenicity in K8 knockdown clones ($p < 0.0005$ and $p < 0.001$) and rescue of phenotype in K8 WT clone ($p < 0.0005$). (**C**) Representative images of excised tumors after sacrificing the mice injected for each of the clones.

The mean volume of the tumors formed by K8 knockdown clones was significantly lowered than the average volume of tumors formed by the vector control cells ($p < 0.0005$ and $p < 0.001$) (**Figure 4.3.2.4 B and C**). To determine that the effects associated with K8 knockdown were not due to off

target effects of the shRNA, a rescue experiment was performed using the construct K8 WT GFP which is resistant to the shRNA, "shRNAK8.2". The stable clones expressing K8 WT GFP showed an early onset and large tumor volume, in the *in vivo* tumorigenicity assay compared to K8 knockdown cells ($p < 0.0005$). This suggested a reversal in the tumorigenic potential of A431 cells upon re-expression of K8 WT GFP in K8 deficient background (**Figure 4.3.2.4 B and C**).

4.3.3 Deciphering molecular mechanism associated with K8 mediated regulation of tumorigenic potential of A431 cells: To understand the molecular basis behind K8 mediated regulation of tumorigenic potential of A431 cells, TMT based quantitative total proteomics was performed for VC, KD2 and KD8 clones at IOB Bangalore (**Figure 4.3.3.1 A & B**). There were a total of 2952 proteins detected in the TMT based total quantitative proteomics, out of which, KD2 clone showed 140 proteins to be differentially expressed whereas, KD8 clone showed 122 proteins to be differentially expressed in comparison to vector control cells (**Figure 4.3.3.1C**). Venn diagram analysis showed 78 common proteins to be significantly altered (up/downregulated) in both the K8 knockdown clones compared to vector control cells (**Figure 4.3.3.1D & E**). Furthermore, the heat-map was plotted for the differentially regulated proteins (with a cut off of 1.5 fold) in response to K8 downregulation. The heat map clearly indicated common proteins which are deregulated among both the knockdown clones (**Figure 4.3.3.2**).

In order to evaluate the global changes upon keratin knockdown we performed Ingenuity pathway analysis (**Figure 4.3.3.3A**) which showed significant alterations in cellular pathways like cancer, cell motility, cell death and survival, cellular growth and proliferation, cell morphology, apoptosis *etc.* (**Figure 4.3.3.3 B**). The associated molecules which demonstrated a substantial level of differential expression included TMS1, Rho GDI2, MARCKSL1, RANBP1, 14-3-3γ, CDK6,

EIF6, SHIP1 (**Figure 4.3.3.3 C**). For authentication of the MS/MS data quantitative spectra were generated for some of these proteins (**Figure 4.3.3.4 A-D, F**) and were considered for further validation and pathway analysis. Together with this our MS/MS data also confirmed a significant reduction in K8 protein levels in both the K8 knockdown clones which could be verified by the quantitative spectra shown in the **Figure 4.3.3.4 E**. To our surprise, apart from these important signaling molecules, some of the keratins like K5, K17 and K15 were also found to be significantly downregulated (quantitative spectra are shown in the **Figure 4.3.3.4 G, H**) after K8 knockdown. Therefore, we went ahead to decipher the mechanism associated with altered keratin expression.

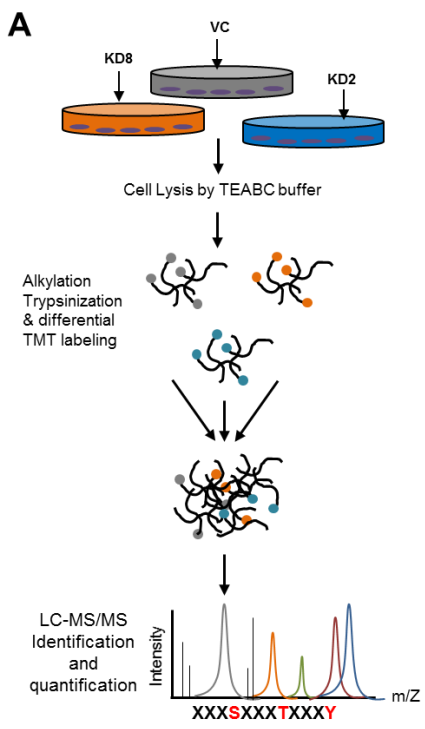

B

		m/z
VC	128N, 128C	128.12, 128.13
KD8	129N, 129C	129.13, 129.14
KD2	130C, 131	130.14, 131.14

C

Cell type	≥ 1.5 fold-up ≥ 1.5 fold-down	No. of proteins
KD8	Up-regulated	81
	Down-regulated	41
KD2	Up-regulated	64
	Down-regulated	76

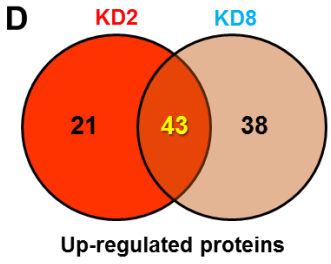

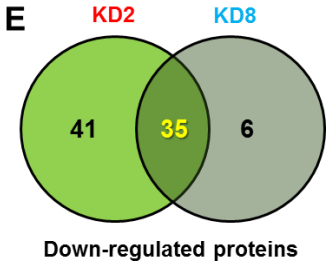

Figure 4.3.3.1: TMT based Differential quantitative proteomics after K8 knockdown in A431 cells: (A) A representative image showing the protocol used for TMT based quantitative proteomics. (B) The table depicts TMT tags used for quantitative proteomics. (C) The table shows differentially expressed proteins in both the K8 knockdown clones (KD2/KD8) compared to vector control cells with a cut off of ≥ 1.5 fold.

Gene Symbol	Description	KD8	KD2
KLF16	Krueppel-like factor 16	3.532	2.669
HMGCS1	hydroxymethylglutaryl-CoA synthase, cytoplasmic	2.831	1.824
ITGB5	integrin beta-5 precursor	2.716	3.373
FAM83H	protein FAM83H	2.316	1.769
PYCARD	apoptosis-associated speck-like protein containing a CARD isoform b	2.312	6.076
FAR1	fatty acyl-CoA reductase 1	2.008	1.652
FDFT1	squalene synthase isoform 1	1.886	1.616
CYCS	cytochrome c	1.879	1.549
CDK6	cyclin-dependent kinase 6	1.863	2.781
LAMC2	laminin subunit gamma-2 isoform b precursor	1.798	1.692
SERPINE1	plasminogen activator inhibitor 1 precursor	1.761	2.488
EGFR	epidermal growth factor receptor isoform a precursor	1.753	1.626
MARCKSL1	MARCKS-related protein	1.74	2.487
ABCE1	ATP-binding cassette sub-family E member 1	1.722	1.688
ACADSB	short/branched chain specific acyl-CoA dehydrogenase, mitochondrial precursor	1.719	1.524
PLAU	urokinase-type plasminogen activator isoform 2	1.687	1.874
MPI	mannose-6-phosphate isomerase isoform 3	1.67	1.63
PTGS1	prostaglandin G/H synthase 1 isoform 5	1.666	1.716
PKN1	serine/threonine-protein kinase N1 isoform 1	1.656	1.585
LANCL2	lanC-like protein 2	1.642	1.626
COX6A1	cytochrome c oxidase subunit 6A1, mitochondrial	1.632	2.2
RHOC	rho-related GTP-binding protein RhoC precursor	1.632	1.559
GLI1	zinc finger protein GLI1 isoform 3	1.629	1.587
TUBB4B	tubulin beta-4B chain	1.629	1.558
LGALS1	galectin-1	1.622	1.541
HSPA5	78 kDa glucose-regulated protein precursor	1.618	1.634
RHOA	transforming protein RhoA precursor	1.603	1.644
PSMD5	26S proteasome non-ATPase regulatory subunit 5 isoform 2	1.596	1.594
SAMD9	sterile alpha motif domain-containing protein 9	1.556	1.561
CHP1	calcineurin B homologous protein 1	1.555	1.548
SH3BGRL2	SH3 domain-binding glutamic acid-rich-like protein 2	1.546	1.564
GALK2	N-acetylgalactosamine kinase isoform 3	1.544	1.559
FAM129B	niban-like protein 1 isoform 2	1.539	1.576
GIGYF2	PERQ amino acid-rich with GYF domain-containing protein 2 isoform c	1.534	1.551
SURF4	surfeit locus protein 4 isoform 3	1.532	1.634
CYP51A1	lanosterol 14-alpha demethylase isoform 2	1.53	1.932
ARHGDIB	rho GDP-dissociation inhibitor 2	1.529	1.848
YWHAG	14-3-3 protein gamma	1.522	1.778
ARL8B	ADP-ribosylation factor-like protein 8B	1.511	1.543
PON2	serum paraoxonase/arylesterase 2 isoform 2	1.509	1.897
MALSU1	mitochondrial assembly of ribosomal large subunit protein 1	1.507	1.524
NUP50	nuclear pore complex protein Nup50 isoform a	1.505	1.588
RAB3D	ras-related protein Rab-3D	1.504	1.568
KRT18	keratin, type I cytoskeletal 18	0.649	0.595
SLC7A5	large neutral amino acids transporter small subunit 1	0.647	0.567
PSPH	phosphoserine phosphatase	0.64	0.594
FGFR1OP	FGFR1 oncogene partner isoform c	0.627	0.564
RNASET2	ribonuclease T2 precursor	0.62	0.542
LZTS2	leucine zipper putative tumor suppressor 2	0.612	0.483
ADA	adenosine deaminase	0.611	0.546
UBE2L3	ubiquitin-conjugating enzyme E2 L3 isoform 3	0.603	0.649
LRRC16A	leucine-rich repeat-containing protein 16A isoform 2	0.599	0.363
SNCG	gamma-synuclein	0.598	0.639
KRT5	keratin, type II cytoskeletal 5	0.595	0.532
INPP5D	phosphatidylinositol 3,4,5-trisphosphate 5-phosphatase 1 isoform b	0.592	0.575
KIF2C	kinesin-like protein KIF2C	0.59	0.431
ANXA11	annexin A11 isoform 2	0.589	0.496
KRT17	keratin, type I cytoskeletal 17	0.587	0.497
MYBPC2	myosin-binding protein C, fast-type	0.587	0.48
PDCD4	programmed cell death protein 4 isoform 3	0.584	0.659
ACTN1	alpha-actinin-1 isoform b	0.583	0.578
MRPL44	39S ribosomal protein L44, mitochondrial	0.583	0.499
NT5C2	cytosolic purine 5'-nucleotidase	0.573	0.608
BID	BH3-interacting domain death agonist isoform 2	0.57	0.578
RANBP1	ran-specific GTPase-activating protein isoform 3	0.568	0.636
GID8	glucose-induced degradation protein 8 homolog	0.565	0.581
ANXA8L1	annexin A8-like protein 1 isoform 1	0.562	0.637
FAM213A	redox-regulatory protein FAM213A isoform 2 precursor	0.556	0.602
EIF1B	eukaryotic translation initiation factor 1b	0.541	0.609
BCAM	basal cell adhesion molecule isoform 2 precursor	0.529	0.642
CRTAP	cartilage-associated protein precursor	0.522	0.601
GSTK1	glutathione S-transferase kappa 1 isoform c	0.52	0.344
CDC23	cell division cycle protein 23 homolog	0.504	0.467
GSTM1	glutathione S-transferase Mu 1 isoform 2	0.49	0.599
GFPT2	glutamine--fructose-6-phosphate aminotransferase [isomerizing] 2	0.444	0.428
CAV1	caveolin-1 isoform alpha	0.405	0.563
KRT8	keratin, type II cytoskeletal 8 isoform 2	0.255	0.159
KRT15	keratin, type I cytoskeletal 15	0.161	0.102

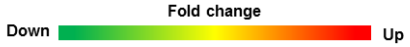

Figure 4.3.3.2: Heat map of differentially expressed (≥1.5 Fold) proteins in KD2 and KD8 cells in comparison to VC cells. The values ≥1.5 represents the upregulated genes and ≤0.66 represents the downregulated genes. The color code represents to the fold change in relative levels of protein expression.

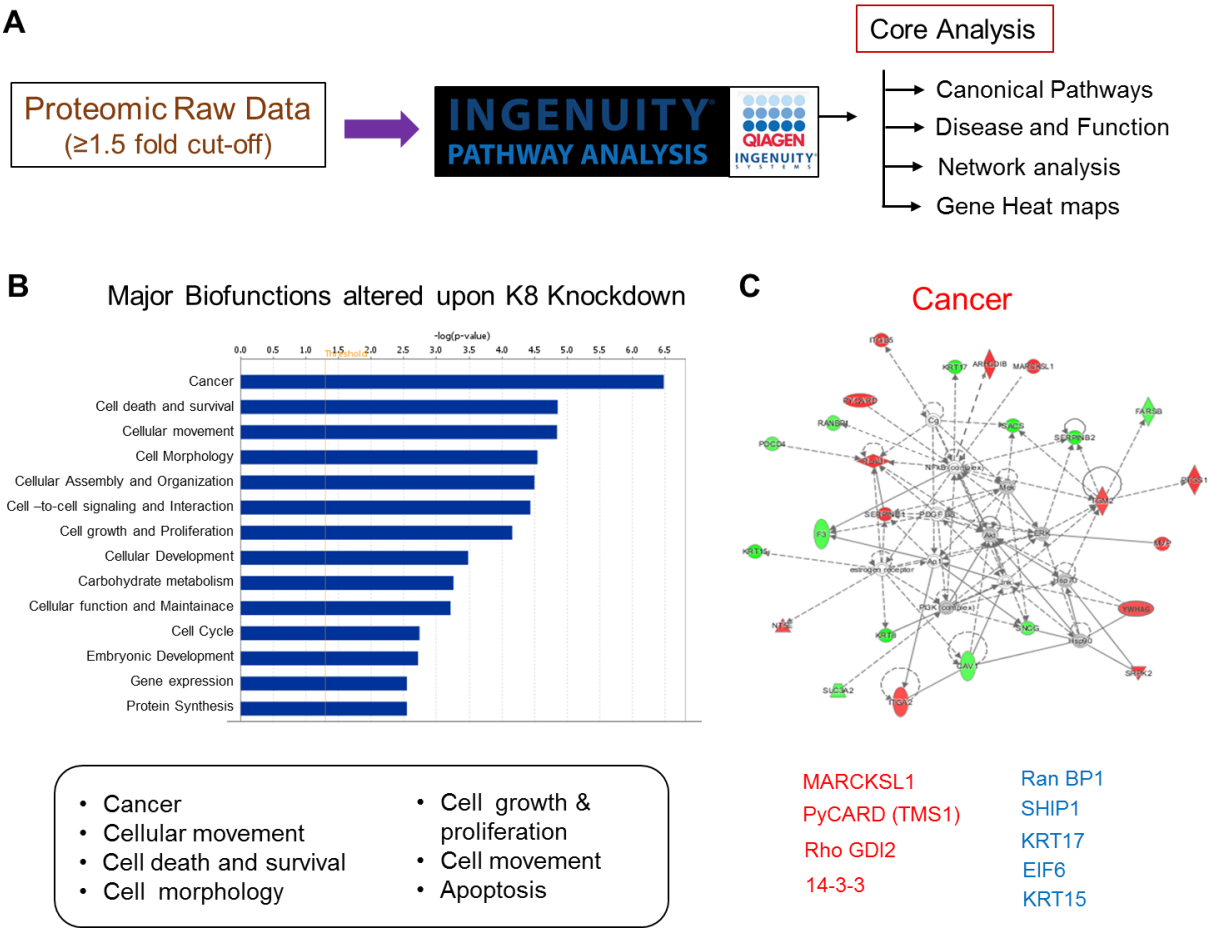

Figure 4.3.3.3: IPA analysis of differential quantitative proteomics data: (**A**) Representative ray diagram showing the protocol followed for IPA analysis. (**B**) The bar graph generated using IPA corresponds to the significantly altered signaling pathways in response to K8 knockdown in A431 cells. A ≥1.5 fold cut off is used to analyze the data. (**C**) A representative IPA network showing differentially regulated proteins belonging to biological pathways like cellular movement and apoptosis. Some of the important proteins are highlighted in the table.

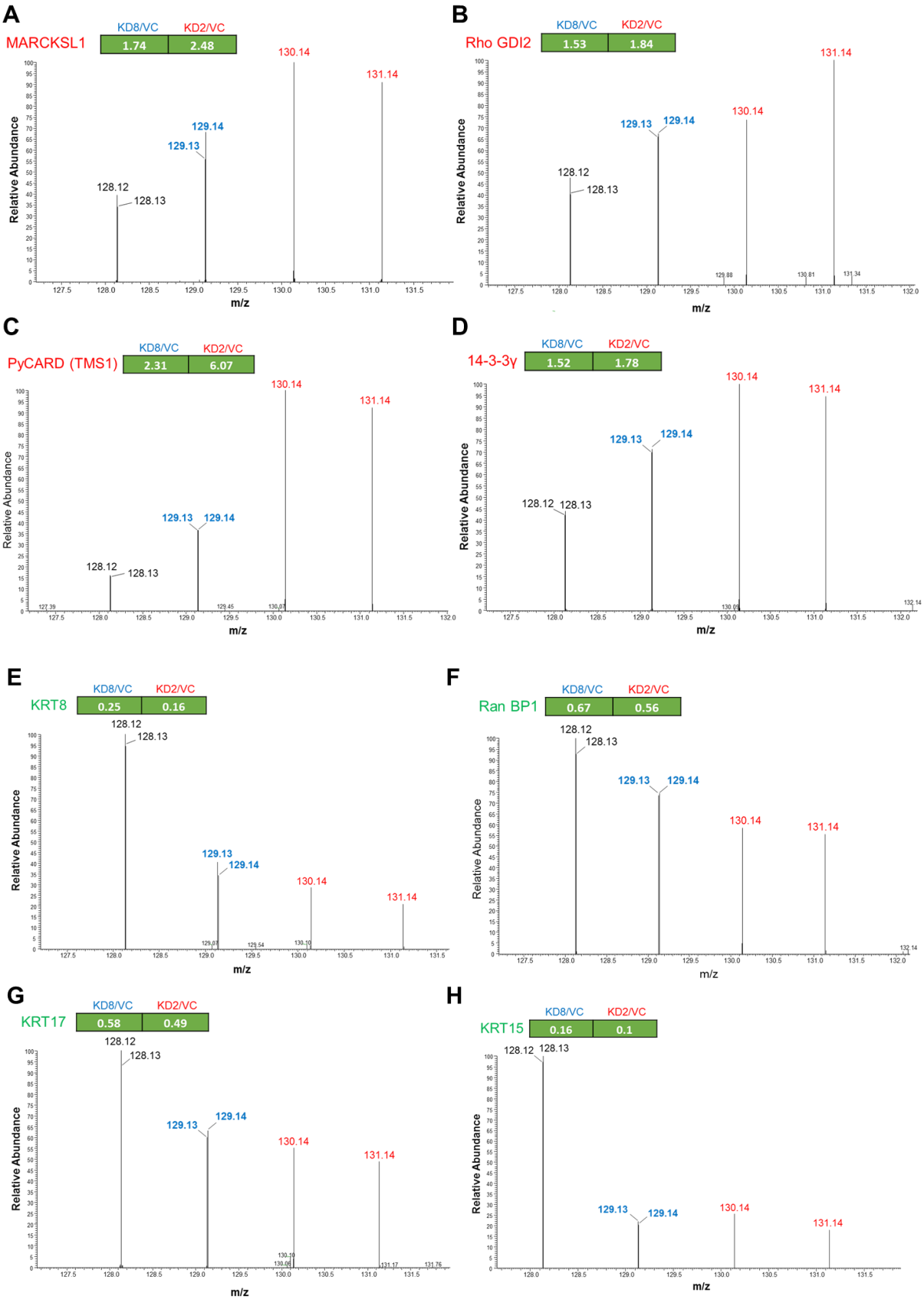
A
MARCKSL1
KD8/VC
KD2/VC
1.74
2.48
B
Rho GDI2
1.53
1.84
C
PyCARD (TMS1)
2.31
6.07
D
14-3-3γ
1.52
1.78
E
KRT8
0.25
0.16
F
Ran BP1
0.67
0.56
G
KRT17
0.58
0.49
H
KRT15
0.16
0.1
Relative Abundance
m/z
128.12
128.13
129.13
129.14
130.14
131.14

Figure: 4.3.3.4: Quantitative MS/MS spectra of differential regulated proteins: Quantitative MS/MS spectra for the upregulated proteins; (**A**) MARCKSL1, (**B**) RhoGDI2, (**C**) PyCARD, (**D**) 14-3-3γ and the downregulated genes (**E**) Keratin 8 (Verifying the K8 knockdown clones), (**F**) RanBP1, (**G**) Keratin 17 (**H**) Keratin15 were generated using Xcalibur version-3.0 software. Representative spectra are shown in the figure. The values in the green boxes represents the relative fold change for the proteins.

4.3.4 Keratin 8 associated changes in keratin 17 expression:

As shown in the quantitative proteomics data, K5/17, another major keratin pair of A431 cells was found to be significantly decreased (~50%) after K8 knockdown. These findings were confirmed by immunoblotting for both K5 and K17 (**Figure 4.3.4A**). Further the transcript levels of these keratins remained unchanged. These results suggest that down regulation of K5/17 upon K8 knockdown could be because of alterations in their protein synthesis or turnover (**Figure 4.3.4 B**). In addition, changes in the filamentous network of K5/17 could be observed after keratin 8 knockdown compared to vector control cells by immunofluorescence analysis. We could observe a significant reduction in the levels of K5/17 together with disrupted filament organization in both the K8 knockdown clones compared to vector control cells (**Figure 4.3.4 C**). Another possibility was the off target effect of shRNA based gene silencing as majority of keratins show a lot of sequence homology although our semi quantitative RT-PCR analysis ruled out this possibility (**Figure 4.3.4B**). Consistent with our quantitative proteomics and immunoblotting data, immunofluorescence staining of Keratin 5/17 showed considerable down- regulation and disrupted filament architecture in K8 knock down clones compared to vector control cells (**Figure 4.3.4C**).

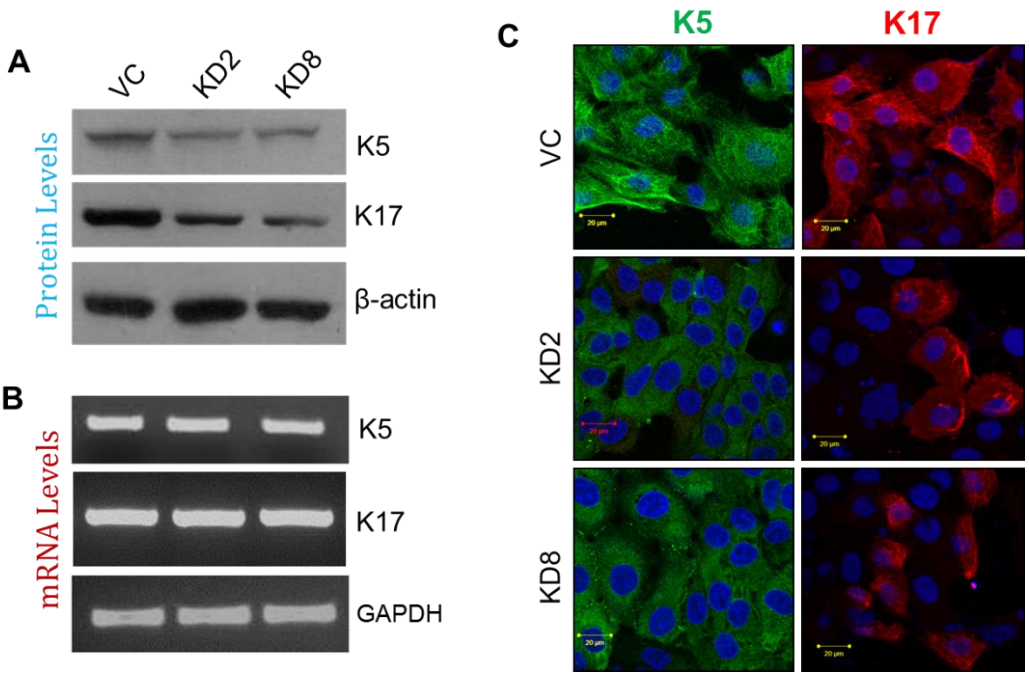

Figure 4.3.4: K8 knockdown leads to reduction in K5/17 levels: (**A**) Western blot and (**B**) RT-PCR analysis of K5 and K17 levels in pTU6 vector control (VC) and both the K8 knockdown clones (KD2/KD8). *β*-actin and GAPDH were used as a loading control, respectively. (**C**) Representative immunofluorescence images of K5/17 showing its protein level as well as filament architecture after K8 downregulation.

4.3.5 Keratin 17 undergoes caspase mediated degradation upon K8 knockdown: Since transcript level of K5/17 was unaffected, we analyzed turnover of these proteins after K8 knockdown. Generally, keratins are very stable proteins and their turnover is more than 48h. The half -life of K17 was drastically reduced to less than 1h in K8 knock down clones in response to CHX (50µg/ml) mediated protein synthesis block for 0 to 24h time points, while K5 showed a half-life of ~12h (**Figure 4.3.5.1 A, B and C**). Although reduction in K5 turnover was also very significant, but it started after 11h of K17 degradation. This suggests that K5 might be getting degraded because of depletion of K17, its preferential binding partner. These results clearly indicate that K8 downregulation affects stability of K17 at protein level which in-turn leads to K5

degradation. Unlike this, K18 levels were consistent in the K8 knockdown clones after CHX treatment suggesting its turnover to be unaffected (**Figure 4.3.5.1 B**).

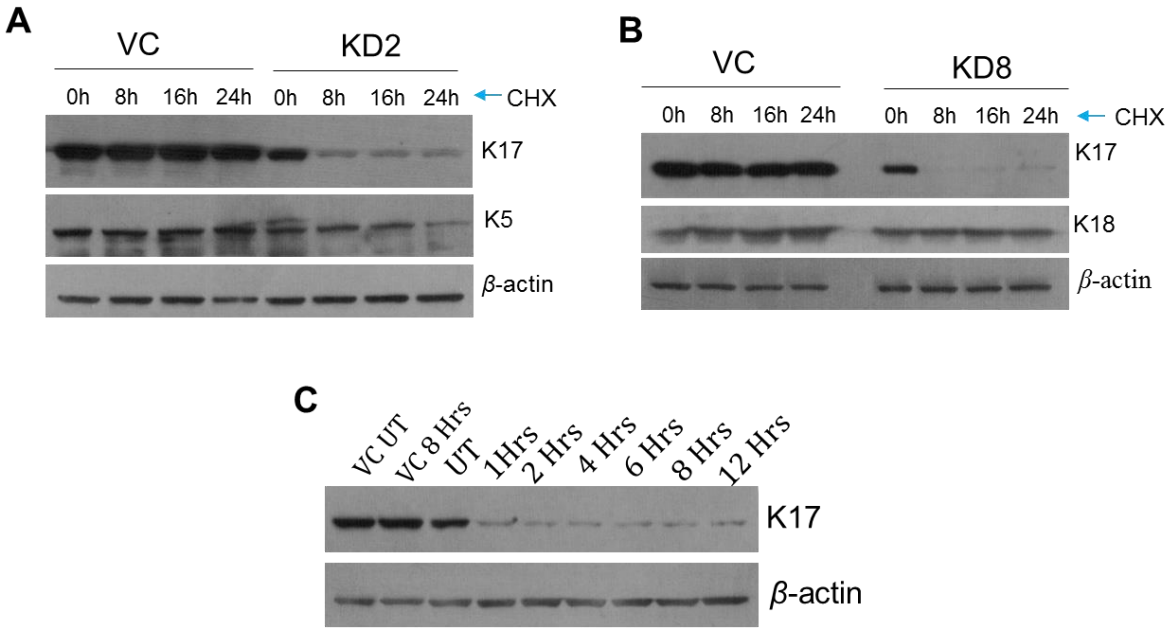

Figure 4.3.5.1: K8 knockdown affects K17 stability: (**A**) Western blot analysis of K5 and K17 levels after CHX treatment (50µg/ml) for 0, 8, 16 and 24h time points in pTU6 vector control (VC) K8 knockdown clone (KD2). (**B**) Western blot analysis of K17 and K18 levels after CHX treatment for 0, 8, 16 and 24h time points in pTU6 vector control (VC) and K8 knockdown clone (KD8). (**C**) Western blot analysis of K17 levels after CHX treatment (50µg/ml) for 0, 1, 2, 4, 6, 8 and 12h time points in pTU6 vector control (VC) and K8 knockdown clone (KD8). *β*-actin was used as a loading control.

Next, to understand the mechanism associated with K17 degradation, we blocked various protein degradation machineries for different time points and assessed stability of K17. For this, the vector control and knockdown cells were treated with specific reagents to block the degradation machinery and at the same time with CHX to block the protein synthesis. For each experiment, untreated (for reagents dissolved in DMSO, media supplemented with required amount of the DMSO served as a vehicle control), only CHX treated, only degradation blocking reagent treated and cells treated with CHX as well as blocking reagent were used. The pattern of K17 degradation was observed for different time points from 0 to 12h by immunoblotting for all the four sets in

vector control and knockdown cells. Proteasomal degradation is known to regulate keratin turnover. Therefore MG132 was used to block proteasomal degradation for different time points till 6h. Immunoblotting followed by proteasomal block did not show any significant alteration in stability of K17 in both the K8 knockdown clones (KD2/KD8) compared to vector control cells (**Figure 4.3.5.2 B**).

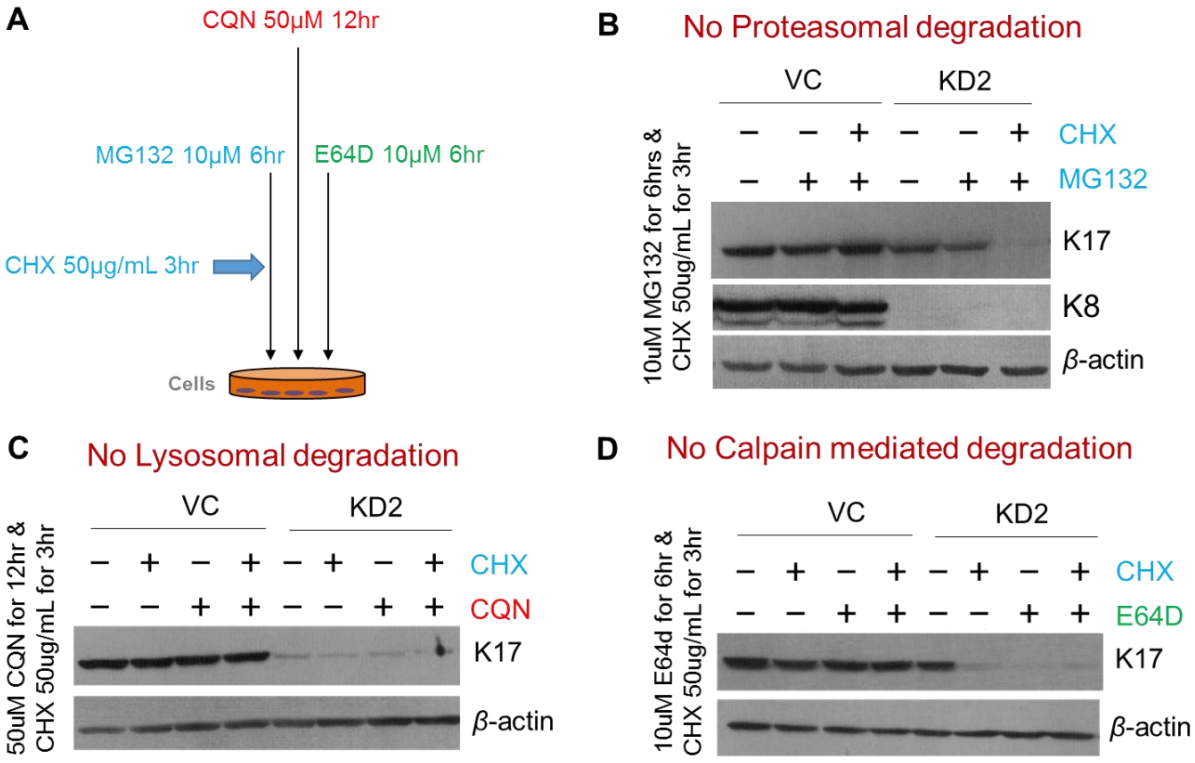

Figure 4.3.5.2: K8 mediated regulation of K17 degradation: (**A**) Schematic representation for CQN, MG132, E64d and CHX treatment protocol used. (**B**) Western blot analysis of K17 levels after treatment with proteasomal inhibitor (MG132-10μM for 6h and CHX 50μg/ml for 3h). (**C**) Western blot analysis of K17 levels after treatment with lysosomal block (CQN-10μM for 12h and and CHX 50μg/ml for 3h) inhibitor. (**D**) Western blot analysis of K17 levels after treatment with Calpain block (E64d-10μM for 6h and CHX 50μg/ml for 3h) inhibitor. **Note:** In each case, cells were treated with 50μg/ml of CHX, 3h prior to completion of the protocol. *β*-actin was used as a loading control.

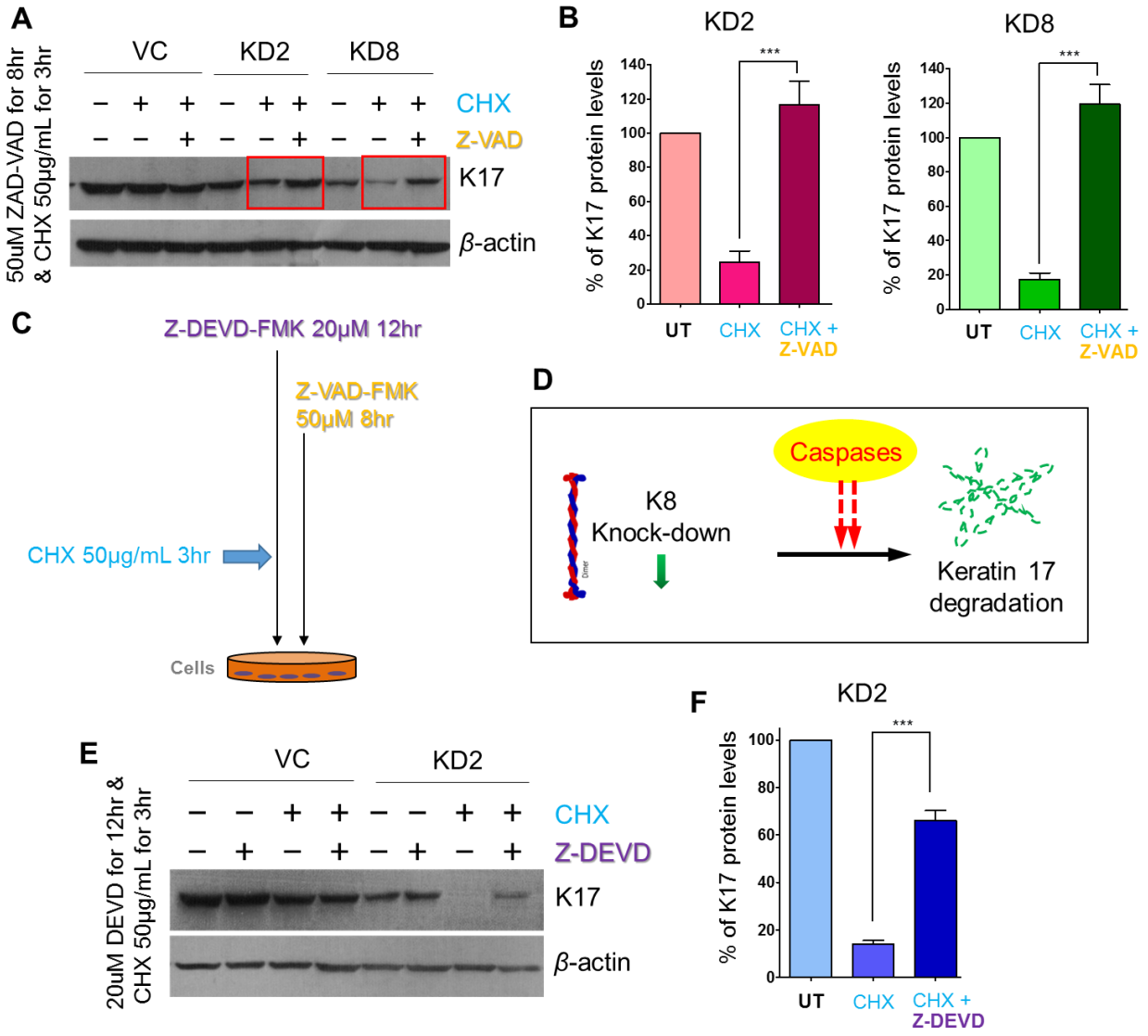

Figure 4.3.5.3: Caspase mediated degradation of K17: (**A**) Western blot analysis of K17 levels after pan caspase inhibition (Z-VAD-FMK-50µM for 8h and CHX 50µg/ml for 3h) in both the pTU6 vector control (VC) and K8 knockdown clones (KD2/KD8). (**B**) Representative bar graphs showing densitometry analysis of K17 levels after pan-caspase inhibition in the respective K8 knockdown clones compared to vector control cells. (**C**) Schematic representation for Z-DEVD-FMK, Z-VAD-FMK and CHX treatment protocol used. (**D**) Cartoon depicting caspase mediated K17 degradation after K8 knockdown. (**E**) Western blot analysis of K17 levels after caspase 3 inhibition (Z-DEVD-FMK- 20µM for 12h and CHX 50µg/ml for 3h) in both the pTU6 vector control (VC) and K8 knockdown clones (KD2/KD8). (**F**) Bar graph depicts the densitometry analysis of K17 levels after Caspase 3 inhibition. **Note:** In each case, cells were treated with 50µg/ml of CHX, 3h prior to completion of the protocol. *β*-actin was used as a loading control.

Further, lysosomal degradation was blocked by Chloroquine treatment for 12h. The western blot data did not show any significant alteration in K17 stability after lysosomal block (**Figure 4.3.5.2 C**). Blocking calpain with E64D for 6h and followed by immunoblotting in similar fashion didn't show any changes in K17 protein stability (**Figure 4.3.5.2 D**). Together, these results suggest, that alterations in K17 stability were not due to changes in any of these major protein degradation machineries.

Another important group of proteases known to cleave keratins are caspases. Therefore, we next blocked caspases with Z-VAD-FMK (a pan-caspase inhibitor) for 8h. Interestingly, a significant stabilization of K17 at protein level could be observed after pan caspase inhibition in K8 knockdown clones (**Figure 4.3.5.3 A & B**). Furthermore, caspase-3 specific inhibitor Z-DEVD-FMK treatment for 12h showed accumulation of K17 but not as significant as pan-caspase inhibition, suggesting the possibility of other caspases to be involved in this process (**Figure 4.3.5.3 E & F**).

4.3.6 K8 and apoptosis:

It is known that K17 together with K15 undergoes caspase mediated degradation during TNF-α induced apoptosis. Therefore, we checked the apoptotic sensitivity of K8 knockdown clones after 18h of TNF-α (20ng/ml) and CHX (50µg/ml) treatment. Annexin-V staining was performed to assess the extent of apoptosis. There was a 2-3 fold increase in apoptotic cells in K8 knockdown clones compared to vector control cells (**Figure 4.3.6 A, B**).

This suggested an increased sensitivity of K8 knockdown clones towards apoptotic stimuli and the same could be responsible for K17 degradation after K8 knockdown. We also assessed the effect of K8 knockdown on autophagy by western blotting and immunofluorescence of LC3B. There was

no change in the levels or appearance of LC3B after K8 knockdown which ruled out the possibility K8 mediated regulation of autophagy and thereby tumorigenicity of A431 cells (**Figure 4.3.6 C**).

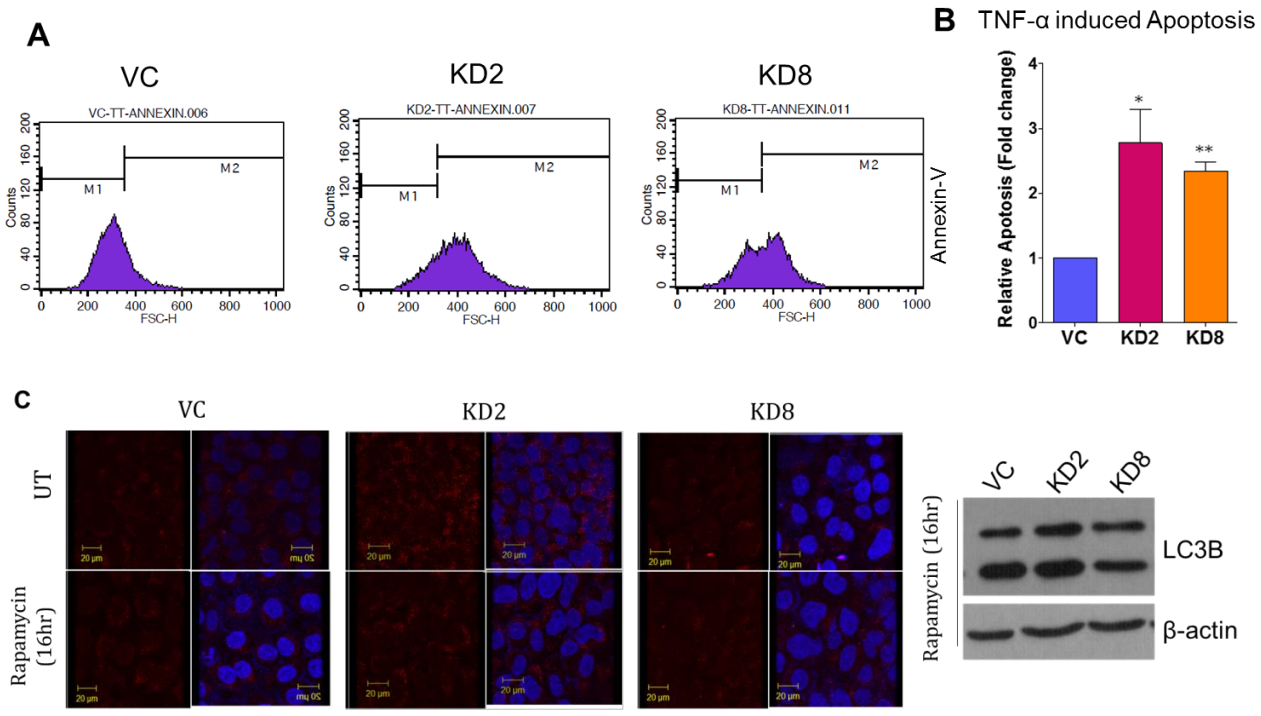

Figure 4.3.6: Effects of K8 knockdown on apoptotic sensitivity and autophagy of A431 cells: (**A, B**) Graphical representation of the apoptotic cell count (Annexin-V positive cells) after TNF-α (20ng/ml) and CHX (50µg/ml) treatment for 18h in both the pTU6 vector control (VC) and K8 knockdown clones (KD2/KD8). (**C**) Immunofluorescence and western blot analysis of LC3B in in both the pTU6 vector control (VC) and K8 knockdown clones (KD2/KD8) after Rapamycin treatment (500µM for 16h), respectively.

4.3.7 K8 regulates apoptosis through NF-κB pathway:

Our quantitative proteomics data showed an upregulation of TMS1/ACS which is known to be a potent regulator of TNF-*α* mediated apoptosis and is epigenetically silenced during various malignancies. Our western-blot analysis showed significant up-regulation of TMS1 which confirmed our MS/MS data (**Figure 4.3.7.1 A**). TMS1 is a known regulator of NF-κB activity both positively and negatively during TNF-*α* induced apoptosis. Therefore, we evaluated transcriptional

activity of NF-κB using luciferase reporter gene assay. The experiment was performed in both TNF-α treated and untreated conditions and the results were normalized with renilla luciferase. The K8 knockdown clones showed 2-2.5-fold downregulation in NF-κB transcriptional activity in both the treated as well as untreated conditions compared to vector control cells (**Figure 4.3.7.1 B, C**). Further, NF-κB transcriptional activity is largely dependent on its nuclear localization therefore we performed immunofluorescence analysis for NF-κB after 20mins of TNF-α treatment. The data showed 2 to 3 fold decrease in NF-κB nuclear translocation in both the K8 knockdown clones compared to vector control cells (**Figure 4.3.7.2 A, B, C)**. RanBP1 an indirect regulator of NF-κB nuclear localization was also found to be significantly decreased in our differential proteomics data which was validated by western blotting as shown in the **Figure 4.3.7.2 D.**

IκB*α* is an upstream regulator of NF-κB therefore the turn-over of IκB*α*, was analyzed post CHX treatment for 0, 8, 12 and 16h time-points (**Figure 4.3.7.3 A**). The western blot analysis demonstrated a significant difference in the stability of IκB*α* in K8 knockdown clones compared to vector control cells. In K8 Knockdown cells IκB*α* was stable for more than 8h whereas in vector control cells it gets degraded much before. Together with this, even after 20min of TNF-α treatment the IκB*α* was more stable in K8 knockdown clones compared to vector control cells (**Figure 4.3.7.3 B)**. This was accompanied by its decreased phosphorylation at Serine^{32}/Serine ^{36} residues after 20min TNF-α treatment. Further, the stability of IκB*α* is largely dependent on its phosphorylation by IκB*α* kinase complex which is required for its degradation (**Figure 4.3.7.3 C**). IκB*α* kinase complex is in-turn activated by IKK*β* Tyrosine^{188} phosphorylation. K8 knockdown clones showed significant reduction in phosphorylation of IKK*β* at Tyrosine^{188} compared to vector control cells as shown by the western blot data. Additionally, the upstream regulator of IKK

phosphorylation during NF-κB mediated apoptosis, PKCδ was found to be downregulated in knockdown clones at total protein levels (**Figure 4.3.7.3 D**). Apart from this, other associated modulators of same pathway like AKT/pAKT, ERK/pERK and JNK/pJNK were also assessed (**Figure 4.3.7.3 E, F**). Amongst these, the stress activated kinase JNK and its phosphorylation levels were significantly increased after K8 knockdown (an important event after diminished NF-κB activity during apoptosis) whereas others were unaffected. Altogether, this data suggests that TMS1 – NF-κB pathway regulates apoptotic sensitivity of A431 cells upon K8 downregulation (**Figure 4.3.7.3 G**).

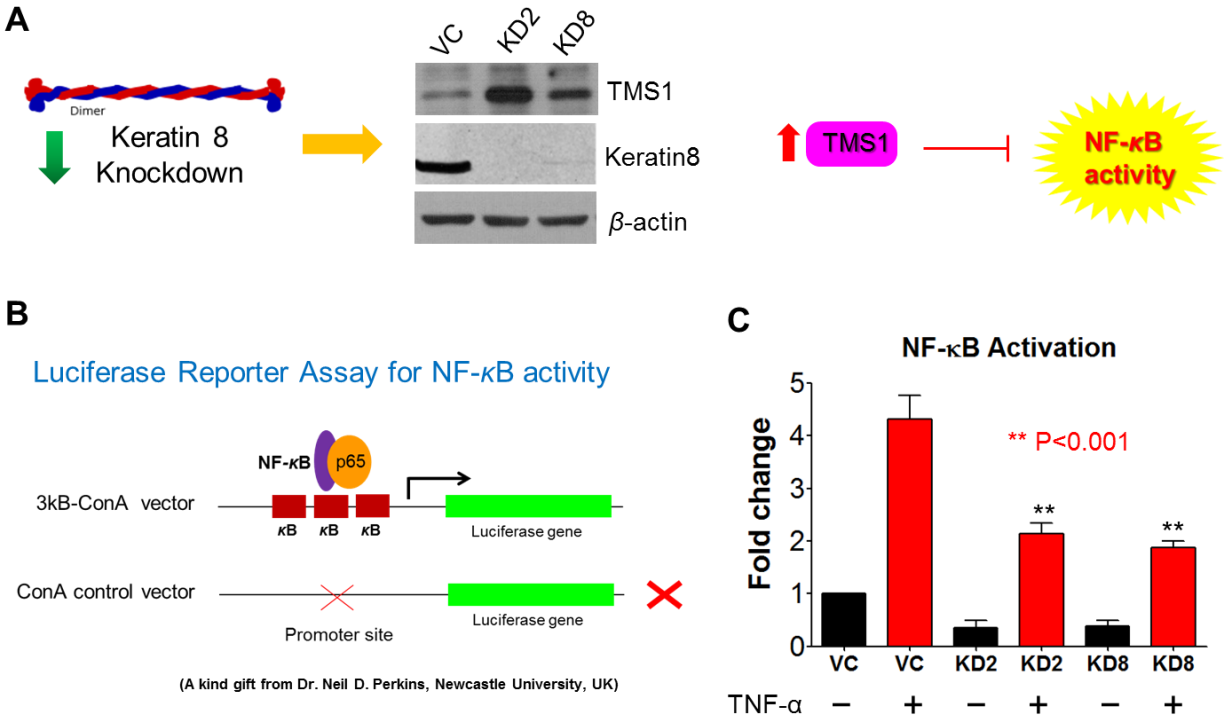

Figure 4.3.7.1: K8 knockdown affects NF-κB pathway in A431 cells: (**A**) Western blot analysis of TMS1 validating differential quantitative proteomics data after keratin 8 knockdown. (**B**) Picture depicting the luciferase reporter assay for NF-κB activity. (**C**) Bar graph showing the NF-κB activity in luciferase assay at the basal level as well as after TNF-α treatment (20ng/ml) in pTU6 vector control (VC) and K8 knockdown cells (KD2/KD8) after normalization with renilla luciferase.

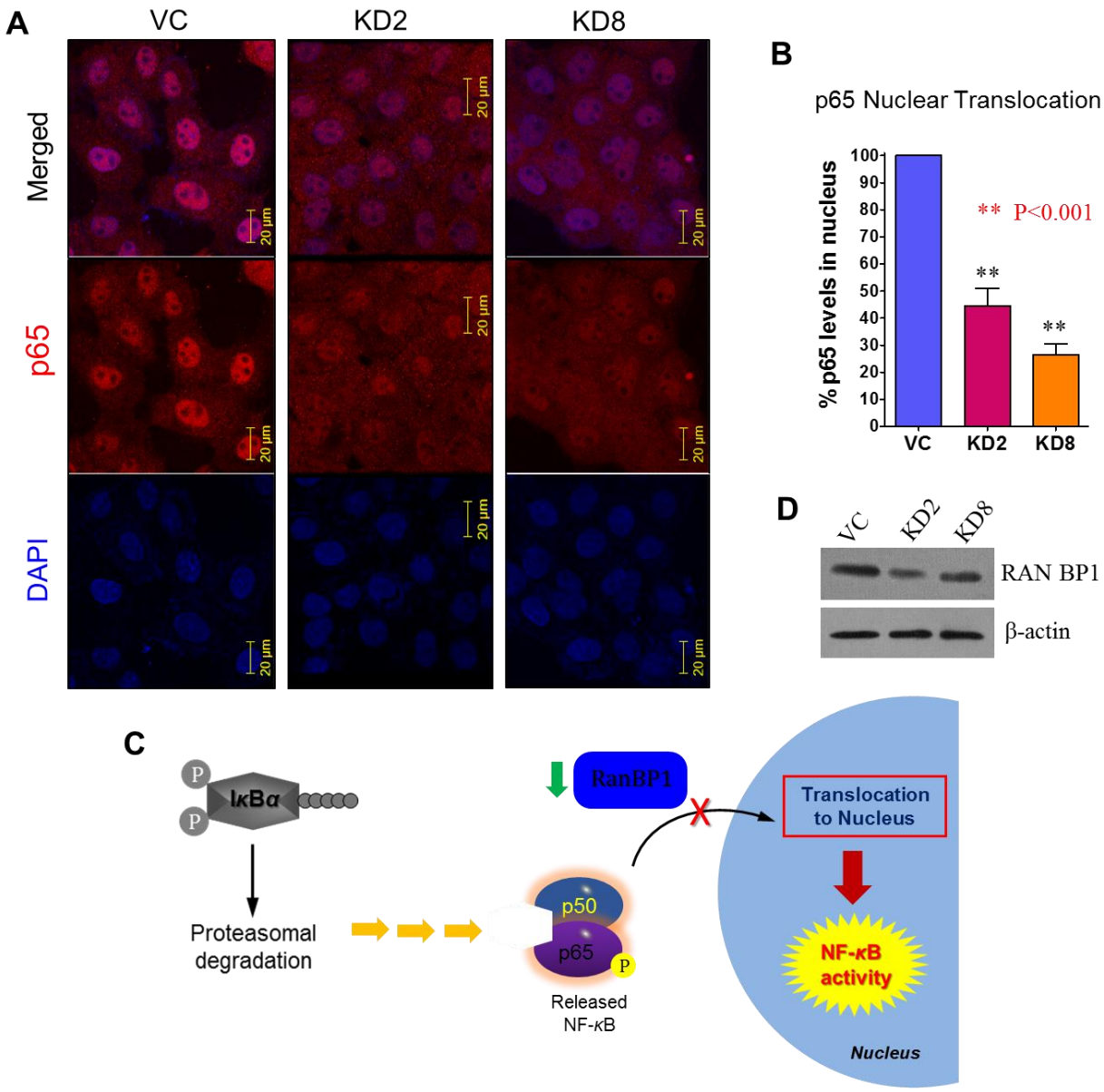

Figure 4.3.7.2: K8 regulates NF-κB translocation to nucleus: (**A**) Immunofluorescence image demonstrating the nuclear localization of NF-κB in pTU6 vector control (VC) and K8 knockdown clones (KD2/KD8) after 20 mins of TNF-*α* treatment (20ng/ml). (**B**) The experiment was performed twice in triplicates and the mean values are plotted as the bar graph showing the quantitation of percent p65 in nucleus in pTU6 vector control (VC) and K8 knockdown (KD2/KD8) cells ($p < 0.001$) after TNF-*α* treatment (20ng/ml). (**C**) The cartoon depicting its probable effect on NF-κB nuclear translocation. (**D**) Western blot analysis of RANBP1 validating differential quantitative proteomics data after keratin 8 knockdown.

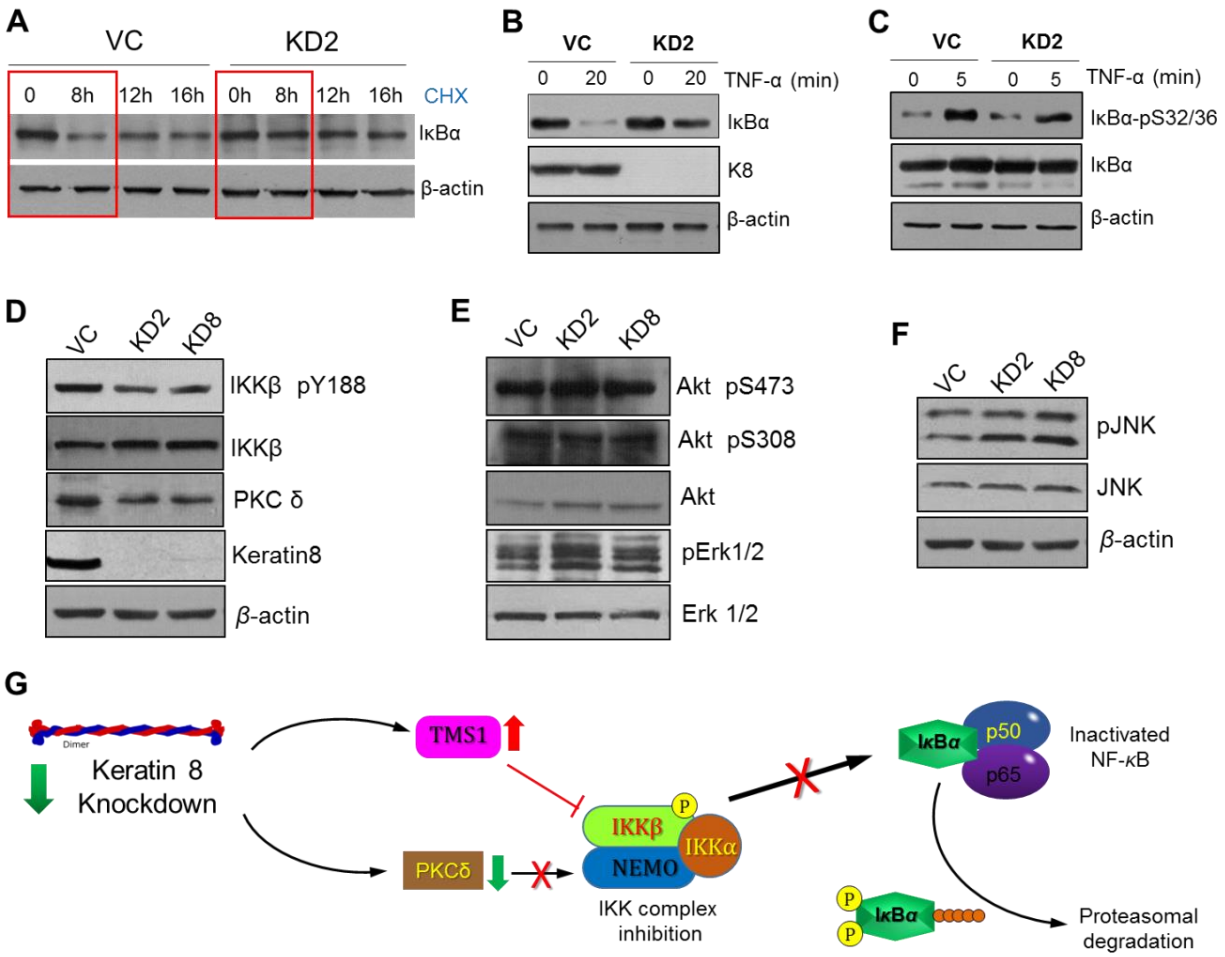

Figure 4.3.7.3: K8 knockdown affects NF-κB activity through regulation of IκBα degradation: (**A**) Western blot analysis of I*κ*B*α* levels after protein synthesis block by CHX (50µg/ml) for 0, 8, 12 and 16h time-points. (**B, C**) Western blot analysis showing I*κ*B*α* degradation and its phosphorylation pattern (at pS32/36 residues) in pTU6 vector control (VC) and K8 knockdown (KD2/KD8) cells after 20min of TNF-*α* treatment (20ng/ml). (**D**) Western blot demonstrating the IKK*β* phosphorylation at Y188 together with PKCδ levels in K8 knockdown clones compared to vector control cells. (**E**) Western blot showing the levels of AKT/pAKT and ERK/pERK in pTU6 vector control (VC) and K8 knockdown clones (KD2/KD8). (**F**) Western blot showing the levels of JNK/pJNK in pTU6 vector control (VC) and K8 knockdown (KD2/KD8) cells. (**G**) Cartoon depicting the possible links between K8 knockdown and NF-κB pathway mediated apoptosis

4.3.8 Cell migration associated signaling pathway is altered upon K8 downregulation:

Consistent with phenotypic assays, IPA analysis of quantitative proteomics data also showed alterations in molecules associated with cell motility, upon K8 downregulation. One of the key

regulators of actin organization MARCKSL1 was found to be significantly upregulated in both the K8 knockdown clones compared to vector control cells in the differential quantitative proteomics data which was further confirmed by western blotting (**Figure 4.3.8.1 A, B**). The downstream effector of MARCKSL1 i.e. Paxillin, showed an increased phosphorylation at Y118 residue, which is known to activate it (**Figure 4.3.8.1 A, B**). Increased phosphorylation of Paxillin is responsible for focal adhesion formation as well as regulation of actin organization in association with FAK. Further, downregulation of K8 led to a decreased phosphorylation of FAK at S397, which is necessary for its activity (**Figure 4.3.8.1 A, B**). Previous studies have shown that paxillin phosphorylation in absence of FAK leads to the formation of shorter actin filaments. We also observed similar alterations in actin organization, when stained with phalloidin-FITC, which binds exclusively to filamentous actin. The K8 knockdown clones showed shorter actin fibers compared to vector control cells with mature elongated cortical actin fibers along the arch (**Figure 4.3.8.1 C**). We could also observe an increased paxillin puncta at the membrane of both K8 knockdown clones (KD2 and KD8) whereas vector control cells showed a paxillin organized at lamellipodia like membrane extensions (**Figure 4.3.8.2**). Contrary to this, FAK did not show any proper staining.

FAK phosphorylation is known to regulate RhoGTPase activity and thereby cell migration. RhoGTPases regulate actin associated membrane protrusions *e.g.* fillopodia (CDC42), lamellipodia (RAC1) and stress fibers (Rho) at the migratory front. To identify, the probable Rho GTPase regulating K8 mediated migratory phenotype, actin staining at migratory edges for K8 knockdown and vector control cells was carried out. This demonstrated a clear mature lamellipodial organization in the migratory edges of vector control cells, whereas knockdown cells showed immature lamellipodial organization (**Figure 4.3.8.3A**). In addition, the lamellipodial

organization post EGF treatment (20ng/ml for 5min) along with cell spreading on laminin was also found to be negatively affected after K8 knockdown compared to vector control cells (**Figure 4.3.8.3 B, C**).

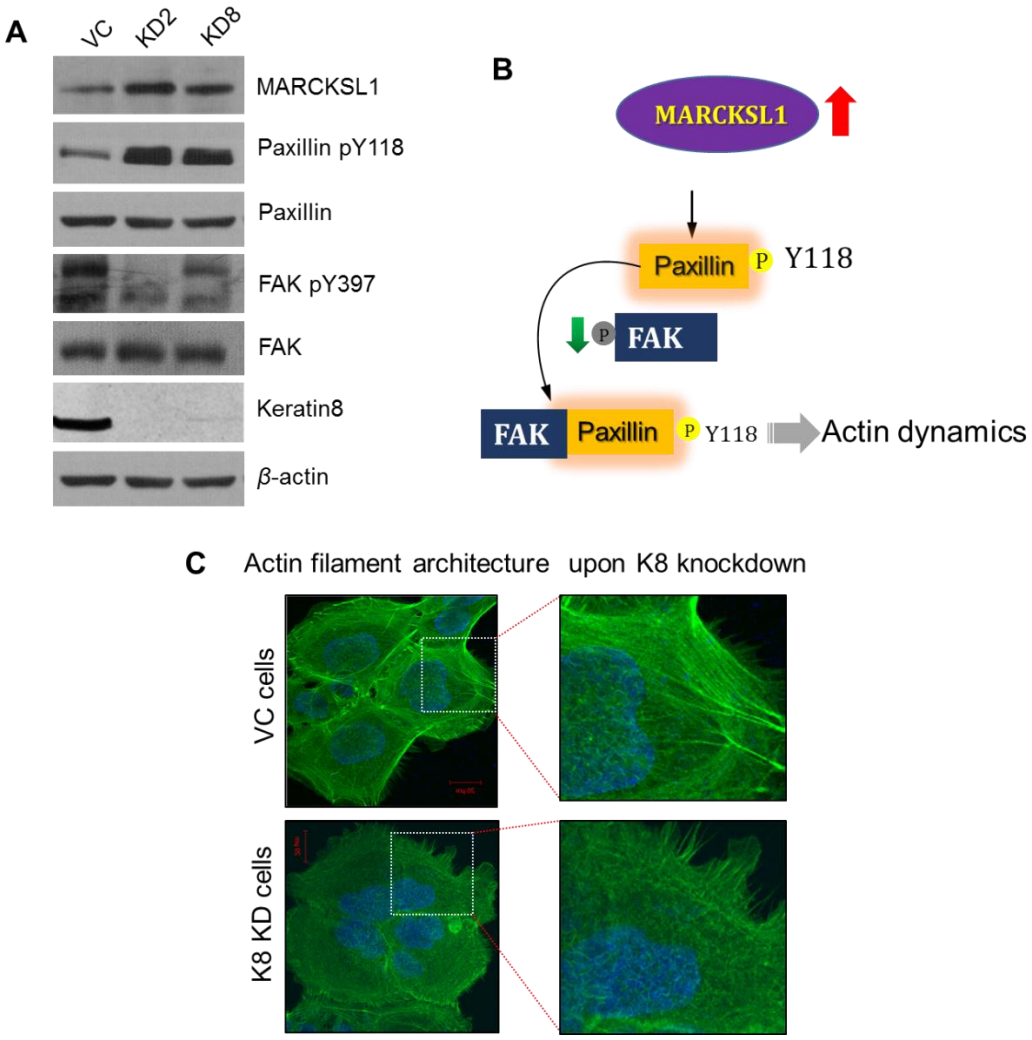

Figure 4.3.8.1: Effect of K8 knockdown on "Cellular movement pathway". (**A**) western blot analysis demonstrating effect of K8 knockdown on the levels of MARCKSL1, Paxillin/pPaxillin, FAK/pFAK. (**B**) Pictorial representation of sequential involvement of these signaling molecules in regulating the cell motility. (**C**) Phalloidin FITC (green) staining followed by immunofluorescence imaging shows defects in actin filament architecture in the K8 knockdown clones compared to vector control cells. The zoomed out images of the same are shown. Nucleus is counter stained with DAPI (blue) in all the cases. (Scale bar 20µm)

In accordance with this observation, active RAC (RAC-GTP) levels were also found to be significantly decreased after 5min of EGF treatment in K8 knockdown cells compared to vector control cells as assessed by RAC-GTP pull down assay. This suggests that RAC activity modulates lamellipodial organization and affects cell migration in K8 dependent manner (**Figure 4.3.8.4 A, B**). Another important protein RhoGDI, which is an upstream regulator of RAC signaling pathway was upregulated after K8 knockdown validating our quantitative proteomics data. Cofilin, an Important downstream modulator of RAC activity which bears actin severing properties and thereby affects actin organization, was further analyzed in K8 knockdown and vector control cells.

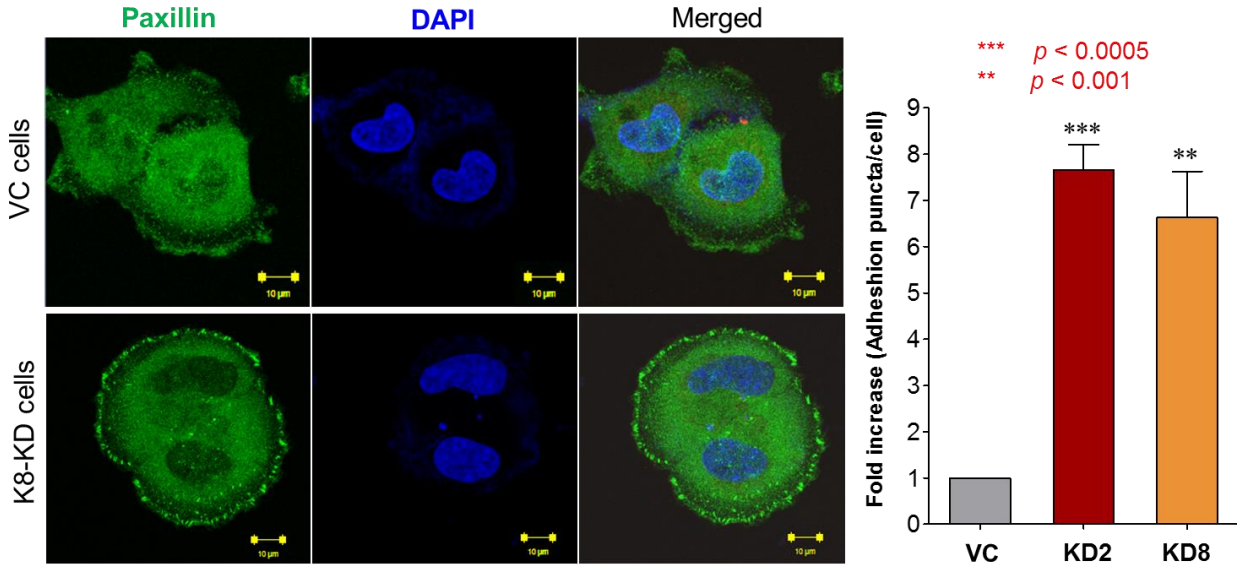

Figure 4.3.8.2: K8 down regulation affects Paxillin and FAK mediated focal adhesion in A431 cells: Immunofluorescence images of paxillin (green) staining in pTU6 vector control (VC) and K8 knockdown (KD2) cells. Nucleus is counter stained with DAPI (blue) in all the cases (Scale bar 20µm). The experiment was performed twice in triplicates and the mean values are plotted as the bar graph showing the quantitation of adhesion puncta per cell in pTU6 vector control (VC) and K8 knockdown (KD2/KD8) cells ($p < 0.001$ and $p<0.0005$).

We did not see any change in total cofilin levels while its phosphorylation at Serine[3] was found to be increased after K8 knockdown, indicating its inactivation and thereby modulation of RAC mediated actin organization. Further, we observed a significant upregulation in 14-3-3γ levels after

K8 knockdown, which validated our total quantitative proteomics data (**Figure 4.3.8.4 C**). Similar observations have been made by Jovceva E *et al.*, where they have shown RAC mediated regulation of Cofilin-1 phosphorylation by inhibition of binding of Slingshot phosphatases to 14-3-3γ. Together, these results indicate that K8 regulates cell migration by modulation of MARCKSL1-FAK- RAC signaling axis in A431 cells (**Figure 4.3.8.4 D**).

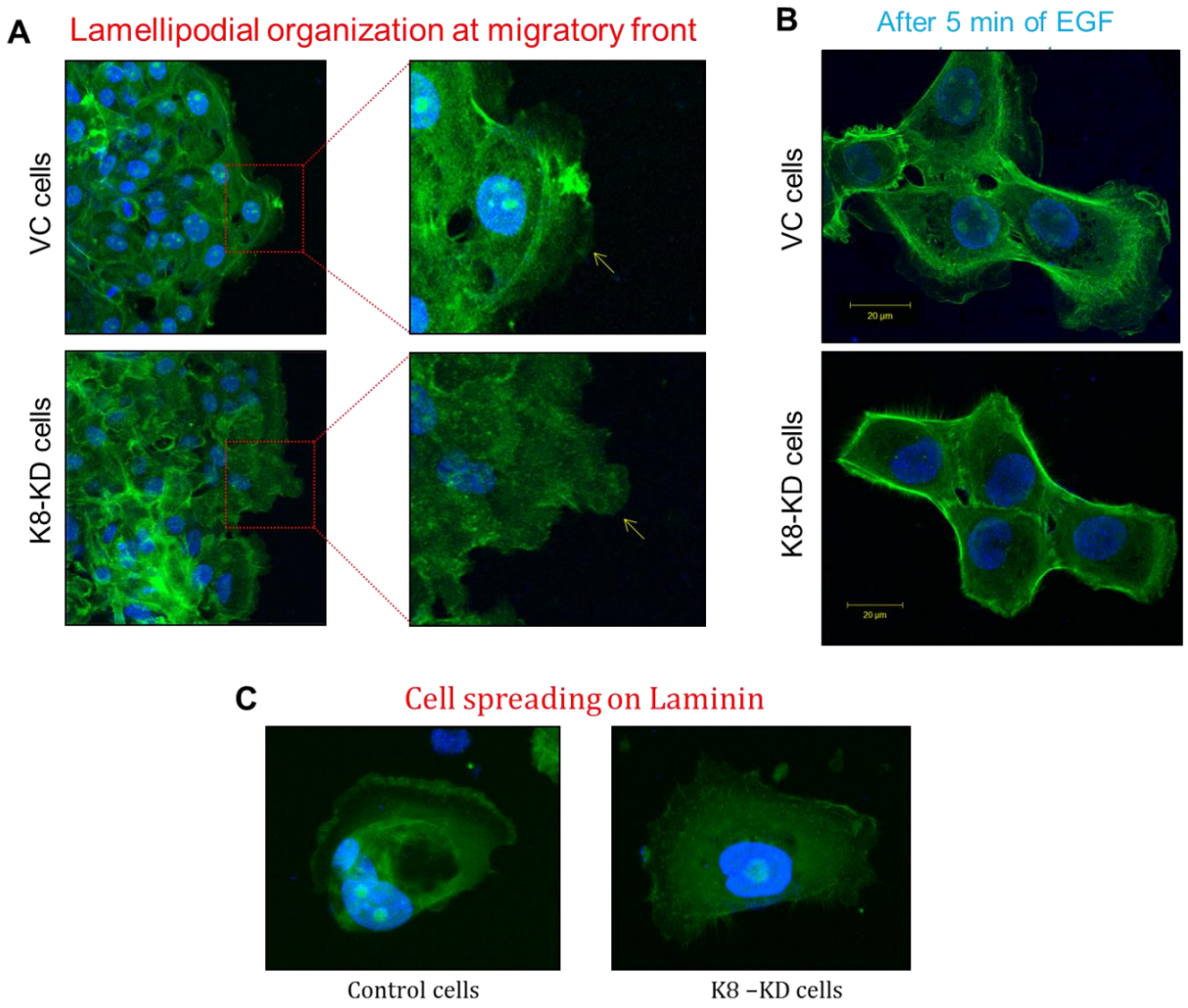

Figure 4.3.8.3: K8 downregulation affects lamellipodial organization in A431 cells: (**A**) Immunofluorescence images of actin phalloidin (FITC-green) staining in pTU6 vector control (VC) and K8 knockdown (KD2/KD8) cells at the migratory edges, post 3h of scratching the wound. (**B**) Representative immunofluorescence images of actin phalloidin staining after EGF treatment (20ng/ml for 5min). (**C**) Cell

spreading on laminin was assessed after actin phalloidin (FITC-green) staining in pTU6 vector control (VC) and K8 knockdown (KD2/KD8) cells. Nucleus is counter stained with DAPI (blue) in all the cases (Scale bar 20µm).

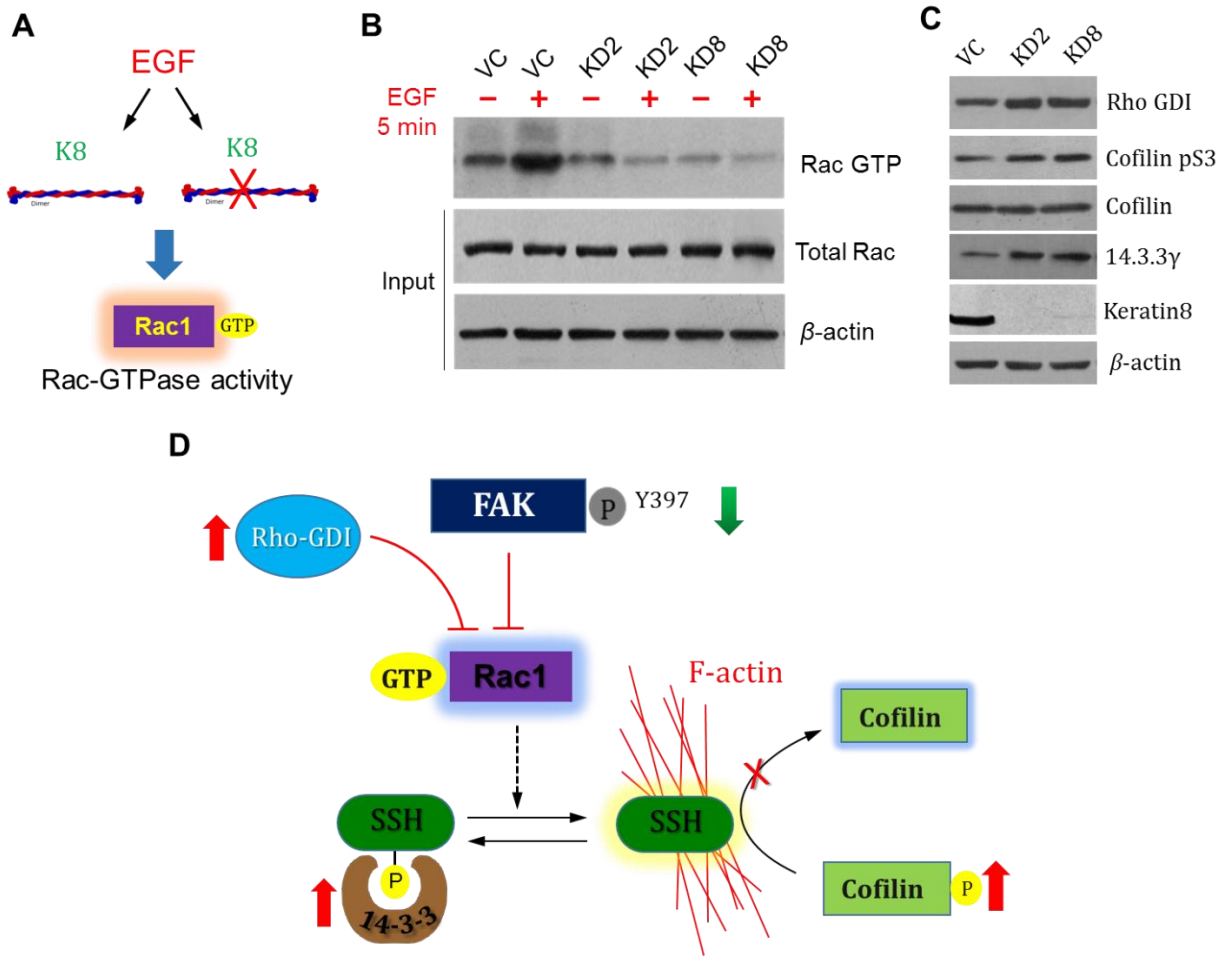

Figure 4.3.8.4: K8 downregulation affects cell motility through RAC mediated actin organization defects at lemmalepodial fronts of A431 cells: (**A**) Pictorial representation of EGF treatment affecting RAC activity in K8 knockdown and vector control cells. (**B**) RAC-GTP pulldown showing effect of K8 downregulation on RAC activity after EGF treatment (20ng/ml for 5min). (**C**) Western blot analysis for RhoGDI, Cofilin/pCofilin and 14-3-3γ. *β*-actin was used as a loading control. (**D**) Cartoon depicting the possible links between K8 knockdown and cellular movement pathway**.**

4.3.9 Rescue of molecular changes observed in K8 knockdown clones by re-expression of shRNA resistant K8 WT GFP:

In order to further confirm that the molecular changes observed are the result of K8 downregulation rather than any off-target effects, rescue experiment was performed. Upon K8 WT GFP expression, the K5 and K17 levels were substantially stabilized as shown in the western blot and immunofluorescence data. The K17 levels were stable upto 12h in K8 WT GFP clone compared to K8 knockdown cells (KD2) **(Figure 4.3.9 A, B)**.

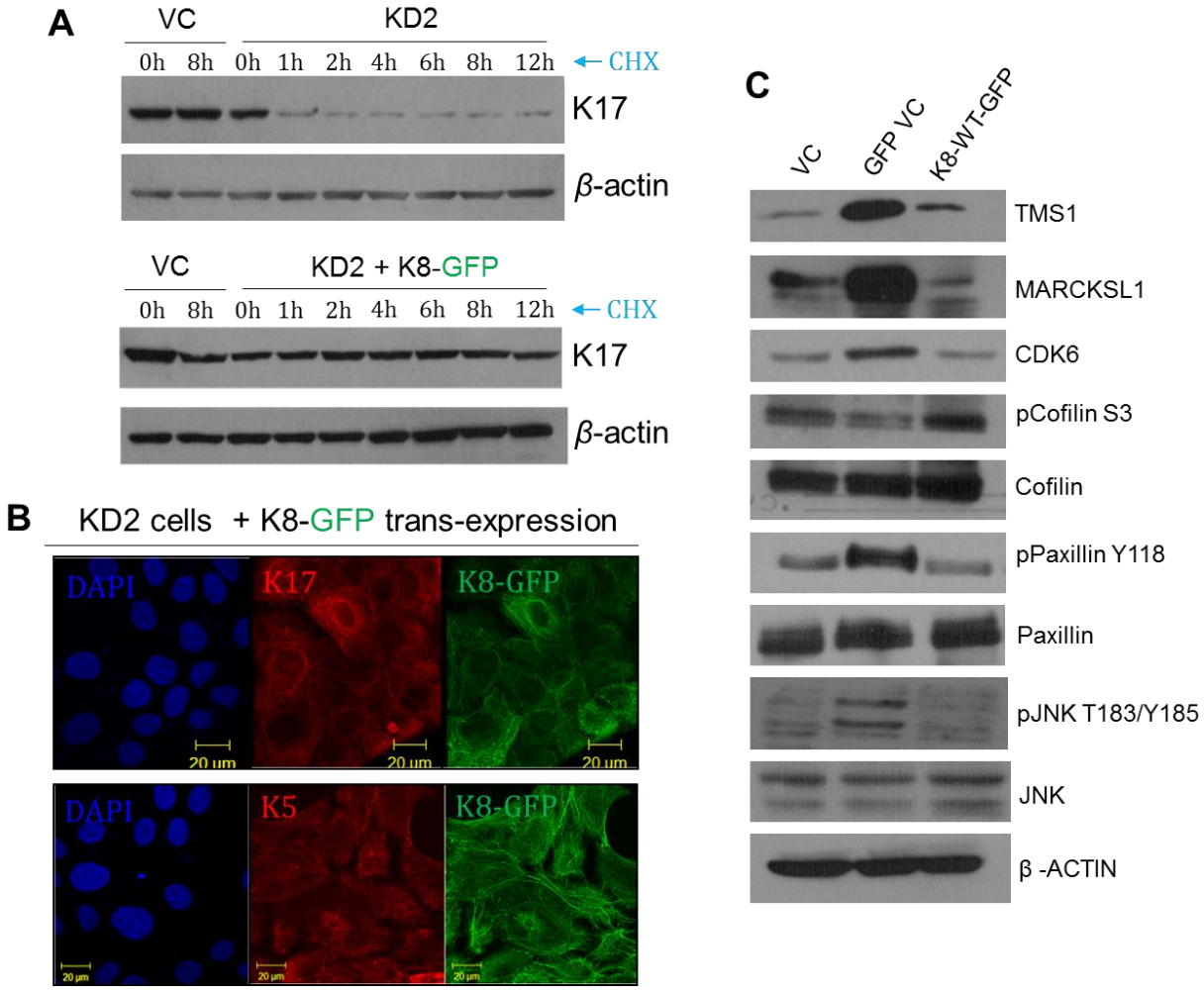

Figure 4.3.9: Rescue of molecular alterations of K8 knockdown cells. (**A**) Western blot analysis of K17 stability after trans-expression of K8 WT GFP in KD2 knockdown clones post CHX treatment (50µg/ml) for 0-12h time points. (**B**) Immunofluorescence imaging showing rescue of K17 and K5 filamentous network (Red) after stable re-expression of K8 WT GFP in KD2 K8 knockdown clones. (**C**) Western blot analysis of stable K8 WT GFP (WT), pEGFP vector control (GFP VC) and pTU6 vector control (VC) cells with antibodies to TMS1, MARCKSL1, CDK6, Cofilin/pCofilin, Paxilin/pPaxilin, JNK/pJNK. *β*-actin was used as a loading control.

Apart from this, there was a reversal in the protein levels of molecules associated with apoptotic and migratory pathways such as TMS1, RANBP1, MARCKSL1, Paxillin/pPaxillin, Cofilin/pCofilin and 14-3-3γ. **(Figure 4.3.9 C)** Together these observations confirmed the role of K8 in neoplastic progression of skin SCC derived A431 cells through the regulation of above mentioned migratory and apoptosis associated proteins.

4.4 To understand the role of Keratin 8 phosphorylation in neoplastic progression of Skin SCC derived A431 cells

4.4.1 Generation of stable clones expressing shRNA-resistant K8 WT and phosphomutants:

Stable clones expressing shRNA-resistant 3X-Flag-(N-term)-GFP-(C-term) tagged K8 WT, phosphodead mutants (K8 S73A & K8 S431A), and phosphomimetic mutants (K8 S73D & K8 S431D) were generated (**Figure 4.4.1.1**), in previously established shRNA-based K8-deficient stable clones of A431 cells.

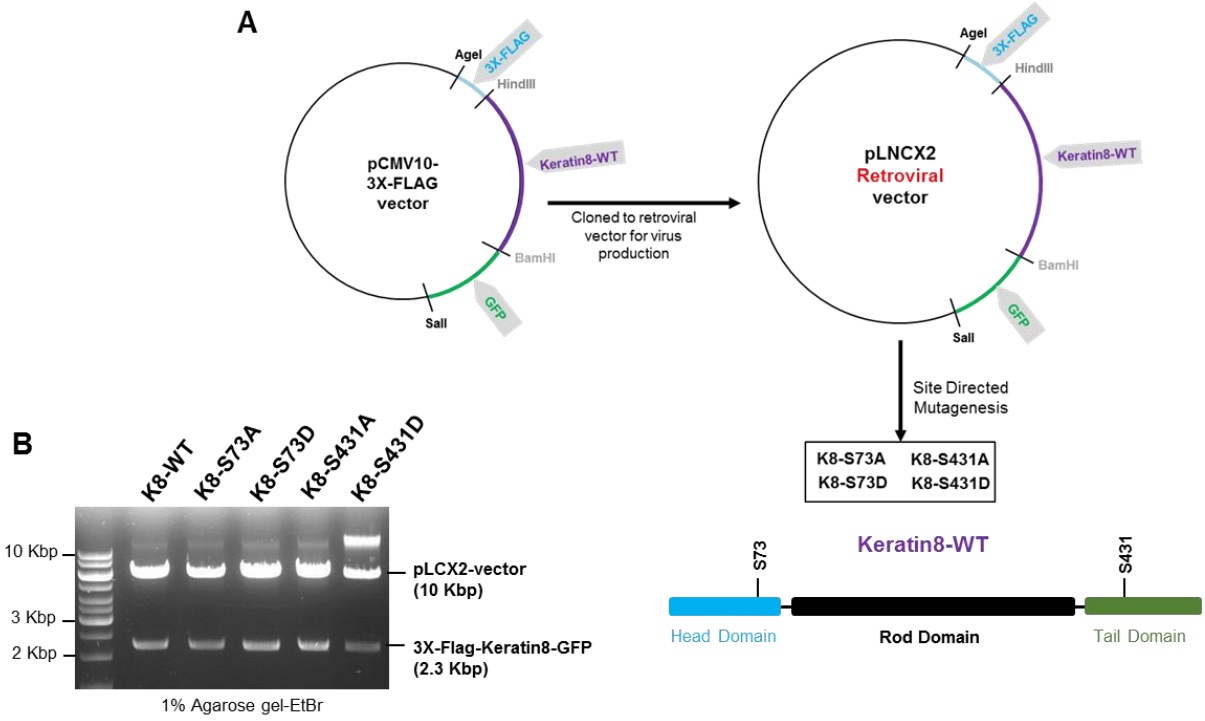

Figure 4.4.1.1: Generation of K8 WT and phosphomutant constructs and their mass spectrometric validation: (**A**) Schematic showing the strategy for cloning K8-WT-GFP, from pCMV-3X flag vector to pLNCX2, a retroviral vector, using AgeI-SalI enzymes. Further site directed mutagenesis was performed to generate phosphodead and phosphomimetic mutants for S73 and S431 sites as shown in the cartoon. (**B**) Gel picture showing the positive clones with a 2.3kbp pop out for K8 GFP after digesting the constructs with AgeI-SalI.

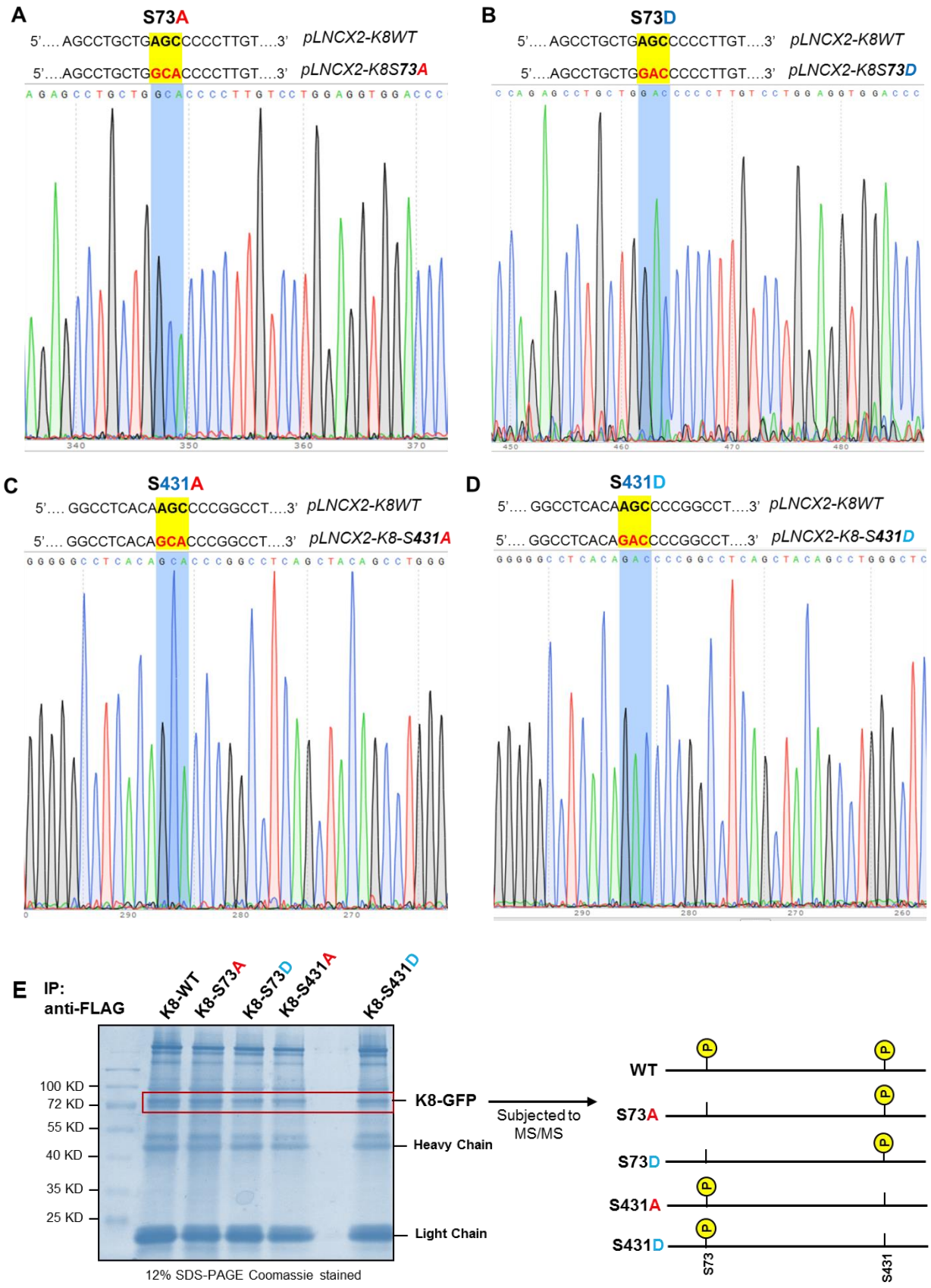
A
S73A
5'.... AGCCTGCTGAGCCCCCTTGT....3' pLNCX2-K8WT
5'....AGCCTGCTGGCACCCCTTGT....3' pLNCX2-K8S73A
B
S73D
5'.... AGCCTGCTGAGCCCCCTTGT....3' pLNCX2-K8WT
5'....AGCCTGCTGGACCCCCTTGT....3' pLNCX2-K8S73D
C
S431A
5'.... GGCCTCACAAGCCCCGGCCT....3' pLNCX2-K8WT
5'.... GGCCTCACAGCACCCGGCCT....3' pLNCX2-K8-S431A
D
S431D
5'.... GGCCTCACAAGCCCCGGCCT....3' pLNCX2-K8WT
5'.... GGCCTCACAGACCCCGGCCT....3' pLNCX2-K8-S431D
E
IP: anti-FLAG
K8-WT
K8-S73A
K8-S73D
K8-S431A
K8-S431D
100 KD
72 KD
55 KD
40 KD
35 KD
25 KD
K8-GFP
Heavy Chain
Light Chain
12% SDS-PAGE Coomassie stained
Subjected to MS/MS
WT
S73A
S73D
S431A
S431D
P
S73
S431

Figure 4.4.1.2 Point mutation validation on K8-constructs: (**A-D**) Sequence verification for pLNCX2-K8 mutant constructs after SDM. (**E**) Mass spectrometric analysis of K8 GFP to validate the phosphorylation status in-vivo for WT as well as respective mutants. Overexpressed WT and phosphomutants K8-GFP were pull down using anti-flag antibody and the corresponding 82 KDa K8 GFP band was excised from Coomassie stained gel. Further, mass spectrometry was carried out and results were analyzed to detect phosphorylation at respective sites as depicted in cartoon.

Genomic DNA sequencing (**Figure 4.4.1.2 A-D**) together with Mass spectrometric **(Figure 4.4.1.2 E)** analysis further confirmed the integration as well as expression of respective phosphomutants clones. Further, immunofluorescence analysis showed appropriate filament organization of trans-expressed K8 GFP in all the five clones **(Figure 4.4.1.3 A).** A significant up-regulation of 3X-Flag(N)-GFP(C) tagged K8-WT and phosphomutants was observed in the western blot analysis for all the clones when probed with total K8 antibody. Further, loss of K8 phosphorylation on respective sites was observed for all four phosphomutant clones (K8 S73A, K8 S73D, K8 S431A and K8 S431D) when probed with K8 Serine^{73} or Serine^{431} phosphorylation specific antibodies **(Figure 4.4.1.3 B).**

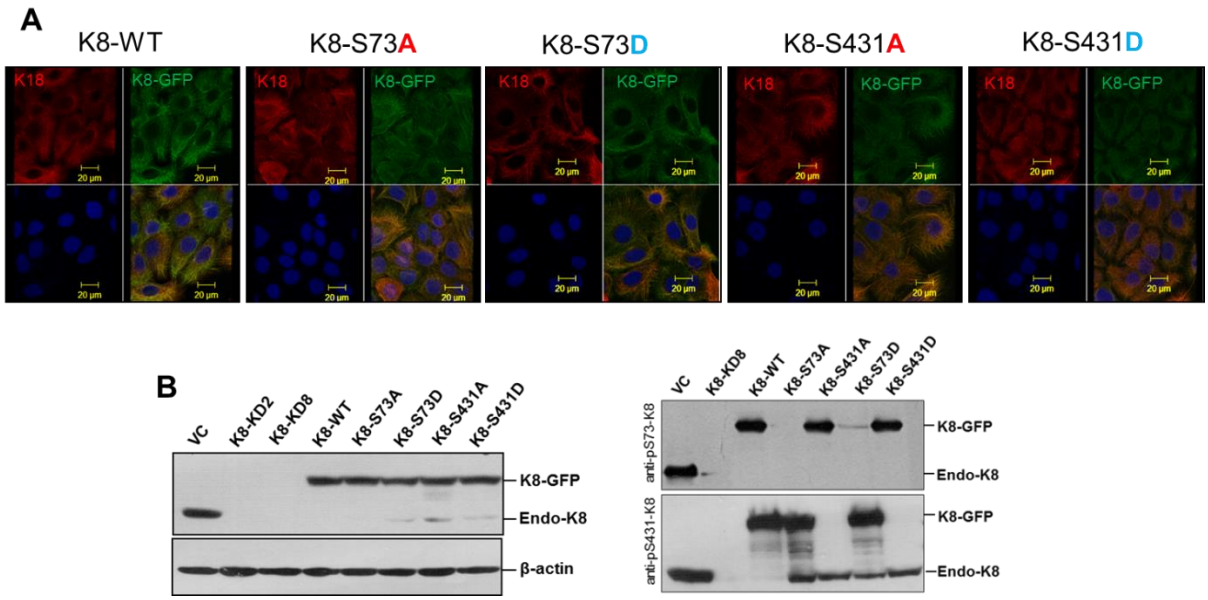

Figure 4.4.1.3: Validation of stable clones trans-expressing K8 GFP (WT/phosphomutants): (**A**) Immunofluorescence imaging of Keratin 8 GFP (WT/phosphodead/phosphomimetic) using LSM 780 Zeiss microscope at 488nm and 568nm wavelength respectively to observe K8/18, filament organization in all five K8 wild type and phosphomutant clones. Green color represents K8 GFP whereas red color represents K18. Nucleus is stained with DAPI, (Scale bar 20µm) (**B**) Western blot analysis of the 5 clones overexpressing wild type and phosphomutants K8 GFP using K8 antibody (left panel) and phosphospecific antibodies (K8 pS73 and K8 pS431) (right panel). VC and K8-KD8 depicts vector control and K8 knockdown clones respectively. Higher molecular weight bands represent trans-expressed K8-GFP (WT/phosphodead/phosphomimetic).

4.4.2 Phosphoproteomic profiling and quantification

Next, we performed a TMT-based quantitative phosphoproteomics for all the five clones, in order to understand the alterations in their global phosphoproteome profile in response to site specific K8 phosphorylation modulation in skin-SCC derived cell-line. A schematic representation of the overall strategy acquired for TMT-based quantitative phosphoproteomics is shown in **Figure 4.4.2.1**.

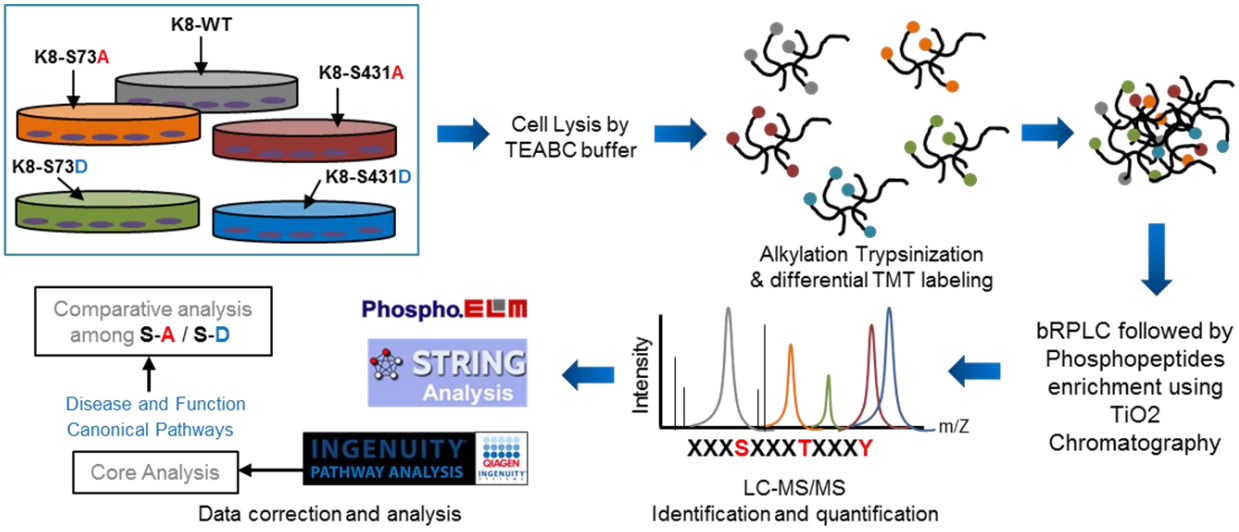

Figure 4.4.2.1: Schematic representation of the methodology acquired for TMT-based quantitative phosphoproteomics.

When searched against human protein database, a total of 5839 unique phosphopeptides corresponding to 2145 proteins were detected. Out of this, a total of 4915 (84.17%), 802 (13.73%) and 122 (2.08%) singly, doubly and phosphopeptides phosphorylated at more than three sites were identified respectively (**Figure 4.4.2.2 A)**. Further, 4644 (86.4%) phospho-Serine, 655 (12.2%) phospho-Threonine and 76 (1.4%) phospho-Tyrosine containing phosphopeptides were detected with a high "phosphoRS Site Probabilities" (**Figure 4.4.2.2 B)**.

A

Details of Phosphoproteomics Data:	
Total no. of unique phosphopeptides	5839
Total no. of Proteins	2145
Total no. of unique phosphosites	5375
Total no. of singly phosphorylated phosphopeptides	4915 (84.17%)
Total no. of doubly phosphorylated phosphopeptides	802 (13.73%)
Total no. of 3 or more phosphorylated phosphopeptides	122 (2.08%)

Phospho-residues	Number	%
Serine	4644	86.4%
Threonine	655	12.2%
Tyrosine	76	1.4%

B

Cell type	≥ 1.5 fold-up ≥ 1.5 fold-down	Known phosphosites	Novel Phosphosites	Total Phosphosites
K8-S73A	Up-regulated	185	161	**346**
	Down-regulated	67	270	**337**
K8-S73D	Up-regulated	174	262	**436**
	Down-regulated	192	495	**687**
K8-S431A	Up-regulated	58	111	**169**
	Down-regulated	81	127	**208**
K8-S431D	Up-regulated	63	197	**260**
	Down-regulated	81	190	**271**

Figure 4.4.2.2: Summary of differential quantitative phosphoproteomics data: (A) The table depicts a total summary of phosphopeptides, phosphoproteins and phosphosites detected after LC-MS/MS analysis together with summary of total number of phospho-serine, phospho-threonine and phospho-tyrosine detected. Table shows number of phospho-serine/tyrosine/threonine detected. (**B**) Table represents differential phosphorylation levels at known and novel phosphorylation sites on proteins in all 4 different clones with a cut-off of ≥1.5-fold change.

Next, Line graphs for entire phosphoproteomics data, representing significant phosphorylation alteration on phosphoproteins detected in all the 4 datasets (K8 S73A, K8 S73D, K8 S431A, K8 S431D) compared to K8 WT were plotted. There were, (346/337), (436/687), (169/208), (260/271) unique phosphosites found to be up/down regulated, amongst the total 5375 phosphosites, with a threshold ≥1.5 fold in case of K8 S73A, K8 S73D, K8 S431A, K8 S431D datasets respectively (**Figure 4.4.2.2 C)**. In addition, to identify total known and novel phosphosites, differentially phosphorylated amongst all the dataset, Phospho-ELM database was used. These results suggested a significant alteration in the phosphoproteomic profile of A431 cells in response to K8 phosphorylation modulation in a site specific manner.

4.4.3 Determining the orthogonal or overlapping phosphoproteomic profile amongst all the datasets

Comparison Analysis of phosphoproteomic profile between phosphodead and phosphomimetic mutants datasets was carried out in order to attribute the effects of site specific K8 phosphorylation in regulating different signaling mechanisms. Significant alterations in the phosphorylation status of corresponding phosphoproteins was observed upon initial overlay analysis of the total phosphoproteome profile between aforementioned datasets for both sites. Furthermore, we observed 79 and 24 common phosphoproteins to be upregulated in phosphodead mutants (K8 S73A and K8 S431A) and downregulated in corresponding phosphomimetic mutants (K8-S73D and K8 S431D) simultaneously, using Venny 2.1 software. Similarly, 48 and 35 common phosphoproteins were upregulated in phosphomimetic mutant (K8 S73D and K8 S431D) datasets and downregulated in corresponding phosphodead mutant (K8 S73A and K8 S431A) datasets alongside. In addition, there were 80 common phosphoproteins upregulated and 97 common

phosphoproteins downregulated within the phosphodead mutant (K8S73A and K8 S431A) datasets. Concurrently, there were 108 common phosphoproteins upregulated and 178 downregulated within the phosphomimetic mutant (K8 S73D and K8 S431D) datasets (**Figure 4.4.3.1 A, B)**.

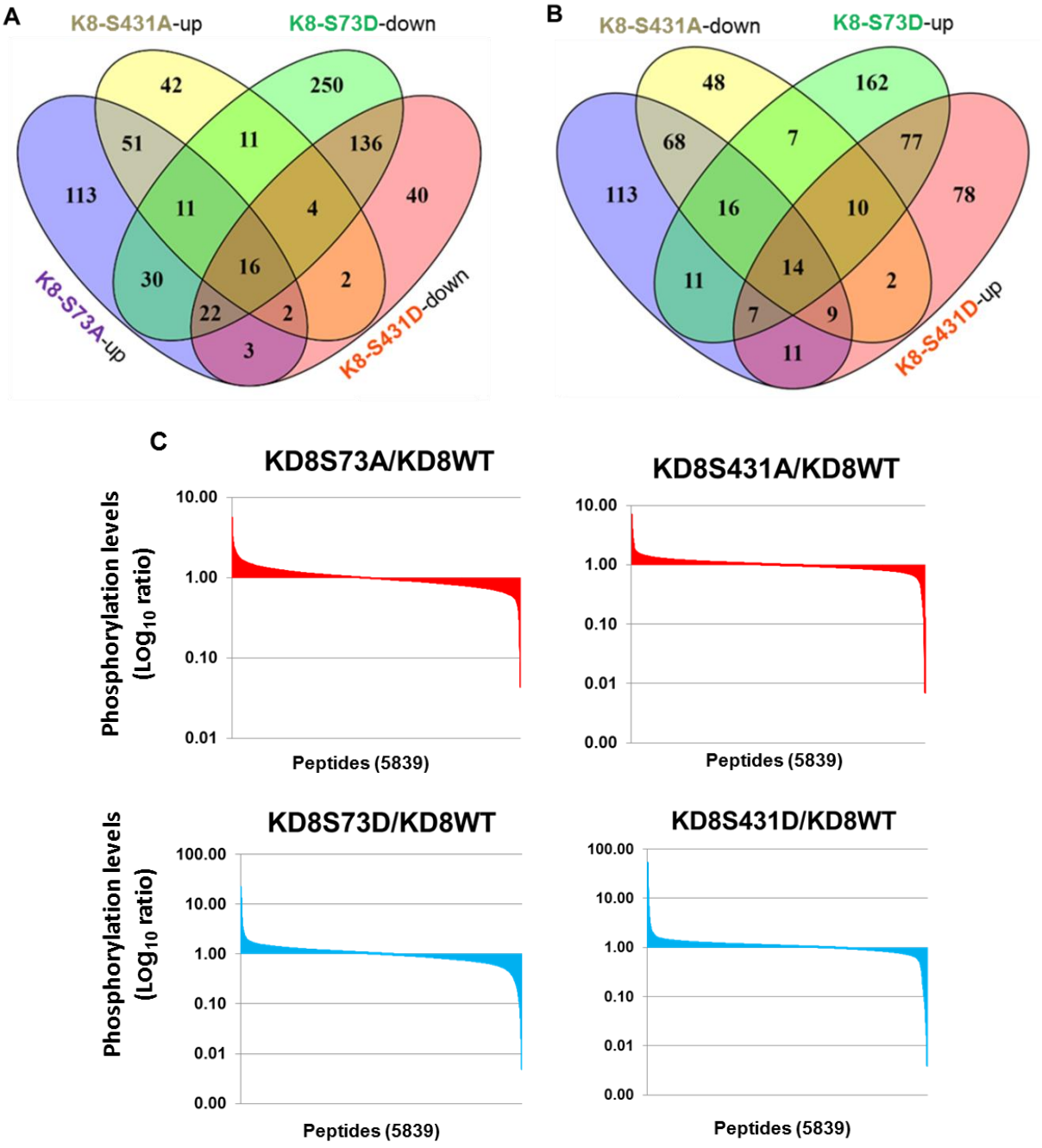

Figure 4.4.3.1: Venn diagram analysis of differential phosphoproteomics data: (**A, B**) Phosphoproteins, with a cut-off of ≥1.5-fold change in their phosphorylation levels from all the 4 data sets were subjected to the Software Venny 2.1 and the diagrams representing the number of orthogonal or within overlapping phosphoproteins the respective clones. (**C**) Line graph showing the total (5839) phosphopeptide distribution in K8 S73A, K8 S431A, K8 S73D and K8 S431D datasets.

A positive correlation between many common effectors with differential phosphorylation within as well as among phosphodead and phosphomimetic mutants could be identified which substantiated their involvement in a site specific K8 phosphorylation mediated biological functions (**Figure 4.4.3.1 C)**.

4.4.4 Functional correlation of Phosphoproteins detected across different datasets

For the intricate analysis of the differential quantitative Phosphoproteomic data different bioinformatics tools were used as shown in the figure above (**Figure 4.4.4**). Ingenuity Pathway analysis (IPA) was performed for independent datasets of phosphomutants in comparison to K8-WT (K8 S73A/WT, K8 S73D/WT, K8 S431A/WT and K8 S431D/WT) to understand the functional relevance of K8 phosphorylation ablation mediated global phosphoproteomic changes. Subsequent to this "Comparison Analysis" within the datasets of K8S73 group (K8 S73A/WT, K8 S73D/WT, K8 S73A/73D) and K8 S431 group (K8 S431A/WT, K8 S431D/WT, K8 S431A/431D) was carried out. Comparison Analysis facilitated the identification of trends or similarities and differences between mutants within the group for both the phosphosites by visualization across multiple analyses. Further, for significantly altered signaling in case of independent and Comparison analysis, extended heat maps and bar charts for the "Canonical pathways", "disease and Biological functions" together with "Networks" were generated.

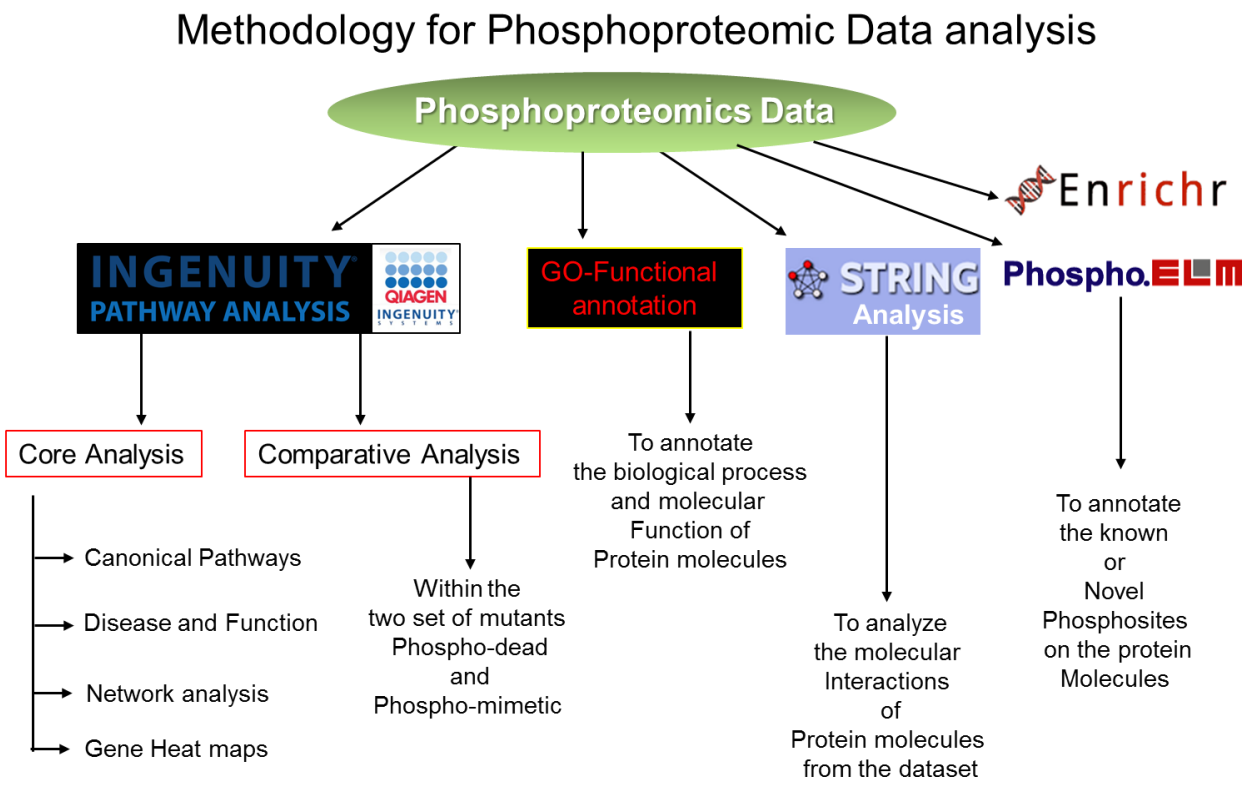

Figure 4.4.4: Schematic representation of methodology for phosphoproteomic data analysis.

4.4.4.1 Functional signaling networks modulated by K8 Serine[73] phosphorylation

The independent IPA-"canonical pathways" analysis showed significant alterations in phosphorylation of proteins involved in the signaling pathways, like: mTOR, ATM, Regulation of eIF4, HIPPO and Apoptosis, for K8 Serine[73] phosphorylation modulation (**Figure 4.4.4.1.1 A)**. Furthermore, the independent "Disease and biological function" analysis of the same revealed many of the differentially phosphorylated proteins associated with RNA Post-Transcriptional Modification, Cancer, Cell Morphology, Cellular Growth and Proliferation, Gene expression and Cell cycle (**Figure 4.4.4.1.1 B)**. Similarly, the differential regulation of phosphoproteins related to "canonical pathways" including Hippo, UVC induced MAPK, Cell cycle control and PKA signaling was observed in K8 S73D dataset (**Figure 4.4.4.1.1 A)**. Interestingly, an inverse

correlation between K8 S73A and K8 S73D datasets could be seen in the IPA-Comparison Analysis for the altered "Canonical pathways" which further strengthened the role of K8 Serine[73] phosphorylation as a potent modulator of these pathways. Some of such pathways significantly modulated included; GNRH, Renin angiotensin, P70 S6K, Integrin, Rho GTPase, ATM pathway *etc*.

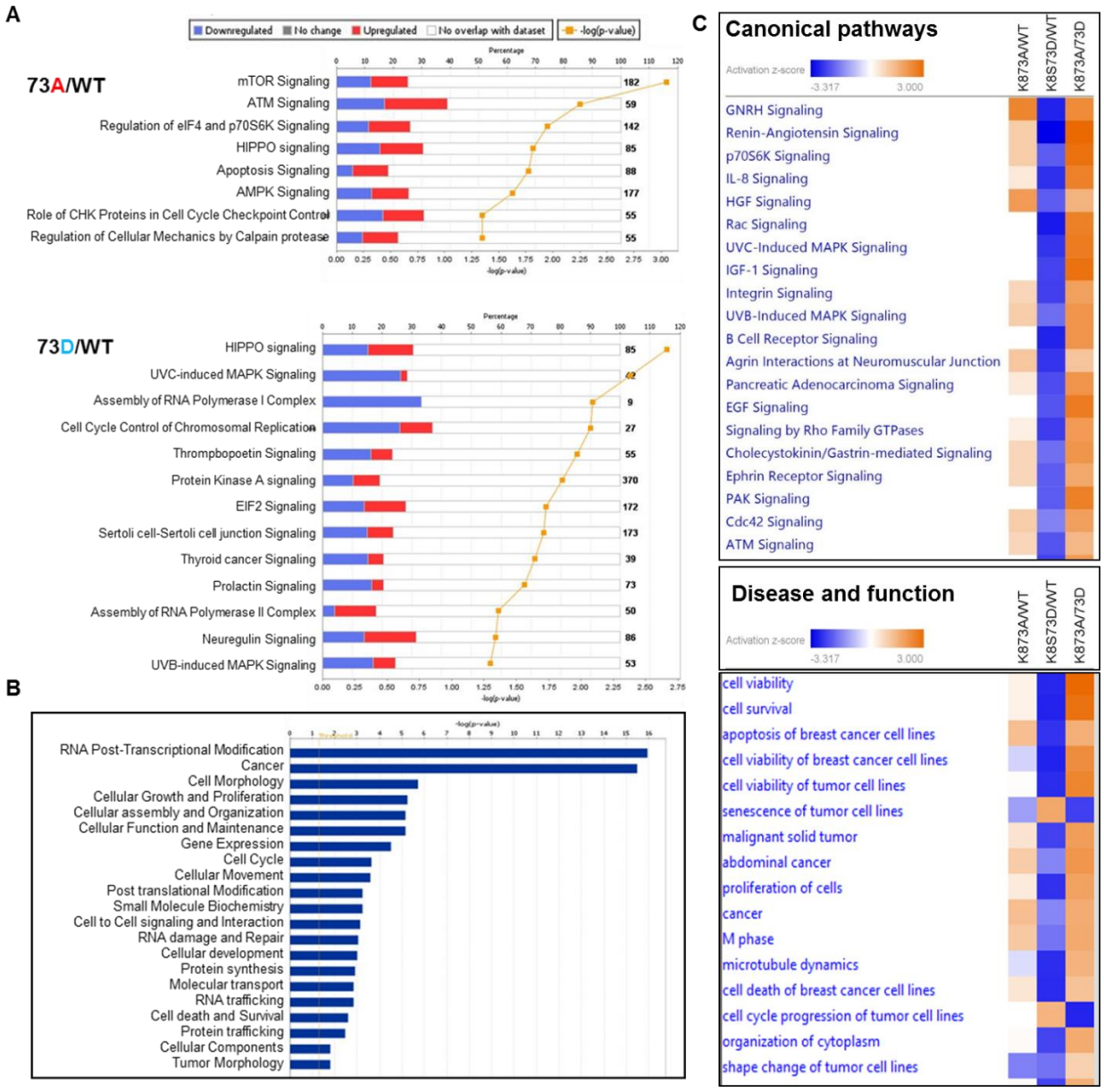

Figure 4.4.4.1.1: Analysis of phosphoproteomic data obtained from TMT-based global phosphoproteome profiling: (**A**) Representative Bar chart for IPA "Canonical Pathways" showed

significantly altered signaling pathways with high -log P-value for both K8 S73A and K8 S73D datasets. The numbers against every bar corresponds to the no. of filtered proteins involved in the mentioned pathway. (**B**) The representative bar chart depicting distribution of the differentially regulated phosphoproteins (with high -log P-value) according to their Biological functions. (**C**) Heat maps generated through IPA for "Comparison Analysis" of K8 Serine[73] datasets (K8 S73A/WT, K8 S73D/WT, K8 S73A/S73D) including "canonical pathways" and "disease and biological function" demonstrate the significantly altered molecular signaling pathways as well as biological functions.

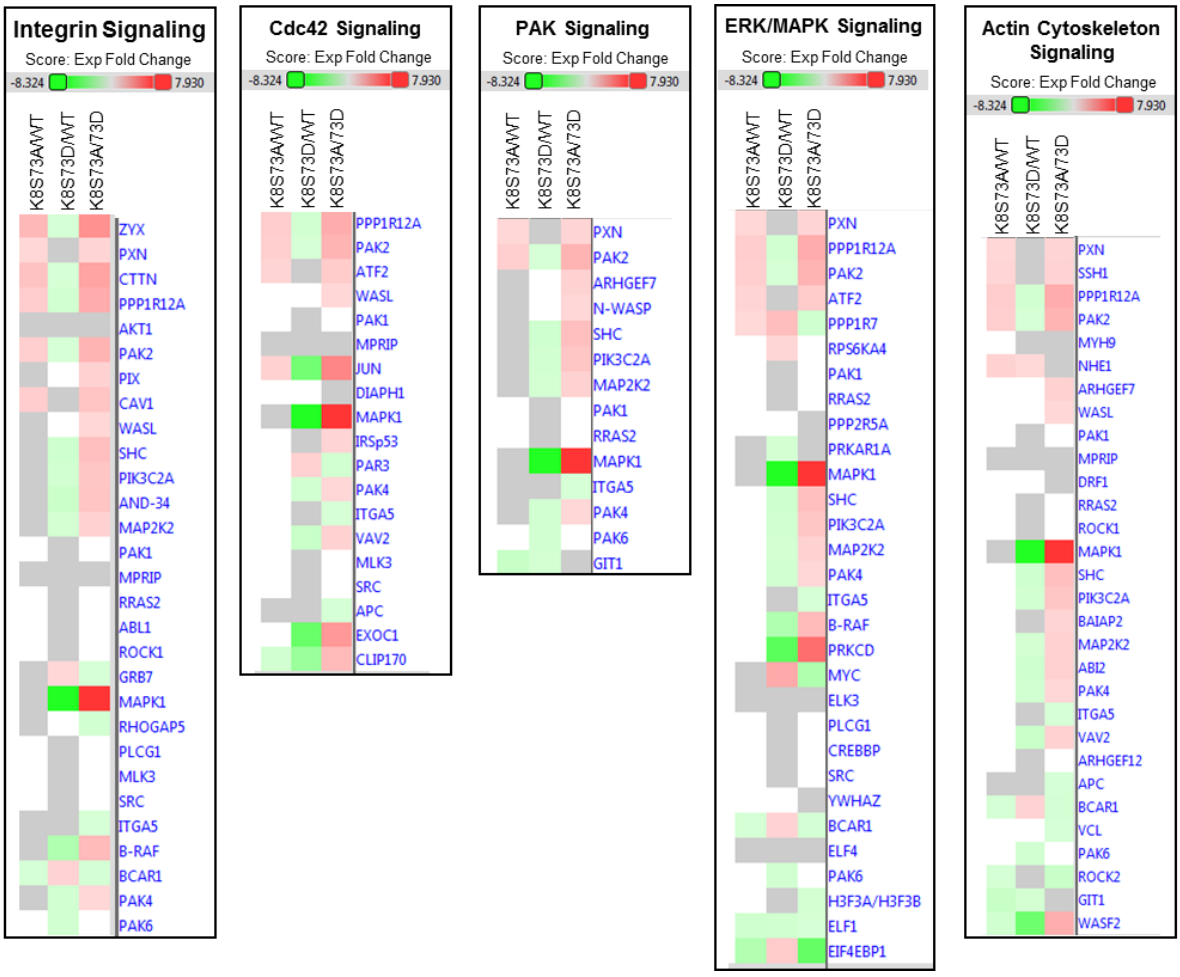

Figure 4.4.4.1.2: Extended IPA Gene Heat Map of "canonical pathway" in K8 Serine[73] dataset: Comparison analysis of K8 Serine[73] dataset using Ingenuity Pathway Analysis (IPA)-"Gene Heat Map" showing phosphoproteins involved in canonical pathways like Integrin, Cdc42, PAK, ERK/MAPK and Actin cytoskeleton organization signaling.

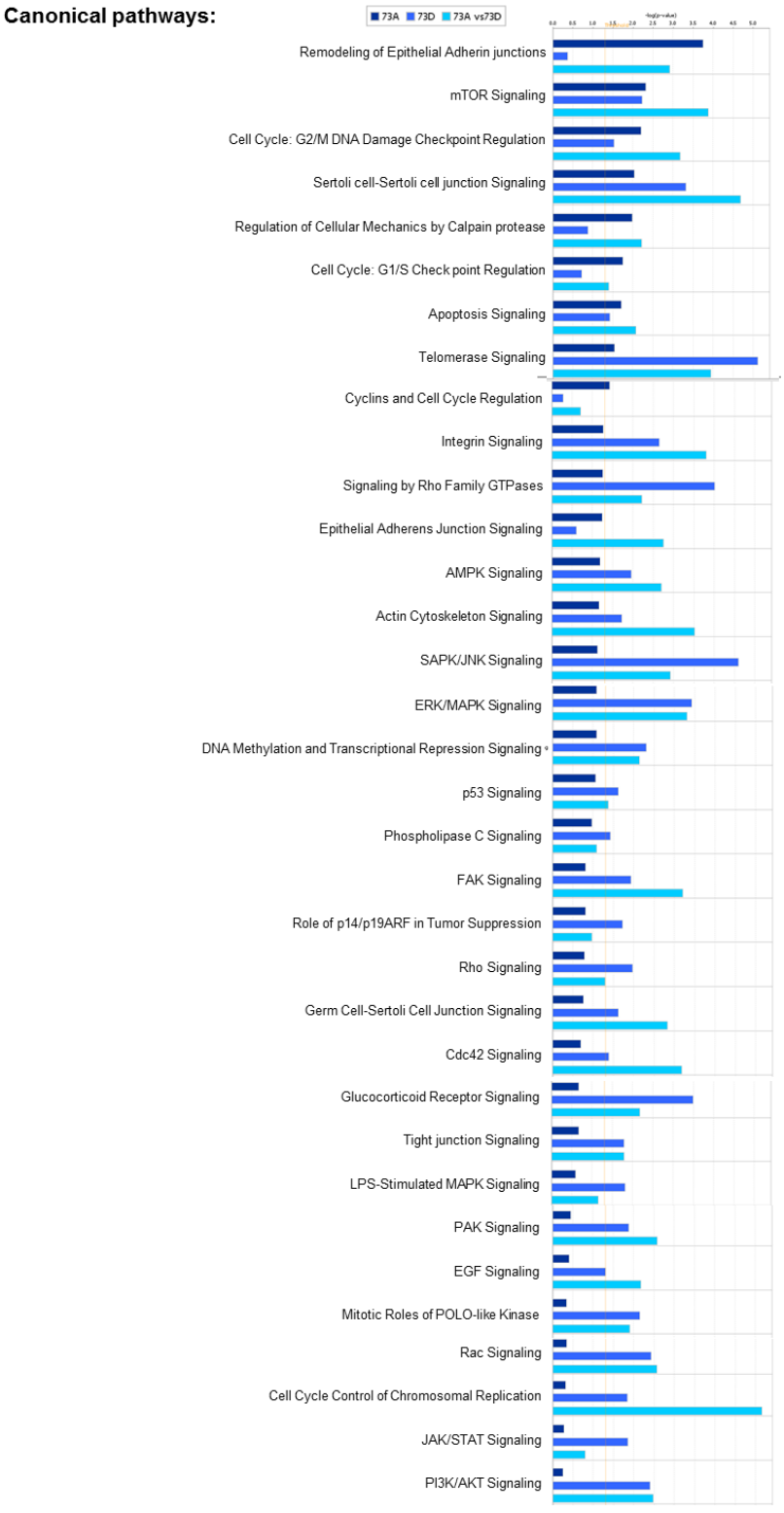

Figure 4.4.4.1.3: Bar chart representing the comparative analysis of significantly altered with high threshold value "Canonical pathways" determined by IPA for K8 Serine[73] dataset.

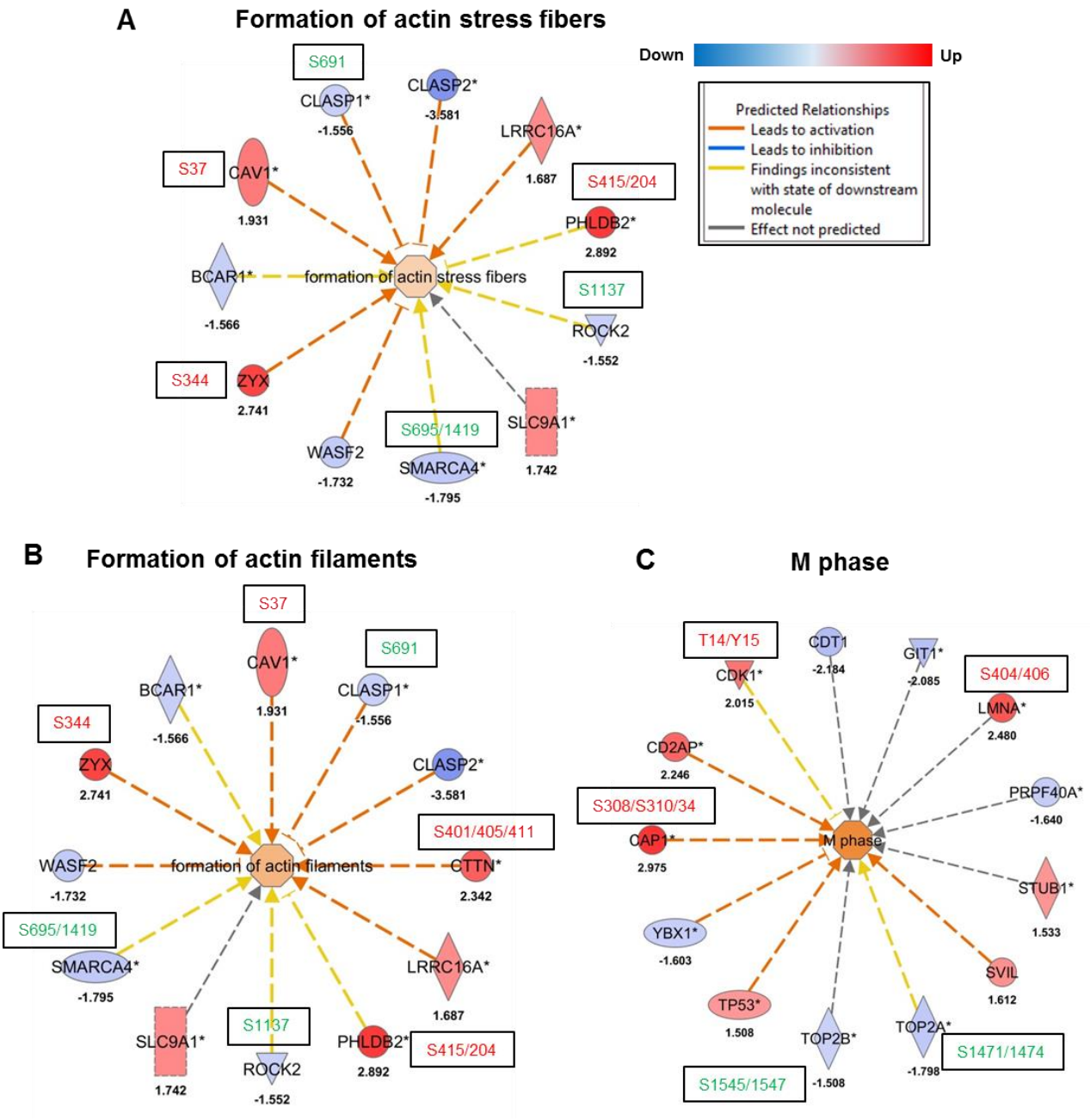

Figure 4.4.4.1.4: Networks showing the phosphorylation status of phosphoproteins involved in biological functions*:* (**A**) Formation of actin stress fibers, (**B**) Formation of actin filaments, (**C**) M-phase for K8 Serine[73] dataset determined by IPA. The value below each molecule represents the up/downregulation of phosphorylation levels at specific residues mentioned aside (Red: up and Green: down).

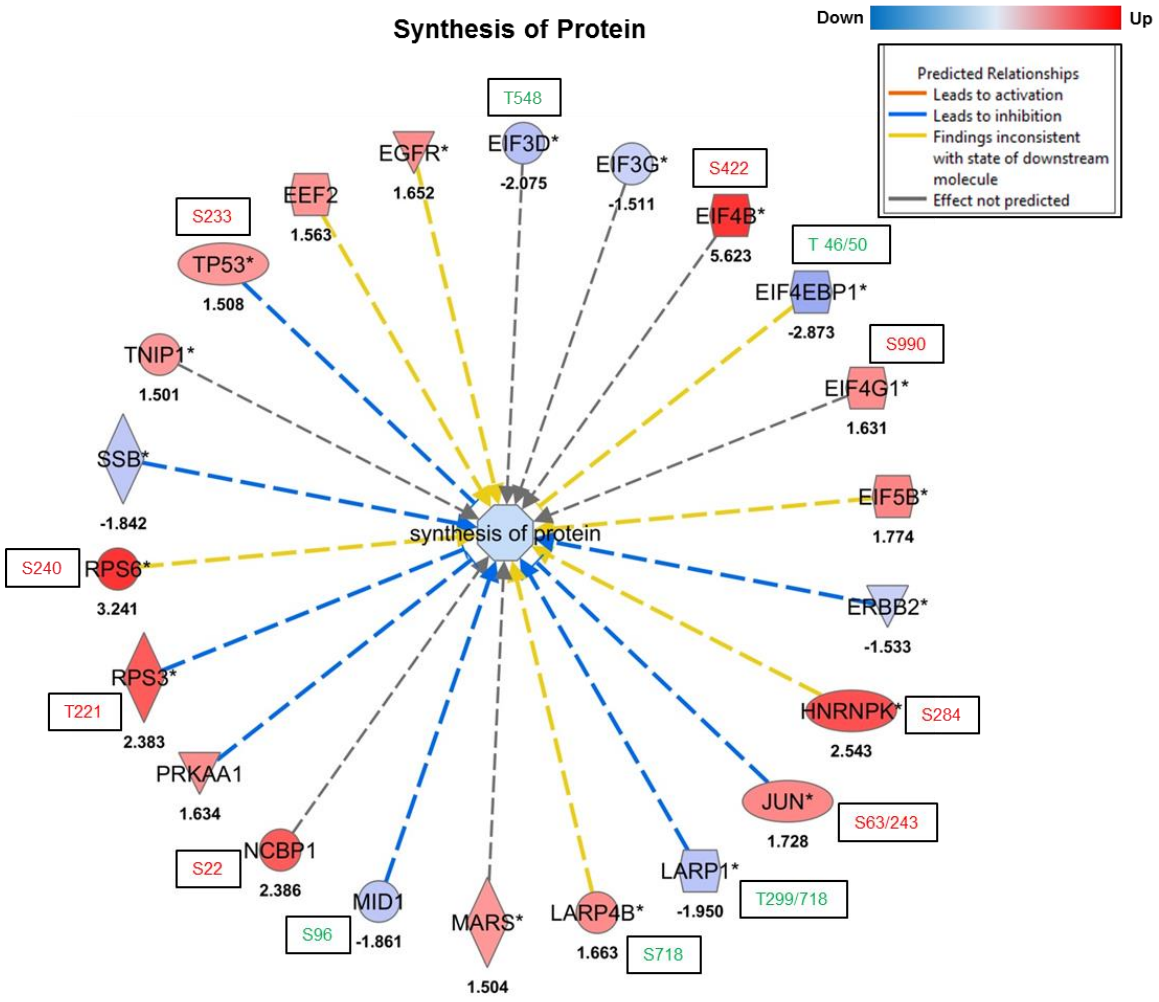

Figure 4.4.4.1.5: Network showing the phosphorylation status of phosphoproteins involved in biological function- "Protein synthesis" for K8 Serine[73] dataset determined by IPA. The value below each molecule represents the up/downregulation of phosphorylation levels at specific residues mentioned aside (Red: up and Green: down).

Moreover, gene heat maps for some major cancer associated pathways including Integrin, cdc42, PAK, ERK/MAPK and Actin cytoskeleton organization signaling were generated, to ascertain the specific phosphoproteins involved. Likewise, IPA-Comparison Analysis for "Disease and biological functions" revealed pathways such as Apoptosis & cell survival, Cell proliferation, Microtubule dynamics and Cell migration to be substantially altered upon deregulation of K8 phosphorylation at Serine[73] residue. This again showed an inverse correlation between

phosphodead and phosphomimetic mutants. Altogether, these results discovered the involvement of many pivotal phosphoproteins including AKT1S1, CTTN, eIF4EBP1, LMNA, CDK1, ZYX and CAV1 as potent modulators of K8 Serine^{73} phosphorylation mediated oncogenesis (**Figure 4.4.4.1.1C)**. For all the important canonical pathways and biological functions, the elaborate gene heat maps, bar charts and ray diagrams are shown in the **Figure 4.4.4.1.2, 4.4.4.1.3, 4.4.4.1.4 (A, B, C), 4.4.4.1.5.**

4.4.4.2 Functional signaling networks modulated by K8 Serine^{431} phosphorylation

The independent IPA- "canonical pathways" analysis determined differential phosphorylation of phosphoproteins involved in pathways comprising Estrogen receptor, Hippo, Sertoli cell junction, JNK/SAPK and CDC42 signaling for K8 Serine^{431} phosphorylation modulation (**Figure 4.4.4.2.1 A)**. The independent "Disease and biological function" analysis for the same exhibited differential regulation of phosphoproteins accompanying; cancer, cell growth, gene expression and cell cycle **(Figure 4.4.4.2.1 B).** Correspondingly, signaling pathways including Sertoli cell junction, Estrogen receptor, Telomerase, JNK/SAPK, CDC42 and Hippo signaling were significantly altered, in K8 S431D dataset (**Figure 4.4.4.2.1 A)**. Furthermore, IPA-Comparison analysis for "Canonical pathways" showed pathways such as; integrin, HIPPO, AMPK, CDC42, Rac, STAT3 and Actin signaling to be significantly altered. Likewise, the "Disease and biological function" analysis for the same, showed most of the phosphoproteins to be involved in Cell survival & viability, Actin dynamics, Microtubule dynamics, Cell proliferation, Invasion and migration. Overall, these results discovered the involvement of many pivotal phosphoproteins including BUB1B, CARHSP1, CTTN, SCRIB, CDK11B and CDK12 as potent modulators of K8 Serine^{431} phosphorylation mediated oncogenesis (**Figure 4.4.4.2.1 C**). For all the important canonical

pathways and biological functions, the elaborate gene heat maps, bar charts and ray diagrams are shown in the figure (**Figure 4.4.4.2.2, 4.4.4.2.3, 4.4.4.2.4, 4.4.4.2.5 A & B, 4.4.4.2.6**).

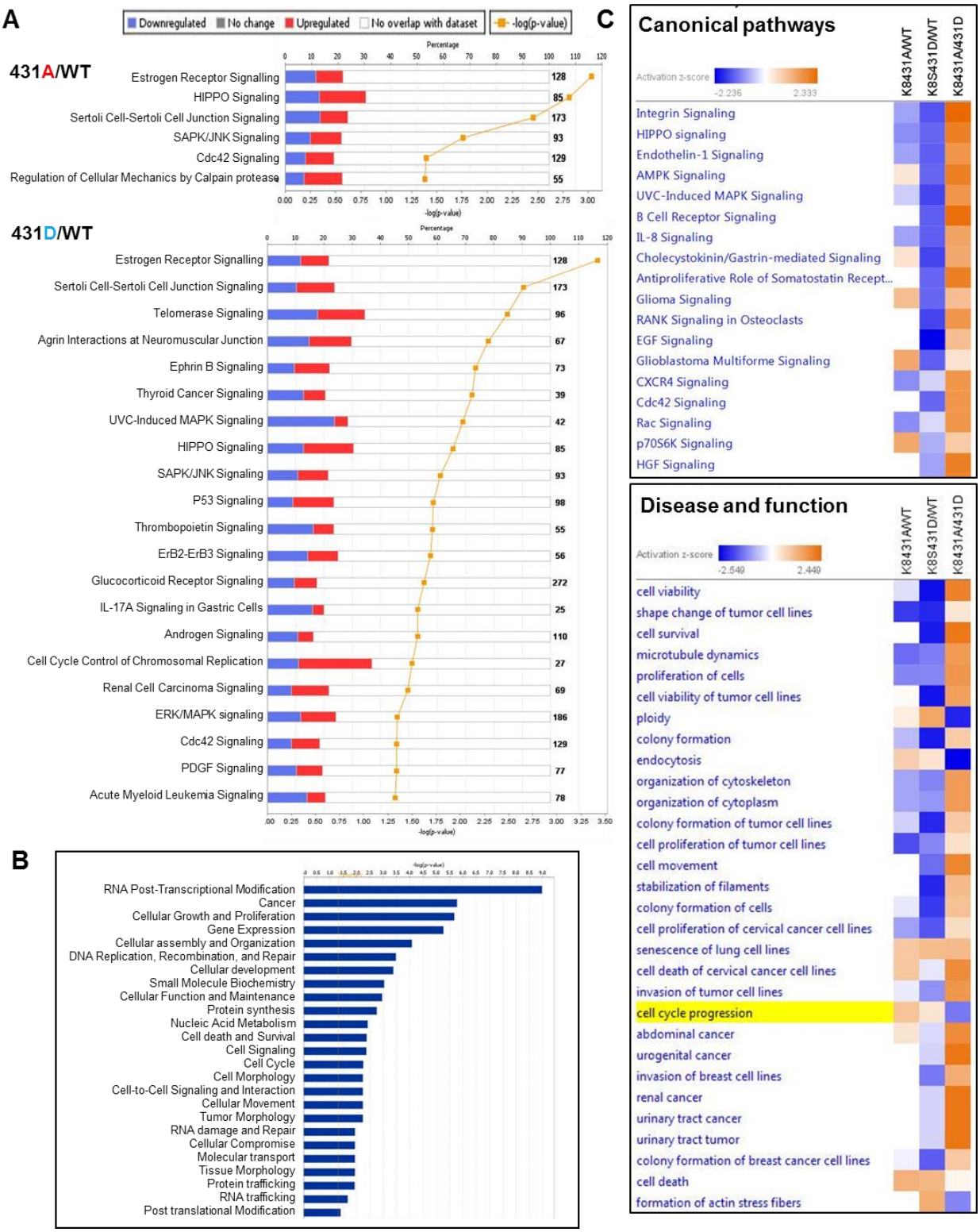

Figure 4.4.4.2.1: Differential phosphoproteomic analysis using IPA for K8 S431A/WT and K8 S431D/WT datasets: (**A**) Representative Bar chart for IPA "Canonical Pathways" shows significantly altered signaling pathways with high-log P-value for both K8 S431A and K8 S431D datasets. The numbers against every bar corresponds to the number of filtered proteins involved in the mentioned pathway. (**B**) Representative bar charts determined by IPA showing Biological function associated with the phosphoproteins for K8 S431A/WT individual dataset. (**C**) Heat maps generated through IPA for "Comparison Analysis" of K8 Serine^{431} dataset (K8 S431A/WT, K8 S431D/WT, K8 S431A/S431D) including "canonical pathways" and "disease and biological function" demonstrate major molecular signaling pathways as well as biological functions affected.

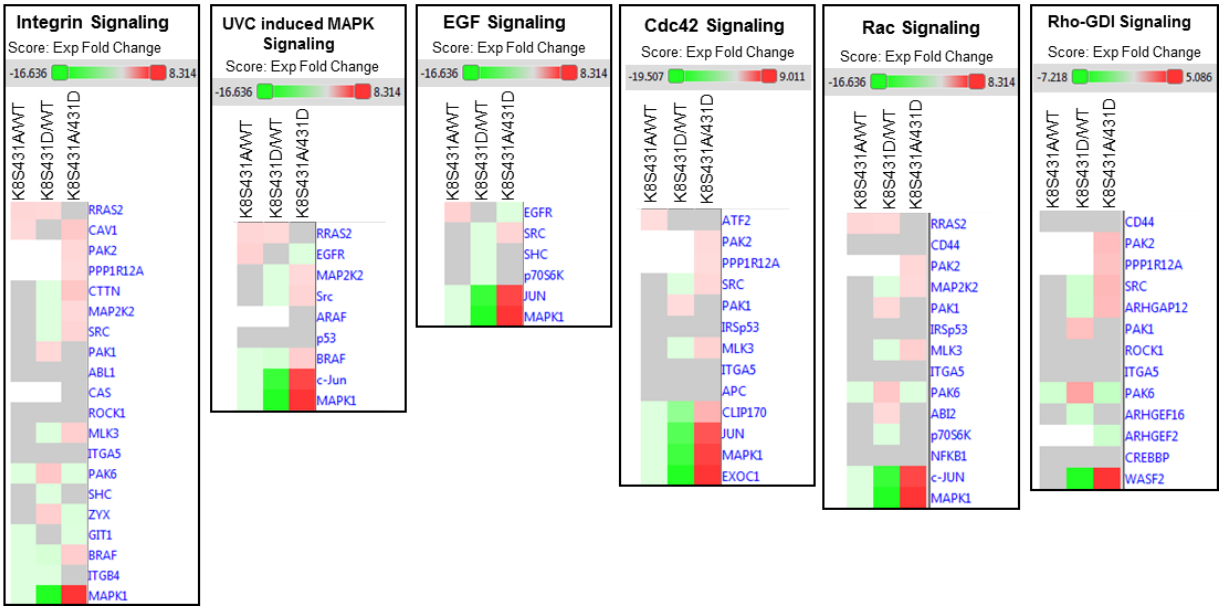

***Figure 4.4.4.2.2: Extended IPA Gene Heat Map of "canonical pathway" in K8 Serine^{431} dataset*:** Comparative analysis of K8 Serine^{431} dataset using IPA "Gene Heat Map" showing phosphoproteins involved in canonical pathways: integrin, UVC induced MAPK signaling, EGF, cdc42, RAC and Rho-GDI signaling.

Canonical pathways:

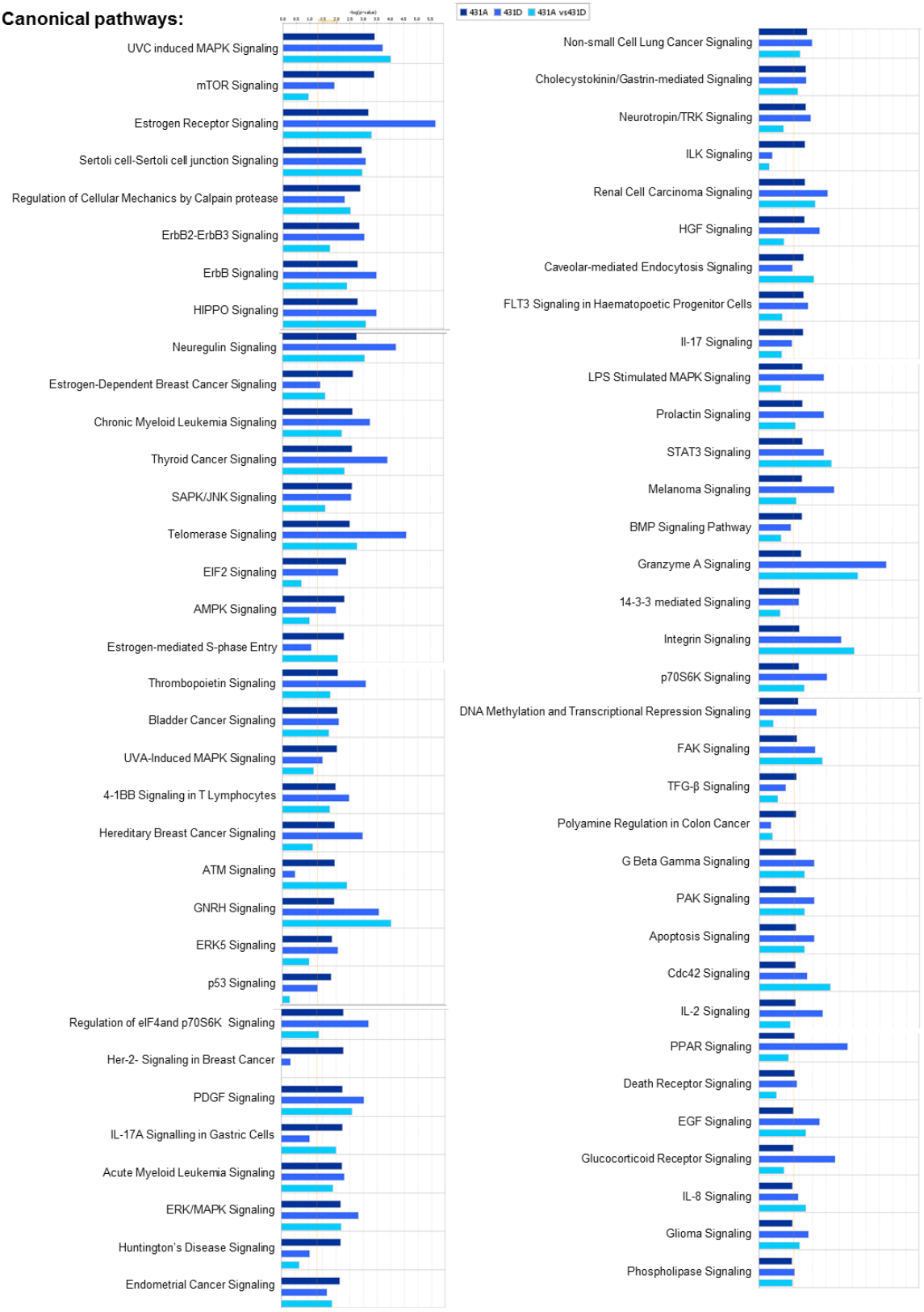

Figure 4.4.4.2.3: Bar chart representing the comparative analysis of significantly altered "Canonical pathways" with high threshold value determined by IPA for K8 Serine^{431} dataset.

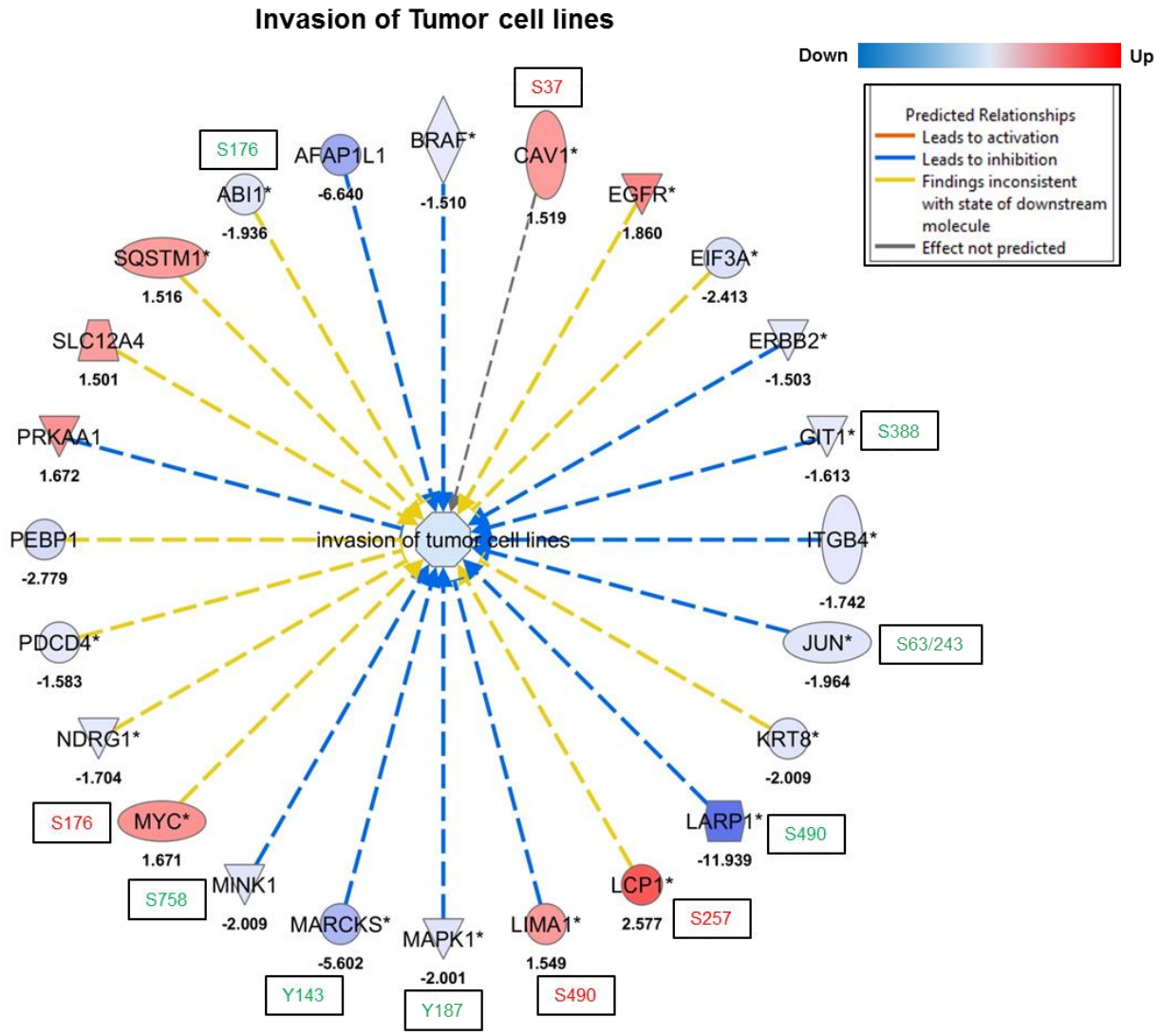

Figure 4.4.4.2.4: Networks showing the phosphorylation status of phosphoproteins involved in biological functions like "Invasion of tumor cell line" for K8 Serine^{431} dataset determined by IPA with a high p-value. The value below each molecule represents the up/downregulation of phosphorylation levels at specific residues mentioned aside (Red: up and Green: down).

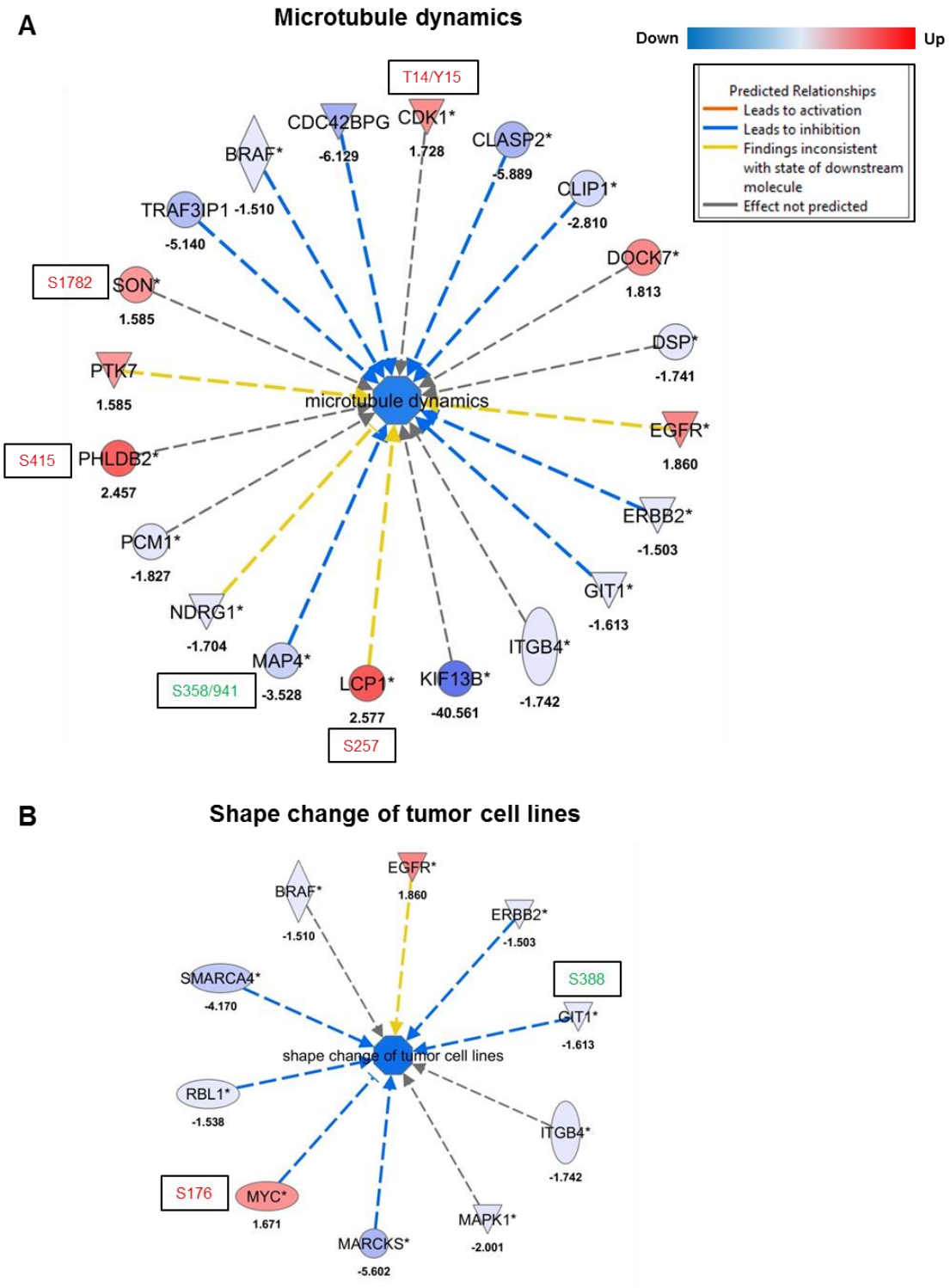

***Figure 4.4.4.2.5*:** Network showing the phosphorylation status of phosphoproteins involved in biological functions like, (**A)** "microtubule dynamics" and (**B**) "shape change of tumor cell line" for K8 Serine[431] dataset determined by IPA with a high p-value. The value below each molecule represents the up/downregulation of phosphorylation levels at specific residues mentioned aside (Red: up and Green: down).

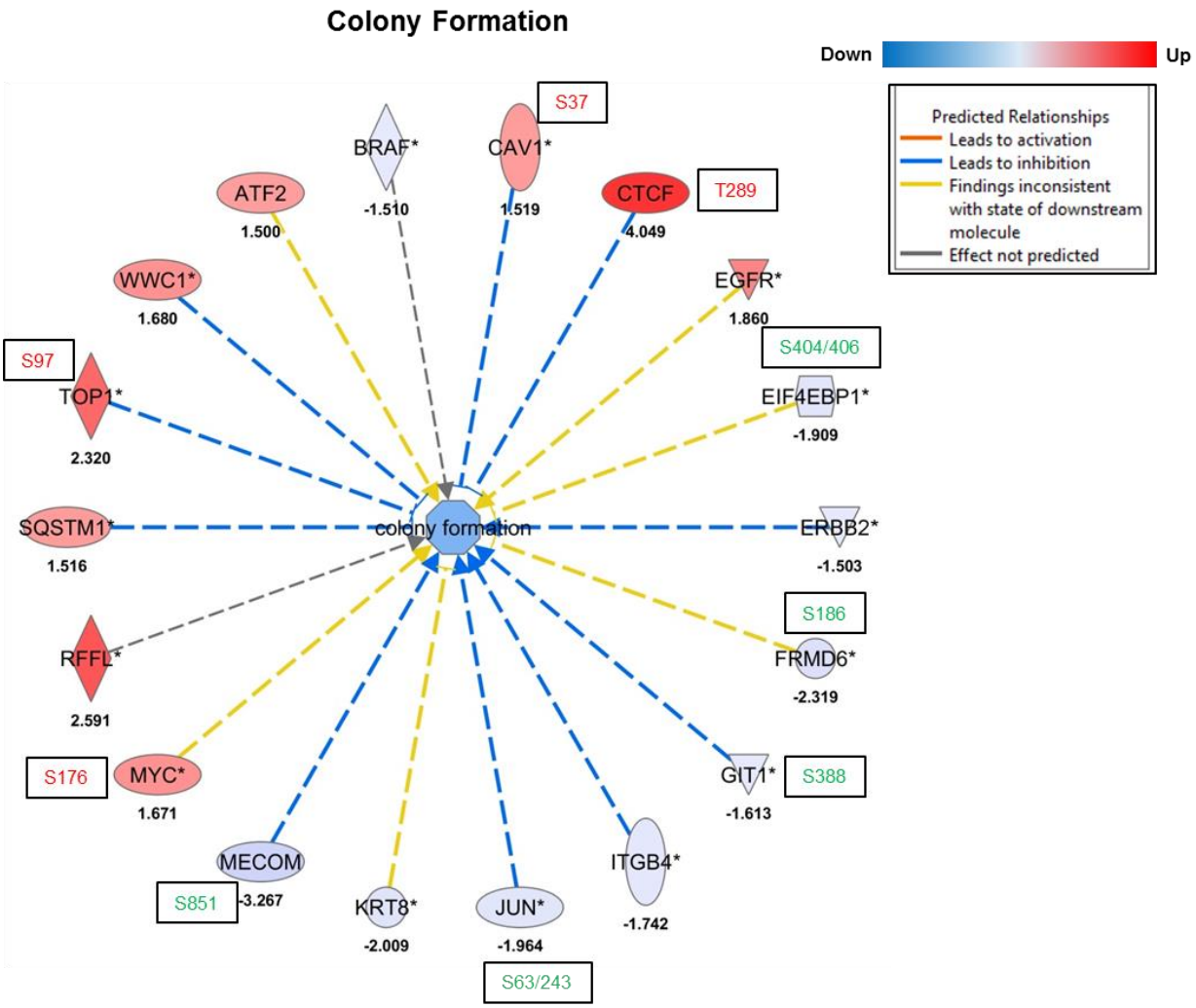

Figure 4.4.4.2.6: Network showing the phosphorylation status of phosphoproteins involved in biological functions like "colony formation" for K8 Serine[431] dataset determined by IPA with a high p-value. The value below each molecule represents the up/downregulation of phosphorylation levels at specific residues mentioned aside (Red: up and Green: down).

4.4.5 Differential phosphorylation pattern of phosphoproteins involved in migration, proliferation and apoptosis in response to K8 phosphorylation

IPA analysis mostly shows signaling pathways or biological functions altered based on the total protein knowledgebase whereas phosphorylation at particular site may affect the function of a protein in many different ways. Therefore, we next focused on the specific phosphosite associated

functions of the phosphoproteins involved in the pathways which were significantly altered as shown in IPA. Further, the phosphoproteins from all 4 datasets were screened according to their involvement in Cell adhesion, migration, proliferation and Apoptosis. These were then subjected to GO-functional annotation. Subsequently, Heat-Maps were generated for the relative phosphorylation levels of selected phosphoproteins using MS-Office-excel. Significant increase in phosphorylation of proteins like CAP1, CTTN, AKT1S1, CDK1, eIF4EBP1, CARHSP1 and LIMA1 could be observed at biologically relevant phosphosites (Sites whose effects on the function of protein upon being phosphorylated or dephosphorylated, is well understood) in case of K8 S73A dataset, whereas K8 S73D dataset showed reversal of the same, in the phosphosite specific heat map. In addition, most of the phosphoproteins were found to be differentially phosphorylated at phosphosites which are novel or less characterized in case of K8 Serine^{431} phosphomutant datasets. Three major phosphoproteins which showed differential phosphorylation at biologically relevant phosphosites with inverse correlation between phosphodead and phosphomimetic mutant for K8 Serine^{431} dataset were; CTTN, BUB1B and CARHSP1 (**Figure 4.4.5.1)**. Heat map for phosphoproteins associated with cell proliferation including, eIF4B, CDK1, eIF4EBP1 and AKT1S1 showed significantly increased phosphorylation at biologically relevant phosphosites in case of K8 S73A dataset with an inverse correlation in K8 S73D dataset. Additionally, similar differential phosphorylation pattern on unidentified/less-characterized phosphosites in case of K8 S73A and K8 S431A mutants together with reversal of the same in K8 S73D and K8 S431D datasets for LAMTOR1, MYC, STK10, BAP1, BRAF, ZYX, LARP1, CDK11B was observed (**Figure 4.4.5.2 A)**. Most of the phosphoproteins like CASP1, BCL2L12, EEF1D and HNRNPK which are involved in apoptotic pathways were found to be differentially phosphorylated at the novel or less-characterized phosphorylation sites among the phosphodead

and phosphomimetic datasets for both the mutants (**Figure 4.4.5.2B)**. Altogether, these computational analyses demonstrated many known and novel phosphorylation sites of phosphoproteins involved in cancer associated phenotypes to be differentially phosphorylated in response to K8 phosphorylation ablation in site specific manner (**Figure 4.4.5.1 and 4.4.5.2 A, B)**.

Cell adhesion and migration

1	2	3	4	5	6	7	8
AHNAK	S2397	3.76	1.28	1.37	1.65	2.94	0.83
TJP2	S986	3.65	1.15	1.40	1.21	3.19	1.16
LIMA1	S604	3.59	0.76	1.40	1.11	4.70	1.26
CAP1	S308; S310	2.98	0.34	0.81	0.13	8.71	6.45
SCRIB	S1437	2.90	1.68	3.07	1.22	1.72	2.52
AHNAK	S5099	2.78	1.09	1.43	1.35	2.54	1.06
ZYX	S344	2.74	0.64	0.75	1.97	4.27	0.38
CAP1	S308; S310	2.66	1.14	1.06	0.79	2.34	1.35
AHNAK	S559	2.56	0.77	0.73	0.54	3.31	1.36
AHNAK	S177	2.55	0.89	0.93	0.91	2.86	1.02
LAD1	S394	2.49	0.84	1.36	0.97	2.96	1.40
LMNA	S404; S406	2.48	0.95	1.21	0.92	2.62	1.32
CDK11A	T570	2.40	1.58	0.87	3.31	1.52	0.26
AHNAK	T490	2.40	1.19	0.97	1.24	2.02	0.78
AJUBA	S137	2.36	0.84	1.32	1.16	2.81	1.14
CTTN	T401; S405; Y421	2.34	0.66	1.05	0.45	3.56	2.32
TJP2	S1159	2.08	0.70	0.96	1.39	2.98	0.69
AKT1S1	S247	2.05	0.91	1.27	0.91	2.25	1.40
CDK1	T14; Y15	2.01	0.82	1.27	0.76	2.47	1.68
ABI1	S176	1.95	0.74	1.35	2.16	2.62	0.63
PHLDB2	S415	1.24	0.44	1.01	0.53	2.81	1.91
FAM83H	S936	1.17	2.54	1.00	0.97	0.46	1.02
SYMPK	S1243	1.16	3.08	1.35	1.38	0.38	0.98
DOCK7	S888	1.12	0.28	0.97	0.68	4.00	1.43
LMNA	S406	1.07	4.44	0.95	1.54	0.24	0.61
INADL	S1661	1.07	2.26	1.89	6.02	0.48	0.31
NDRG1	S271	1.06	0.18	0.59	0.18	5.92	3.20
DLG1	S158	1.03	0.50	1.29	1.22	2.05	1.06
ZC3HC1	S395	1.00	0.52	0.64	0.31	1.94	2.04
CDC42EP1	S192	0.98	0.45	0.87	1.40	2.19	0.62
PALLD	S393	0.98	2.05	1.06	2.26	0.48	0.47
CTNND1	S248	0.93	0.42	0.74	1.02	2.24	0.73
JUN	S243	0.90	0.19	0.51	0.07	4.67	7.49
ABI1	S119	0.87	0.37	0.52	0.38	2.37	1.37
MINK1	S758	0.87	0.21	0.50	0.08	4.13	6.53
BRAF	S446	0.87	0.39	0.66	0.33	2.24	2.00
MICAL3	S2002	0.82	0.10	0.82	1.22	8.00	0.68
FRMD6	S186	0.81	0.16	0.43	0.06	5.04	7.53
KRT5	S82	0.81	0.36	0.76	1.00	2.26	0.76
PNN	S692	0.80	2.65	1.56	2.96	0.30	0.53
PKP2	S151	0.80	0.24	0.42	0.27	3.32	1.54
LLGL2	S653	0.76	0.27	0.77	0.71	2.78	1.08
PKP3	S180	0.72	0.12	0.38	0.08	6.11	4.66
KRT8	T218	0.72	0.83	0.50	1.46	0.86	0.34
ANKRD26	S530	0.71	2.67	1.09	1.18	0.27	0.92
PTK7	S654	0.71	1.66	1.59	2.14	0.43	0.74
RIN1	S337	0.59	1.08	1.10	2.20	0.54	0.50
EIF4EBP1	T46; T50	0.35	1.99	0.52	1.01	0.17	0.52

Fold change

Down — Up

1. Gene Symbol
2. Phosphorylation sites on protein
3. K8-S73A/ K8-WT
4. K8-S73D/ K8-WT
5. K8-S431A/ K8-WT
6. K8-S431D/ K8-WT
7. K8-S73A/ K8-S73D
8. K8-S431A/ K8-S431D

***Figure 4.4.5.1*:** Phosphorylation oriented functional annotation Heat-maps for Cell adhesion-migration depicting the differential phosphorylation sites on the phosphoproteins; mentioned in column-1 & 2. The color code represents to the fold change in relative levels of phosphorylation at specific sites.

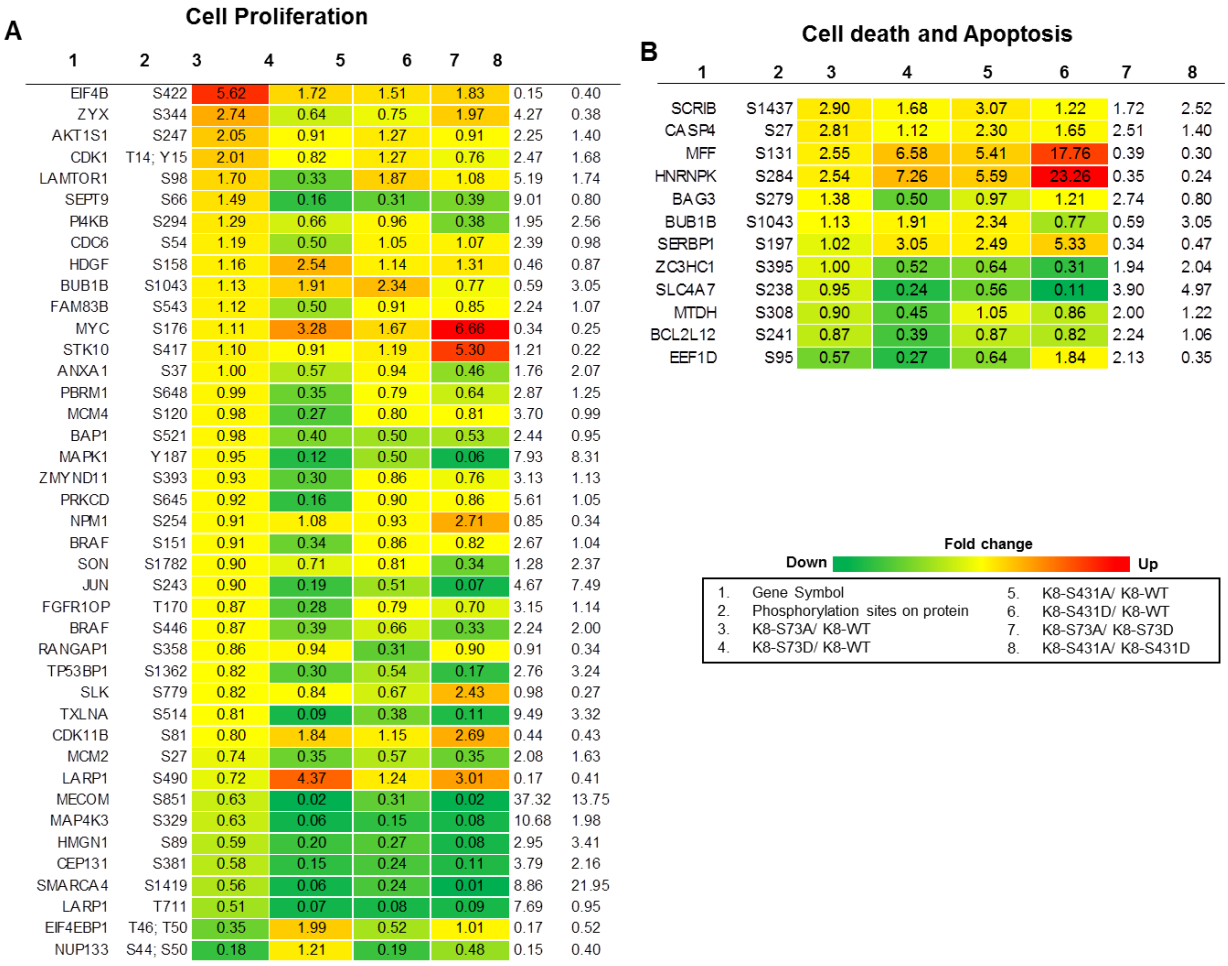

***Figure 4.4.5.2*:** Phosphorylation oriented functional annotation Heat-maps for (**A**) "Cell proliferation" and (**B**) "cell death and apoptosis" depicting the differential phosphorylation sites on the phosphoproteins; mentioned in column-1 & 2. The color code represents to the fold change in relative levels of phosphorylation at specific sites.

4.4.6 Interaction analysis of different Phosphoproteins detected across different phosphomutant datasets

Next, to elucidate the Protein-Protein Interaction (PPI) amongst the large variety of aforementioned phosphoproteins, we performed STRING analysis for all the datasets as there were a significant proportion of total phosphoproteome altered in response to a single twitch i.e., K8 site specific phosphorylation. A significant number of interactions between phosphoproteins with

high –log P-values could be confirmed by PPI network analysis (**Figure 4.4.6.1 A, 4.4.6.2 A, 4.4.6.3 A, 4.4.6.4 A**). We selected cell migration associated signaling network (**Figure 4.4.6.1 B, 4.4.6.2 B, 4.4.6.3 B, 4.4.6.4 B**)., one of the significantly altered biological function as shown in our IPA analysis and GO-Functional annotation, as a proof of principle and plotted separately (**Figure 4.4.6.5**). There were strong interactions between CAP1, CDK1, ZYX, CTTN, TJP2, DSP, PKP3, MAPK1, JUN, MYC, PNN and KRT8 as shown in PPI analysis. The pictorial representation in figure shows the predicted interactions within phosphoproteins associated with Cell migration. The differentially regulated phosphosites were annotated on the respective phosphoproteins. Nevertheless, to establish their chronology in the pathway, further validation of the phosphorylation status together with the interactions of these proteins is essential.

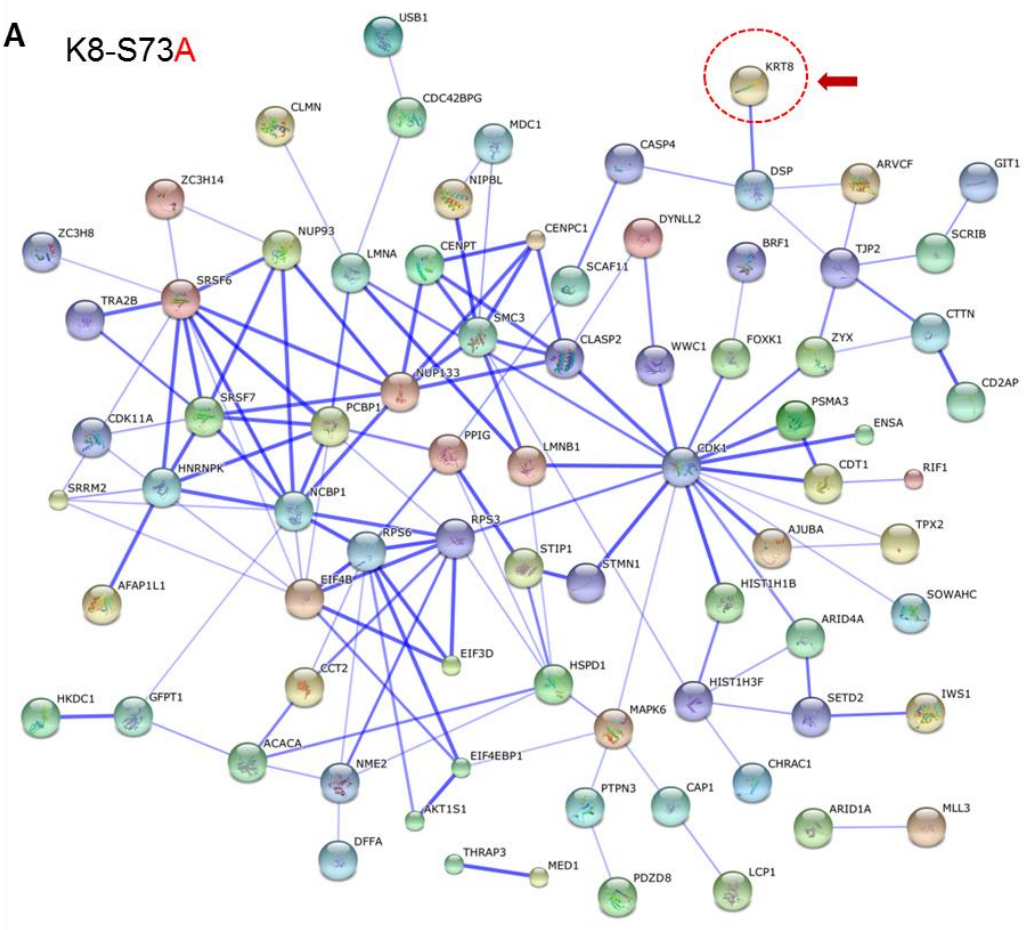

Figure 4.4.6.1**:** (**A**) STRING analysis for biological interactions with significant alteration in their relative phosphorylation levels) for K8 S73A/WT dataset. (**B**) STRING analysis for the differential regulated genes in K8 S73A/WT dataset; associated with cell migration function. The blue line represents the confidence levels and thickness indicates the strength of data support. The red-dotted circle indicates Keratin 8 position in the networks.

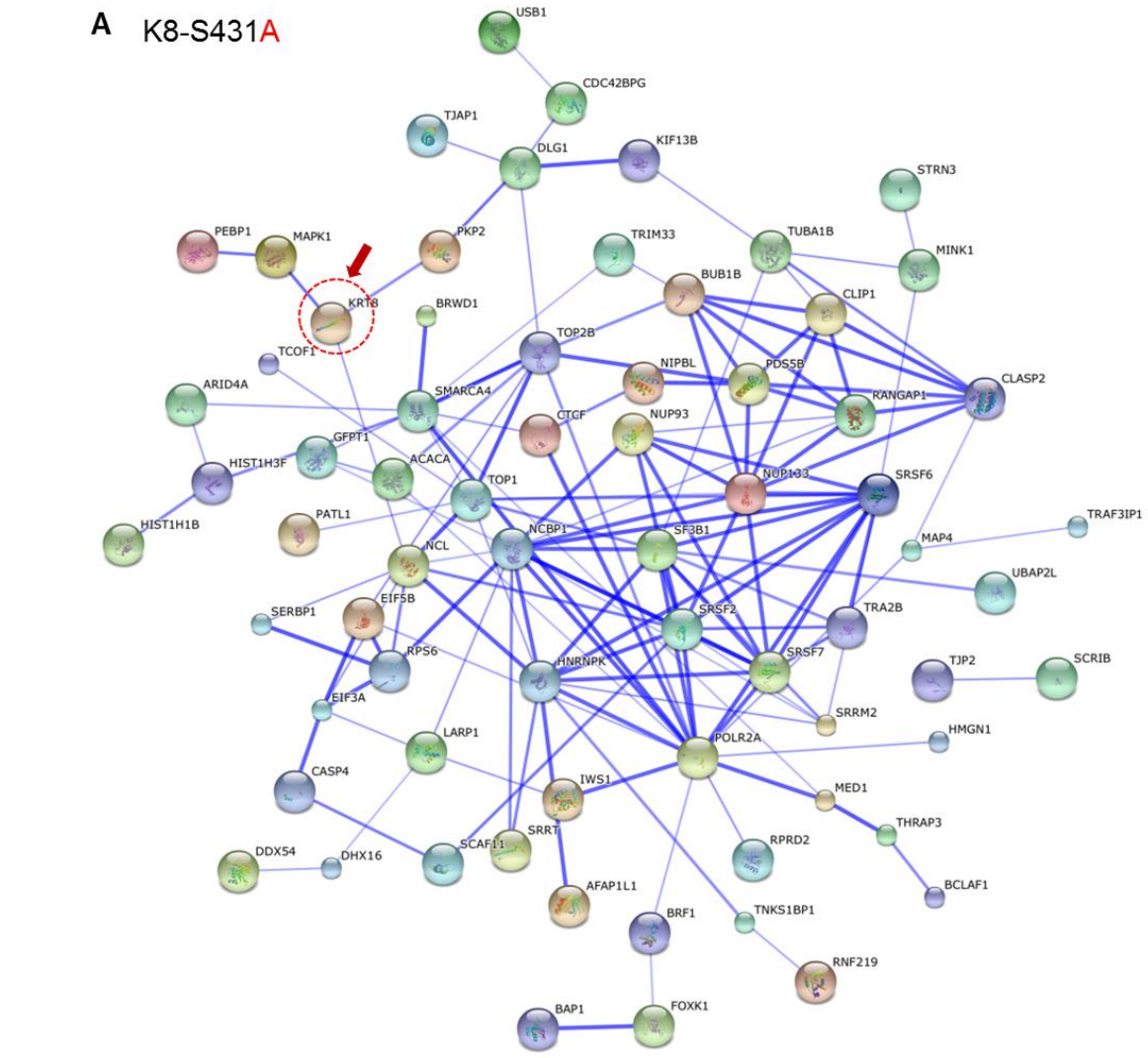

Figure 4.4.6.2: (**A**) STRING analysis for biological interactions within phosphoproteins with significant alteration change in their relative phosphorylation levels for K8 431A/WT dataset. (**B**) STRING analysis for the differential regulated genes in K8 S431A/WT dataset; associated with cell migration function. The blue line represents the confidence levels and thickness indicates the strength of data support. The red-dotted circle indicates Keratin 8 position in the networks.

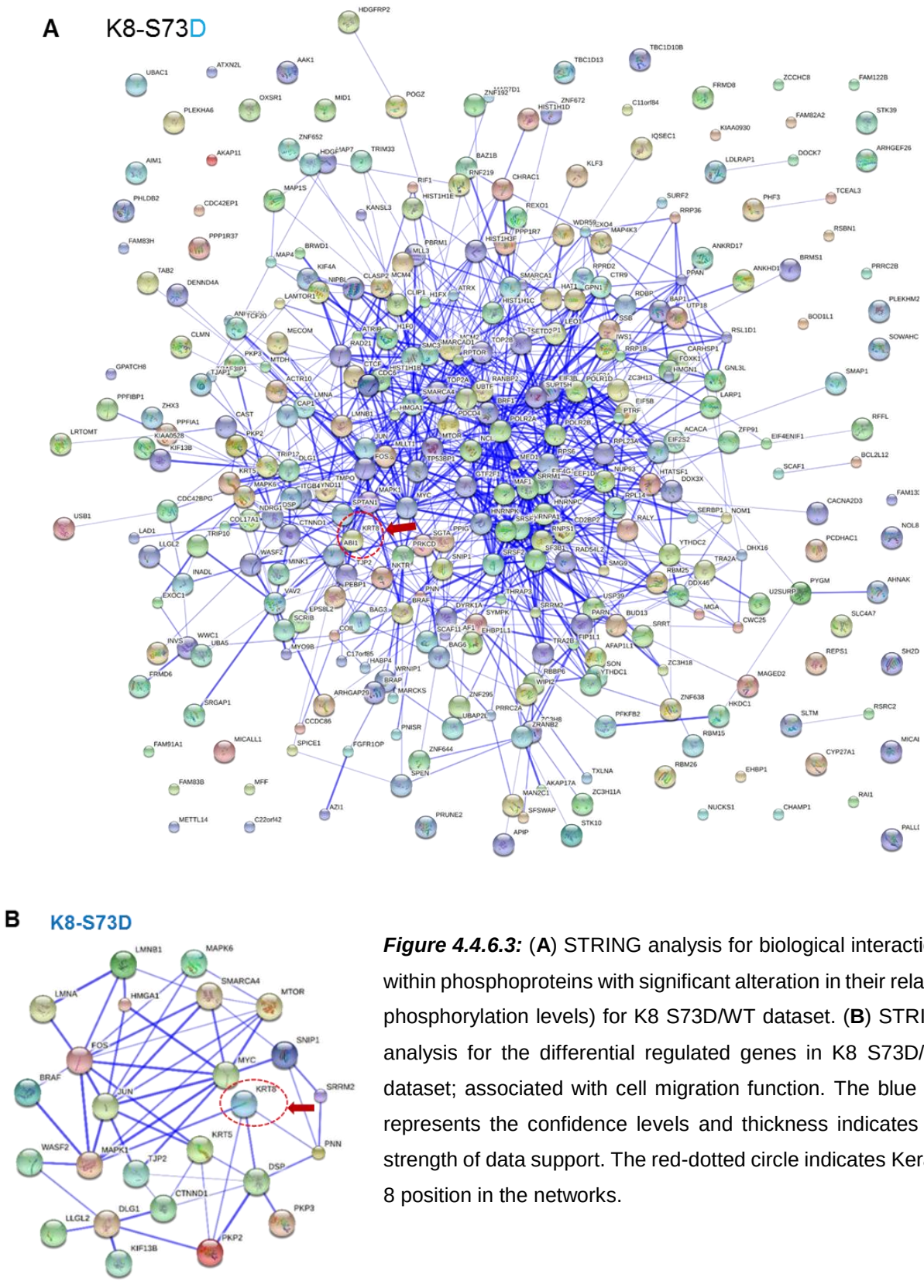

Figure 4.4.6.3: (**A**) STRING analysis for biological interactions within phosphoproteins with significant alteration in their relative phosphorylation levels) for K8 S73D/WT dataset. (**B**) STRING analysis for the differential regulated genes in K8 S73D/WT dataset; associated with cell migration function. The blue line represents the confidence levels and thickness indicates the strength of data support. The red-dotted circle indicates Keratin 8 position in the networks.

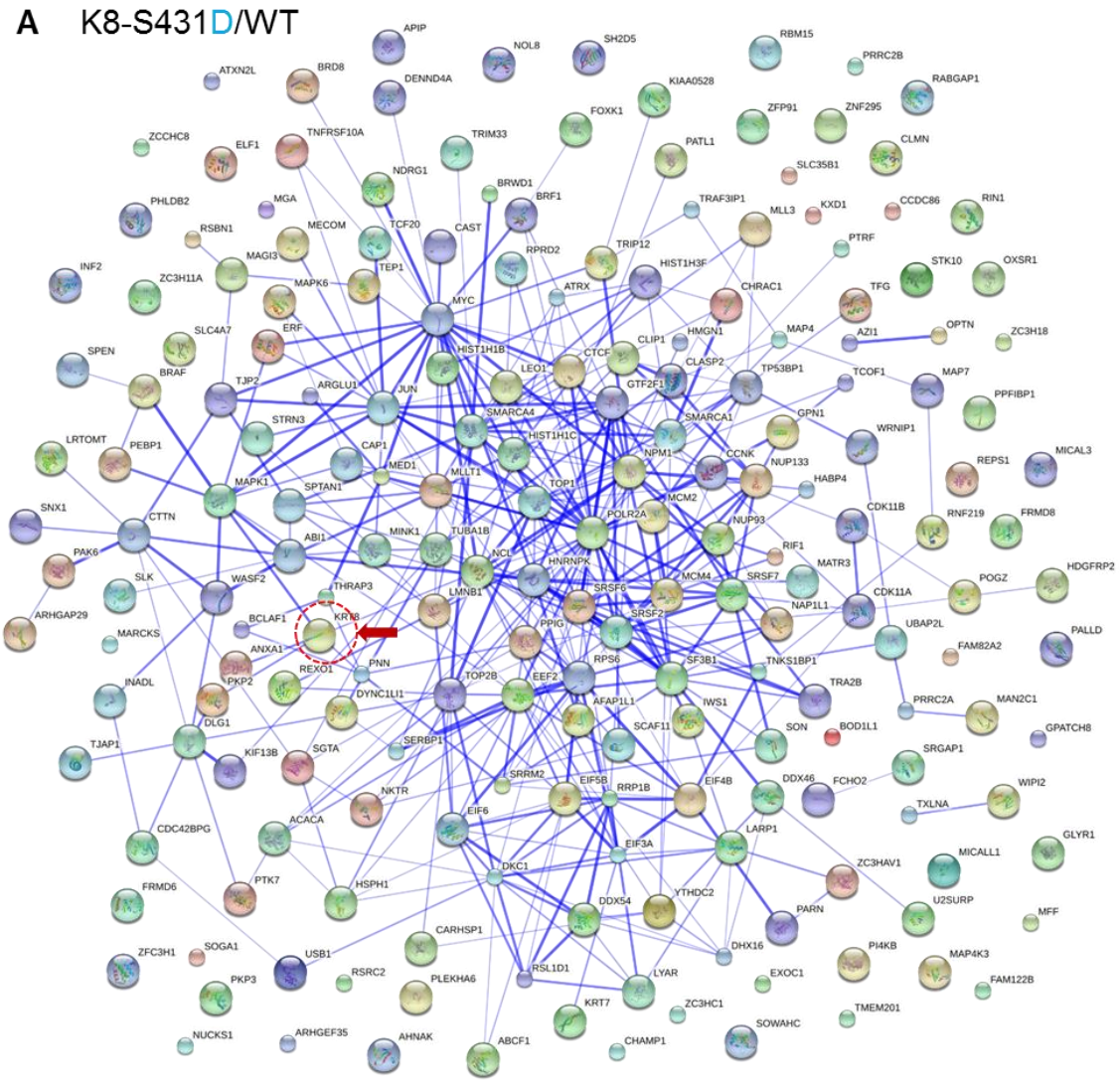

Figure 4.4.6.4: **(A)** STRING analysis for biological interactions within phosphoproteins with significant alteration change in their relative phosphorylation levels for K8 431D/WT dataset. (**B**) STRING analysis for the differential regulated genes in K8 S431D/WT dataset; associated with cell migration function. The blue line represents the confidence levels and thickness indicates the strength of data support. The red-dotted circle indicates Keratin8 position in the networks.

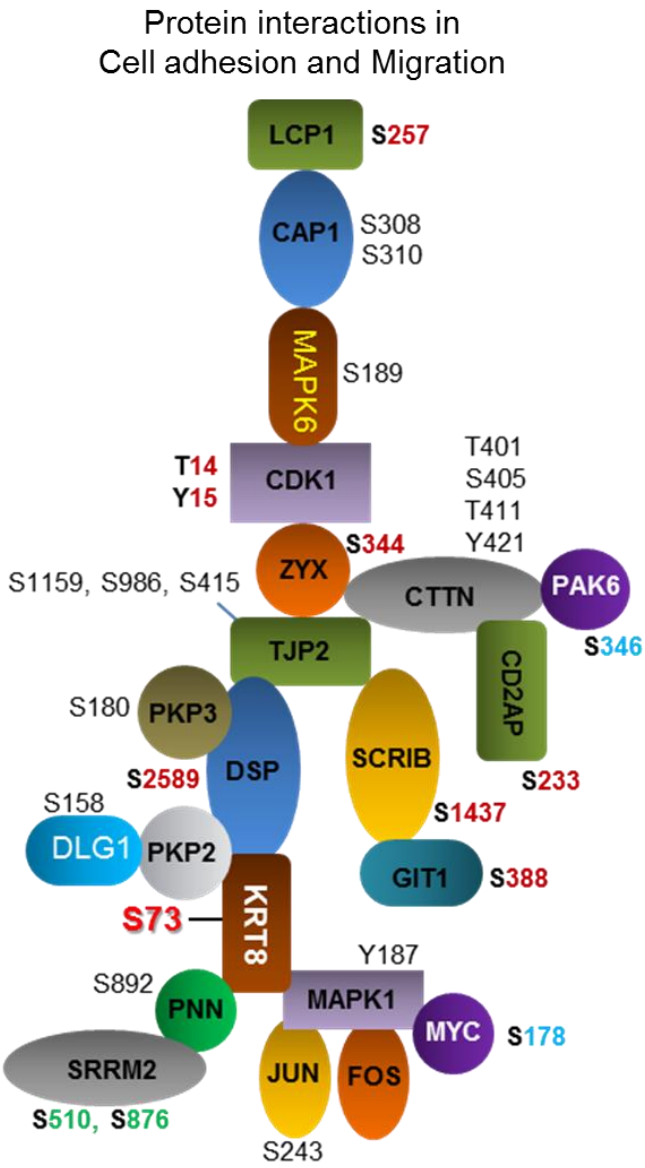

Figure 4.4.6.5: Schematic model representing possible interactions within the phosphoproteins derived from STRING analysis for cell migration and adhesion function.

In addition, we used Enrichr analysis web server to determine the PPI hub proteins (The key regulators) upstream to the significantly altered phosphoproteins with inverse correlation in both K8 Serine[73] and K8 Serine[431] datasets. Majority of phosphoproteins from our dataset were found to be clustered under CDK2, GSK3β, MAPK14, CDK1 and MAPK1 like protein kinases in the Clustergrammer with 'protein kinase' as enriched term. This enabled us to narrow down to major

key kinases and their corresponding downstream effectors (which showed differential phosphorylation and an inverse correlation between the phosphodead and phosphomimetic mutants) befall together in the dataset. For instance, SRRM2, eIF4EBP1, ZYX, CTTN; which fall in the K8 Serine^{73} dataset together with CDK1 the key upstream kinase for them. Such kinases were considered for further analysis based on the biological relevance of their corresponding phosphosites (**Figure 4.4.6.6 A, B)**. In addition, we subjected the phosphoproteins with significantly altered phosphorylation (showing reversal of differential phosphorylation status between phosphodead and phosphomimetic datasets) to "Panther classification system". According to protein class the distribution of such phosphoproteins showed 7 kinases (CDK1, CDK10, MAPK1, AAK1, PGK1, CDK12 and CDK11B) and 3 kinases (CDK12, CDK11B and MAP3K11) in K8 Serine^{73} and K8 Serine^{431} datasets respectively (**Figure 4.4.6.7 A, B)**. These results put forward a hypothesis that under the effect of K8 site specific phosphorylation modulation, these kinases may regulate the phosphorylation of many phosphoproteins and thereby govern cancer associated signaling pathways. Based upon the intricate analysis of phosphoproteomics data, comprehensive model pathways were then reconstructed using IPA tool for functions which were predominantly altered in response to site specific K8 phosphorylation ablation. Major signaling cascades emphasized many phosphoproteins associated with Cell proliferation, Actin organization, Cell survival and Gene expression regulation to be deregulated by K8 phosphorylation modulation, (the pathways were depicted with phosphorylation annotation) (**Figure 4.4.6.8 and 4.4.6.9**).

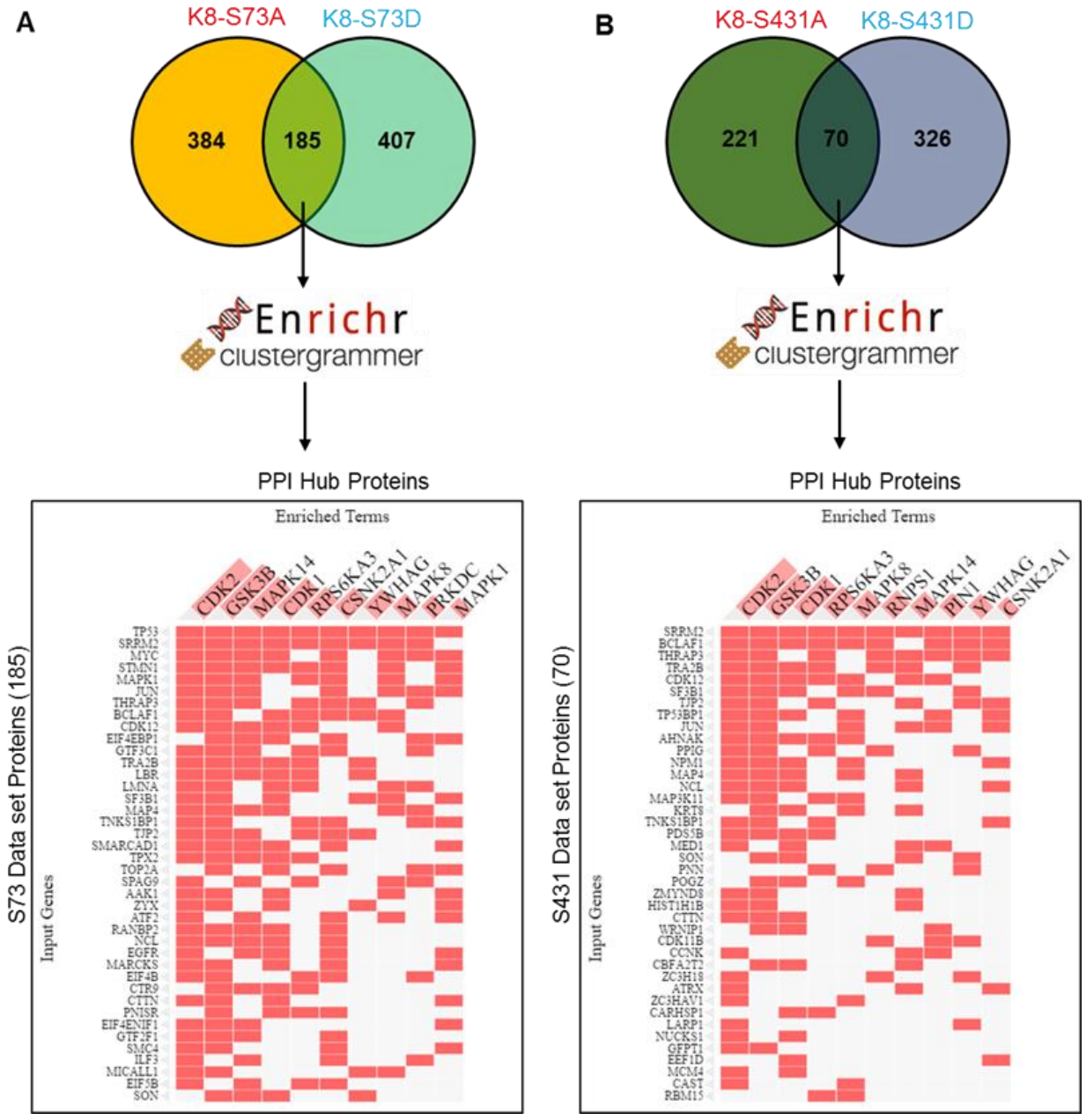

Figure 4.4.6.6: Extended clustergrammer and network analysis for differentially regulated phosphoproteins: (**A, B**) "Enrichr-PPI hub proteins" analysis of common phosphoproteins (differentially regulated with inverse correlation) within both the phosphodead and phosphomimetic mutant pair; (**A**) K8 S73A/D and (**B**) K8 431A/D dataset. The clustergrammer chart depicts the PPI hub proteins clustered under kinases as Enriched Terms, with highest p-value at left-hand side, upstream to the corresponding phosphoproteins.

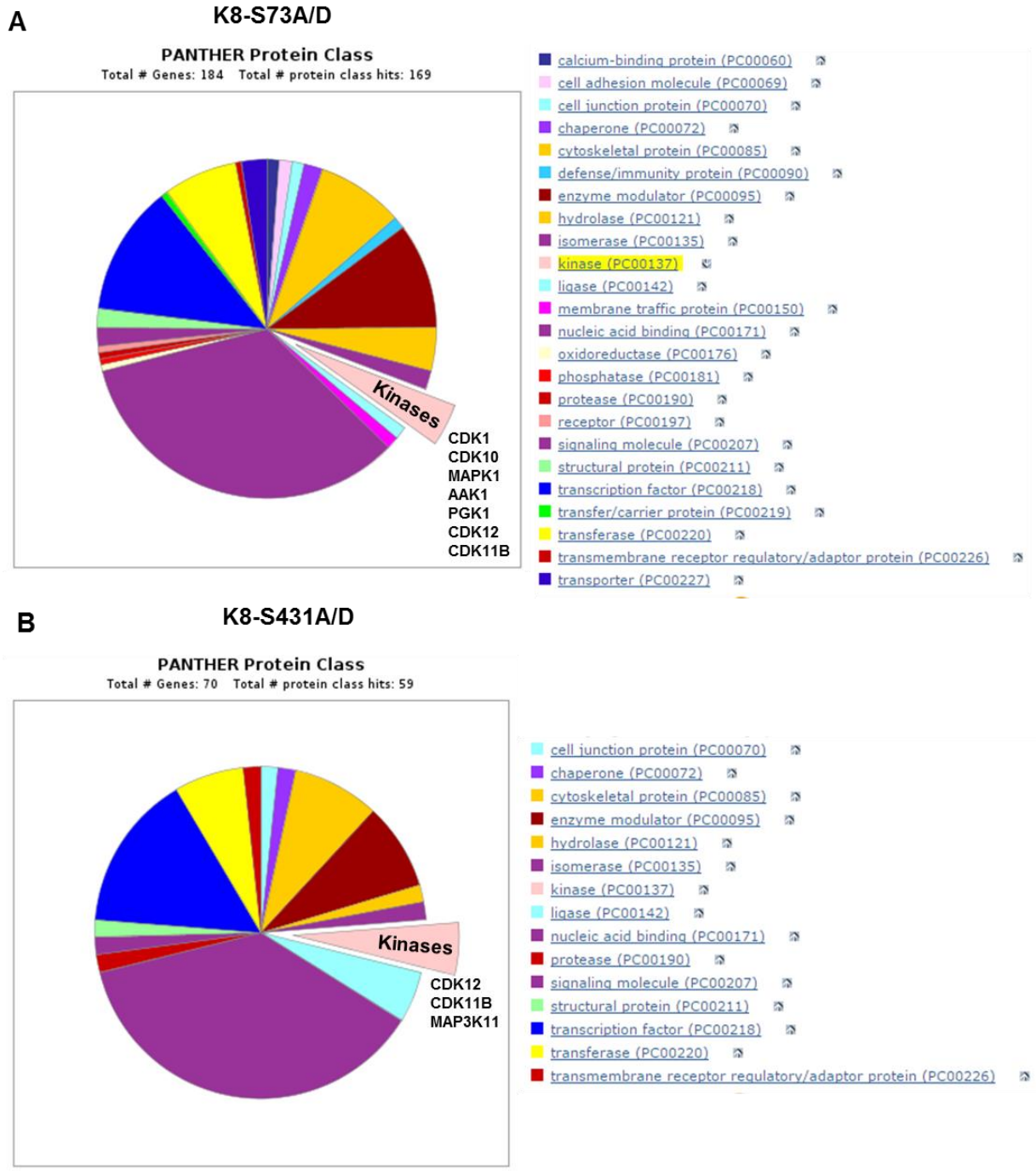

Figure 4.4.6.7: Panther analysis for protein class of the phosphoproteins showed significantly reversal phosphorylation levels within the two phosphodead and phosphomimetic pairs; (**A)** K8 S73A/D and (**B**) K8 431A/D dataset. Pie chart shows the protein class with highlighted kinase molecules within the list inserted.

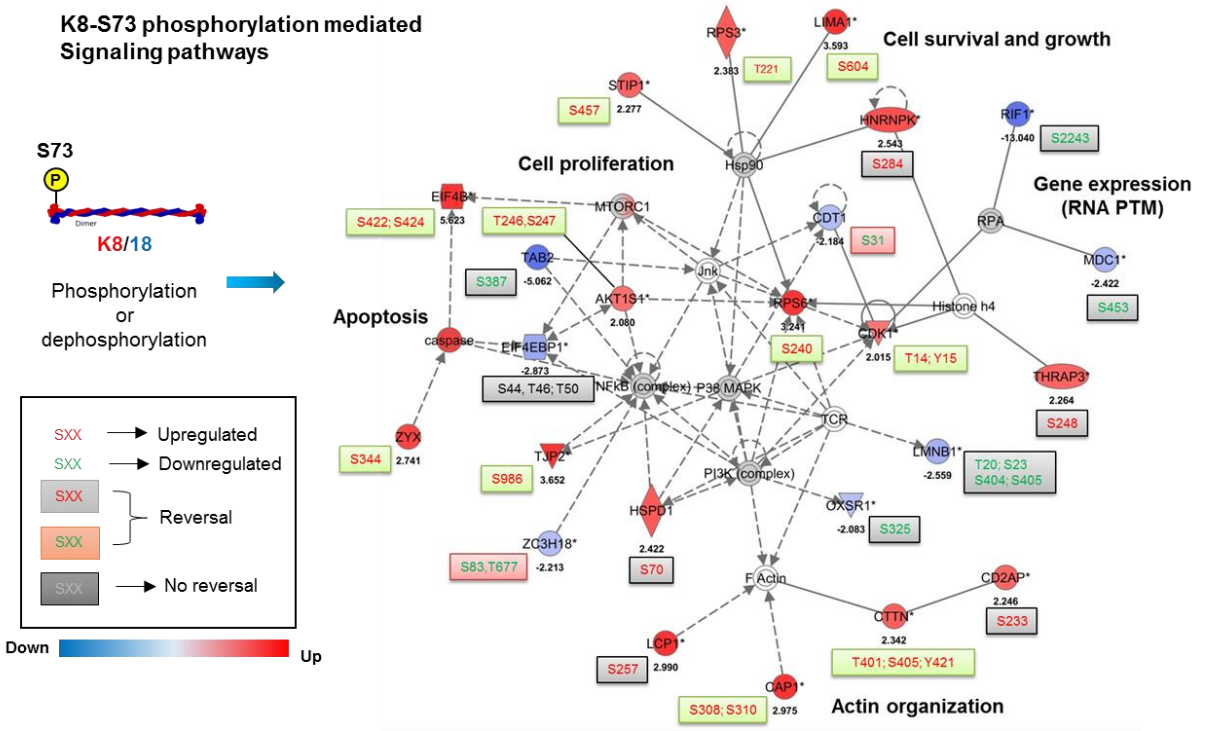

Figure 4.4.6.8: K8 Serine[73] phosphorylation mediated signaling pathways mapped by IPA. The phosphorylation sites detected were assigned with the phosphoproteins.

4.4.7 Validation of identified proteins by Western blotting:

Western blot analysis was then performed to validate differentially phosphorylated phosphoproteins within K8 Serine[73] and K8 Serine[431] datasets with phospho-specific antibodies whereas total protein antibodies of the respective phosphoproteins were used as control. The distribution of the phosphoproteins according to the protein class showed 7 kinases (CDK1, CDK10, MAPK1, AAK1, PGK1, CDK12 and CDK11B) in K8 Serine[73] dataset and 3 kinases (CDK12, CDK11B and MAP3K11) in K8 Serine[431] dataset to be differentially phosphorylated. Generation of qualitative and quantitative MS/MS spectra using Xcalibur software for specific phosphopeptides of some representative Kinases (CDK1, MAPK1, CDK11B and CDK12) and signaling molecules (eIF4EBP1$^{T37/T46}$, AKTS1^{T246}, eIF4B^{S422}, CTTN^{Y421}, and cJUN^{S243}) further authenticated our phosphoproteomics data (**Figure 4.4.7.1-4.4.7.6 A, B).**

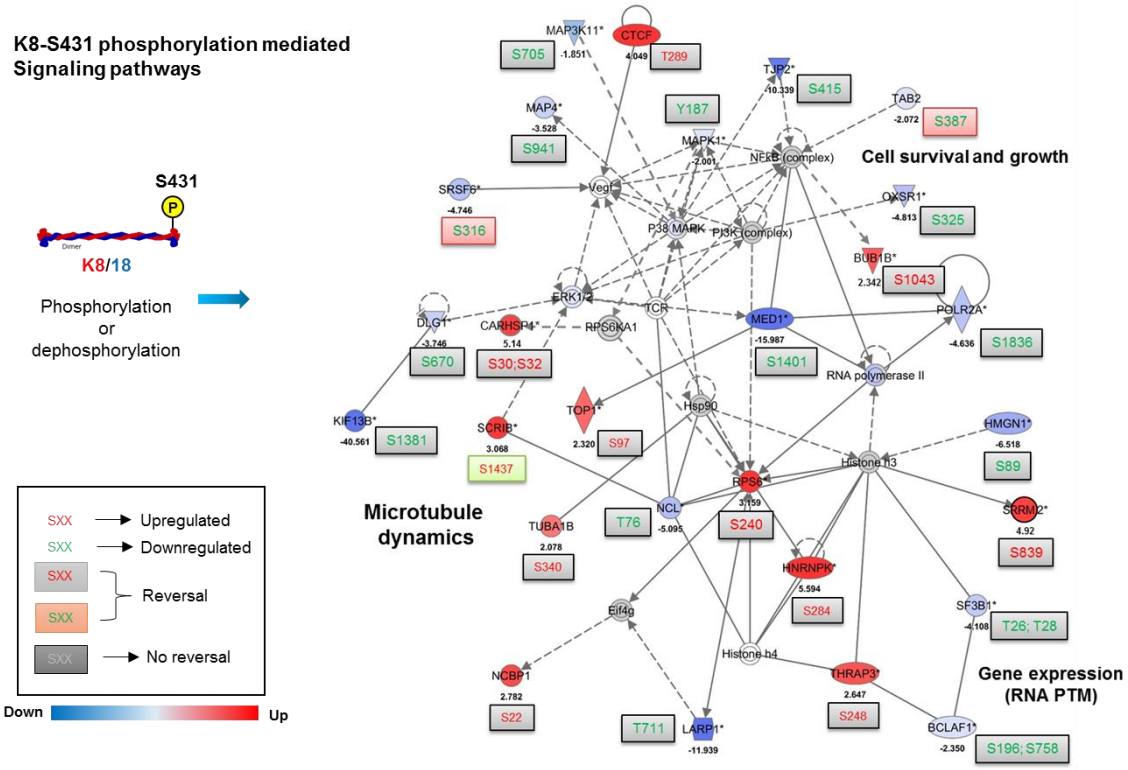

Figure 4.4.6.9: K8 Serine[73] phosphorylation mediated signaling pathways mapped by IPA. The phosphorylation sites detected were assigned with the phosphoproteins.

For biochemical validation by western blotting, we selected some of the kinases and corresponding signaling molecules as per our computational analysis. Western blot analysis showed an increased phosphorylation at Threonine[14]/Tyrosine[15] of CDK1 in K8 Serine[73] phosphodead mutant expressing clones in comparison to WT and phosphomimetic mutants. Similarly, MAPK1 phosphorylation at Tyrosine[187] was significantly decreased in K8 S73D mutant compared to WT and phosphodead mutants in concordance to our MS/MS data. In addition, the corresponding signaling molecules (eIF4EBP1$^{T37/T46}$, AKTS1^{T246}, eIF4B^{S422}, CTTN^{Y421}, and cJUN^{S243}) which were shown to be associated with tumorigenic potential, were validated by respective phosphosite specific antibodies (**Figure 4.4.7.7 A)**. Western blot analysis of these phosphoproteins correlated well with the MS/MS data. In case of K8 Serine[431] dataset, western blot validated the differential phosphorylation of CTTN for phosphorylation at Tyrosine[421] (**Figure 4.4.7.7 B**).

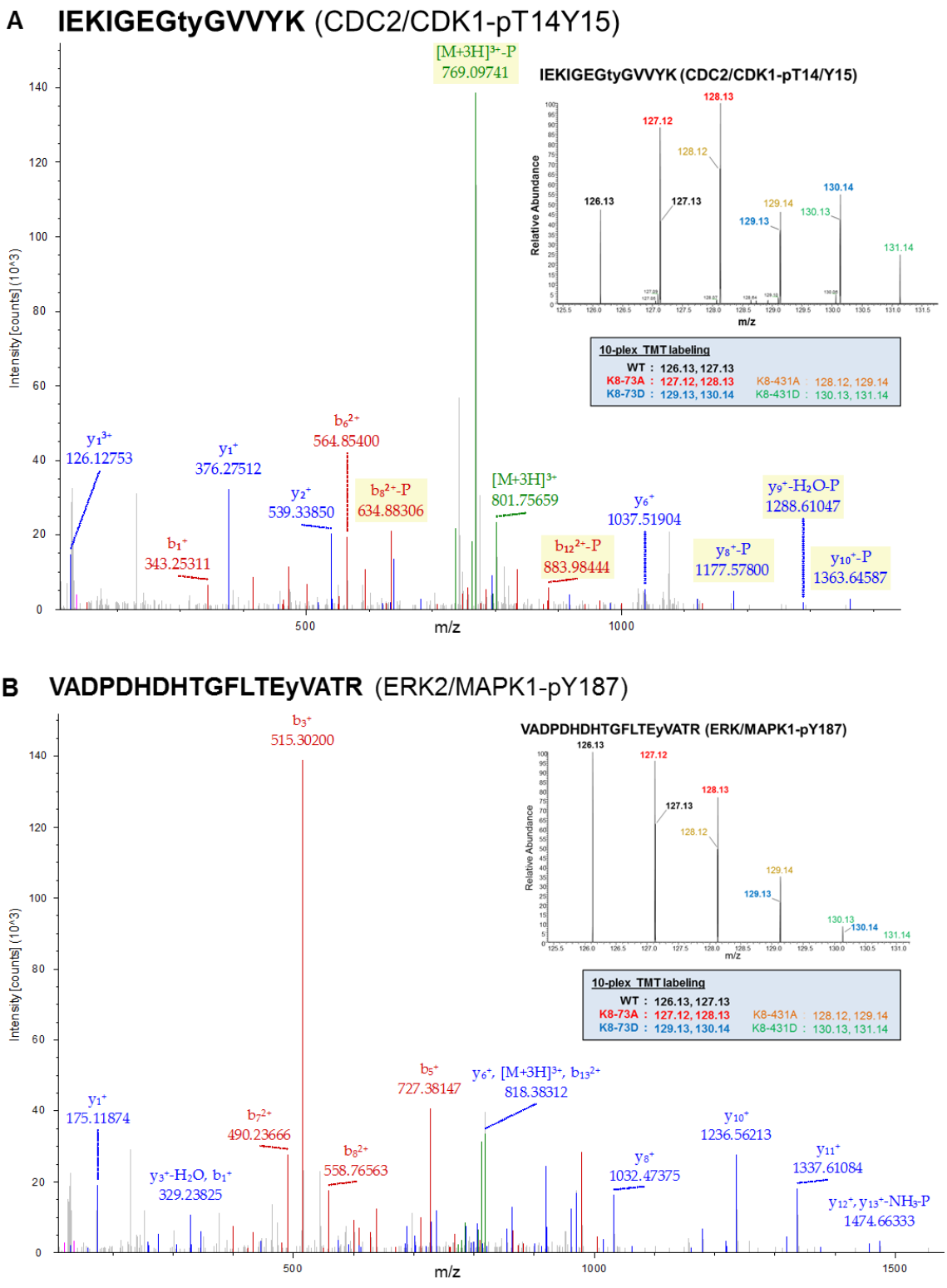

Figure 4.4.7.1: Quantitative and qualitative MS/MS spectra of CDK1 and MAPK1 for the given phosphopeptides. For the verification of MS/MS data, representative quantitative and qualitative spectra for selected kinases were generated using Xcalibur software version-3.0 and Proteome discoverer version

1.4.1.14, Thermo Scientific respectively. The representative spectra for kinases, CDK1 and MAPK1 are shown in the figures.

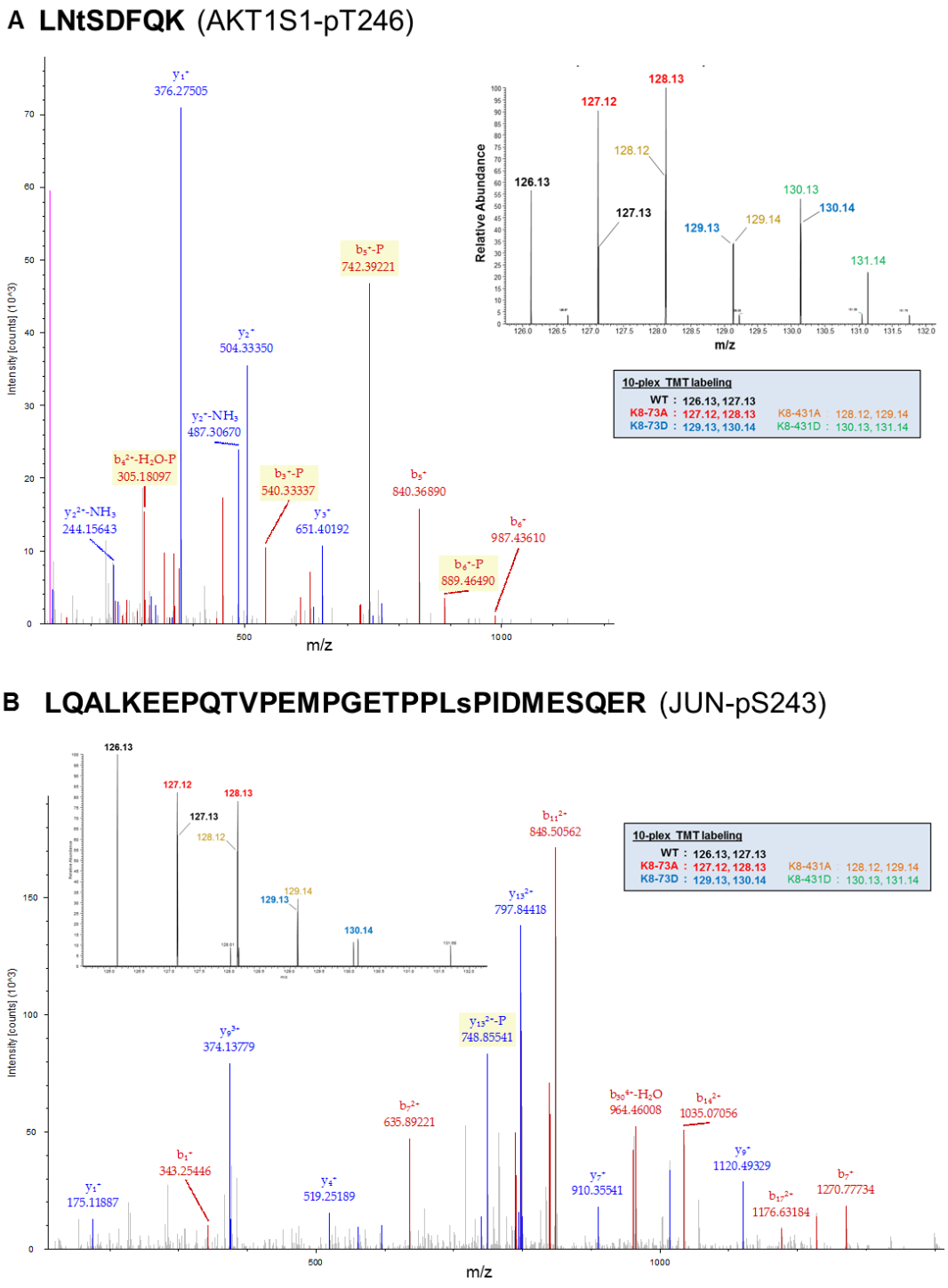

Figure 4.4.7.2: Quantitative and qualitative MS/MS spectra of AKT and JUN for the given phosphopeptides. For the verification of MS/MS data, representative quantitative and qualitative spectra for selected kinases were generated using Xcalibur software version-3.0 and Proteome discoverer version

1.4.1.14, Thermo Scientific respectively. The representative spectra for AKT and c-JUN are shown in the figures.

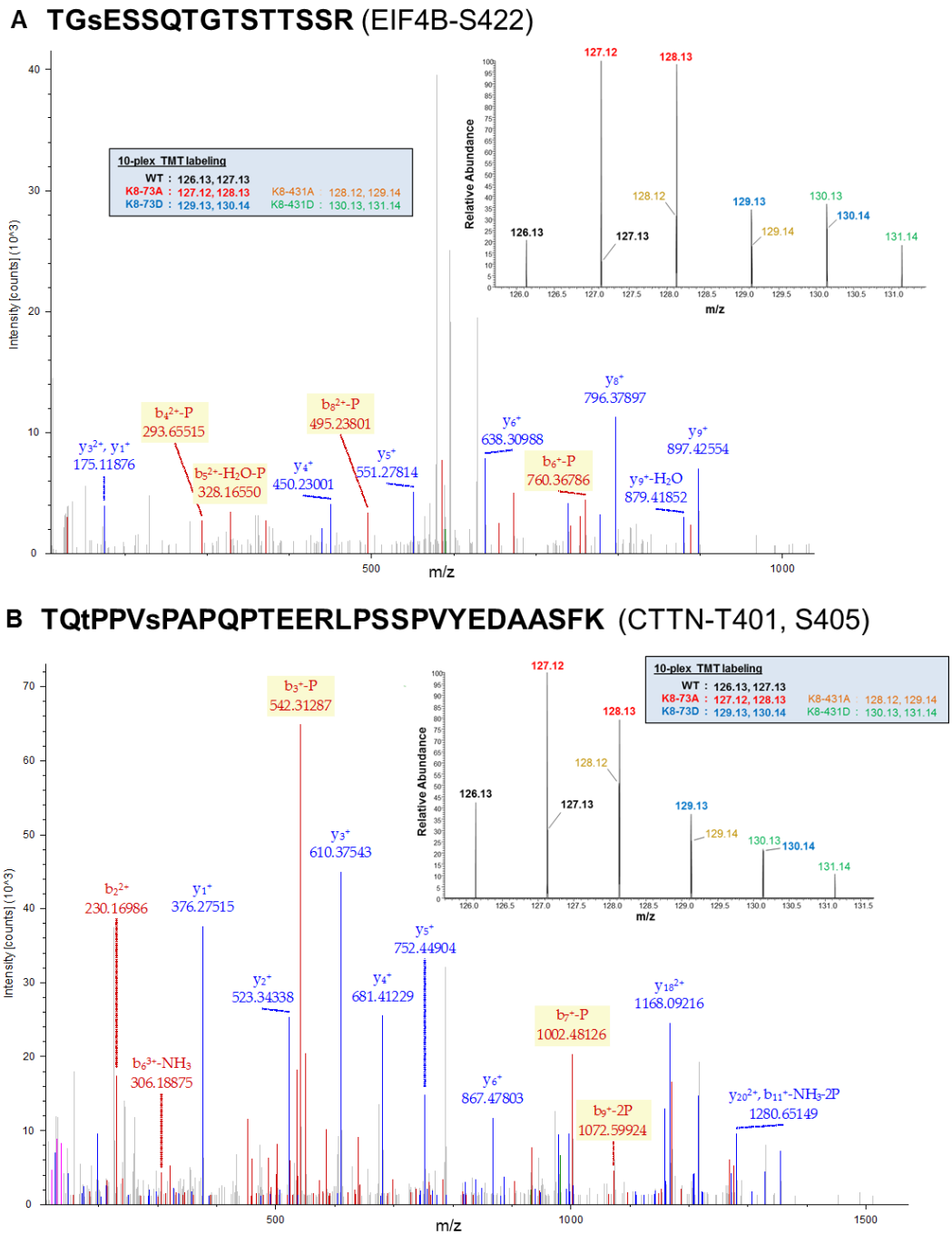

Figure 4.4.7.3: Quantitative and qualitative MS/MS spectra of eIF4B and CTTN for the given phosphopeptides. For the verification of MS/MS data, representative quantitative and qualitative spectra for selected kinases were generated using Xcalibur software version-3.0 and Proteome discoverer version 1.4.1.14, Thermo Scientific respectively. The representative spectra for eIF4B and CTTN are shown in the figures.

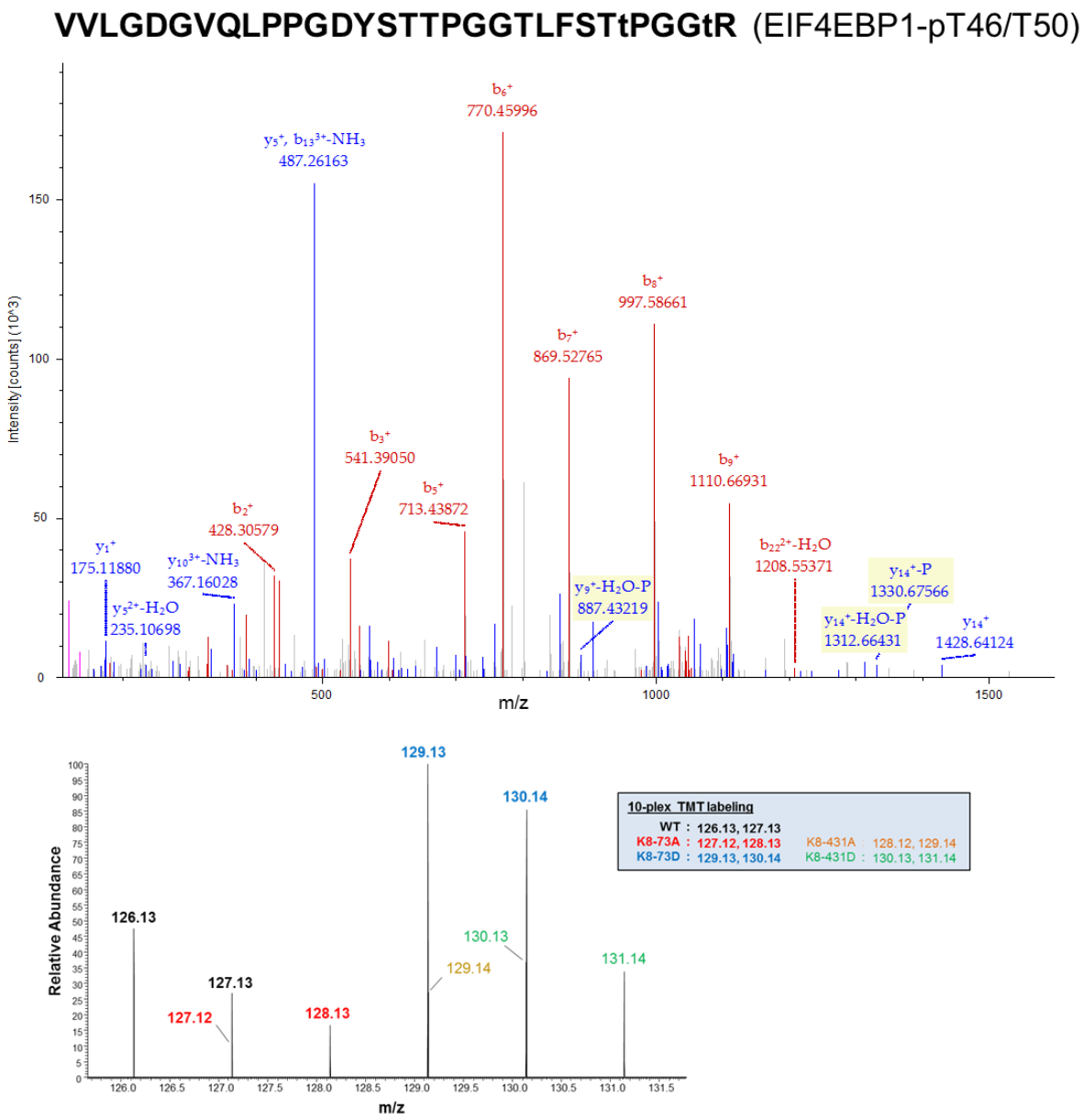

Figure 4.4.7.4: Quantitative and qualitative MS/MS spectra of eIF4EBP1 for the given phosphopeptides. For the verification of MS/MS data, representative quantitative and qualitative spectra for selected kinases were generated using Xcalibur software version-3.0 and Proteome discoverer version 1.4.1.14, Thermo Scientific respectively. The representative spectra eIF4EBP1 is shown in the figures.

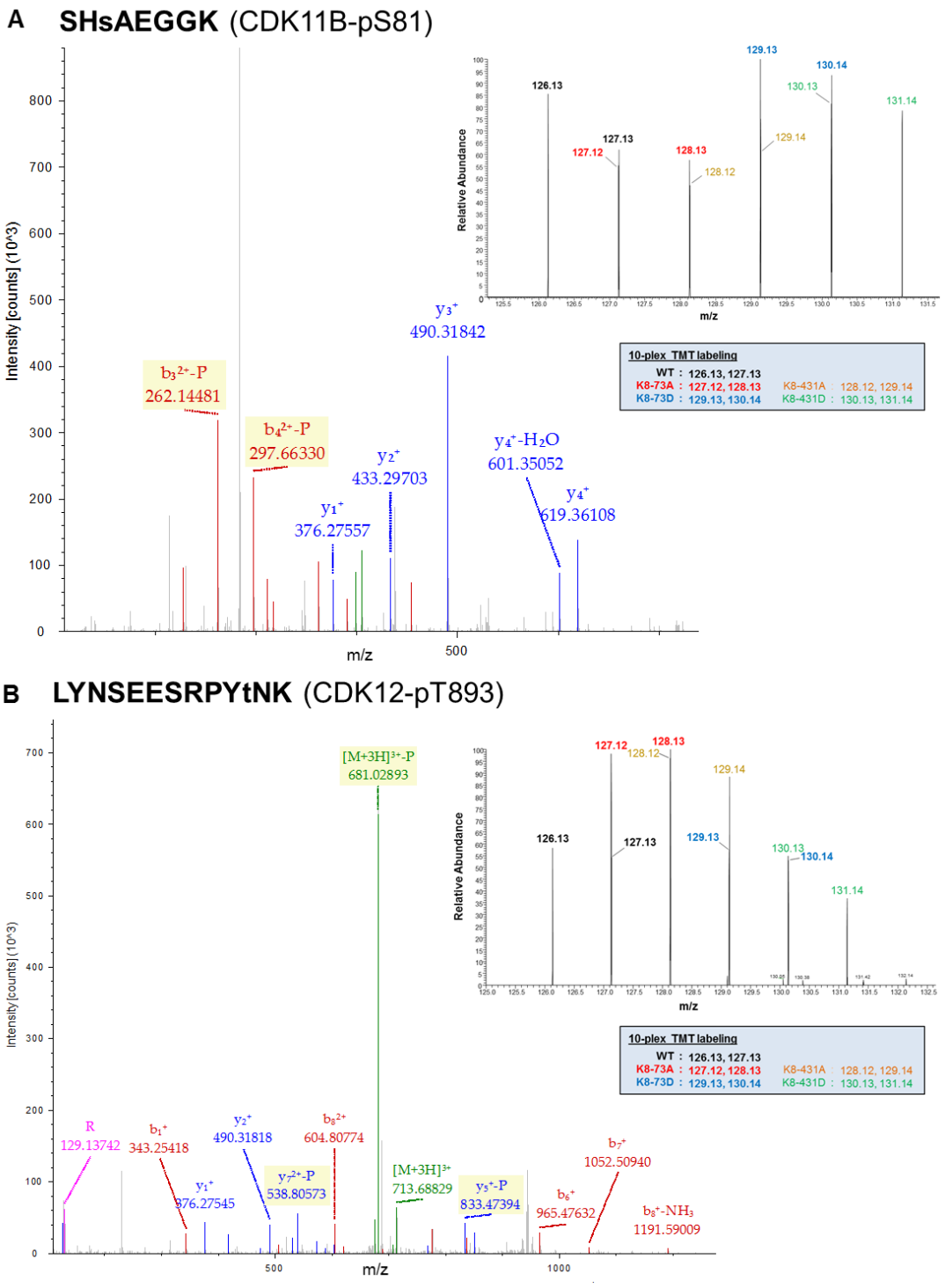

Figure. 4.4.7.5: Quantitative and qualitative MS/MS spectra of CDK11B and CDK12 for the given phosphopeptides. For the verification of MS/MS data, representative quantitative and qualitative spectra for selected kinases were generated using Xcalibur software version-3.0 and Proteome discoverer version 1.4.1.14, Thermo Scientific respectively. The representative spectra for kinases, CDK11B and CDK12 are shown in the figures.

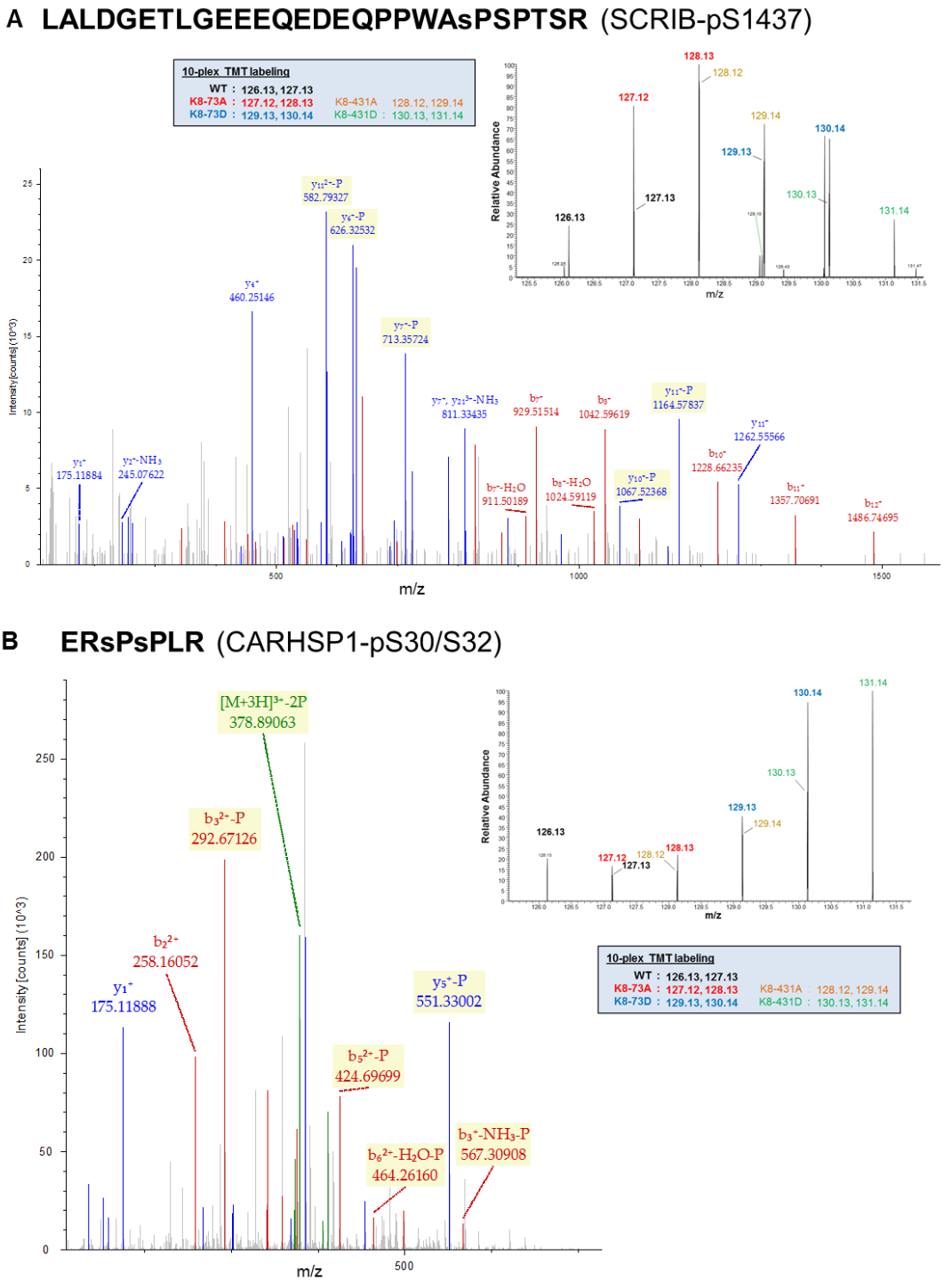

Figure 4.4.7.6: Quantitative and qualitative MS/MS spectra of SCRIB and CARHSP1 for the given phosphopeptides. For the verification of MS/MS data, representative quantitative and qualitative spectra for selected kinases were generated using Xcalibur software version-3.0 and Proteome discoverer version

1.4.1.14, Thermo Scientific respectively. The representative spectra for SCRIB and CARHSP1 are shown in the figures.

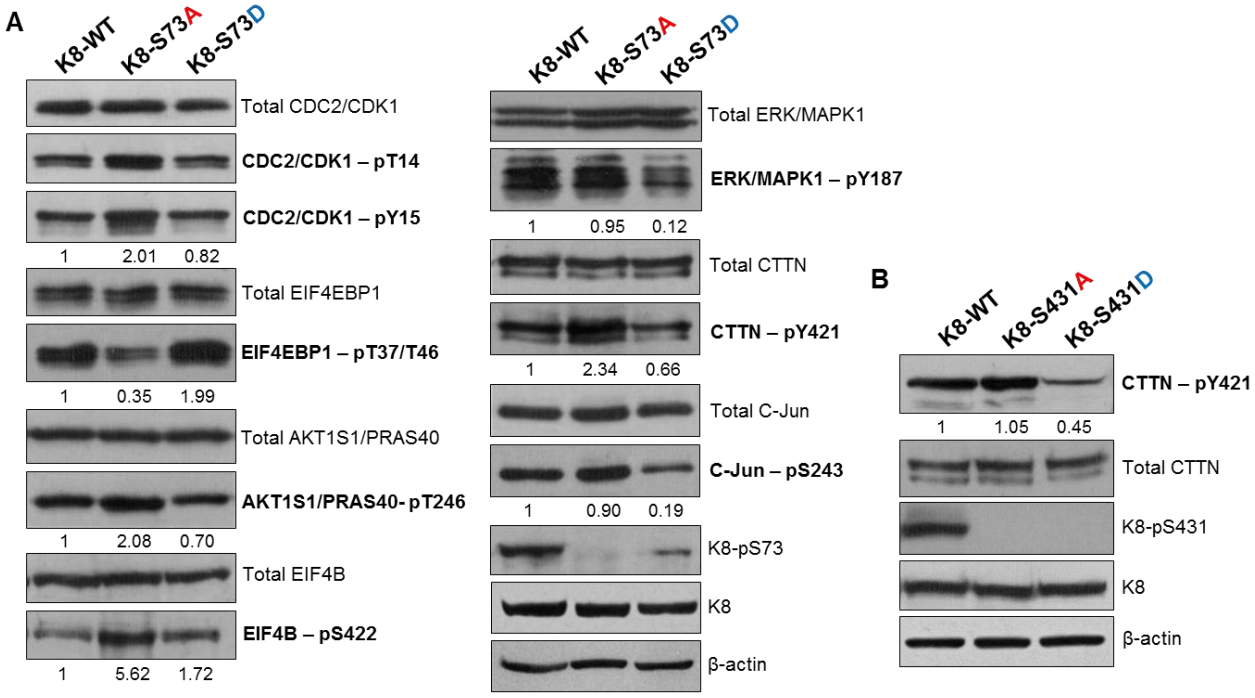

Figure 4.4.7.7: Validation of MS results for selected phosphoproteins: Validation of MS results by western blot analysis for selected proteins. Western blot analysis was carried out (n = 3, ±SD) for some of the selected phosphoproteins with high statistical and biological significance. Western blots using phosphospecific antibodies for CDK1 (pT14/Y15), MAPK1 (pY187), eIF4B (pS422), AKT1S1 (pT221), eIF4EBP1 (pT37/T46), CTNN1 (pT401/S405), c-JUN (pS243) showed expected differential expression verifying the MS-MS Data in S73A/D (**A**) and S431A/D (**B)** datasets. Quantitative values for the specific phosphopeptides from the MS/MS data are indicated below the respective western blots (blots obtained using phosphorylation specific antibodies). Respective blots for total proteins were used as control together with *β*-actin. A representative blot for K8 overexpression and its phosphorylation status (for both the sites K8 Serine^{73} and Serine^{431}) is also shown in the figures. Quantitative spectra could only be used to authenticate differential phosphorylation of such proteins. Overall, the mass-spectrometric data could be confirmed by western blot analysis of the biologically relevant phosphoproteins thereby substantiating their role in Keratin 8 phosphorylation mediated oncogenic pathways.

4.4.8 Site specific phosphorylation on K8 regulates cellular migration, invasion and proliferation in A431 cells

IPA analysis, heat map profiling and Western blot validation for all the four datasets indicated significant alterations in cell migration, invasion, and proliferation associated signaling pathways. This prompted us to validate our observations by phenotypic assays. Hence, we performed scratch wound healing and Boyden chamber migration assay along with matrigel invasion and MTT cell proliferation assay for all the clones. In scratch wound healing assay, the clones expressing K8 phosphodead mutants (K8 S73A and K8 S431A) showed a significant decrease (30–40%) in cell migration rate as compared to K8-WT expressing clone **(Figure. 4.4.8 A)**. Whereas, both the clones expressing K8 phosphomimetic mutants (K8 S73D and K8 S431D) showed a migration rate of 80–90%. For matrigel invasion assay, the K8 phosphodead mutant cells showed 50–60% decrease in invasive potential compared to K8 WT expressing cells whereas, both the K8 phosphomimetic mutant expressing cells showed an invasive potential of 90–100% **(Figure. 4.4.8 B)**. Boyden chamber migration assay correlated well with the scratch wound healing assay **(Figure. 4.4.8 C)**. In addition, K8 phosphodead mutant expressing clones showed 30–40% decrease in the cell proliferation compared to K8 WT expressing clones. Whereas, cell proliferation potential for both the K8 phosphomimetic mutant clones was found to be 80–100% **(Figure. 4.4.8 D)**. The data clearly indicates that the K8 phosphomimetic mutant cells exhibit a reversal of migratory, invasive, and proliferative potential as compared to phosphodead mutant cells. These results are in concordance to our phosphoproteomics data. In summation, these results suggest that K8 phosphorylation at Serine^{73} and Serine^{431} significantly modulated the migratory, invasive, and proliferative ability of A431 cells. This subsequently strengthens our findings of K8 phosphorylation to be a modulator of tumorigenic potential of A431 cells.

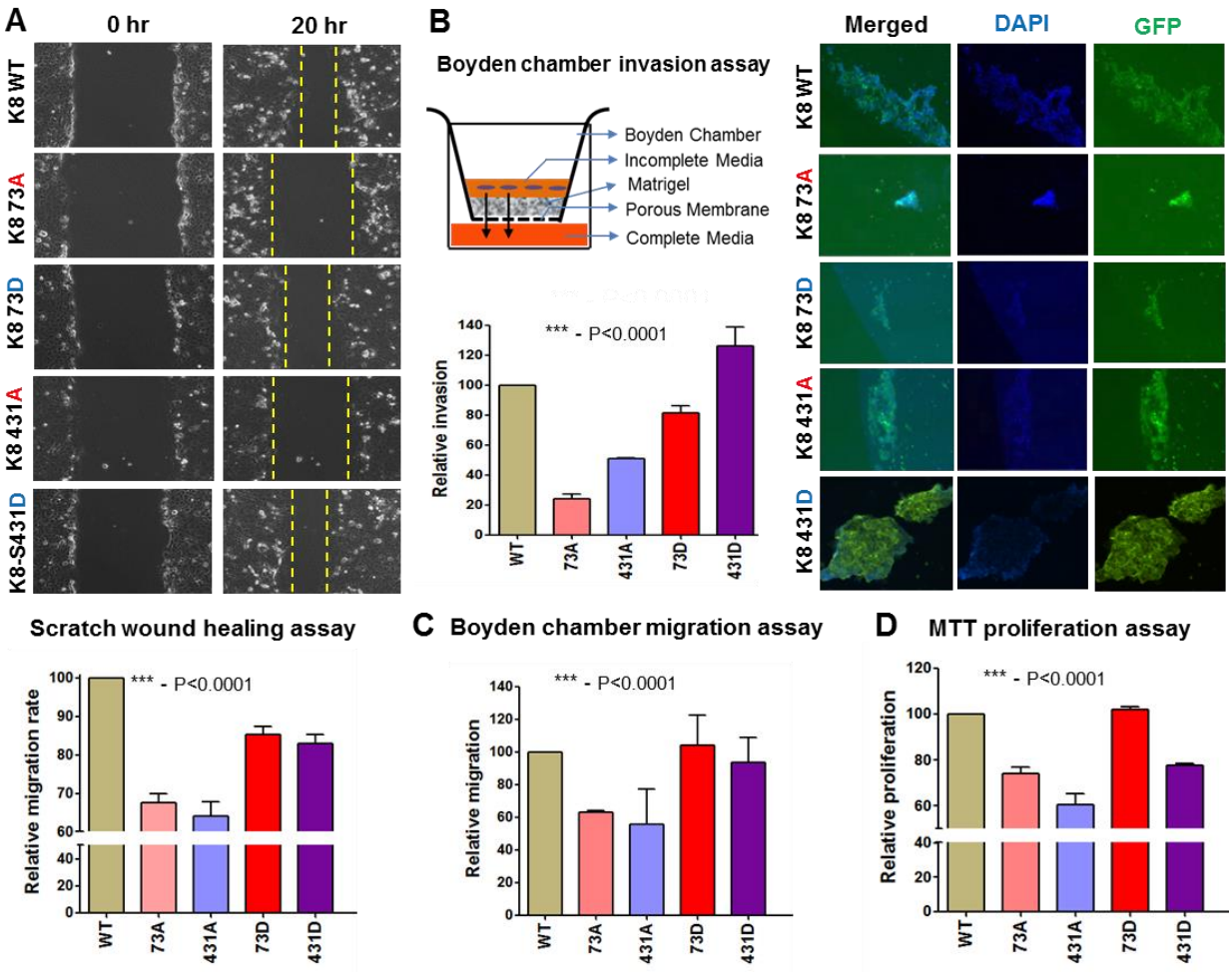

Figure 4.4.8 : K8 Phosphorylation at Serine[73] and Serine[431] residue regulates tumorigenic potential of A431 cells. (**A**) Scratch wound healing assay was performed for all 5 different clones (K8 WT, phosphodead and phosphomimetic mutants) following the protocol described as materials and methods. Representative time lapse microscopy images showing wound healing at 0h and 20h time points. Rate of migration was calculated by MacBiophotonics–ImageJ software. The graph represents relative migration rate ± SEM of three independent experiments done in triplicates. (**B**) Boyden chamber matrigel invasion assay was performed as described in materials and method section. The graph represents average number of invaded cells (stained with DAPI) ± SEM of three independent experiments done in triplicates. Representative images depicting invaded cells visualized for GFP and DAPI under upright microscope. (**C**) Boyden chamber migration assay was performed as described in materials and method section. The graph represents average number of migrated cells (stained with DAPI) ± SEM of three independent experiments done in triplicate. (**D**) MTT-based cell proliferation assay was performed for all 5 clones till six days. The relative proliferation was plotted for each of the clones. [Each bar graph data represents ± standard error mean (SEM) of three independent experiments].

Chapter-V

Discussion

5.1 To study the role of K8 phosphorylation in neoplastic progression of SCC using transgenic mouse model.

Keratin 8 undergoes phosphorylation at two main residues Serine^{73} (Head domain) as well as Serine^{431} (tail domain) and thereby performs different regulatory functions [11]. Deregulation of phosphorylation at these two sites regulates tumor progression either positively or negatively in different malignancies, in a context dependent manner as shown by various cell line based *in vitro* studies [39-41]. Although cell line based studies provide important information, the major drawback of this system is lack of tissue microenvironment and cell-cell/cell- tissue interaction and therefore cannot be directly extrapolated to human systems. Apart from this, cell lines are usually transformed, exhibiting different gene expression and cell cycle profiles than those of cells in the living organism. Therefore, to understand the exact role of K8 phosphorylation in cancer initiation and progression, a model that mimics the multistep tumorigenesis of human cancers, from the initial genetic insults in single cells to malignant progression in a proper tissue environment is required. Tumors arising in genetically modified mouse models (GEMMs) mimic the histopathological and molecular features of their human counterparts, display genetic heterogeneity, and are able to spontaneously progress toward metastatic disease. Furthermore, two-stage skin carcinogenesis studies using transgenic mouse model provide valuable tools to study the mechanisms underlying processes such as cancer initiation, progression, organ-specific metastasis formation, and role of tumor microenvironment. As opposed to, cancer cell line based studies and xenograft models, GEMMs develop *de novo* tumors in a natural immune-proficient microenvironment and are therefore important tool in deciphering the contribution of tumor cell-extrinsic factors such as cancer-associated fibroblasts (CAFs) and immune cells in tumorigenesis. Also, the development of methods for targeting genetic modifications in a tissue specific manner

avoids complications such as embryonic lethality or systemic effects [111-113]. Hence, in order to understand the exact role of K8 phosphorylation in neoplastic progression of SCC and to monitor the effects at different stages of skin SCC in a stepwise manner, we generated tissue specific transgenic mouse model expressing K8 wild type and phosphodead mutants under K14 promoter. This was followed by DMBA-TPA mediated skin carcinogenesis. Here we used K14 promoter which drives the expression of a gene in the basal keratinocytes of skin. We chose to use tissue specific model of transgenesis since it has been reported earlier by Nom On Ku et, al that mice expressing K8 S73A under a CMV a ubiquitous promoter enhanced the susceptibility of mice to hepatotoxic injury upon apoptotic stimulation [66].

To generate tissue specific transgenic mice expressing K8 wild type as well as phosphomutants under K14 promoter, the expression cassettes were electroporated to the spermatogonial stem cells of the male mice. In the third attempt we obtained few of the transgene positive pups for all the three constructs as shown by the tail genomic DNA PCR data using GFP primers. This suggested a successful integration of the transgene into the mouse genome. In addition, in the western blot analysis, an 82kD high molecular weight band corresponding to K8 GFP was observed in the skin tissue lysates for all three constructs. Apart from this, we observed a dark patch at the region of 50 to 55kD. This is the region where most of the type two keratins appear. Similar observations have been made by Cassanova et.al., when they generated K8 expressing transgenic mice. According to them, appearance of this band might be because of the sporadic expression of K8 in the hair follicles and Whiskers cells of the skin [66, 87, 92]. Furthermore, we could verify the transgene positive mice from all the three lines by immunofluorescence analysis, using both K8 as well as GFP antibodies. Together these results suggest that not only the transgene is integrated in the genome but is also being expressed at protein level. The two major problems generally

encountered while performing these studies in relation to keratins are; 1) Keratins are obligate hetero-polymers, generally unstable when expressed alone and 2) as stated earlier, during neoplastic progression an aberrant expression of endogenous K8 starts which might interfere with the effects of ectopically expressed phosphomutants. In this context, it has been reported by Cassanova et,al., that K8 might get stabilized by K14, in absence of its type two binding partner K18 in the skin as shown by their electron microscopy results [66, 87, 92]. This could be true in our case also. Apart from this, it is well known that K8 phosphomutants are dominant negative, which ruled out possibility of interference of endogenous K8 phosphorylation to mask the effects of the ectopically expressed phosphodead mutants of K8 . After successful generation of transgenic lines for all the three K8 wild type and phosphomutant constructs, initially, three male mice from each set (K14-K8 WT/S73A/S431A GFP) were subjected to DMBA TPA mediated skin carcinogenesis protocol, as a pilot study. Here, we could observe that, amongst the three sets, K8 WT GFP expressing transgenic mice showed the onset of tumors the earliest, followed by K8 S431A and then K8 S73A expressing mice. It is known that at basal level, K8 is generally phosphorylated at Serine^{431} residue which further increases during specific conditions like mitosis. In contrast, K8 Serine^{73} acts as a switch on switch off mechanism and thus is a more potent regulator of K8 functions compared to K8 Serine^{431}. Therefore, when there is an insufficiency of K8 Serine^{73} phosphorylation, it leads to less tumorigenic phenotype in transgenic mice compared to K8 Serine^{431}. Furthermore, two of the wild type expressing transgenic mice showed a 12-14 mm sized tumors to be formed by 6th week where as one of them showed the regression by 4th week of TPA application. There are few reports which suggest that the regression during chemical carcinogenesis may occur because of metastasis. This could be the possible reason behind our observation regarding the regression of tumor in one of K8 wild type mice. Altogether this data

indicate that K8 phosphorylation might be providing more aggressiveness to the skin SCC cells under *in vivo* conditions. Our data supports the report by Tanaka et.al. This group has recently shown that depletion of Sec8 in HSC3, a human oral squamous cell carcinoma-derived metastatic cell line, suppressed its migration by controlling the phosphorylation of K8 at Serine^{73}. They also showed that this reduced K8 phosphorylation at Serine^{73} is regulated by the activation of ERK and p38 mitogen-activated protein kinases (MAPK) signaling pathways [41]. In agreement with this study, results of our *in vitro* studies have shown that, forced expression of shRNA-resistant phosphodead mutants in K8 deficient-skin epidermoid carcinoma derived A431 cells resulted in a decreased tumorigenic potential when compared to wild type expressing cells (as discussed in 5.3). Notably, the phosphomimetic mutant expressing cells showed an inverse correlation when compared to phosphodead mutant. Thus, our preliminary *in vivo* data presented here supports the hypothesis that K8 phosphorylation provides more aggressiveness to the cells during neoplastic progression of skin SCC, which goes along with our *in vitro* data. We have also shown possible mechanisms behind the effects of site specific K8 phosphorylation on aggressiveness of Skin SCC in our *in vitro* study. Future studies are required to ascertain whether these observations hold true in the *in vivo* conditions. Apart from this, it has been shown by different groups that K8 phosphorylation is required during proliferation, protects cells from apoptosis by working as a phosphate sponge as well as is required for its binding to other proteins like 14-3-3 during various signaling mechanisms [32]. Its dephosphorylated form might be negatively affecting the proliferative and anti-apoptotic properties and thereby tumorigenic potential. In addition, human skin SCC tissue samples can be probed for K8 phospho-specific antibodies to further establish its function in skin SCC.

5.2 To study the role of K8 in neoplastic progression of skin SCC derived cells:

One of the major characteristics of keratins is their tissue specific and differentiation state dependent expression pattern [4, 54]. Keratin 8/18, a preferential keratin pair of simple epithelial tissue is reported to be aberrantly expressed in different squamous cell carcinomas. Its aberrant expression has been correlated with increased invasiveness and poor prognosis of these tissues[4, 33, 93]. Skin SCCs (Non-melanoma skin cancers -NMSC), one of the most common neoplasms which is known to cause serious morbidity and mortality, is curable at early stages, but delayed diagnosis leads to metastasis [42]. Although, K8/18 pair is known to be aberrantly expressed in skin cancers [24], till now, there are no reports about the involvement of K8 in the neoplastic progression of skin SCCs and the mechanisms associated with it. To investigate if this keratin pair has any role in tumorigenic potential of skin SCC and if yes what is the molecular mechanism, K8 was depleted from an human epidermoid carcinoma derived cell line A431. This led to a significant decrease in tumorigenic potential of A431 cells *in vitro* as well as in *in vivo* tumorigenicity assay. In case of *in vivo* tumorigenicity assay the effect of K8 downregulation could be rescued by re-expression of K8 WT GFP in the K8 deficient background. Together, these results suggest that K8 regulates tumorigenic potential in A431 cells *in vitro* as well as *in vivo*. Further, these results were in accordance with an earlier report from our laboratory, in which K8 downregulation in an oral SCC derived AW13516 cells resulted in decreased tumorigenic potential of these cells [36]. In addition, Consistent with our data, a previous report by Casanova et al., demonstrated that K8 expressing transgenic mice undergo alterations in epidermal differentiation markers. The severity of the skin phenotype of these transgenic mice increase with age, leading to areas of pre-neoplastic transformation. Furthermore, Skin carcinogenesis in these mice showed that K8 alters the epidermal cell differentiation, favors the neoplastic transformation of cells, and is responsible for

the invasive behavior of transformed epidermal cells, leading to faster conversion of benign tumors to malignant once [87, 92].

Next, to understand the associated mechanism, we performed a differential quantitative proteomics for keratin 8 knockdown clones (KD2/KD8) and vector control cells. The data showed a total of 140 and 122 proteins to be differentially expressed in KD2 and KD8 knockdown clones respectively, compared to vector control cells. There were 78 common proteins which were significantly altered (up/down-regulated) in both the K8 knockdown clones compared to vector control cells. The quantitative proteomics confirmed a substantial down-regulation of K8 expression upto 80% in both the knockdown clones. Together with this, K18 (a normal binding partner of K8) also showed a down-regulation of Up to 30-40%, which could be further verified by the western blot data. This might be because of destabilization of K18 in the absence of its preferential type II binding partner K8, which is in line with earlier observations [36]. Conversely, to our surprise, there was a significant decrease in the levels of K5, K17 and K15 upon K8 knockdown as shown in the differential proteomics data. Our western blot analysis confirmed a significant down-regulation of K5/17 at protein level. Furthermore, it is well known that, in A431 cells, K5/17 form a major keratin pair apart from K8/18 [114]. Our immunofluorescence data showed that upon K8 downregulation, neither K8/18 nor K5/17 could form proper filamentous network. Nonetheless the transcript levels of K5/17 were largely unaffected. This observation ruled out any likelihood of off target effects of the shRNA, which was a possibility because keratins share a large amount of sequence homology. This also indicates the possibility of defects in protein synthesis or their turnover. Generally keratins, like other cytoskeletal proteins are very stable with a half-life of more than 48h [60]. Interestingly, after K8 knockdown, the turnover of K5 and K17 was decreased upto less than 12 and 1h after CHX treatment respectively, which

suggested a possible alteration in the degradation pattern of these proteins. Altogether this data indicated that K8 down-regulation affects the turnover of K17 and the fast depletion of K17 probably makes it unavailable to hetero-dimerize and stabilize K5, leading to its further degradation. In addition, the cells expressing K8 WT GFP showed a considerable stabilization of K5/17 levels compared to GFP vector control cells, further strengthening our hypothesis. Inhibition of major degradation machineries (proteasome, lysosome, Calpain) did not show any changes in K17 stability whereas caspase inhibition resulted in substantial stabilization of the same. An earlier report has shown that TNF-α induced apoptosis resulted in the caspase mediated degradation of K15 as well as K17 [115]. This suggested that depletion of K8 might be causing increased sensitivity of A431 cells towards apoptotic stimuli, which was confirmed by Annexin V staining after TNF-α treatment. Altogether this data suggested that K8 might be favoring the resistance towards TNF-α mediated apoptosis in A431 cells. In case of simple epithelia, K8/18 is a major keratin pair and one of its important functions is to provide resistance towards stress and apoptosis [70, 116]. It is also suggested that during apoptosis or stress conditions, keratins undergo caspase cleavage and reorganization which may initiate the orderly processing of the filament proteins during apoptosis in epithelial cells [117, 118] . K5/17 degradation after K8 knockdown may have the same function as it is the major keratin pair of A431 cells. In addition to this, annexin V staining suggested that K8 might be responsible for providing resistance towards apoptosis to A431 cells. Therefore, its down-regulation leads to increased sensitivity of A431 cells which might be resulting in the degradation of K17 for the survival of these cells. This also explains a probable reason behind the slow growing capacity of K8 knockdown clones as shown by the clonogenic and soft agar assays. Apart from K8/18, there is an emerging role of K17 in proliferation as well as apoptosis. The type I keratin 17 is co-expressed with its type II partners such as, K5 and K6, in

epithelial appendages like in the hair follicles, nails, various glands, oral papillae *etc*. In hair follicles, K17 is important for mechanical support and promotes the anagen phase of the hair cycle by antagonizing TNF-α-induced apoptosis. K17 expression is also shown to be induced in regenerative epithelia and different types of cancers [5]. Furthermore induction of K17 expression has been observed in various malignancies which could be associated with poor prognosis [119-121]. Increased K17 expression is also considered as a marker of keratinocyte proliferation [122]. It is known to play an important role in regulation of signaling pathways such as Akt/mTOR in OSCC and Hedgehog (Hh) in (BCC) Besal cell carcinomas [121, 123]. Altogether, these reports support our *in vitro* data and suggest a possible role of K17 mediated regulation of cell growth and apoptosis to be involved in decreased tumourigenic potential of A431 cells upon K8 knockdown. In accordance with this, our differential proteomics data showed that there was a 2 to 6 fold up-regulation of TMS1, a card domain containing apoptosis associated protein, in K8 knockdown clones compared to vector control cells. TMS1 is shown to be epigenetically silenced in many cancers and is associated with their tumorigenic potential [124-126].These observations support our phenotypic analysis. Furthermore, TMS1 regulates apoptosis through NF-κB signaling by modulating IKK phosphorylation and in-turn IκB alpha stability [127]. Our data showed a significant reduction in NF-κB activity and its nuclear translocation after K8 downregulation through decreased IKK phosphorylation and thereby decreased IκB alpha degradation. NF-κB itself is a dual regulator of apoptosis, although in majority of the cases it regulates the transcription of anti-apoptotic genes [128-130].

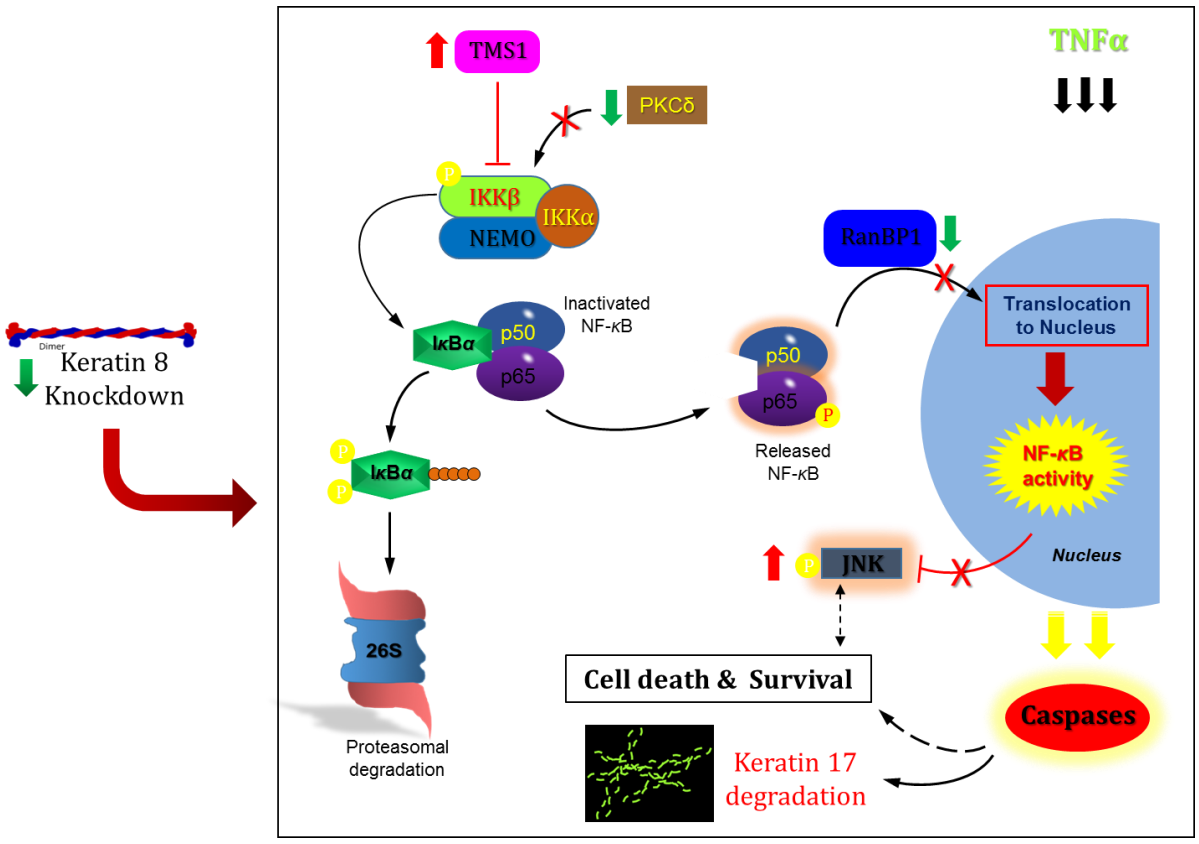

Figure 5.2.1: Schematic representation of proposed model pathway for the probable mechanism of K8 mediated regulation of apoptosis in A431 cells

A significant reduction in PKC and activation of JNK pathway supports reduction in its anti-apoptotic function. Reports suggesting contrasting Roles of PKC**δ** in Cell Survival vis a vis Cell Death and its involvement in activation of IκB Kinase b further supported our data [131, 132]. Further more, it has been reported that the absence of NF-κB-mediated Inhibition of c-Jun N-Terminal Kinase activation Contributes to Tumor Necrosis Factor alpha-induced Apoptosis [133]. In addition to this, RanBP1, one of the key factors involved in nuclear import and export of NLS sequence containing proteins, was found to be two fold down-regulated in quantitative proteomics data. NF-κB is also a NLS containing protein and its nuclear localization has been shown to be regulated by RCC a Ran GTP binding protein. RCC functions in association with RanBP1. This might be one of the factors resulting in impaired NF-κB nuclear localization after K8 knockdown.

Apart from this, literature suggests that RanBP1 is up-regulated in many malignancies and also is associated with apoptosis. In agreement with our data, one of the reports suggests that reduction in RanBP1 levels results in an increased sensitization of cancer cells towards taxol [134]. Altogether, our data in association with the available literature, suggest that K8 might be providing survival benefits to A431 cells by differentially regulating many pro and anti-apoptotic signalling molecules and thereby apoptosis (**Figure 5.2.1)**.

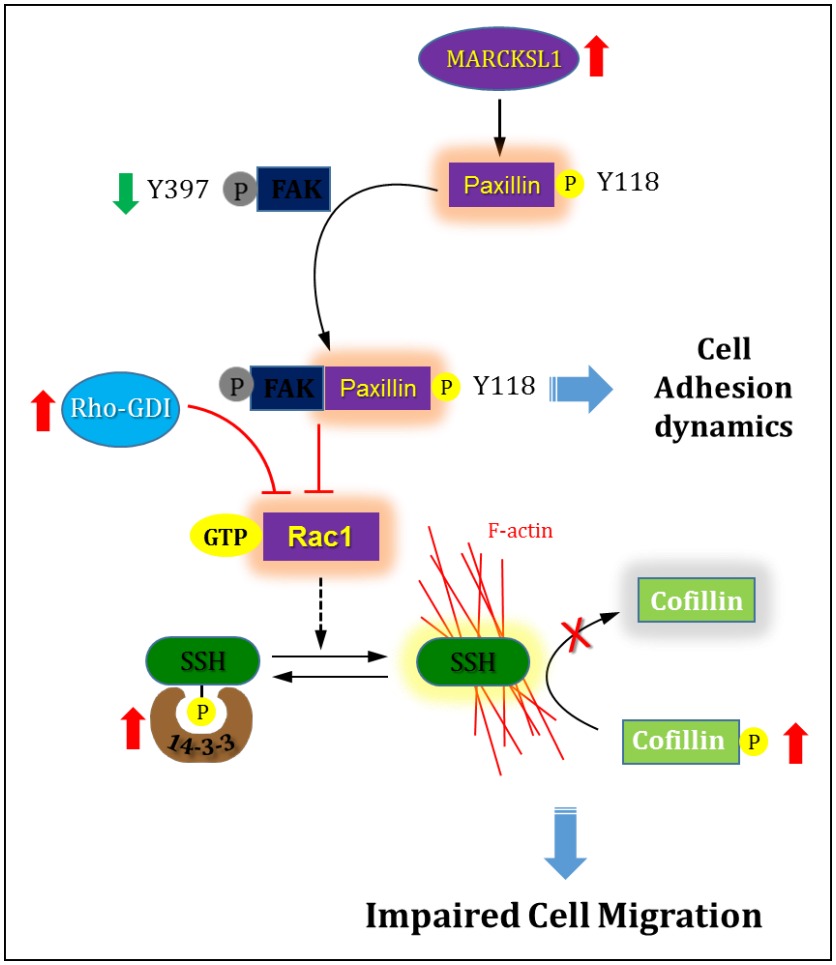

Figure 5.2.2: Schematic representation of proposed model pathway for the probable mechanism of K8 mediated regulation of migratory potential of A431 cells

Apart from apoptosis and proliferation, another important factor involved in metastatic potential of a cancer cell is its migratory and invasive potential. We could observe a significant decrease in

the migratory and invasive potential of A431 cells upon K8 downregulation as shown in our phenotypic data. In relation to this, our IPA analysis revealed "actin organization" and "cellular movement" pathways to be affected upon K8 downregulation. It is well documented that cell migration is a highly integrated multistep process that is initiated by the protrusions of the cell membrane. Protruding structures formed by migrating and invading cells could be either filopodia, lamellipodia, or invadopodia/podosomes, on the basis of their morphological, structural, and functional Characters [135]. Formation of these structures is driven by spatially- and temporally-regulated actin polymerization at the leading edges. MARCKSL1 which is significantly upregulated upon K8 downregulation (as shown in the differential proteomics data) is one of the important regulator of cellular movement (**Figure 5.2.2**).

MARCKSL1 regulates actin cytoskeleton homeostasis together with filopodium and lamellipodium formation during cell migration. The key downstream target of MARCKSL1 is paxillin [136-138]. Number of reports suggest that paxillin localizes to discrete structures in the cells called focal adhesions, which are sites of close cellular contact with the underlying extracellular matrix. The Tyrosine^{118} phosphorylation of Paxillin is important for its activity at focal contacts during fibrillogenesis and cell migration in association with focal adhesion kinase (FAK) [139, 140]. Paxillin phosphorylation initiates focal contact formation together with FAK. Further maturation and disassembly of focal contacts for proper cell migration requires FAK phosphorylation [141]. In this study, when K8 was downregulated, it resulted in an increased paxillin phosphorylation at Tyrosine^{118}, while decreased FAK phosphorylation at Serine^{397} was seen. According to a previous report, paxillin in absence of FAK phosphorylation can initiate the focal contact formation while maturation and fibrillogenesis of these focal contacts is inhibited leading to decreased migratory potential of such cells. This might be the reason why K8

knockdown cells are less migratory as we could observe a more of paxillin at the cell periphery of the K8 knockdown cells (thick pin point paxillin dots) whereas vector control cells showed paxillin to be localized in the lamellipodial fronts. Additionally, we observed shorter actin filaments in K8 knockdown clones which corroborated with an earlier observation where more paxillin phosphorylation resulted in shorter actin bundles [138]. Furthermore, FAK dephosphorylation regulates cell migration through Rho-GTPases [142, 143]. Our actin staining showed mature lamellipodial organization in vector control cells together with more RAC activity. This suggests that decreased FAK phosphorylation together with less RAC activity might be responsible for less migratory phenotype of A431 cells, after K8 knockdown. Rac activity regulates actin dynamics through cofilin Serine^{3} phosphorylation. Cofilin is a actin severing protein which gets inactivated upon Serine^{3} phosphorylation [144]. In association with the above data we could observe a significant increase in cofilin phosphorylation. Previous reports suggest that when RAC is activated it leads to activation of slingshot phosphatases by releasing it from 14-3-3γ. In the absence of RAC activity, slingshot phosphatases are inactivated resulting in more and more accumulation of phosphorylated and inactivated cofilin [145-147]. Our quantitative proteomics as well as immunoblotting data showed significant upregulation of 14-3-3γ levels in both the K8 knockdown clones suggesting its role in the increased phosphorylation of cofilin after K8 downregulation. In accordance with this, it has been shown that if there are shorter actin filament bundles in a cell, it causes the inactivation of cofilin by increased Serine^{3} phosphorylation to seize its actin severing activity as a feedback loop [148]. In addition to the earlier observations, re-expression of K8 WT GFP in the K8 knockdown background resulted in the rescue of the molecular changes associated with both apoptosis (TMS1, RanBP1) as well as migration (MRCKSL1, Paxillin1/pPaxillin1, Cofillin/pCofillin). This further strengthened the involvement

of K8 in regulation of these pathways. Together with this, we did not get any changes in Fascin/pFascin, AKT/pAKT or ERK/pERK levels suggesting that these pathways might not be involved in K8 mediated regulation of skin SCC. Altogether our results provide a new insight in to the role of K8 in neoplastic progression of skin SCC derived A431 cells possibly by regulating apoptosis and migration.

5.3 To understand the role of K8 phosphorylation in neoplastic progression of skin SCC derived A431 cell line:

Phosphorylation is a proven modulator of K8 conventional functions; however, its role in malignant transformation and the mechanism involved to bring about the same is still obscure. In this part of our study, we carried out the total phospho-proteome profiling and quantification after K8 phosphorylation modulation in a skin carcinoma derived A431 cell-line using TMT-based quantitative phosphoproteomics. Comparative data analysis using various computational bioinformatics tools facilitated identification of number of differentially regulated signaling pathways associated with biological functions like cell proliferation, migration, invasion and metastasis. Additionally, protein phosphorylation levels validations together with phenotypic analysis correlated well with our phosphoproteomics data, signifying K8 phosphorylation to impart increased aggressiveness to skin-SCC derived cells.

In our phosphoproteomic study, in response to K8 phosphorylation modulation, we could observe a considerable proportion of the total phosphoproteome to be altered. A number of overlapping and orthogonal phosphoproteins were found to be up or down-regulated between the different datasets as shown in Venn diagram analysis. The data demonstrated many phosphoproteins with increased phosphorylation upon K8 phosphodead mutant expression while expression of

phosphomimetic mutants resulted in decreased phosphorylation of these phosphoproteins and vice-versa. These results indicated that the effects of K8 phosphodead mutants might be reversed by K8 phosphomimetic mutants through phosphorylation modulation of such common target proteins.

Next, for comprehensive understanding of the system wide phosphoproteome data, "Ingenuity pathway analysis" was carried out for all the four datasets. This uncovered many cancer associated phosphoproteins to be differentially phosphorylated. Surprisingly, as indicated in the results, regulation of "RNA post transcriptional modification" followed by "Cancer" in K8 S73A as well as K8 S73D independent data sets were the most significant biological functions altered. Further, deregulation of mTOR and ATM signaling pathways in K8 S73A dataset whereas Hippo signaling in K8 S73D dataset which have never been reported earlier in context of K8 phosphorylation were identified during Canonical pathway analysis for the same. Comparison Analysis of K8 Serine[73] dataset demonstrated changes in many signaling pathways, most importantly GNRH, Renin angiotensin, P70S6K, mTOR and ATM signaling, which were not reported previously in relation to K8 phosphorylation ablation. Earlier studies have shown deregulation of GnRH signaling in many different malignancies together with high GnRH-Receptor's altered expression [149] . Similarly, there are accumulating molecular and in-vivo evidences showing that the Renin–angiotensin system (RAS) increases cell proliferation and modulates the growth of vascular cells during angiogenesis [150]. In addition, p70S6K which is a Serine/Threonine kinase regulated by PI3K/mTOR pathway, plays a crucial role in controlling cell cycle, growth and survival [151]. ATM and mTOR signaling pathways are also well established critical effectors which are commonly deregulated in human cancers [152, 153] . Together with this, antagonists/inhibitors of these pathways are being considered as probable candidates in cancer therapy [149-153].

Altogether, the data analysis on the backdrop of the available literature shows an expanding role of K8 Serine^{73} phosphorylation in cancer.

Similarly, to identify signaling mechanisms and associated phosphoproteins which are differentially regulated in case of K8 Serine^{431} dataset, the "biological function analysis" for K8 S431A and K8 S431D independent datasets was carried out. This showed most of the differentially regulated phosphoproteins to be associated with RNA post transcriptional modifications and cancer. The "canonical pathway" analysis for the same revealed estrogen receptor, Hippo and JNK/SAPK signaling to be significantly altered in both the datasets. Some of the phosphoproteins like CAV1 and ZYX which are a part of integrin mediated signaling network, could be possible new links between K8 Serine^{431} phosphorylation and cancer progression. Recent studies have implicated a loss of caveolin-1, in driving early tumor recurrence, metastasis, and poor prognosis [154] . Zyxin, an actin associated protein, which concentrates at focal adhesions along the actin cytoskeleton, is reported to regulate actin dynamics, apoptosis, cell migration and metastasis in many different cancers [155]. These results along with the available literature collectively indicated the role of K8 Serine^{431} phosphorylation modulation in regulation of phosphorylation dependent functions of many phosphoproteins and thereby cancer.

In addition to IPA tool based functional analysis, we have also carried out phosphorylation site annotation using online databases including PhosphoELM, PhosphoSitePlus, HPRD and Uniprot. This helped us to attribute the exact function which these site specific phosphorylation provides to the phosphoproteins. This revealed many biologically relevant phosphosites to be altered in different datasets. For instance, in case of K8 Serine^{73} dataset, differential phosphorylation of Threonine^{401} Serine^{405} and Tyrosine^{421} of cortactin was identified. The phosphorylation of cortactin at these residues regulates actin cytoskeletal network reorganization and in turn cell

motility [156]. Similarly, the phosphosites Serine^{307} and Serine^{309} identified on CAP1 regulate its binding to cofilin resulting in accumulation of actin stress fibers and in turn cancer cell migration and metastasis [157]. In addition to this, K8 Serine^{431} dataset demonstrated differential phosphorylation of BUB1B at Serine^{1043}, which has importance in the processes like cell proliferation and apoptosis [158]. Although, many phosphorylation sites from our data have been reported in the published literature, we have also unraveled many less characterized or novel phosphosites on biologically relevant protein molecules. For instance, MAP3K11^{S705} and ZYX^{S344} are novel phosphorylation sites found to be altered in our dataset, but their biological functions are still unknown [159, 160]. Validation of these novel phosphosites by mutational studies can provide new insights into their functional relevance and may open new avenues in the area of cancer research.

Systematic analysis of phosphorylation site dependent complex interaction dynamics by "STRING" analysis not only highlighted the hub proteins but also uncovered many relevant interactions in our study. For example, PPI network for cell migration suggested many multifaceted indirect interactions between phosphoproteins. These might contribute to novel cross-talk in cancer signaling upon K8 phosphorylation modulation. Furthermore, our "Enrichr" analysis for key upstream regulators identified many upstream kinases which could bridge the gap between K8 site-specific phosphorylation and the final downstream effectors identified by the same. For example, CDK1 and its target eIF4EBP1 seem to be good candidates to elucidate K8 Serine^{73} phosphorylation mediated signaling cascade, based on the biological relevance of corresponding phosphosites. Moreover, IPA comprehensive model pathways together with phosphosite annotation featured many phosphoproteins accompanying functions like Cell proliferation, Actin organization, Cell survival and Gene expression regulation being deregulated by K8

phosphorylation modulation. Consistent with these observations, the protein phosphorylation level validation of few of such phosphoproteins including; eIF4B, AKT1S1, CTNN1, 4EBP1 and upstream kinases like MAPK1, CDK1 in K8 Serine^{73} datasets confirmed our phosphoproteomics data.

Furthermore, to validate the major biological pathways shown to be altered in computational analysis such as those regulating cell migration, invasion and proliferation; different phenotypic assays were carried out. Skin SCC derived A431 cells, upon expressing either of the phosphodead mutants, showed abolition of oncogenic potential for all the three assays and regained the tumorigenic potential upon expressing either of the phosphomimetic mutants. In agreement with our present data, a recent report demonstrated reduced K8 Serine^{73} phosphorylation via p38 MAPK pathway upon Sec8 downregulation. This in turn resulted in decreased cell migration in case of oral SCC derived cell-line [41]. Contrary to these findings, Mizuuchi et al. have demonstrated correlation of PRL-3 dependent K8 dephosphorylation at Serine^{73} and Serine^{431} with increased cell motility in colorectal cancer derived-cells [39]. This data is further supported by the data from our laboratory in an OSCC derived cell-line [40]. These reports suggest that K8 phosphorylation associated effects in cancer progression might be context dependent. Our quantitative phosphoproteomics and immunoblotting data suggests an upregulation of CDK1 inhibitory phosphorylation at Threonine^{14}/Tyrosine^{15} in case of K8 Serine^{73} phosphodead mutant. It is reported that wee1 and myt1 mediated inactivation of CDK1 by phosphorylation at Threonine^{14}/Tyrosine^{15} leads to G2-M arrest and in turn decrease proliferation [161, 162]. We also observed similar phenotypic changes which validated our phosphoproteomics data. eIF4EBP1, an important regulator of mitotic cap-dependent translation which is downstream to CDK1, was found to be dephosphorylated at the residues Serine^{44}, Threonine^{46} and Threonine^{50}. The hierarchical

phosphorylation of these sites on eIF4EBP1 is essential for release of eIF4E [163] which further associates with eIF4F and eIF4A at the initiation complex and hence is indispensable for cap-dependent translation initiation [164]. eIF4E-BP1 phosphorylation at Threonine^{37}/Threonine^{46} residues is governed by CDK1 [165].

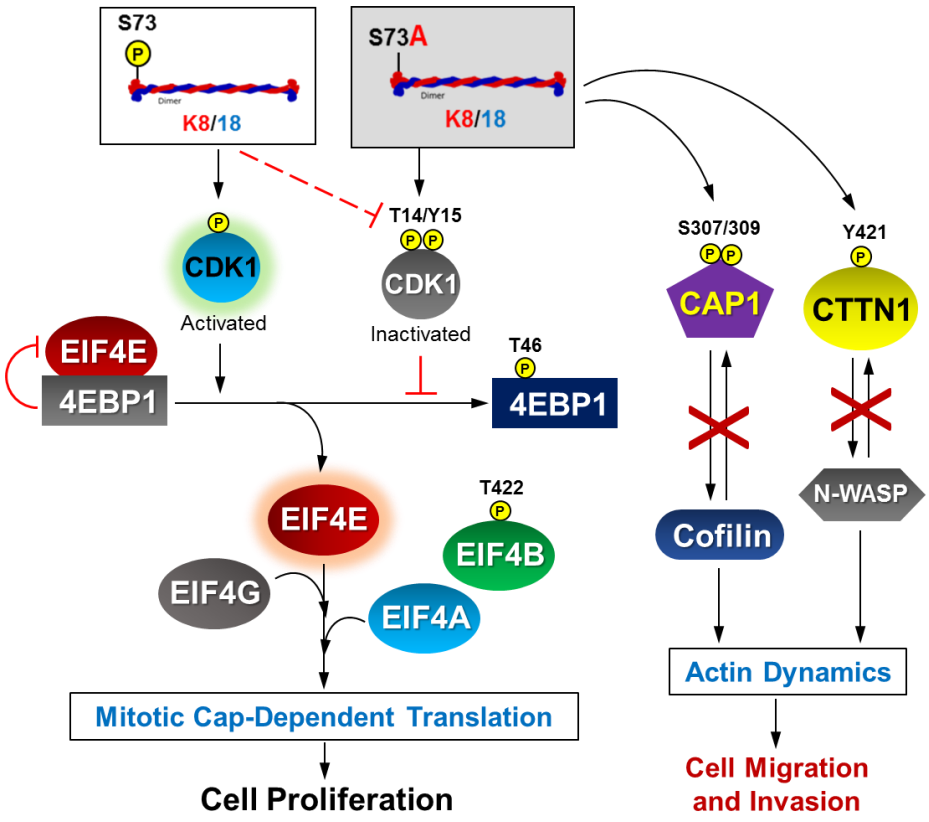

Figure 5.3: Model pathway summarizing possible molecular mechanism associated with K8 Serine^{73} Phosphorylation mediated regulation of proliferation, cellular migration and invasion.

Our results have shown decreased phosphorylation of 4EBP1 at these residues probably because of CDK1 inactivation. This might be leading to reduced mitotic cap-dependent translation and hence shows less proliferation. Although, eIF4EBP1 has another potent modulator for its phosphorylation vis mTORC1; it has been reported that CDK1 can substitute its function in mitotic cap-dependent translation [165-167]. However, we observed a 5-fold up-regulation of eIF4B

phosphorylation at Serine^{422} residue which is an indirect downstream target of mTORC1. Furthermore, some other kinases such as PKB can directly phosphorylate eIF4B, which again suggests that mTORC1 might be inactivated in K8 S73A mutant cells [168]. eIF4B, when phosphorylated at Serine^{422}, acts as co-activator of eIF4A helicase activity during cap-dependent translation initiation [169]. Because of the consistent impaired cap-dependent translation, the upstream kinases like AKT/PKB, might be activated in a feedback loop which is reflected in an enhancement of pRAS40 phosphorylation at Threonine^{246} and eIF4B at Serine^{422} as observed in our data. Nevertheless, the initial step of translation initiation complex formation i.e. release of eIF4E from eIF4E-BP1 might be abrogated because of decreased phosphorylation of eIF4E-BP1. Hence, hyperphosphorylated form of eIF4B and pRAS40 as observed, might not be sufficient for driving the translation initiation and hence it is stalled and shows reduced proliferation in these cells. We have also observed increased phosphorylation of cortactin at Serine^{405} and Tyrosine^{421}. Mutational analysis has shown that ERK mediated Serine^{405} phosphorylation of cortactin enhances its binding with N-WASP and WASP but is inhibited by Src mediated Tyrosine^{421} phosphorylation of cortactin [170]. This inhibits further activation of the Arp2/3 complex and in turn affects actin nucleation and dynamics. Similarly, GSK3 mediated phosphorylation of CAP1 at Serine^{307} and Serine^{309} was increased on K8 S73A mutation, which is known to inhibit its binding to cofilin and further accumulation of actin stress fibers [157]. Both these molecules are important modulators of actin dynamics and in turn cell migration and invasion which is also validated by our phenotypic data. Altogether, our data suggests K8 phosphorylation at Serine^{73} position can modulated intricate pathways and thereby migration and metastatic potential of the cells. Earlier reports have shown aberrant accumulation of an important oncogenic transcription factor c-Jun upon dephosphorylation at Serine^{243} leading to accelerated G1/S transition and thereby hyper-

proliferation [171] as observed in our K8 S73D phosphomimetic mutant dataset . In case of K8 Serine^{431} dataset, despite the significant phenotypic alteration, majority of the differentially regulated phosphosites were novel/less characterized, hence we could not propose any phosphorylation based model pathway. However, a protein level comprehensive model pathway generated by IPA, provides multiple start-points for further mechanistic studies for elucidating K8 Serine^{431} phosphorylation mediated oncogenic pathways (**Figure 5.3)**.

Overall, the bioinformatics analysis suggested that the K8 phosphorylation might be modulating cancer related phenotype by differentially regulating an important part of the cellular phosphoproteome. In concordance with our global phosphoproteome profiling, the biochemical and phenotypic validations confirmed a potential role of K8 phosphorylation in neoplastic progression of skin-SCCs. In addition, our phosphoproteomic analysis not only ratifies previous findings but also unravels many novel K8 phosphorylation mediated functional networks and signaling mechanisms, underlining its much broader regulatory role in cancer.

Chapter-VI

Summary & Conclusions

6.1 Part 1: Objective 1 and 2

6.1.1 Summary:

- Transgenic mice for K14-K8 WT GFP, K14-K8 S73A GFP and K14-K8 S431A GFP could successfully be generated.
- DMBA/TPA mediated skin carcinogenesis was carried out and the preliminary data suggest an early initiation in K8 WT expressing mice compared to phosphodead mutants.

6.1.2 Conclusion:

➢ Our preliminary results showed a delayed onset of tumors in K8 phosphorylation deficient mice compared to the K8 WT mice. Conducting the DMBA/TPA experiment in the large number of mice is required to further strengthen this hypothesis.

6.2 Part 2: Objective 1

6.2.1 Summary

- Depletion of K8 in a human epidermoid carcinoma derived A431 cells leads to a significant decrease in its **tumorigenic potential.**
- TMT based differential quantitative proteomics profiling revealed key regulators including **MARCKSL1, Rho GDI, TMS1, RANBP1, 14-3-3γ, K17** to be involved in K8 mediated oncogenic pathways**.**

- K8 knockdown leads to apoptotic sensitization of A431 cells probably through **TMS1-PKCδ-NF-κB signaling pathway.**
- K8 downregulation **affects actin organization** and thereby cell migration probably through **MARCKSL1-Paxillin-Rac signaling** pathway.

6.2.2 Conclusion:

➢ This part of the study suggests a potent role of keratin 8 in regulating tumorigenic potential of Skin SCC derived A431 cell line possibly by modulating **MARCKSL1-Paxillin-Rac** and **TMS1-PKCδ-NF-κB** axis and thereby cell motility and apoptosis. Human skin SCC tissue sample based studies and intricate analysis of these proposed model pathways will be required to further endorse its role in skin SCC.

6.3 Part 2: Objective 2

6.3.1 Summary:

- Quantitative phosphoproteomic analysis identified differential phosphorylation of many known and novel phosphosites of proteins, which are well established key players in cancer and are associated with cell migration, proliferation and apoptosis, in response to K8 phosphorylation deregulation.

- In concordance with our global phosphoproteome profiling, the biochemical and phenotypic validations confirmed a potential role of K8 phosphorylation in neoplastic progression of skin-SCCs.

6.3.2 Conclusion:

- To the best of our knowledge, this study represents the first report investigating regulatory role of site specific K8 phosphorylation, and could identify many phosphoproteins and signaling pathways to be altered upon K8 phosphorylation modulation. Intricate analysis of these proposed pathways will be useful to further define association between K8 phosphorylation and cancer.

6.4 Significance of the study:

In the current study, for the first time, we have performed a quantitative total proteomics and differential phosphoproteomic analysis to understand the role of K8 and its site-specific phosphorylation, respectively in neoplastic progression of skin squamous cell carcinoma. We have identified many proteins and signaling networks which are known to play a crucial role in cancer biology and are associated with cell migration, proliferation, invasion, and apoptosis to be differentially regulated in a skin carcinoma derived cell line. Preliminary data of our transgenic study is in agreement with the results of our *in vitro* study. Thus our study underlines the importance of not only K8 aberrant expression, but also its phosphorylation in progression of skin cancers. If validated in human skin tumor samples, both K8 and its phosphorylation can be used in prognostication as well as novel therapeutic targets for skin cancer.

Chapter-VII

Bibliography

1. Godsel LM, Hobbs RP, Green KJ: **Intermediate filament assembly: dynamics to disease**. *Trends in cell biology* 2008, **18**(1):28-37.
2. Bousquet O, Coulombe PA: **Cytoskeleton: missing links found?** *Current biology : CB* 1996, **6**(12):1563-1566.
3. Coulombe PA, Omary MB: **'Hard' and 'soft' principles defining the structure, function and regulation of keratin intermediate filaments**. *Current opinion in cell biology* 2002, **14**(1):110-122.
4. Moll R, Franke WW, Schiller DL, Geiger B, Krepler R: **The catalog of human cytokeratins: patterns of expression in normal epithelia, tumors and cultured cells**. *Cell* 1982, **31**(1):11-24.
5. Moll R, Divo M, Langbein L: **The human keratins: biology and pathology**. *Histochemistry and cell biology* 2008, **129**(6):705-733.
6. Schweizer J, Bowden PE, Coulombe PA, Langbein L, Lane EB, Magin TM, Maltais L, Omary MB, Parry DA, Rogers MA *et al*: **New consensus nomenclature for mammalian keratins**. *The Journal of cell biology* 2006, **174**(2):169-174.
7. Omary MB, Ku NO, Strnad P, Hanada S: **Toward unraveling the complexity of simple epithelial keratins in human disease**. *The Journal of clinical investigation* 2009, **119**(7):1794-1805.
8. Nelson WG, Sun TT: **The 50- and 58-kdalton keratin classes as molecular markers for stratified squamous epithelia: cell culture studies**. *The Journal of cell biology* 1983, **97**(1):244-251.
9. Herrmann H, Aebi U: **Intermediate filaments: molecular structure, assembly mechanism, and integration into functionally distinct intracellular Scaffolds**. *Annual review of biochemistry* 2004, **73**:749-789.
10. Fuchs E, Weber K: **Intermediate filaments: structure, dynamics, function, and disease**. *Annual review of biochemistry* 1994, **63**:345-382.
11. Omary MB, Ku NO, Tao GZ, Toivola DM, Liao J: **"Heads and tails" of intermediate filament phosphorylation: multiple sites and functional insights**. *Trends in biochemical sciences* 2006, **31**(7):383-394.
12. Omary MB, Ku NO, Liao J, Price D: **Keratin modifications and solubility properties in epithelial cells and in vitro**. *Sub-cellular biochemistry* 1998, **31**:105-140.
13. Fuchs E, Cleveland DW: **A structural scaffolding of intermediate filaments in health and disease**. *Science* 1998, **279**(5350):514-519.
14. Gu LH, Coulombe PA: **Keratin function in skin epithelia: a broadening palette with surprising shades**. *Current opinion in cell biology* 2007, **19**(1):13-23.
15. Coulombe PA, Tong X, Mazzalupo S, Wang Z, Wong P: **Great promises yet to be fulfilled: defining keratin intermediate filament function in vivo**. *European journal of cell biology* 2004, **83**(11-12):735-746.
16. Magin TM, Vijayaraj P, Leube RE: **Structural and regulatory functions of keratins**. *Experimental cell research* 2007, **313**(10):2021-2032.
17. Paramio JM, Jorcano JL: **Beyond structure: do intermediate filaments modulate cell signalling?** *BioEssays : news and reviews in molecular, cellular and developmental biology* 2002, **24**(9):836-844.
18. Owens DW, Lane EB: **The quest for the function of simple epithelial keratins**. *BioEssays : news and reviews in molecular, cellular and developmental biology* 2003, **25**(8):748-758.
19. Kim S, Wong P, Coulombe PA: **A keratin cytoskeletal protein regulates protein synthesis and epithelial cell growth**. *Nature* 2006, **441**(7091):362-365.
20. Oshima RG: **Apoptosis and keratin intermediate filaments**. *Cell death and differentiation* 2002, **9**(5):486-492.
21. Bordeleau F, Myrand Lapierre ME, Sheng Y, Marceau N: **Keratin 8/18 regulation of cell stiffness-extracellular matrix interplay through modulation of Rho-mediated actin cytoskeleton dynamics**. *PloS one* 2012, **7**(6):e38780.

22. Salas PJ, Forteza R, Mashukova A: **Multiple roles for keratin intermediate filaments in the regulation of epithelial barrier function and apico-basal polarity**. *Tissue barriers* 2016, **4**(3):e1178368.
23. Pallari HM, Eriksson JE: **Intermediate filaments as signaling platforms**. *Science's STKE : signal transduction knowledge environment* 2006, **2006**(366):pe53.
24. Karantza V: **Keratins in health and cancer: more than mere epithelial cell markers**. *Oncogene* 2011, **30**(2):127-138.
25. Paramio JM, Casanova ML, Segrelles C, Mittnacht S, Lane EB, Jorcano JL: **Modulation of cell proliferation by cytokeratins K10 and K16**. *Molecular and cellular biology* 1999, **19**(4):3086-3094.
26. Hyder CL, Pallari HM, Kochin V, Eriksson JE: **Providing cellular signposts--post-translational modifications of intermediate filaments**. *FEBS letters* 2008, **582**(14):2140-2148.
27. Sawant MS, Leube RE: **Consequences of Keratin Phosphorylation for Cytoskeletal Organization and Epithelial Functions**. *International review of cell and molecular biology* 2017, **330**:171-225.
28. Paramio JM: **A role for phosphorylation in the dynamics of keratin intermediate filaments**. *European journal of cell biology* 1999, **78**(1):33-43.
29. Liao J, Ku NO, Omary MB: **Stress, apoptosis, and mitosis induce phosphorylation of human keratin 8 at Ser-73 in tissues and cultured cells**. *The Journal of biological chemistry* 1997, **272**(28):17565-17573.
30. Ku NO, Omary MB: **Phosphorylation of human keratin 8 in vivo at conserved head domain serine 23 and at epidermal growth factor-stimulated tail domain serine 431**. *The Journal of biological chemistry* 1997, **272**(11):7556-7564.
31. Snider NT, Omary MB: **Post-translational modifications of intermediate filament proteins: mechanisms and functions**. *Nature reviews Molecular cell biology* 2014, **15**(3):163-177.
32. Kim HJ, Choi WJ, Lee CH: **Phosphorylation and Reorganization of Keratin Networks: Implications for Carcinogenesis and Epithelial Mesenchymal Transition**. *Biomolecules & therapeutics* 2015, **23**(4):301-312.
33. Fillies T, Werkmeister R, Packeisen J, Brandt B, Morin P, Weingart D, Joos U, Buerger H: **Cytokeratin 8/18 expression indicates a poor prognosis in squamous cell carcinomas of the oral cavity**. *BMC cancer* 2006, **6**:10.
34. Vaidya MM, Borges AM, Pradhan SA, Bhisey AN: **Cytokeratin expression in squamous cell carcinomas of the tongue and alveolar mucosa**. *European journal of cancer Part B, Oral oncology* 1996, **32B**(5):333-336.
35. Raul U, Sawant S, Dange P, Kalraiya R, Ingle A, Vaidya M: **Implications of cytokeratin 8/18 filament formation in stratified epithelial cells: induction of transformed phenotype**. *International journal of cancer* 2004, **111**(5):662-668.
36. Alam H, Kundu ST, Dalal SN, Vaidya MM: **Loss of keratins 8 and 18 leads to alterations in alpha6beta4-integrin-mediated signalling and decreased neoplastic progression in an oral-tumour-derived cell line**. *Journal of cell science* 2011, **124**(Pt 12):2096-2106.
37. Alam H, Bhate AV, Gangadaran P, Sawant SS, Salot S, Sehgal L, Dange PP, Chaukar DA, D'Cruz A K, Kannanl S *et al*: **Fascin overexpression promotes neoplastic progression in oral squamous cell carcinoma**. *BMC cancer* 2012, **12**:32.
38. Lee EJ, Park MK, Kim HJ, Kim EJ, Kang GJ, Byun HJ, Lee CH: **Epithelial membrane protein 2 regulates sphingosylphosphorylcholine-induced keratin 8 phosphorylation and reorganization: Changes of PP2A expression by interaction with alpha4 and caveolin-1 in lung cancer cells**. *Biochimica et biophysica acta* 2016, **1863**(6 Pt A):1157-1169.
39. Mizuuchi E, Semba S, Kodama Y, Yokozaki H: **Down-modulation of keratin 8 phosphorylation levels by PRL-3 contributes to colorectal carcinoma progression**. *International journal of cancer* 2009, **124**(8):1802-1810.

40. Alam H, Gangadaran P, Bhate AV, Chaukar DA, Sawant SS, Tiwari R, Bobade J, Kannan S, D'Cruz A K, Kane S *et al*: **Loss of keratin 8 phosphorylation leads to increased tumor progression and correlates with clinico-pathological parameters of OSCC patients**. *PloS one* 2011, **6**(11):e27767.
41. Tanaka T, Iino M: **Sec8 regulates cytokeratin8 phosphorylation and cell migration by controlling the ERK and p38 MAPK signalling pathways**. *Cellular signalling* 2015, **27**(6):1110-1119.
42. Chinembiri TN, du Plessis LH, Gerber M, Hamman JH, du Plessis J: **Review of natural compounds for potential skin cancer treatment**. *Molecules* 2014, **19**(8):11679-11721.
43. Darwiche N, Ryscavage A, Perez-Lorenzo R, Wright L, Bae DS, Hennings H, Yuspa SH, Glick AB: **Expression profile of skin papillomas with high cancer risk displays a unique genetic signature that clusters with squamous cell carcinomas and predicts risk for malignant conversion**. *Oncogene* 2007, **26**(48):6885-6895.
44. Herrmann H, Strelkov SV, Burkhard P, Aebi U: **Intermediate filaments: primary determinants of cell architecture and plasticity**. *The Journal of clinical investigation* 2009, **119**(7):1772-1783.
45. Bray DJ, Walsh TR, Noro MG, Notman R: **Complete Structure of an Epithelial Keratin Dimer: Implications for Intermediate Filament Assembly**. *PloS one* 2015, **10**(7):e0132706.
46. Eriksson JE, Dechat T, Grin B, Helfand B, Mendez M, Pallari HM, Goldman RD: **Introducing intermediate filaments: from discovery to disease**. *The Journal of clinical investigation* 2009, **119**(7):1763-1771.
47. Steinert PM, North AC, Parry DA: **Structural features of keratin intermediate filaments**. *The Journal of investigative dermatology* 1994, **103**(5 Suppl):19S-24S.
48. Omary MB, Coulombe PA, McLean WH: **Intermediate filament proteins and their associated diseases**. *The New England journal of medicine* 2004, **351**(20):2087-2100.
49. Lee CH, Coulombe PA: **Self-organization of keratin intermediate filaments into cross-linked networks**. *The Journal of cell biology* 2009, **186**(3):409-421.
50. Kim JS, Lee CH, Coulombe PA: **Modeling the self-organization property of keratin intermediate filaments**. *Biophysical journal* 2010, **99**(9):2748-2756.
51. Kolsch A, Windoffer R, Wurflinger T, Aach T, Leube RE: **The keratin-filament cycle of assembly and disassembly**. *Journal of cell science* 2010, **123**(Pt 13):2266-2272.
52. Windoffer R, Beil M, Magin TM, Leube RE: **Cytoskeleton in motion: the dynamics of keratin intermediate filaments in epithelia**. *The Journal of cell biology* 2011, **194**(5):669-678.
53. Chu PG, Weiss LM: **Keratin expression in human tissues and neoplasms**. *Histopathology* 2002, **40**(5):403-439.
54. Fuchs E, Green H: **Changes in keratin gene expression during terminal differentiation of the keratinocyte**. *Cell* 1980, **19**(4):1033-1042.
55. Bragulla HH, Homberger DG: **Structure and functions of keratin proteins in simple, stratified, keratinized and cornified epithelia**. *Journal of anatomy* 2009, **214**(4):516-559.
56. Strnad P, Guldiken N, Helenius TO, Misiorek JO, Nystrom JH, Lahdeniemi IA, Silvander JS, Kuscuoglu D, Toivola DM: **Simple Epithelial Keratins**. *Methods in enzymology* 2016, **568**:351-388.
57. Srikanth B, Vaidya MM, Kalraiya RD: **O-GlcNAcylation determines the solubility, filament organization, and stability of keratins 8 and 18**. *The Journal of biological chemistry* 2010, **285**(44):34062-34071.
58. Kakade PS, Budnar S, Kalraiya RD, Vaidya MM: **Functional Implications of O-GlcNAcylation-dependent Phosphorylation at a Proximal Site on Keratin 18**. *The Journal of biological chemistry* 2016, **291**(23):12003-12013.
59. Snider NT, Weerasinghe SV, Iniguez-Lluhi JA, Herrmann H, Omary MB: **Keratin hypersumoylation alters filament dynamics and is a marker for human liver disease and keratin mutation**. *The Journal of biological chemistry* 2011, **286**(3):2273-2284.

60. Ku NO, Omary MB: **Keratins turn over by ubiquitination in a phosphorylation-modulated fashion**. *The Journal of cell biology* 2000, **149**(3):547-552.
61. Snider NT, Leonard JM, Kwan R, Griggs NW, Rui L, Omary MB: **Glucose and SIRT2 reciprocally mediate the regulation of keratin 8 by lysine acetylation**. *The Journal of cell biology* 2013, **200**(3):241-247.
62. Ku NO, Liao J, Chou CF, Omary MB: **Implications of intermediate filament protein phosphorylation**. *Cancer metastasis reviews* 1996, **15**(4):429-444.
63. Ku NO, Darling JM, Krams SM, Esquivel CO, Keeffe EB, Sibley RK, Lee YM, Wright TL, Omary MB: **Keratin 8 and 18 mutations are risk factors for developing liver disease of multiple etiologies**. *Proceedings of the National Academy of Sciences of the United States of America* 2003, **100**(10):6063-6068.
64. Omary MB: **"IF-pathies": a broad spectrum of intermediate filament-associated diseases**. *The Journal of clinical investigation* 2009, **119**(7):1756-1762.
65. Tao GZ, Toivola DM, Zhou Q, Strnad P, Xu B, Michie SA, Omary MB: **Protein phosphatase-2A associates with and dephosphorylates keratin 8 after hyposmotic stress in a site- and cell-specific manner**. *Journal of cell science* 2006, **119**(Pt 7):1425-1432.
66. Ku NO, Omary MB: **A disease- and phosphorylation-related nonmechanical function for keratin 8**. *The Journal of cell biology* 2006, **174**(1):115-125.
67. Ridge KM, Linz L, Flitney FW, Kuczmarski ER, Chou YH, Omary MB, Sznajder JI, Goldman RD: **Keratin 8 phosphorylation by protein kinase C delta regulates shear stress-mediated disassembly of keratin intermediate filaments in alveolar epithelial cells**. *The Journal of biological chemistry* 2005, **280**(34):30400-30405.
68. Marceau N, Gilbert S, Loranger A: **Uncovering the roles of intermediate filaments in apoptosis**. *Methods in cell biology* 2004, **78**:95-129.
69. Pan X, Hobbs RP, Coulombe PA: **The expanding significance of keratin intermediate filaments in normal and diseased epithelia**. *Current opinion in cell biology* 2013, **25**(1):47-56.
70. Gilbert S, Loranger A, Daigle N, Marceau N: **Simple epithelium keratins 8 and 18 provide resistance to Fas-mediated apoptosis. The protection occurs through a receptor-targeting modulation**. *The Journal of cell biology* 2001, **154**(4):763-773.
71. Gilbert S, Loranger A, Marceau N: **Keratins modulate c-Flip/extracellular signal-regulated kinase 1 and 2 antiapoptotic signaling in simple epithelial cells**. *Molecular and cellular biology* 2004, **24**(16):7072-7081.
72. Tong X, Coulombe PA: **Keratin 17 modulates hair follicle cycling in a TNFalpha-dependent fashion**. *Genes & development* 2006, **20**(10):1353-1364.
73. Kongara S, Kravchuk O, Teplova I, Lozy F, Schulte J, Moore D, Barnard N, Neumann CA, White E, Karantza V: **Autophagy regulates keratin 8 homeostasis in mammary epithelial cells and in breast tumors**. *Molecular cancer research : MCR* 2010, **8**(6):873-884.
74. Harada M, Strnad P, Toivola DM, Omary MB: **Autophagy modulates keratin-containing inclusion formation and apoptosis in cell culture in a context-dependent fashion**. *Experimental cell research* 2008, **314**(8):1753-1764.
75. Galarneau L, Loranger A, Gilbert S, Marceau N: **Keratins modulate hepatic cell adhesion, size and G1/S transition**. *Experimental cell research* 2007, **313**(1):179-194.
76. Woll S, Windoffer R, Leube RE: **Dissection of keratin dynamics: different contributions of the actin and microtubule systems**. *European journal of cell biology* 2005, **84**(2-3):311-328.
77. Windoffer R, Kolsch A, Woll S, Leube RE: **Focal adhesions are hotspots for keratin filament precursor formation**. *The Journal of cell biology* 2006, **173**(3):341-348.
78. Bordeleau F, Galarneau L, Gilbert S, Loranger A, Marceau N: **Keratin 8/18 modulation of protein kinase C-mediated integrin-dependent adhesion and migration of liver epithelial cells**. *Molecular biology of the cell* 2010, **21**(10):1698-1713.

79. Mazzalupo S, Wong P, Martin P, Coulombe PA: **Role for keratins 6 and 17 during wound closure in embryonic mouse skin**. *Developmental dynamics : an official publication of the American Association of Anatomists* 2003, **226**(2):356-365.
80. Hendrix MJ, Seftor EA, Chu YW, Trevor KT, Seftor RE: **Role of intermediate filaments in migration, invasion and metastasis**. *Cancer metastasis reviews* 1996, **15**(4):507-525.
81. Chu YW, Seftor EA, Romer LH, Hendrix MJ: **Experimental coexpression of vimentin and keratin intermediate filaments in human melanoma cells augments motility**. *The American journal of pathology* 1996, **148**(1):63-69.
82. Chu YW, Runyan RB, Oshima RG, Hendrix MJ: **Expression of complete keratin filaments in mouse L cells augments cell migration and invasion**. *Proceedings of the National Academy of Sciences of the United States of America* 1993, **90**(9):4261-4265.
83. Knosel T, Emde V, Schluns K, Schlag PM, Dietel M, Petersen I: **Cytokeratin profiles identify diagnostic signatures in colorectal cancer using multiplex analysis of tissue microarrays**. *Cellular oncology : the official journal of the International Society for Cellular Oncology* 2006, **28**(4):167-175.
84. Vijayaraj P, Sohl G, Magin TM: **Keratin transgenic and knockout mice: functional analysis and validation of disease-causing mutations**. *Methods in molecular biology* 2007, **360**:203-251.
85. Baribault H, Price J, Miyai K, Oshima RG: **Mid-gestational lethality in mice lacking keratin 8**. *Genes & development* 1993, **7**(7A):1191-1202.
86. Habtezion A, Toivola DM, Butcher EC, Omary MB: **Keratin-8-deficient mice develop chronic spontaneous Th2 colitis amenable to antibiotic treatment**. *Journal of cell science* 2005, **118**(Pt 9):1971-1980.
87. Casanova ML, Bravo A, Ramirez A, Morreale de Escobar G, Were F, Merlino G, Vidal M, Jorcano JL: **Exocrine pancreatic disorders in transsgenic mice expressing human keratin 8**. *The Journal of clinical investigation* 1999, **103**(11):1587-1595.
88. Toivola DM, Nakamichi I, Strnad P, Michie SA, Ghori N, Harada M, Zeh K, Oshima RG, Baribault H, Omary MB: **Keratin overexpression levels correlate with the extent of spontaneous pancreatic injury**. *The American journal of pathology* 2008, **172**(4):882-892.
89. Chen J, Cheng X, Merched-Sauvage M, Caulin C, Roop DR, Koch PJ: **An unexpected role for keratin 10 end domains in susceptibility to skin cancer**. *Journal of cell science* 2006, **119**(Pt 24):5067-5076.
90. Depianto D, Kerns ML, Dlugosz AA, Coulombe PA: **Keratin 17 promotes epithelial proliferation and tumor growth by polarizing the immune response in skin**. *Nature genetics* 2010, **42**(10):910-914.
91. Schaafsma HE, Van Der Velden LA, Manni JJ, Peters H, Link M, Rutter DJ, Ramaekers FC: **Increased expression of cytokeratins 8, 18 and vimentin in the invasion front of mucosal squamous cell carcinoma**. *The Journal of pathology* 1993, **170**(1):77-86.
92. Casanova ML, Bravo A, Martinez-Palacio J, Fernandez-Acenero MJ, Villanueva C, Larcher F, Conti CJ, Jorcano JL: **Epidermal abnormalities and increased malignancy of skin tumors in human epidermal keratin 8-expressing transgenic mice**. *FASEB journal : official publication of the Federation of American Societies for Experimental Biology* 2004, **18**(13):1556-1558.
93. Frohwitter G, Buerger H, PJ VAND, Korsching E, Kleinheinz J, Fillies T: **Cytokeratin and protein expression patterns in squamous cell carcinoma of the oral cavity provide evidence for two distinct pathogenetic pathways**. *Oncology letters* 2016, **12**(1):107-113.
94. Ku NO, Strnad P, Zhong BH, Tao GZ, Omary MB: **Keratins let liver live: Mutations predispose to liver disease and crosslinking generates Mallory-Denk bodies**. *Hepatology* 2007, **46**(5):1639-1649.
95. Stevens HP, Rustin MH: **Keratin gene mutations in human skin disease**. *Postgraduate medical journal* 1994, **70**(829):775-779.
96. Uitto J, Richard G, McGrath JA: **Diseases of epidermal keratins and their linker proteins**. *Experimental cell research* 2007, **313**(10):1995-2009.

97. Ku NO, Michie SA, Soetikno RM, Resurreccion EZ, Broome RL, Omary MB: **Mutation of a major keratin phosphorylation site predisposes to hepatotoxic injury in transgenic mice**. *The Journal of cell biology* 1998, **143**(7):2023-2032.
98. Hofmann A, Kessler B, Ewerling S, Weppert M, Vogg B, Ludwig H, Stojkovic M, Boelhauve M, Brem G, Wolf E *et al*: **Efficient transgenesis in farm animals by lentiviral vectors**. *EMBO reports* 2003, **4**(11):1054-1060.
99. Sehgal L, Thorat R, Khapare N, Mukhopadhaya A, Sawant M, Dalal SN: **Lentiviral mediated transgenesis by in vivo manipulation of spermatogonial stem cells**. *PLoS One* 2011, **6**(7):e21975.
100. Usmani A, Ganguli N, Sarkar H, Dhup S, Batta SR, Vimal M, Ganguli N, Basu S, Nagarajan P, Majumdar SS: **A non-surgical approach for male germ cell mediated gene transmission through transgenesis**. *Scientific reports* 2013, **3**:3430.
101. Peterson GL: **A simplification of the protein assay method of Lowry et al. which is more generally applicable**. *Analytical biochemistry* 1977, **83**(2):346-356.
102. Laemmli UK: **Cleavage of structural proteins during the assembly of the head of bacteriophage T4**. *Nature* 1970, **227**(5259):680-685.
103. Towbin H, Staehelin T, Gordon J: **Electrophoretic transfer of proteins from polyacrylamide gels to nitrocellulose sheets: procedure and some applications. 1979**. *Biotechnology* 1992, **24**:145-149.
104. Wiśniewski JR, Zougman A, Nagaraj N, Mann M: **Universal sample preparation method for proteome analysis**. *Nature methods* 2009, **6**(5):359-362.
105. Selvan LD, Renuse S, Kaviyil JE, Sharma J, Pinto SM, Yelamanchi SD, Puttamallesh VN, Ravikumar R, Pandey A, Prasad TS *et al*: **Phosphoproteome of Cryptococcus neoformans**. *J Proteomics* 2014, **97**:287-295.
106. Wisniewski JR, Zougman A, Nagaraj N, Mann M: **Universal sample preparation method for proteome analysis**. *Nat Methods* 2009, **6**(5):359-362.
107. Dinkel H, Chica C, Via A, Gould CM, Jensen LJ, Gibson TJ, Diella F: **Phospho.ELM: a database of phosphorylation sites--update 2011**. *Nucleic Acids Res* 2011, **39**(Database issue):D261-267.
108. Chen EY, Tan CM, Kou Y, Duan Q, Wang Z, Meirelles GV, Clark NR, Ma'ayan A: **Enrichr: interactive and collaborative HTML5 gene list enrichment analysis tool**. *BMC Bioinformatics* 2013, **14**:128.
109. Mi H, Poudel S, Muruganujan A, Casagrande JT, Thomas PD: **PANTHER version 10: expanded protein families and functions, and analysis tools**. *Nucleic Acids Res* 2016, **44**(D1):D336-342.
110. Mosmann T: **Rapid colorimetric assay for cellular growth and survival: application to proliferation and cytotoxicity assays**. *Journal of immunological methods* 1983, **65**(1-2):55-63.
111. Walrath JC, Hawes JJ, Van Dyke T, Reilly KM: **Genetically engineered mouse models in cancer research**. *Advances in cancer research* 2010, **106**:113-164.
112. Kersten K, de Visser KE, van Miltenburg MH, Jonkers J: **Genetically engineered mouse models in oncology research and cancer medicine**. *EMBO molecular medicine* 2017, **9**(2):137-153.
113. Neagu M, Caruntu C, Constantin C, Boda D, Zurac S, Spandidos DA, Tsatsakis AM: **Chemically induced skin carcinogenesis: Updates in experimental models (Review)**. *Oncology reports* 2016, **35**(5):2516-2528.
114. Chung BM, Murray CI, Van Eyk JE, Coulombe PA: **Identification of novel interaction between annexin A2 and keratin 17: evidence for reciprocal regulation**. *The Journal of biological chemistry* 2012, **287**(10):7573-7581.
115. Badock V, Steinhusen U, Bommert K, Wittmann-Liebold B, Otto A: **Apoptosis-induced cleavage of keratin 15 and keratin 17 in a human breast epithelial cell line**. *Cell Death Differ* 2001, **8**(3):308-315.
116. Marceau N, Loranger A, Gilbert S, Daigle N, Champetier S: **Keratin-mediated resistance to stress and apoptosis in simple epithelial cells in relation to health and disease**. *Biochemistry and cell biology = Biochimie et biologie cellulaire* 2001, **79**(5):543-555.

117. Caulin C, Salvesen GS, Oshima RG: **Caspase cleavage of keratin 18 and reorganization of intermediate filaments during epithelial cell apoptosis**. *The Journal of cell biology* 1997, **138**(6):1379-1394.
118. Weerasinghe SV, Ku NO, Altshuler PJ, Kwan R, Omary MB: **Mutation of caspase-digestion sites in keratin 18 interferes with filament reorganization, and predisposes to hepatocyte necrosis and loss of membrane integrity**. *Journal of cell science* 2014, **127**(Pt 7):1464-1475.
119. Wang YF, Lang HY, Yuan J, Wang J, Wang R, Zhang XH, Zhang J, Zhao T, Li YR, Liu JY *et al*: **Overexpression of keratin 17 is associated with poor prognosis in epithelial ovarian cancer**. *Tumour biology : the journal of the International Society for Oncodevelopmental Biology and Medicine* 2013, **34**(3):1685-1689.
120. Ide M, Kato T, Ogata K, Mochiki E, Kuwano H, Oyama T: **Keratin 17 expression correlates with tumor progression and poor prognosis in gastric adenocarcinoma**. *Annals of surgical oncology* 2012, **19**(11):3506-3514.
121. Khanom R, Nguyen CT, Kayamori K, Zhao X, Morita K, Miki Y, Katsube K, Yamaguchi A, Sakamoto K: **Keratin 17 Is Induced in Oral Cancer and Facilitates Tumor Growth**. *PloS one* 2016, **11**(8):e0161163.
122. Leigh IM, Navsaria H, Purkis PE, McKay IA, Bowden PE, Riddle PN: **Keratins (K16 and K17) as markers of keratinocyte hyperproliferation in psoriasis in vivo and in vitro**. *The British journal of dermatology* 1995, **133**(4):501-511.
123. Hutchin ME, Kariapper MS, Grachtchouk M, Wang A, Wei L, Cummings D, Liu J, Michael LE, Glick A, Dlugosz AA: **Sustained Hedgehog signaling is required for basal cell carcinoma proliferation and survival: conditional skin tumorigenesis recapitulates the hair growth cycle**. *Genes & development* 2005, **19**(2):214-223.
124. Zhang C, Li H, Zhou G, Zhang Q, Zhang T, Li J, Zhang J, Hou J, Liew CT, Yin D: **Transcriptional silencing of the TMS1/ASC tumour suppressor gene by an epigenetic mechanism in hepatocellular carcinoma cells**. *The Journal of pathology* 2007, **212**(2):134-142.
125. Okada N, Fujii C, Matsumura T, Kitazawa M, Okuyama R, Taniguchi S, Hida S: **Novel role of ASC as a regulator of metastatic phenotype**. *Cancer medicine* 2016, **5**(9):2487-2500.
126. Virmani A, Rathi A, Sugio K, Sathyanarayana UG, Toyooka S, Kischel FC, Tonk V, Padar A, Takahashi T, Roth JA *et al*: **Aberrant methylation of TMS1 in small cell, non small cell lung cancer and breast cancer**. *International journal of cancer* 2003, **106**(2):198-204.
127. Parsons MJ, Vertino PM: **Dual role of TMS1/ASC in death receptor signaling**. *Oncogene* 2006, **25**(52):6948-6958.
128. Barkett M, Gilmore TD: **Control of apoptosis by Rel/NF-kappaB transcription factors**. *Oncogene* 1999, **18**(49):6910-6924.
129. Van Antwerp DJ, Martin SJ, Verma IM, Green DR: **Inhibition of TNF-induced apoptosis by NF-kappa B**. *Trends in cell biology* 1998, **8**(3):107-111.
130. Karin M, Lin A: **NF-kappaB at the crossroads of life and death**. *Nature immunology* 2002, **3**(3):221-227.
131. Basu A, Pal D: **Two faces of protein kinase Cdelta: the contrasting roles of PKCdelta in cell survival and cell death**. *ScientificWorldJournal* 2010, **10**:2272-2284.
132. Lallena MJ, Diaz-Meco MT, Bren G, Paya CV, Moscat J: **Activation of IkappaB kinase beta by protein kinase C isoforms**. *Molecular and cellular biology* 1999, **19**(3):2180-2188.
133. Lin A: **Activation of the JNK signaling pathway: breaking the brake on apoptosis**. *BioEssays : news and reviews in molecular, cellular and developmental biology* 2003, **25**(1):17-24.
134. Rensen WM, Roscioli E, Tedeschi A, Mangiacasale R, Ciciarello M, Di Gioia SA, Lavia P: **RanBP1 downregulation sensitizes cancer cells to taxol in a caspase-3-dependent manner**. *Oncogene* 2009, **28**(15):1748-1758.

135. Yamaguchi H, Condeelis J: **Regulation of the actin cytoskeleton in cancer cell migration and invasion**. *Biochimica et biophysica acta* 2007, **1773**(5):642-652.
136. Li J, Zhu Z, Bao Z: **Role of MacMARCKS in integrin-dependent macrophage spreading and tyrosine phosphorylation of paxillin**. *J Biol Chem* 1996, **271**(22):12985-12990.
137. Bjorkblom B, Padzik A, Mohammad H, Westerlund N, Komulainen E, Hollos P, Parviainen L, Papageorgiou AC, Iljin K, Kallioniemi O *et al*: **c-Jun N-terminal kinase phosphorylation of MARCKSL1 determines actin stability and migration in neurons and in cancer cells**. *Molecular and cellular biology* 2012, **32**(17):3513-3526.
138. Jamieson JS, Tumbarello DA, Halle M, Brown MC, Tremblay ML, Turner CE: **Paxillin is essential for PTP-PEST-dependent regulation of cell spreading and motility: a role for paxillin kinase linker**. *Journal of cell science* 2005, **118**(Pt 24):5835-5847.
139. Zaidel-Bar R, Milo R, Kam Z, Geiger B: **A paxillin tyrosine phosphorylation switch regulates the assembly and form of cell-matrix adhesions**. *Journal of cell science* 2007, **120**(Pt 1):137-148.
140. Turner CE: **Paxillin interactions**. *Journal of cell science* 2000, **113 Pt 23**:4139-4140.
141. Schaller MD: **Paxillin: a focal adhesion-associated adaptor protein**. *Oncogene* 2001, **20**(44):6459-6472.
142. Hanna S, El-Sibai M: **Signaling networks of Rho GTPases in cell motility**. *Cellular signalling* 2013, **25**(10):1955-1961.
143. Schaller MD: **FAK and paxillin: regulators of N-cadherin adhesion and inhibitors of cell migration?** *The Journal of cell biology* 2004, **166**(2):157-159.
144. Yang N, Higuchi O, Ohashi K, Nagata K, Wada A, Kangawa K, Nishida E, Mizuno K: **Cofilin phosphorylation by LIM-kinase 1 and its role in Rac-mediated actin reorganization**. *Nature* 1998, **393**(6687):809-812.
145. Nagata-Ohashi K, Ohta Y, Goto K, Chiba S, Mori R, Nishita M, Ohashi K, Kousaka K, Iwamatsu A, Niwa R *et al*: **A pathway of neuregulin-induced activation of cofilin-phosphatase Slingshot and cofilin in lamellipodia**. *The Journal of cell biology* 2004, **165**(4):465-471.
146. Sehgal BU, DeBiase PJ, Matzno S, Chew TL, Claiborne JN, Hopkinson SB, Russell A, Marinkovich MP, Jones JC: **Integrin beta4 regulates migratory behavior of keratinocytes by determining laminin-332 organization**. *The Journal of biological chemistry* 2006, **281**(46):35487-35498.
147. Kligys K, Claiborne JN, DeBiase PJ, Hopkinson SB, Wu Y, Mizuno K, Jones JC: **The slingshot family of phosphatases mediates Rac1 regulation of cofilin phosphorylation, laminin-332 organization, and motility behavior of keratinocytes**. *The Journal of biological chemistry* 2007, **282**(44):32520-32528.
148. Jovceva E, Larsen MR, Waterfield MD, Baum B, Timms JF: **Dynamic cofilin phosphorylation in the control of lamellipodial actin homeostasis**. *Journal of cell science* 2007, **120**(Pt 11):1888-1897.
149. Kraus S, Naor Z, Seger R: **Intracellular signaling pathways mediated by the gonadotropin-releasing hormone (GnRH) receptor**. *Archives of medical research* 2001, **32**(6):499-509.
150. George AJ, Thomas WG, Hannan RD: **The renin-angiotensin system and cancer: old dog, new tricks**. *Nature reviews Cancer* 2010, **10**(11):745-759.
151. Heinonen H, Nieminen A, Saarela M, Kallioniemi A, Klefstrom J, Hautaniemi S, Monni O: **Deciphering downstream gene targets of PI3K/mTOR/p70S6K pathway in breast cancer**. *BMC genomics* 2008, **9**:348.
152. Guertin DA, Sabatini DM: **Defining the role of mTOR in cancer**. *Cancer cell* 2007, **12**(1):9-22.
153. Cremona CA, Behrens A: **ATM signalling and cancer**. *Oncogene* 2014, **33**(26):3351-3360.
154. Sotgia F, Martinez-Outschoorn UE, Howell A, Pestell RG, Pavlides S, Lisanti MP: **Caveolin-1 and cancer metabolism in the tumor microenvironment: markers, models, and mechanisms**. *Annu Rev Pathol* 2012, **7**:423-467.
155. Hirata H, Tatsumi H, Sokabe M: **Zyxin emerges as a key player in the mechanotransduction at cell adhesive structures**. *Commun Integr Biol* 2008, **1**(2):192-195.

156. Lua BL, Low BC: **Cortactin phosphorylation as a switch for actin cytoskeletal network and cell dynamics control**. *FEBS Lett* 2005, **579**(3):577-585.
157. Zhou GL, Zhang H, Wu H, Ghai P, Field J: **Phosphorylation of the cytoskeletal protein CAP1 controls its association with cofilin and actin**. *J Cell Sci* 2014, **127**(Pt 23):5052-5065.
158. Elowe S, Dulla K, Uldschmid A, Li X, Dou Z, Nigg EA: **Uncoupling of the spindle-checkpoint and chromosome-congression functions of BubR1**. *J Cell Sci* 2010, **123**(Pt 1):84-94.
159. Daub H, Olsen JV, Bairlein M, Gnad F, Oppermann FS, Korner R, Greff Z, Keri G, Stemmann O, Mann M: **Kinase-selective enrichment enables quantitative phosphoproteomics of the kinome across the cell cycle**. *Mol Cell* 2008, **31**(3):438-448.
160. Olsen JV, Blagoev B, Gnad F, Macek B, Kumar C, Mortensen P, Mann M: **Global, in vivo, and site-specific phosphorylation dynamics in signaling networks**. *Cell* 2006, **127**(3):635-648.
161. Lew DJ, Kornbluth S: **Regulatory roles of cyclin dependent kinase phosphorylation in cell cycle control**. *Curr Opin Cell Biol* 1996, **8**(6):795-804.
162. Lindqvist A, Rodriguez-Bravo V, Medema RH: **The decision to enter mitosis: feedback and redundancy in the mitotic entry network**. *J Cell Biol* 2009, **185**(2):193-202.
163. Gingras AC, Raught B, Gygi SP, Niedzwiecka A, Miron M, Burley SK, Polakiewicz RD, Wyslouch-Cieszynska A, Aebersold R, Sonenberg N: **Hierarchical phosphorylation of the translation inhibitor 4E-BP1**. *Genes Dev* 2001, **15**(21):2852-2864.
164. Pyronnet S, Dostie J, Sonenberg N: **Suppression of cap-dependent translation in mitosis**. *Genes Dev* 2001, **15**(16):2083-2093.
165. Shuda M, Velasquez C, Cheng E, Cordek DG, Kwun HJ, Chang Y, Moore PS: **CDK1 substitutes for mTOR kinase to activate mitotic cap-dependent protein translation**. *Proc Natl Acad Sci U S A* 2015, **112**(19):5875-5882.
166. Choo AY, Yoon SO, Kim SG, Roux PP, Blenis J: **Rapamycin differentially inhibits S6Ks and 4E-BP1 to mediate cell-type-specific repression of mRNA translation**. *Proc Natl Acad Sci U S A* 2008, **105**(45):17414-17419.
167. Livingstone M, Bidinosti M: **Rapamycin-insensitive mTORC1 activity controls eIF4E:4E-BP1 binding**. *F1000Res* 2012, **1**:4.
168. van Gorp AG, van der Vos KE, Brenkman AB, Bremer A, van den Broek N, Zwartkruis F, Hershey JW, Burgering BM, Calkhoven CF, Coffer PJ: **AGC kinases regulate phosphorylation and activation of eukaryotic translation initiation factor 4B**. *Oncogene* 2009, **28**(1):95-106.
169. Gallie DR: **The role of the initiation surveillance complex in promoting efficient protein synthesis**. *Biochem Soc Trans* 2004, **32**(Pt 4):585-588.
170. Martinez-Quiles N, Ho HY, Kirschner MW, Ramesh N, Geha RS: **Erk/Src phosphorylation of cortactin acts as a switch on-switch off mechanism that controls its ability to activate N-WASP**. *Mol Cell Biol* 2004, **24**(12):5269-5280.
171. Taira N, Mimoto R, Kurata M, Yamaguchi T, Kitagawa M, Miki Y, Yoshida K: **DYRK2 priming phosphorylation of c-Jun and c-Myc modulates cell cycle progression in human cancer cells**. *J Clin Invest* 2012, **122**(3):859-872.

Publication

DOI 10.1002/pmic.201600254 *Proteomics 17, 7,* 2017, 1600254

RESEARCH ARTICLE

Quantitative phosphoproteomic analysis reveals system-wide signaling pathways regulated by site-specific phosphorylation of Keratin-8 in skin squamous cell carcinoma derived cell line

Richa Tiwari[1,2], Indrajit Sahu[1,2,3], Bihari lal Soni[1,2,4], Gajanan J. Sathe[5], Keshava K. Datta[5], Pankaj Thapa[1,2], Shruti Sinha[1], Chella Krishna Vadivel[1], Bharti Dhaka[5], Harsha Gowda[5] and Milind M. Vaidya[1,2]

[1] Advanced Centre for Treatment, Research and Education in Cancer, Navi Mumbai, India
[2] Homi Bhabha National Institute, Training School Complex, Anushakti Nagar, Mumbai, India
[3] Department of Biology, Technion–Israel Institute of Technology, Haifa, Israel
[4] Medical College of Wisconsin, Milwaukee, WI, USA
[5] Institute of Bioinformatics, Bangalore, India

Received: June 15, 2016
Revised: January 14, 2017
Accepted: February 1, 2017

Keratin 8/18, a simple epithelia specific keratin pair, is often aberrantly expressed in squamous cell carcinomas (SCC) where its expression is correlated with increased invasion and poor prognosis. Majority of Keratin 8 (K8) functions are governed by its phosphorylation at Serine^{73} (head-domain) and Serine^{431} (tail-domain) residues. Although, deregulation of K8 phosphorylation is associated with progression of different carcinomas, its role in skin-SCC and the underlying mechanism is obscure. In this direction, we performed tandem mass tag-based quantitative phosphoproteomics by expressing K8 wild type, phosphodead, and phosphomimetic mutants in K8-deficient A431 cells. Further analysis of our phosphoproteomics data showed a significant proportion of total phosphoproteome associated with migratory, proliferative, and invasive potential of these cells to be differentially phosphorylated. Differential phosphorylation of CDK1^{T14,Y15}, EIF4EBP1^{T46,T50}, EIF4B^{S422}, AKT1S1^{T246,S247}, CTTN1^{T401,S405,Y421}, and CAP1$^{S307/309}$ in K8-S73A/D mutant and CTTN1^{T401,S405,Y421}, BUB1B^{S1043}, and CARHSP1^{S30,S32} in K8-S431A/D mutants as well as some anonymous phosphosites including MYC^{S176}, ZYX^{S344}, and PNN^{S692} could be potential candidates associated with K8 phosphorylation mediated tumorigenicity. Biochemical validation followed by phenotypic analysis further confirmed our quantitative phosphoproteomics data. In conclusion, our study provides the first global picture of K8 site-specific phosphorylation function in neoplastic progression of A431 cells and suggests various potential starting points for further mechanistic studies.

Keywords:
IPA / Keratin 8 / 18 Phosphorylation / Quantitative phosphoproteomics / Tumorigenic potential

Additional supporting information may be found in the online version of this article at the publisher's web-site

Correspondence: Dr. Milind M. Vaidya, Advanced Centre for Treatment, Research and Education in Cancer, Navi Mumbai 410210, India.
E-mail: mvaidya@actrec.gov.in

Abbreviations: **GFP**, green fluorescence protein; **HPRD**, human RefSeq protein database; **IPA**, ingenuity pathway analysis; **K8**, Keratin 8; **MTT**, 3-(4,5-dimethylthiazol-2-yl)-2,5-diphenyltetrazolium bromide; **PPI**, protein–protein interaction; **SCC**, squamous cell carcinoma; **TMT**, tandem mass tag; **WT**, wild type

Colour Online: See the article online to view Figs. 1–7 in colour.

Significance of the study

In the current study, for the first time, we have performed a quantitative phosphoproteomic analysis to understand the role of site-specific K8 phosphorylation in neoplastic progression of skin squamous cell carcinomas using an epidermoid carcinoma derived cell-line A431. We have identified differential phosphorylation of many known and novel phosphosites of proteins, which are well-established key players in cancer biology and are associated with cell migration, proliferation, invasion, and apoptosis. In addition, our phosphoproteomic analysis uncovered many novel K8 phosphorylation mediated functional networks together with signaling mechanisms and also confirmed previous findings, thereby revealing its much broader regulatory role in cancer. Our protein phosphorylation level validation followed by phenotypic analysis further correlated well with our phosphoproteomics data. Hence, this study adds on to the existing knowledge about the role of K8 phosphorylation in modulating different signaling mechanisms and thereby cancer progression.

1 Introduction

Keratins are the largest subgroup of intermediate filament proteins expressed in a tissue specific and differentiation-dependent manner. They are stable as 10 nm obligate heteropolymeric filaments of a Type-I (K9–K28, K31–K40) and Type-II (K1–K8, K71–K86) keratin each. Keratin 8/18 (K8/18), the simple epithelia-specific keratin-pair, typically executes various mechanical and regulatory functions [1]. However, its aberrant expression is broadly correlated with increased invasiveness and poor prognosis of squamous cell carcinomas [2]. K8/18 share a common prototype structure comprising of a central coiled coil alpha helical rod domain flanked by two nonhelical head and tail domains [1]. The head and tail domains provide heterogeneity to all the keratins and harbor sites for major PTMs, predominantly phosphorylation.

Phosphorylation imparts various functions to K8/18, such as filament organization, solubility, binding to other proteins and protecting cells from stress and apoptosis [3]. K8 contains three major physiological phosphorylation sites, Serine^{23}, Serine^{73} in head-domain and Serine^{431} in tail-domain. Phosphorylation at Serine^{23} is highly conserved among all type-II keratins, rendering several common functions to them, whereas Serine^{73} and Serine^{431} are unique to K8 [4]. Many kinases (JNK, p38-MAP kinase, PKCδ) and phosphatases (PP2A, PRL3) are known to regulate K8 phosphorylation under specific conditions including stress, mitosis, and apoptosis (Serine^{73}/Serine^{431}) or in basal condition (Serine^{23}/Serine^{431}) and consequently modulate its functions [4, 5]. Although phosphorylation is associated with many diverse physiological functions of K8, the reports related to its role in the neoplastic progression of different carcinomas and the underlying mechanisms are inconsistent.

Nonmelanoma skin cancers, one of the most common neoplasms, known to cause serious morbidity and mortality, are curable at early stages, but delayed diagnosis leads to metastasis [6]. Although, K8/18 pair is known to be aberrantly expressed in skin cancers [7] till now, to our knowledge, there are no reports about the involvement of K8 phosphorylation and related mechanistic pathways in basal squamous cell carcinomas (SCCs). In this study, we carried out system-wide phosphoproteomic profiling after ablation of K8 phosphorylation at Serine^{73} and Serine^{431} in A431 cells, a skin epidermoid carcinoma derived cell-line followed by phenotypic validation. Tandem mass tag (TMT)-based phosphoproteomic profiling and high-throughput analysis revealed many known and novel cancer associated pathways to be modulated significantly after deregulating site-specific K8 phosphorylation. These results were well supported by our protein phosphorylation level validation as well as phenotypic analysis. Our study provides a unique resource of phosphoproteins and phosphorylation sites that may give better insight into signaling mechanisms associated with K8 phosphorylation mediated regulation of skin-SCC progression.

2 Materials and methods

2.1 Plasmids and cloning

The shRNA-resistant pLNCX2-3XFlag-K8-WT-GFP construct was first generated as described in the Supporting Information Fig. 1. Further, shRNA-resistant phosphodead mutants (pLNCX2-3XFlag-K8-73A-GFP and pLNCX2-3XFlag-K8-431A-GFP) and phosphomimetic mutants (pLNCX2-3XFlag-K8-S73D-GFP and pLNCX2-3XFlag-K8-S431D-GFP) were generated by site-directed mutagenesis of the pLNCX2-3XFlag-K8-WT-GFP following the protocol as described earlier [8]. The point-mutations were verified by sequencing. The list of primers used for site-directed mutagenesis is given in Supporting Information Fig. 2.

2.2 Cell-lines, viral particle preparation, and generation of stable clones

Human epidermoid carcinoma derived cell-line (A431) and HEK293-FT cell-line were maintained in DMEM media supplemented with 10% FBS, 5% CO_2 and grown at 37°C. High-titer retroviral particles for all the constructs were

generated as described in Supporting Information-Methodology. K8-deficient cells (previously generated K8 knockdown cells) were transduced with the respective viral particles and stable clones were maintained in 500 ng/ml of puromycin and 600 μg/ml of G418 sulphate containing complete DMEM.

2.3 Western blot and Immunofluorescence analysis

Western blotting and Immunofluorescence analysis were performed as described in previous report [8]. The list of antibodies used is given in Supporting Information Fig. 2.

2.4 Differential quantitative phosphoproteomics

Mammalian cell lysis, Protein digestion, TMT labeling, b-RPLC, Phosphopeptides enrichment using TiO_2 Chromatography followed by LC-MS/MS were carried out for all the clones as described in detail in Supporting Information-Methodology.

2.5 LC-MS/MS analysis

The enriched phosphopeptides were analyzed on Orbitrap Fusion™ Tribrid™ Mass Spectrometer (Thermo Electron, Bremen, Germany) interfaced with Easy-nLC 1000 liquid chromatography system (Thermo Scientific, Odense, Denmark). The peptide digests were reconstituted in 0.1% formic acid and loaded onto trap column (75 μm × 2 cm) packed in-house with Magic C18 AQ (Michrom Bioresources, Inc., Auburn, CA, USA). Peptides were resolved on an analytical column (75 μm x 20 cm) at a flow rate of 350 nL/min using a linear gradient of 10–35% solvent B (0.1% formic acid in 95% acetonitrile) over 80 min. Data-dependent acquisition with full scans in 350–1700 *m/z* range was carried out using an Orbitrap mass analyzer at a mass resolution of 120 000 at 400 *m/z*. Fifteen most intense precursor ions from a survey scan were selected for MS/MS fragments using HCD fragmentation with 32% normalized collision energy and detected at a mass resolution of 30 000 at 400 *m/z*. Dynamic exclusion was set for 30 s with a 10 ppm mass window. Internal calibration was carried out using lock mass option (*m/z* 445.1200025) from ambient air.

2.6 MS data analysis

The MS derived data were searched against "Human RefSeq protein database" (Version 65, containing 36 211 protein entries with common contaminants added) using "SEQUEST" and "Mascot" search algorithms through "Proteome Discoverer" platform (version 1.4.1.14, Thermo Scientific) as described in earlier report [9, 10]. The search parameters for both algorithms included: carbamidomethylation of cysteine and TMT 10-plex (C229.163) modification at N-terminus of peptide and lysine as fixed modifications; N-terminal acetylation, oxidation of methionine, phosphorylation at serine, threonine, and tyrosine (+79.966 Da) as variable modifications. MS/MS spectra were searched with a precursor mass tolerance of 10 ppm and fragment mass tolerance of 0.05 Da. Trypsin was specified as protease and a maximum of two missed cleavages were allowed. The data was searched against decoy database and the false discovery rate was set to 1% at the PSM level. The probability of phosphosite localization for each Serine/Threonine site on each protein was calculated by the phosphoRS 3.1 node in the Proteome Discoverer (version 1.4, Thermo Scientific). Phosphopeptides with >75% localization probability were considered. The phosphorylation sites that were identified with >75% localization probability but were assigned to different sites by the search algorithm were manually corrected based on the phosphoRS localization probability for a given residue. Peptides with ≥1.5-fold cut-off were considered as differentially phosphorylated phosphosites. The FDR between the technical replicates was calculated and shown in the Supporting Information Spreadsheet as FDR based on technical replicate ratio (Supporting Information-Datasheet-1). Briefly, FDR estimation was carried out by calculating the number of differentially phosphorylated peptides identified between the technical replicates with ≥1.5-fold cut-off out of the total identified phosphopeptides. The FDR thus obtained, was approximately in the range of 10–20% that is within acceptable limits for further analysis. The MS proteomics data have been deposited to the "ProteomeXchange Consortium" (http://proteomecentral.proteomexchange.org) via the PRIDE partner repository [11] with the dataset identifier PXD005301.

2.7 Bioinformatics analysis

The MS-derived data were searched against human RefSeq protein database (HPRD) (Version 65, containing 36 211 protein entries with common contaminants added) using "SEQUEST" and "Mascot" search algorithms through "Proteome Discoverer" platform (version 1.4.1.14, Thermo Scientific) as described in earlier report [9, 10]. Phosphopeptides with a fold change of ≥1.5 (up/downregulated) were considered for further bioinformatics analysis. "PhosphoELM" [12], "PhosphoSitePlus," and "Uniprot" database were referred to determine the known and novel phosphosites identified in our MS data. To determine the orthogonal or overlapping phosphoproteomic profile among all the datasets "Venny2.1 tool" was used. "STRING analysis tool" was used for protein–protein interaction analysis of different Phosphoproteins. All quantified phosphopeptides were analyzed using "Ingenuity Pathway Analysis" (IPA, Ingenuity systems, Qiagen, used in collaboration with IOB, Bangalore) (with a cut off ≥ 1.5 fold). The overrepresented "Canonical pathways", "Disease & biological functions" and "Networks", deregulated in K8 phosphorylation dependent manner, were generated based on

information contained in the Ingenuity Pathway Knowledge Base. The significance of the association between the dataset and the canonical pathway was measured in two ways: (1) A ratio of the number of molecules from the dataset that map to the pathway divided by the total number of molecules that map to the canonical pathway is displayed. (2) Fisher's exact test was used to calculate a *p*-value determining the probability that the association between the genes in the dataset and the "Canonical pathways" is explained by chance alone. Comparative analysis was carried out using IPA core analysis tool to identify common pathways showing reversal between phosphodead and phosphomimetic mutants expressing clones. The phosphopeptides involved in canonical or biological pathways showing reversal with a high log *p*-value (level of significance as per IPA manual) were considered for further analysis. "Enrichr tool" [13], was used to analyze "PPI hub proteins" of the set of phosphoproteins, showed significant reversal of phosphorylation levels. "PANTHER GO-functional annotation" [14] was used to determine "Protein class" within the datasets showing significant reversal in phosphorylation levels. Proteome Discoverer version 1.4.1.14 and Xcalibur version-3.0 were used to determine the qualitative and quantitative spectra for phosphopeptides respectively.

2.8 Cell migration, proliferation, and invasion assay

For phenotypic validation, Scratch Wound healing, Boyden chamber cell migration, MTT, and Matrigel cell Invasion assays were performed as described in earlier reports [15, 16]. Migrated or invaded cells were stained with DAPI. Results obtained from three independent experiments each in triplicate were represented as mean values using ±SEM obtained from software Graphpad prism 5.

3 Results

3.1 Generation of stable clones expressing shRNA-resistant K8 WT and phosphomutants

To examine the effect of K8 site-specific phosphorylation in neoplastic progression of skin SCC, stable clones expressing shRNA resistant 3XFlag-(N-terminus)-GFP-(C-terminus) tagged K8-WT, phosphodead mutants (K8-S73A & K8-S431A), and phosphomimetic mutants (K8-S73D & K8-S431D) were generated (Supporting Information Fig. 1A, B) in previously established shRNA-based K8-deficient stable clones of A431 cells. Western blot analysis of all the clones showed significant upregulation of 3XFlag-K8-GFP WT (wild type) and phosphomutants when probed with K8 antibody (Fig. 1A). To verify the K8 phosphorylation status, lysates from all the clones were probed with K8 Serine^{73} or K8 Serine^{431} phosphorylation-specific antibodies. The clones expressing phosphomutants (K8-S73A, K8-S73D, K8-S431A, and K8-S431D) showed the loss of K8 phosphorylation on respective sites (Fig. 1B). To reevaluate the phosphorylation status of transexpressed 3XFlag-K8-GFP (WT and phosphomutants), coimmunoprecipitation from whole cell lysates of respective clones with anti-flag antibody, followed by in-gel digestion and nano-LC-MS/MS analysis were performed. The mass spectrometric data analysis further supported Western blot data, i.e. the loss of phosphorylation at respective sites in all the phosphomutant clones (Supporting Information Fig. 1C). Next, immunofluorescence analysis showed appropriate filament organization of trans-expressed K8-GFP in all the five clones (Fig. 1C).

3.2 Phosphoproteomic profiling and quantification

In order to understand the alterations in global phosphoproteome profile in response to K8 phosphorylation modulation in skin-SCC derived cell-line, we performed a TMT-based quantitative phosphoproteomic analysis for all the clones (Fig. 1D). A total of 5839 unique phosphopeptides corresponding to 2145 proteins were detected when searched against human protein database (Supporting Information-Datasheet-1). A total of 4915 (84.17%), 802 (13.73%), and 122 (2.08%) singly, doubly, and phosphopeptides phosphorylated at more than three sites were detected, respectively. Further, 4644 (86.4%) phospho-Serine, 655 (12.2%) phospho-Threonine, and 76 (1.4%) phospho-Tyrosine containing phosphopeptides were identified with a high "phosphoRS Site Probabilities" (Fig. 1E). The entire phosphoproteomics data were plotted as line graphs representing significant phosphorylation alteration on phosphoproteins detected in all the four datasets (K8-S73A, K8-S73D, K8-S431A, K8-S431D) when compared with K8-WT (Fig. 1F). Among the total 5375 phosphosites, (346/337), (436/687), (169/208), (260/271) unique phosphosites were found to be up/downregulated with a threshold ≥1.5-fold in case of K8-S73A, K8-S73D, K8-S431A, K8-S431D datasets, respectively (Fig. 1G). In addition, Phospho-ELM database was used to identify total known and novel phosphosites, differentially phosphorylated among all the datasets (Fig. 1G). These results suggest a significant alteration in phosphoproteomic landscape, emerged upon K8 phosphorylation modulation in a site-specific manner.

3.3 Determining the orthogonal or overlapping phosphoproteomic profile among all the datasets

To visualize the orthogonal or overlapping phosphopeptides differentially phosphorylated with ≥1.5-fold cut-off, among two different phosphomutant datasets, we performed Venn diagram analysis using Venny 2.1 software. Based on this criteria phosphopeptides showing upregulation of phosphorylation in case of phosphodead mutants and downregulation of phosphorylation in case of phosphomimetic mutants for both the sites were subjected to Venn diagram analysis

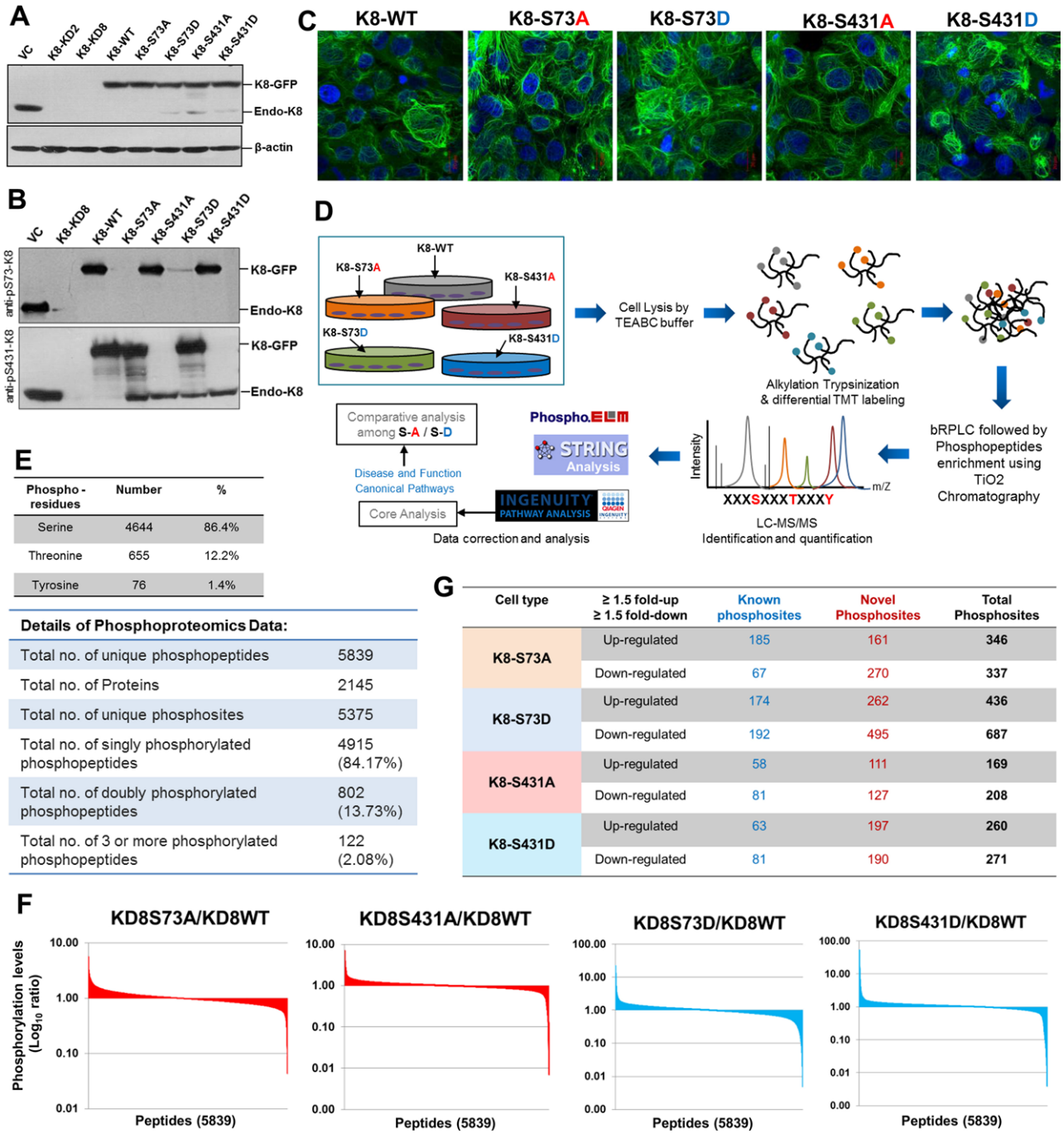

E

Phospho-residues	Number	%
Serine	4644	86.4%
Threonine	655	12.2%
Tyrosine	76	1.4%

Details of Phosphoproteomics Data:	
Total no. of unique phosphopeptides	5839
Total no. of Proteins	2145
Total no. of unique phosphosites	5375
Total no. of singly phosphorylated phosphopeptides	4915 (84.17%)
Total no. of doubly phosphorylated phosphopeptides	802 (13.73%)
Total no. of 3 or more phosphorylated phosphopeptides	122 (2.08%)

G

Cell type	≥ 1.5 fold-up ≥ 1.5 fold-down	Known phosphosites	Novel Phosphosites	Total Phosphosites
K8-S73A	Up-regulated	185	161	346
	Down-regulated	67	270	337
K8-S73D	Up-regulated	174	262	436
	Down-regulated	192	495	687
K8-S431A	Up-regulated	58	111	169
	Down-regulated	81	127	208
K8-S431D	Up-regulated	63	197	260
	Down-regulated	81	190	271

Figure 1. Verification of stable clones trans-expressing 3XFlag-K8-GFP (WT/phosphomutants) and summary of TMT-based global phosphoproteome profiling: Western blot analysis of all the five clones expressing 3XFlag-K8-GFP wild type and phosphomutants using K8 antibody (A), and phosphospecific antibodies (K8 Serine^{73} and K8 Serine^{431}) (B). Here "VC" depicts vector control A431 cells; "K8-KD2" & "K8-KD8" depict two different K8 knockdown clones in A431 cells. Higher molecular weight bands (82KDa) represent trans-expressed 3XFlag-K8-GFP (WT/phosphodead/phosphomimetic) in K8 knockdown background. (C) Immunofluorescence imaging of 3XFlag-K8-GFP (WT/phosphodead/phosphomimetic) using LSM780 Zeiss microscope at 488 nm wavelength to observe K8 filament organization. Green color represents K8-GFP and nucleus is stained with DAPI. (D) Schematic representation of the methodology for TMT-based quantitative phosphoproteomics. (E) The table depicts a total summary of phosphopeptides, phosphoproteins, and phosphosites detected after LC-MS/MS analysis together with summary of total number of phosphoserine, phosphothreonine, and phosphotyrosine detected. (F) Line graph showing the total (5839) phosphopeptide distribution in K8-S73A, K8-S431A, K8-S73D, and K8-S431D datasets. (G) Table represents differential phosphorylation levels at known and novel phosphorylation sites on proteins in all four different clones with a cut-off of ≥1.5-fold.

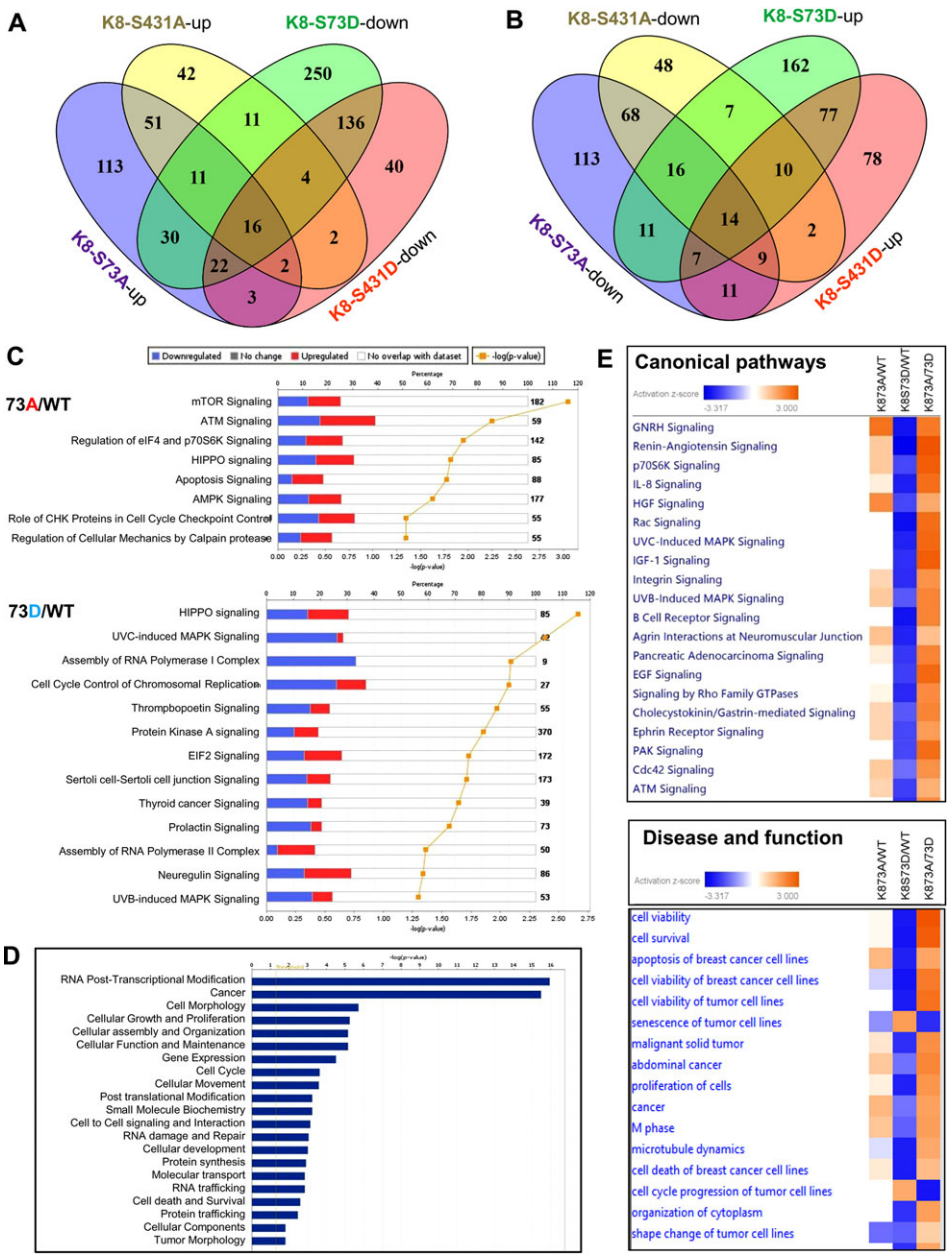

Figure 2. Analysis of phosphoproteomics data obtained from TMT-based global phosphoproteome profiling: (A and B) Phosphopeptides, with a cut-off of ≥1.5-fold in their phosphorylation levels from all the four data sets were subjected to the Software Venny 2.1. The diagrams represent the number of orthogonal or overlapping phosphopeptides among the respective datasets. (C) Representative Bar chart for IPA "Canonical Pathways" showed significantly altered signaling pathways with high –log *p*-value for both K8-S73A and K8-S73D datasets. The numbers against every bar correspond to the number of filtered proteins involved in the mentioned pathway. (D) The representative bar chart depicting distribution of the differentially regulated phosphoproteins (with high –log *p*-value) according to their Biological functions. (E) Heat maps generated through IPA for "Comparison Analysis" of K8-S73 datasets (K8-S73A/WT, K8-S73D/WT, K8-S73A/S73D) including "Canonical pathways" and "Disease and biological functions" demonstrating the significantly altered molecular signaling pathways as well as biological functions.

(Fig. 2A, B and Supporting Information-Datasheet-2). There were 79 and 24 common phosphopeptide upregulated in phosphodead mutants (K8-S73A and K8-S431A) and downregulated in corresponding phosphomimetic mutants (K8-S73D and K8-S431D), respectively (Fig. 2A). Besides, there were 80 common phosphopeptides upregulated within the phosphodead mutant (K8-S73A and K8-S431A) and 178 common phosphopeptides downregulated within the phosphomimetic mutants (K8-S73D and K8-S431D) (Fig. 2A). Similarly, phosphopeptides showing downregulation of phosphorylation in case of phosphodead mutants and upregulation of phosphorylation in case of phosphomimetic mutants for both the sites were subjected to Venn diagram analysis (Fig. 2B). There were 48 and 35 common phosphopeptides upregulated in phosphomimetic mutants (K8-S73D and K8-S431D) and downregulated in corresponding phosphodead mutants (K8-S73A and K8-S431A), respectively. Concomitantly, there were 97 common phosphopeptides downregulated within the phosphodead mutant (K8-S73A and K8-S431A) and 108 common phosphopeptides upregulated within the phosphomimetic mutants (K8-S73D and K8-S431D) (Fig. 2B). In addition, the scatter plot for differentially phosphorylated phosphopeptides with ≥1.5-fold cut-off, further suggested an inverse correlation between the phosphodead and phosphomimetic mutant dataset (K8-S73A versus K8-S73D and K8-S431A versus S431D) independently (Supporting information Fig. 3). These results showed a positive relationship between many common effectors with differential phos-

phorylation within and among phosphodead and phosphomimetic mutants substantiating their involvement in a site-specific K8 phosphorylation mediated biological functions.

3.4 Functional correlation of phosphoproteins detected across different datasets

In order to understand the functional relevance of K8 phosphorylation ablation mediated global phosphoproteomic changes, Ingenuity Pathway analysis (IPA) was performed for independent datasets of phosphomutants in comparison to K8-WT (K8-S73A/WT, K8-S73D/WT, K8- S431A/WT, and K8-S431D/WT). This was followed by "Comparison Analysis" within the datasets of K8-S73 group (K8-S73A/WT, K8-S73D/WT, K8-S73A/73D) and K8-S431 group (K8-S431A/WT, K8-S431D/WT, K8-S431A/431D). Comparison analysis enabled us to identify trends or similarities and differences between mutants within the group for both the phosphosites by visualization across multiple analyses. Extended heat maps and bar charts for the "Canonical pathways," "Disease and Biological functions" together with "Networks" were generated for significantly altered signaling in case of independent and comparison analysis.

3.4.1 Functional signaling networks modulated by K8 Serine73 phosphorylation

Upon K8 Serine^{73} phosphorylation modulation, the independent IPA-"Canonical pathways" analysis showed significantly altered differential phosphorylation of proteins involved in the signaling pathways, for instance; mTOR, ATM, regulation of eIF4, HIPPO, and apoptosis (Fig. 2C, Supporting Information Fig. 4A and Supporting Information-Enlarged Fig. 1). Furthermore, the independent "Disease and biological functions" analysis of the same showed most of the differentially phosphorylated molecules to be involved in RNA Post-Transcriptional Modification, Cancer, Cell Morphology, Cellular Growth, and Proliferation, Gene expression, and Cell cycle (Fig. 2D, Supporting Information Fig. 4B and Supporting Information-Enlarged Fig. 2). Similarly, in K8-S73D dataset, the differential regulation of phosphoproteins related to "Canonical pathways" including Hippo, UVC-induced MAPK, Cell cycle control, and PKA signaling was observed (Fig. 2C). Interestingly, IPA-Comparison Analysis showed an inverse correlation between K8-S73A and K8-S73D datasets for the altered "Canonical pathways" strengthening the role of K8 Serine^{73} phosphorylation as a potent modulator of these pathways. Some of these pathways including GNRH, Renin angiotensin, P70 S6K, Integrin, Rho GTPase, ATM were significantly modulated (Fig. 2E, Supporting Information Fig. 6). In addition, gene heat maps were generated for some major cancer associated pathways including Integrin, cdc42, PAK, ERK/MAPK, and Actin cytoskeleton organization signaling, to find out the specific phosphoproteins involved (Supporting Information Fig. 5). Furthermore, IPA-Comparison Analysis for "Disease and biological functions" revealed pathways such as apoptosis & cell survival, cell proliferation, microtubule dynamics, and cell migration to be significantly modulated upon deregulation of K8 phosphorylation at Serine^{73} residue and showing inverse correlation between phosphodead and phosphomimetic mutants (Fig. 2E, Supporting Information Figs. 7 and 8). Altogether, these analyses revealed the involvement of many crucial phosphoproteins including AKT1S1, CTTN, EIF4EBP1, LMNA, CDK1, ZYX, and CAV1 as potent modulators of K8 Serine^{73} phosphorylation-mediated oncogenesis.

3.4.2 Functional signaling networks modulated by K8 Serine^{431} phosphorylation

Upon K8 Serine^{431} phosphorylation modulation, the independent IPA-"Canonical pathways" analysis determined differential phosphorylation of phosphoproteins involved in pathways including Estrogen receptor, Hippo, Sertoli cell junction, JNK/SAPK, and CDC42 signaling (Fig. 3A, Supporting Information Fig. 9A and Supporting Information-Enlarged Fig. 3). The independent "Disease and biological functions" analysis showed differential regulation of phosphoproteins associated with cancer, cell growth, gene expression and cell cycle (Fig 3B, Supporting Information Fig. 9B and Supporting Information-Enlarged Fig. 4). Similarly, in K8-S431D dataset, signaling pathways including Sertoli cell junction, Estrogen receptor, Telomerase, JNK/SAPK, CDC42, and Hippo signaling were significantly altered. Furthermore, IPA-Comparison Analysis determined "Canonical pathways" such as; integrin, HIPPO, AMPK, CDC42, Rac, STAT3, and Actin signaling to be significantly altered (Fig. 3C, Supporting Information Figs. 9 and 11). In addition, the "Disease and biological functions" analysis was carried out for the same dataset. Heat maps showed most of the molecules to be involved in cell survival & viability, actin dynamics, microtubule dynamics, cell proliferation, invasion, and migration (Fig 3C, Supporting Information Fig. 4). Altogether, these analyses revealed the involvement of many crucial phosphoproteins including BUB1B, CARHSP1, CTTN, SCRIB, CDK11B, and CDK12 as potent modulators of K8 Serine^{431} phosphorylation mediated oncogenesis. The elaborate gene heat maps, bar charts, ray diagrams for all the important pathways and biological functions are given in Supporting Information Figs. 12–14.

3.5 Differential phosphorylation pattern of phosphoproteins involved in migration, proliferation and apoptosis in response to K8 phosphorylation

Since IPA data suggested significant alterations in many cancer associated signaling mechanisms upon modulation of

Figure 3. Differential phosphoproteomic analysis using IPA for K8-S431A/WT and K8- S431D/WT datasets: (A) Representative Bar chart for IPA "Canonical Pathways" shows significantly altered signaling pathways with high –log *p*-value for both K8-S431A and K8- S431D datasets. The numbers against every bar correspond to the number of filtered proteins involved in the mentioned pathway. (B) Representative bar charts determined by IPA showing Biological function associated with the phosphoproteins for K8-S431A/WT individual dataset. (C) Heat maps generated through IPA for "Comparison Analysis" of K8-S431 dataset (K8- S431A/WT, K8-S431D/WT, K8-S431A/S431D) including "Canonical pathways" and "Disease and biological functions" demonstrating major molecular signaling pathways as well as biological functions affected.

K8 phosphorylation at Serine[73] and Serine[431] residues, we next focused on the site-specific phosphorylation and related functions of the phosphoproteins involved in such pathways. GO-functional annotation was carried out for the phosphoproteins from all four datasets and was screened according to their involvement in cell adhesion, migration, proliferation, and apoptosis. Further, the relative phosphorylation levels of selected phosphoproteins were subjected to MSOffice-excel for Heat-map generation. Heat-map for cell migration associated proteins such as CAP1, CTTN, AKT1S1, CDK1, EIF4EBP1, CARHSP1, and LIMA1 showed significantly increased phosphorylation at biologically relevant phosphosites in case of K8-S73A dataset, whereas K8-S73D dataset showed reversal of the same (Fig. 4A). Besides, in case of K8-S431 phosphomutant datasets, most of the phosphoproteins were found to be differentially phosphorylated at phosphosites that are novel or less characterized. Three major phosphoproteins CTTN, BUB1B, and CARHSP1 showed differential phosphorylation at biologically relevant phosphosites with reversal of the same in case of K8S431D dataset. Heat map for proteins involved in cell proliferation including, EIF4B, CDK1, EIF4EBP1, and AKT1S1 showed significantly increased phosphorylation at biologically relevant phosphosites in case of K8-S73A dataset with an inverse correlation in K8-S73D dataset (Fig. 4B). Additionally, LAMTOR1, MYC, STK10, BAP1, BRAF, ZYX, LARP1, CDK11B showed similar differential phosphorylation pattern on unidentified/less-characterized phosphosites in case of K8-S73A and K8-S431A mutants together with reversal of the same in K8-S73D and K8-S431D datasets as shown in Fig. 4B. Most of the phosphoproteins involved in apoptotic pathways like CASP1, BCL2L12, EEF1D and HNRNPK were found to be differentially phosphorylated at the novel or less-characterized phosphorylation sites among the phosphodead and phosphomimetic datasets for both the mutants (Supporting Information Fig. 15). Altogether, this analysis substantiates many known and novel phosphorylation sites belonging to phosphoproteins involved in cancer associated phenotypes to be modulated in response to K8 phosphorylation ablation in site-specific manner.

3.6 Interaction analysis of different phosphoproteins detected across different phosphomutants

Since a large variety of phosphoproteins showed such significant alteration in phosphorylation status in response to a single twitch, i.e. K8 site-specific phosphorylation, we wanted to determine the protein–protein Interaction (PPI) among themselves. Hence, to elucidate the phosphoprotein interaction network in all the datasets, we performed STRING analysis. PPI network analysis confirmed significant number of interactions between phosphoproteins with high –log *p*-values (Supporting Information Figs. 16–19). As a proof of principle, we selected cell migration-associated signaling network, one of the significantly altered biological function as shown in our IPA analysis together with GO-Functional annotation and plotted separately (Fig. 4C). The PPI showed strong interactions between CAP1, CDK1, ZYX, CTTN, TJP2, DSP, PKP3, MAPK1, JUN, MYC, PNN, and KRT8. The pictorial representation in Fig. 4D highlights the predicted interactions within phosphoproteins involved in cell migration. The differentially regulated phosphosites were annotated on the respective phosphoproteins. However, further validation of the phosphorylation status together with the interactions of these proteins is essential to establish their chronology in the pathway. In order to determine the PPI hub proteins upstream to the significantly altered phosphoproteins with inverse correlation in both K8-S73 and K8-S431 datasets, we used Enrichr analysis web server. [The excel file of phosphoprotein lists with their upstream hub proteins determined by Enrichr-PPI hub protein analysis was provided in Supporting Information-Datasheet-3]. The Clustergrammer results showed majority of phosphoproteins from our dataset to be clustered under enriched term as protein kinases; CDK2, GSK3β, MAPK14, CDK1, and MAPK1 (Fig. 5A). This facilitated us to narrow down our focus to determine which of the kinases and their corresponding downstream effectors befall together in the dataset. For instance, CDK1 and its target proteins SRRM2, EIF4EBP1, ZYX, CTTN; which were then considered for further analysis based on the biological relevance of their corresponding phosphosites. In addition, we subjected the phosphoproteins that showed significant reversal in differential phosphorylation status between phosphodead and phosphomimetic in case of both the datasets to "PANTHER classification system." The distribution of the phosphoproteins according to the protein class showed seven kinases (CDK1, CDK10, MAPK1, AAK1, PGK1, CDK12, and CDK11B) and three kinases (CDK12, CDK11B, and MAP3K11) to be differentially phosphorylated in K8-S73 and K8-S431 datasets, respectively (Supporting Information Fig. 20). This data suggest that upon K8 site-specific phosphorylation, modulation of these kinases may regulate the phosphorylation of many phosphoproteins and thereby govern cancer-associated signaling pathways. Based upon the intricate analysis of phosphoproteomics data we then reconstructed comprehensive model pathways using IPA tool (the corresponding phosphorylation sites were assigned with the phosphoproteins) that were predominantly altered in response to site-specific K8 phosphorylation ablation. These signaling cascade highlighted many phosphoproteins associated with cell proliferation, actin organization, cell survival, and gene expression regulation being deregulated by K8 phosphorylation modulation (Fig. 5B and Supporting Information Fig. 21).

3.7 Validation of identified proteins by Western blotting

We then performed Western blot analysis to validate differentially phosphorylated phosphoproteins within K8-S73 and K8-S431 datasets using commercially available phospho-specific antibodies. According to "PANTHER

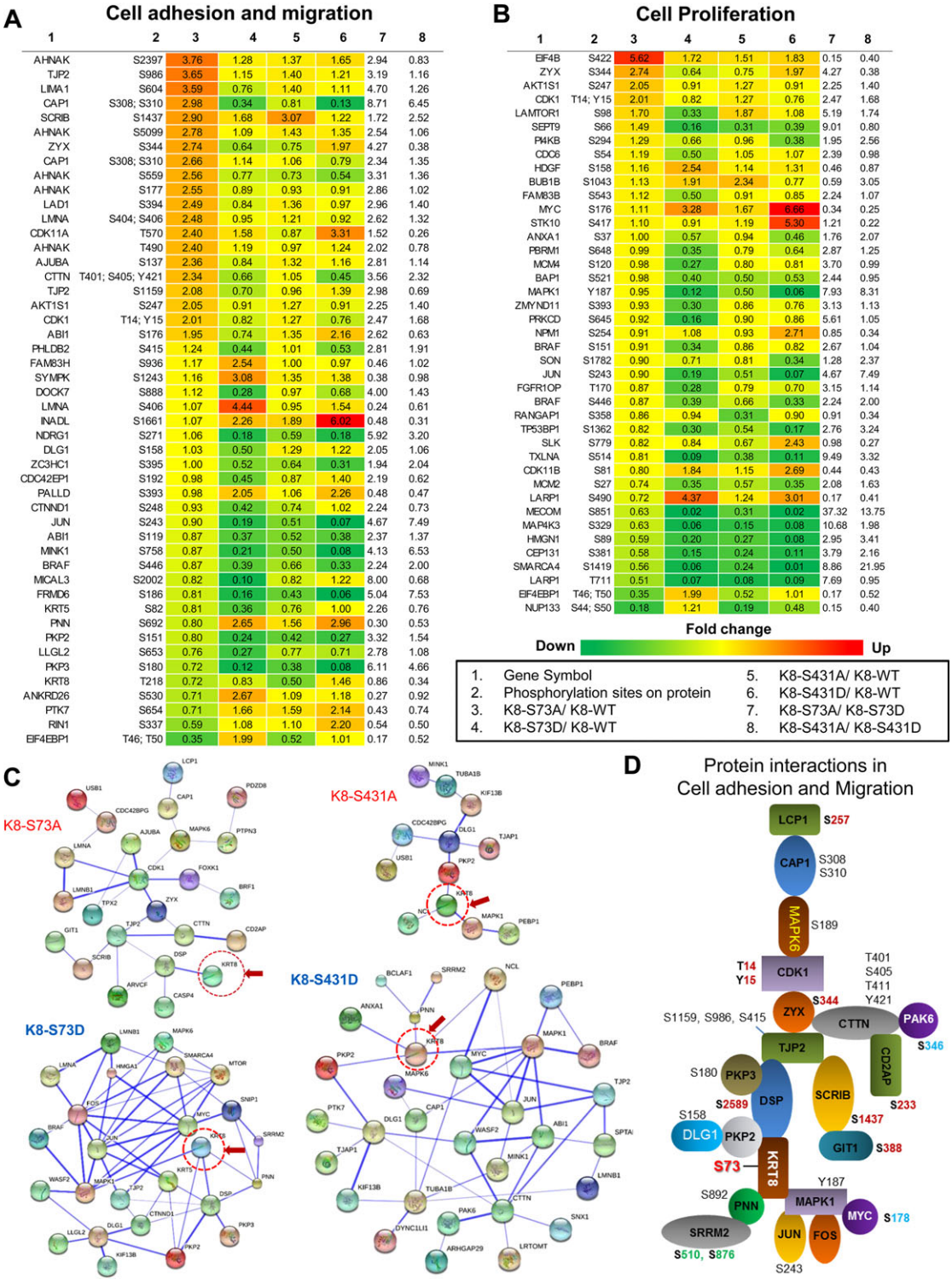

1	2	3	4	5	6	7	8
AHNAK	S2397	3.76	1.28	1.37	1.65	2.94	0.83
TJP2	S986	3.65	1.15	1.40	1.21	3.19	1.16
LIMA1	S604	3.59	0.76	1.40	1.11	4.70	1.26
CAP1	S308; S310	2.98	0.34	0.81	0.13	8.71	6.45
SCRIB	S1437	2.90	1.68	3.07	1.22	1.72	2.52
AHNAK	S5099	2.78	1.09	1.43	1.35	2.54	1.06
ZYX	S344	2.74	0.64	0.75	1.97	4.27	0.38
CAP1	S308; S310	2.66	1.14	1.06	0.79	2.34	1.35
AHNAK	S559	2.56	0.77	0.73	0.54	3.31	1.36
AHNAK	S177	2.55	0.89	0.93	0.91	2.86	1.02
LAD1	S394	2.49	0.84	1.36	0.97	2.96	1.40
LMNA	S404; S406	2.48	0.95	1.21	0.92	2.62	1.32
CDK11A	T570	2.40	1.58	0.87	3.31	1.52	0.26
AHNAK	T490	2.40	1.19	0.97	1.24	2.02	0.78
AJUBA	S137	2.36	0.84	1.32	1.16	2.81	1.14
CTTN	T401; S405; Y421	2.34	0.66	1.05	0.45	3.56	2.32
TJP2	S1159	2.08	0.70	0.96	1.39	2.98	0.69
AKT1S1	S247	2.05	0.91	1.27	0.91	2.25	1.40
CDK1	T14; Y15	2.01	0.82	1.27	0.76	2.47	1.68
ABI1	S176	1.95	0.74	1.35	2.16	2.62	0.63
PHLDB2	S415	1.24	0.44	1.01	0.53	2.81	1.91
FAM83H	S936	1.17	2.54	1.00	0.97	0.46	1.02
SYMPK	S1243	1.16	3.08	1.35	1.38	0.38	0.98
DOCK7	S888	1.12	0.28	0.97	0.68	4.00	1.43
LMNA	S406	1.07	4.44	0.95	1.54	0.24	0.61
INADL	S1661	1.07	2.26	1.89	6.02	0.48	0.31
NDRG1	S271	1.06	0.18	0.59	0.18	5.92	3.20
DLG1	S158	1.03	0.50	1.29	1.22	2.05	1.06
ZC3HC1	S395	1.00	0.52	0.64	0.31	1.94	2.04
CDC42EP1	S192	0.98	0.45	0.87	1.40	2.19	0.62
PALLD	S393	0.98	2.05	1.06	2.26	0.48	0.47
CTNND1	S248	0.93	0.42	0.74	1.02	2.24	0.73
JUN	S243	0.90	0.19	0.51	0.07	4.67	7.49
ABI1	S119	0.87	0.37	0.52	0.38	2.37	1.37
MINK1	S758	0.87	0.21	0.50	0.08	4.13	6.53
BRAF	S446	0.87	0.39	0.66	0.33	2.24	2.00
MICAL3	S2002	0.82	0.10	0.82	1.22	8.00	0.68
FRMD6	S186	0.81	0.16	0.43	0.06	5.04	7.53
KRT5	S82	0.81	0.36	0.76	1.00	2.26	0.76
PNN	S692	0.80	2.65	1.56	2.96	0.30	0.53
PKP2	S151	0.80	0.24	0.42	0.27	3.32	1.54
LLGL2	S653	0.76	0.27	0.77	0.71	2.78	1.08
PKP3	S180	0.72	0.12	0.38	0.08	6.11	4.66
KRT8	T218	0.72	0.83	0.50	1.46	0.86	0.34
ANKRD26	S530	0.71	2.67	1.09	1.18	0.27	0.92
PTK7	S654	0.71	1.66	1.59	2.14	0.43	0.74
RIN1	S337	0.59	1.08	1.10	2.20	0.54	0.50
EIF4EBP1	T46; T50	0.35	1.99	0.52	1.01	0.17	0.52

1	2	3	4	5	6	7	8
EIF4B	S422	5.62	1.72	1.51	1.83	0.15	0.40
ZYX	S344	2.74	0.64	0.75	1.97	4.27	0.38
AKT1S1	S247	2.05	0.91	1.27	0.91	2.25	1.40
CDK1	T14; Y15	2.01	0.82	1.27	0.76	2.47	1.68
LAMTOR1	S98	1.70	0.33	1.87	1.08	5.19	1.74
SEPT9	S66	1.49	0.16	0.31	0.39	9.01	0.80
PI4KB	S294	1.29	0.66	0.96	0.38	1.95	2.56
CDC6	S54	1.19	0.50	1.05	1.07	2.39	0.98
HDGF	S158	1.16	2.54	1.14	1.31	0.46	0.87
BUB1B	S1043	1.13	1.91	2.34	0.77	0.59	3.05
FAM83B	S543	1.12	0.50	0.91	0.85	2.24	1.07
MYC	S176	1.11	3.28	1.67	6.66	0.34	0.25
STK10	S417	1.10	0.91	1.19	5.30	1.21	0.22
ANXA1	S37	1.00	0.57	0.94	0.46	1.76	2.07
PBRM1	S648	0.99	0.35	0.79	0.64	2.87	1.25
MCM4	S120	0.98	0.27	0.80	0.81	3.70	0.99
BAP1	S521	0.98	0.40	0.50	0.53	2.44	0.95
MAPK1	Y187	0.95	0.12	0.50	0.06	7.93	8.31
ZMYND11	S393	0.93	0.30	0.86	0.76	3.13	1.13
PRKCD	S645	0.92	0.16	0.90	0.86	5.61	1.05
NPM1	S254	0.91	1.08	0.93	2.71	0.85	0.34
BRAF	S151	0.91	0.34	0.86	0.82	2.67	1.04
SON	S1782	0.90	0.71	0.81	0.34	1.28	2.37
JUN	S243	0.90	0.19	0.51	0.07	4.67	7.49
FGFR1OP	T170	0.87	0.28	0.79	0.70	3.15	1.14
BRAF	S446	0.87	0.39	0.66	0.33	2.24	2.00
RANGAP1	S358	0.86	0.94	0.31	0.90	0.91	0.34
TP53BP1	S1362	0.82	0.30	0.54	0.17	2.76	3.24
SLK	S779	0.82	0.84	0.67	2.43	0.98	0.27
TXLNA	S514	0.81	0.09	0.38	0.11	9.49	3.32
CDK11B	S81	0.80	1.84	1.15	2.69	0.44	0.43
MCM2	S27	0.74	0.35	0.57	0.35	2.08	1.63
LARP1	S490	0.72	4.37	1.24	3.01	0.17	0.41
MECOM	S851	0.63	0.02	0.31	0.02	37.32	13.75
MAP4K3	S329	0.63	0.06	0.15	0.08	10.68	1.98
HMGN1	S89	0.59	0.20	0.27	0.08	2.95	3.41
CEP131	S381	0.58	0.15	0.24	0.11	3.79	2.16
SMARCA4	S1419	0.56	0.06	0.24	0.01	8.86	21.95
LARP1	T711	0.51	0.07	0.08	0.09	7.69	0.95
EIF4EBP1	T46; T50	0.35	1.99	0.52	1.01	0.17	0.52
NUP133	S44; S50	0.18	1.21	0.19	0.48	0.15	0.40

Figure 4. Heat-map and PPI analysis of phosphoproteins: (A, B) Phosphorylation oriented functional annotation Heat-maps for Cell adhesion-migration and cell proliferation depicting the differential phosphorylation sites on the phosphoproteins; mentioned in column-1 and 2. The color code indicates the fold change in relative levels of phosphorylation at specific sites. (C) STRING analysis for biological interactions within phosphoproteins of all four datasets, involved in Cell adhesion, migration function. The blue line represents the confidence level and thickness indicates the strength of the interaction among the proteins. The red-dotted circle indicates Keratin8 position in the networks. (D) Schematic model representing possible interactions within the phosphoproteins derived from STRING analysis for cell migration and adhesion function.

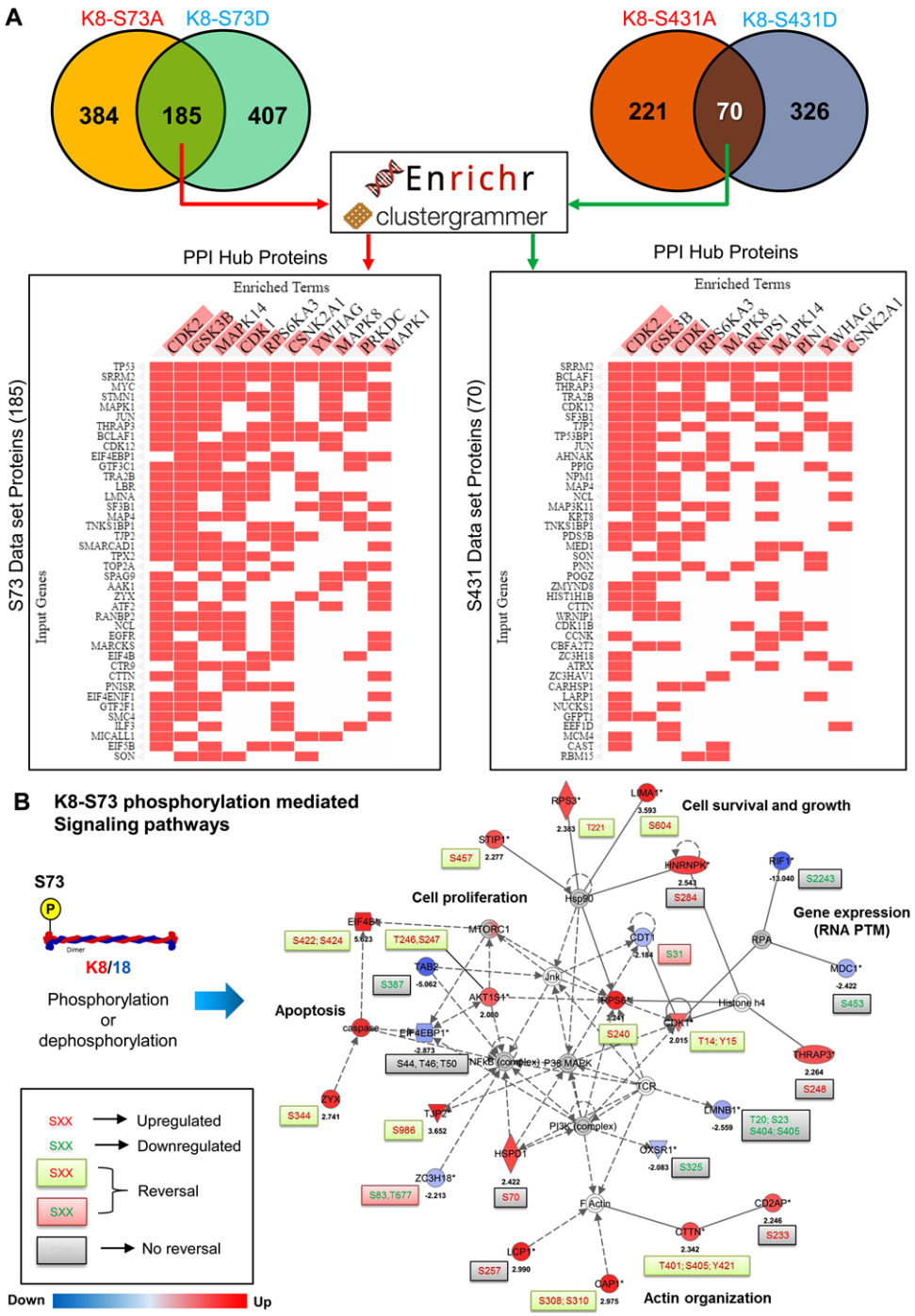

Figure 5. Extended clustergrammer and network analysis for differentially regulated phosphoproteins: (A) "Enrichr-PPI hub proteins" analysis of common phosphoproteins (differentially regulated with inverse correlation) within both the phosphodead and phosphomimetic mutant pair. The clustergrammer chart depicts the PPI hub proteins clustered under kinases as Enriched Terms, with highest *p*-value at left-hand side, upstream to the corresponding phosphoproteins. (B) K8 Serine[73] phosphorylation mediated signaling pathways mapped by IPA considering the differentially phosphorylated phosphopeptides (with cut-off ≥1.5-fold) in response to site-specific K8 phosphorylation ablation. The representative network depicts intricate signaling cascade within the phosphoproteins and some hub proteins involved in cell proliferation, cell survival, and growth, actin organization, apoptosis, and gene expression. The phosphorylation sites detected are assigned with the phosphoproteins.

analysis" the distribution of the phosphoproteins based on protein class showed seven kinases (CDK1, CDK10, MAPK1, AAK1, PGK1, CDK12, and CDK11B) in K8-S73 dataset and three kinases (CDK12, CDK11B, and MAP3K11) in K8-S431 dataset to be differentially phosphorylated. For authentication, qualitative and quantitative MS/MS spectra of specific phosphopeptides for some representative Kinases (CDK1, MAPK1, CDK11B, and CDK12) were generated using Proteome Discoverer and Xcalibur software (Fig. 6A, Supporting Information Figs. 22 and 26). For further validation, we selected kinases depending on availability of the commercial antibodies. Western blot analysis using phospho-specific antibodies for T14/Y15 of CDK1 showed increased phosphorylation at this phosphosites in K8-S73A (phosphodead) mutant expressing clones in comparison to K8-WT and K8-S73D (phosphomimetic) mutants (Fig. 6B). Moreover, in case of MAPK1, phosphorylation at Y187 was significantly decreased in K8-S73D (phospho-

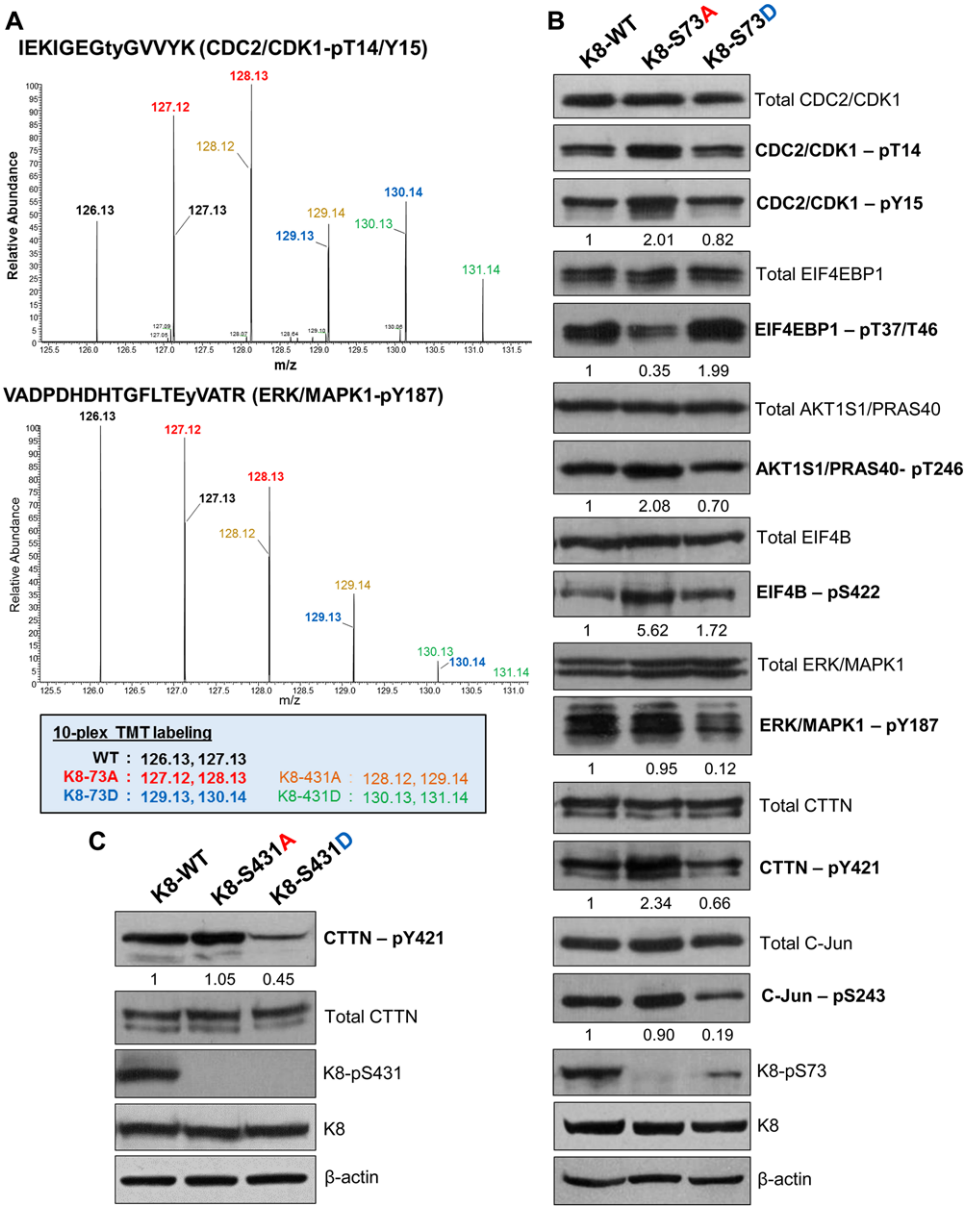

Figure 6. Validation of MS results for selected phosphoproteins. (A) For the verification of MS/MS data, representative quantitative spectra for selected kinases were generated using Xcalibur software tool version-3.0. The representative spectra for kinases, CDK1 and MAPK1 are shown in the figures. (B, C) Validation of MS results by Western blot analysis for selected proteins. Western blot analysis was carried out (n = 3, ± SD) for some of the selected phosphoproteins with high statistical and biological significance. Western blots using phospho-specific antibodies for CDK1 (pT14/Y15), MAPK1 (pY187), EIF4B (pS422), AKT1S1 (pT221), EIF4EBP1 (pT37/T46), CTNN1 (pT401/S405), c-JUN (pS243) showed expected differential expression verifying the MS/MS Data in S73A/D and S431A/D datasets. Quantitative values for the specific phosphopeptides from the MS/MS data are indicated below the respective Western blots (blots obtained using phosphorylation-specific antibodies). Respective blots for total proteins were used as control together with beta actin. A representative blot for K8 overexpression and its phosphorylation status (for both the sites K8 Serine^{73} and Serine^{431}) is also shown in the Fig. B and C.

mimetic) mutant compared to K8-WT and K8-S73A (phosphodead) mutant in concordance to our MS/MS data. Next, we validated the phosphorylation levels of proteins associated with tumorigenic potential as per computational analysis including EIF4EBP1$^{T37/T46}$, AKTS1^{T246}, EIF4B^{S422}, CTTN^{Y421}, and cJUN^{S243} using Western blot analysis (Fig. 6B, C) which correlated well with the MS/MS data. In addition, quantitative and qualitative spectra were generated for further authentication (Supporting Information Figs. 23–25). In case of K8S431 dataset, CTTN was validated using Western blotting for phosphorylation at Y421 (Fig. 6C). Since other relevant proteins were differentially phosphorylated at novel/less characterized phosphosites, their respective antibodies were not available commercially. Therefore, differential phosphorylation of some representative proteins was authenticated using only qualitative and quantitative spectra (Supporting Information Fig. 27). Altogether, our Western blot analysis of the biologically relevant phosphoproteins confirmed the mass-spectrometric data thereby substantiating their role in Keratin 8 phosphorylation mediated oncogenic pathways.

3.8 Site-specific phosphorylation on K8 regulates cellular migration, invasion, and proliferation in A431 cells

IPA analysis, heat map profiling together with Western blot validation for all the four datasets indicated the significant alterations in cell migration, invasion, and proliferation associated signaling pathways. This led us to validate our

observations by phenotypic assays. Hence, we performed scratch wound healing and Boyden chamber migration assay together with matrigel invasion and MTT cell proliferation assay in all the clones. In scratch wound healing assay the clones expressing K8 phosphodead mutants (K8-S73A and K8-S431A) showed a significant decrease (~30–40%) in cell migration rate compared to K8-WT expressing clone (Fig. 5A). Both the clones expressing K8 phosphomimetic mutants (K8-S73D and K8-S431D) showed a migration rate of ~80–90%. Similarly, for matrigel invasion assay, the K8 phosphodead mutant cells showed ~50–60% decrease in invasive potential compared to K8-WT expressing cells whereas, both the K8 phosphomimetic mutant expressing cells showed an invasive potential to be ~90–100% (Fig. 5B). Boyden chamber migration assay correlated well with the scratch wound healing assay (Fig. 5C). In addition, K8 phosphodead mutant expressing clones showed ~30–40% decrease in the cell proliferation compared to K8-WT expressing clones whereas, cell proliferation potential for both the K8 phosphomimetic mutant clones was found to be ~80–100% (Fig. 5D). Altogether, the data clearly indicates that the K8 phosphomimetic mutant cells exhibit a reversal of migratory, invasive, and proliferative potential compared to phosphodead mutant cells in concordance to our phosphoproteomics data. Overall these results suggest that K8 phosphorylation at Serine^{73} and Serine^{431} significantly modulated the migratory, invasive, and proliferative ability of A431 cells and strengthen our findings of K8 phosphorylation to be a modulator of tumorigenic potential of A431 cells.

4 Discussion

Phosphorylation is established as a potent modulator of conventional functions of K8; however, its role in malignant transformation and the mechanism involved to bring about the same is still ambiguous. Here, we present the total phosphoproteome profiling and quantification after K8 phosphorylation modulation in a skin carcinoma cell-line using TMT-based quantitative phosphoproteomics. Comparative data analysis using various analysis software tools allowed us to identify number of differentially regulated signaling pathways associated with biological functions like cell proliferation, migration, invasion, and metastasis. Furthermore, protein phosphorylation level validation along with phenotypic analysis correlated well with our phosphoproteomics data, signifying K8 phosphorylation to impart increased aggressiveness to skin-SCC-derived cell line.

In our current phosphoproteomic study, we observed a significant proportion of the total phosphoproteome to be altered in response to K8 phosphorylation modulation. The Venn diagram analysis indicated number of overlapping and orthogonal phosphoproteins to be up or downregulated between the different datasets. We found many phosphoproteins with increased phosphorylation upon K8 phosphodead mutant expression, simultaneously showing decreased phosphorylation upon K8 phosphomimetic mutant expression and vice versa. This data suggest that the phenotypic effects of K8 phosphodead mutants might be reversed by K8 phosphomimetic mutants through alteration of some common pathways involving phosphorylation modulation of common target proteins.

Next, for comprehensive understanding of the system wide phosphoproteome data, "Ingenuity Pathway Analysis" (IPA) was performed for all the four datasets that elucidated many differentially phosphorylated proteins to be associated with "cancer." Surprisingly, as stated in the results, the most significant biological function altered was regulation of "RNA post-transcriptional modification" followed by "Cancer" in K8-S73A as well as K8-S73D-independent datasets. Canonical pathway analysis for the same showed deregulation of mTOR and ATM signaling pathways in K8-S73A dataset and of Hippo signaling in K8-S73D dataset which have never been reported earlier in context of K8 phosphorylation. Comparison Analysis of K8-S73 dataset showed alterations in many signaling pathways most importantly, GnRH, Renin angiotensin, P70S6K, mTOR, and ATM signaling, which were not reported before in relation to K8 phosphorylation ablation. It is evident that GnRH signaling is altered in many different malignancies together with high GnRH-Receptor's altered expression [17]. There is accumulating molecular and *in vivo* evidence indicating that the Renin–angiotensin system (RAS) increases cell proliferation and modulates the growth of vascular cells during angiogenesis [18]. p70S6K, a serine/threonine kinase regulated by PI3K/mTOR pathway, plays a crucial role in controlling cell cycle, growth, and survival [19]. ATM and mTOR signaling pathways have also emerged as critical effectors commonly deregulated in human cancers [20, 21]. Available literature also suggests that antagonists/inhibitors of these pathways could be useful in cancer therapy [17–21]. Altogether, the data analysis on the backdrop of the available literature shows an expanding role of K8 Serine^{73} phosphorylation in cancer.

Similarly, we made an attempt to identify signaling mechanisms and associated phosphoproteins that are differentially regulated in case of K8-S431 dataset. The "Biological functions" analysis showed most of the differentially regulated phosphoproteins to be associated with "RNA post-transcriptional modification" and "Cancer" for K8-S431A and K8-S431D independent datasets. The "Canonical pathway" analysis for the same showed estrogen receptor, Hippo, and JNK/SAPK signaling to be significantly altered in both the datasets. Few of the molecules like CAV1 and ZYX are involved in integrin mediated signaling network that could prove possible new links between K8 Serine^{431} phosphorylation and cancer progression. Recent studies have implicated loss of caveolin-1 driving early tumor recurrence, metastasis, and poor prognosis [22]. Zyxin concentrates at focal adhesions along the actin cytoskeleton and is well reported to regulate actin dynamics, apoptosis, cell migration, and metastasis in many different cancers [23]. This data in association with available reports collectively

revealed that K8 Serine^{431} phosphorylation modulation regulates phosphorylation-dependent function of many phosphoproteins and thereby cancer.

In addition to functional analysis by IPA tool, we had also performed phosphorylation site annotation using online database including PhosphoELM, PhosphoSitePlus, HPRD, and Uniprot to attribute the site-specific phosphorylation function to these phosphoproteins. This revealed many biologically relevant phosphosites to be altered, for instance in case of K8-S73 dataset, Threonine^{401} Serine^{405}, and Tyrosine,^{421} on cortactin that play a role in phosphorylation-dependent regulation of actin cytoskeletal networks and in turn cell motility [24]. Similarly the phosphosites Serine^{307} and Serine^{309} identified on CAP1 regulate its binding to cofilin resulting in accumulation of actin stress fibers, thereby cancer cell migration and metastasis [25]. Apart from this, K8-S431 dataset showed differential phosphorylation of BUB1B at Serine^{1043} that correlated with functions like cell proliferation and apoptosis [26]. Although many phosphorylation sites from our data recapitulate the published literature, we have also unraveled many less characterized or novel phosphosites on biologically relevant protein molecules; for instance MAP3K11^{S705} and ZYX^{S344} [27, 28]. Validation of those novel phosphosites by mutational studies can provide new insights into their functional relevance and may open new avenues in the area of cancer research.

Systematic analysis of phosphorylation site-dependent complex interaction dynamics by "STRING" not only highlighted the hub proteins but also emphasized on many relevant interactions in our study. For instance, PPI network for cell migration suggested many multifaceted indirect interactions between phosphoproteins that might contribute to novel cross-talk in cancer signaling in response to K8 phosphorylation. Furthermore, our "PPI hub protein" analysis by "Enrichr" underlined many upstream kinases that could bridge the gap between K8 site-specific phosphorylation and the final downstream effectors identified herein. For example, based on biological relevance of the corresponding phosphosites, CDK1, and its target EIF4EBP1 seem to be good candidates to elucidate K8 Serine^{73} phosphorylation-mediated signaling cascade. Additionally, IPA comprehensive model pathways highlighted many phosphoproteins associated with cell proliferation, actin organization, cell survival, and gene expression regulation being deregulated by K8 phosphorylation modulation. Further, protein phosphorylation level validation for few of these phosphoproteins such as; EIF4B, AKT1S1, CTNN1, 4EBP1 including some of upstream kinases like MAPK1, CDK1 in K8-S73 datasets confirmed our phosphoproteomics data.

Next, in the same line, as a proof of principle, we made an attempt to validate the major phenotypic pathways shown to be altered in our computational analysis such as; cell migration, invasion, and proliferation. Skin-SCC derived A431 cells, upon expressing either of the phosphodead mutants, showed abolition of oncogenic potential for all the three assays and radically regained the tumorigenic potential upon expressing either of the phosphomimetic mutants. In agreement with our present data, a recent report demonstrated reduced K8-S73 phosphorylation via p38 MAPK pathway upon Sec 8 downregulation that in turn resulted in decreased cell migration in case of oral-SCC derived cell-line [29]. Contrary to these findings, Mizuuchi et al. have also demonstrated correlation of PRL-3-dependent K8 dephosphorylation at Serine^{73} and Serine^{431} with increased cell motility in colorectal cancer-derived cells [30]. These data are further supported by the data from our lab in an oral-SCC derived cell-line [8]. These reports suggest that K8 phosphorylation associated effects in cancer progression might be context dependent.

The quantitative phosphoproteomics and immunoblotting data suggests an upregulation of CDK1 inhibitory phosphorylation at Threonine^{14}/Tyrosine^{15} in case of K8-S73 phosphodead mutant. It is well reported that wee1 and myt1 mediated inactivation of CDK1 by phosphorylation at Threonine^{14}/Tyrosine^{15} leads to G2-M arrest and in turn decrease proliferation [31, 32]. We also observed similar phenotypic changes that validated our phosphoproteomics data. eIF4E-BP1, an important regulator of mitotic cap-dependent translation that is downstream to CDK1, was found to be dephosphorylated at the residues Serine^{44}, Threonine,^{46} and Threonine.^{50} The hierarchical phosphorylation of these sites on eIF4E-BP1 is essential for release of eIF4E [33] that further associates with eIF4F and eIF4A at the initiation complex hence indispensable for cap-dependent translation initiation [34]. eIF4E-BP1 phosphorylation at Threonine^{37}/Threonine^{46} residues is governed by CDK1 [35]. Our results have shown decreased phosphorylation of 4EBP1 at these residues probably because of CDK1 inactivation. This might be leading to reduced mitotic cap-dependent translation and thereby less proliferation. Although, mTORC1 is another potent phosphorylation modulator of eIF4E-BP1; it has been reported that CDK1 can substitute its function in mitotic cap-dependent translation [35–37]. However, we observed a fivefold upregulation of eIF4B phosphorylation at S422 residue that is an indirect downstream target of mTORC1. Furthermore, some other kinases such as PKB can directly phosphorylate eIF4B, which again suggests that mTORC1 might not be involved here in this process [38].

eIF4B, when phosphorylated at Serine^{422}, acts as coactivator of eIF4A helicase activity during cap-dependent translation initiation [39]. Because of the consistent impaired cap-dependent translation, the upstream kinases like AKT/PKB, might be activated in a feedback loop that is reflected by enhanced pRAS40 phosphorylation at Threonine^{246} and eIF4B at Serine^{422} in our data. Nevertheless, the initial step of translation initiation complex formation, i.e. release of eIF4E from eIF4E-BP1 might be abrogated because of decreased phosphorylation of eIF4E-BP1. Hence, hyperphosphorylated forms of eIF4B and pRAS40 as observed might not be sufficient for driving the translation initiation, indicating that the initiation complex would have been stalled, consequently resulting in reduced proliferation of these cells (Fig. 7). We have also observed increased phosphorylation of cortactin

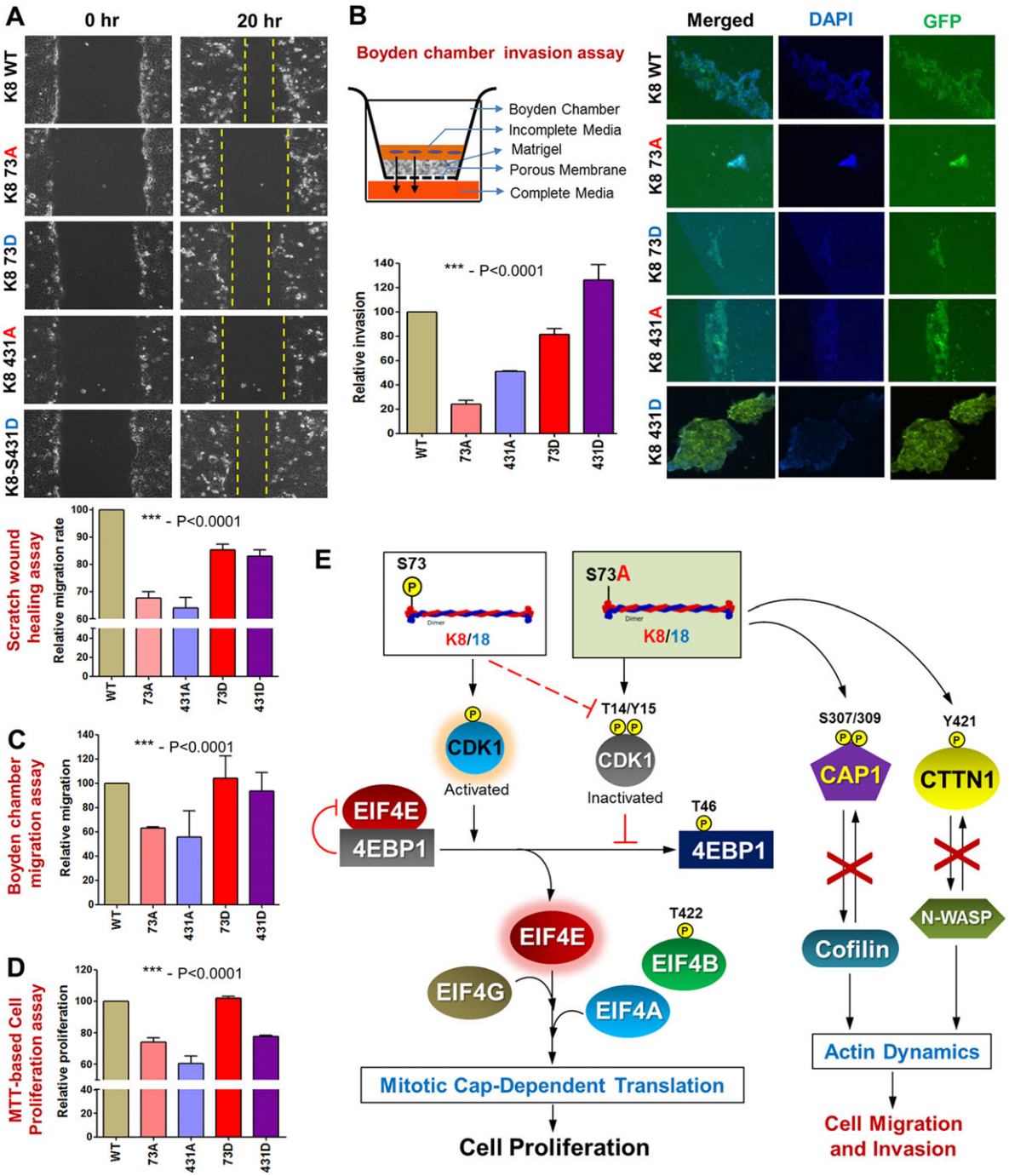

Figure 7. Tumorigenic potential of A431 cells regulated by site specific K8 phosphorylation: (A) Scratch wound healing assay was performed for all five different clones (K8-WT, phosphodead, and phosphomimetic mutants) following the protocol described as materials and methods. Representative time lapse microscopy images showing wound healing at 0 and 20 h time points. Rate of migration was calculated by MacBiophotonics–ImageJ software. The graph represents relative migration rate ± SEM of three independent experiments done in triplicates. (B) Boyden chamber matrigel invasion assay was performed as described in materials and method section. The graph represents average number of invaded cells (stained with DAPI) ± SEM of three independent experiments done in triplicates. Representative images depicting invaded cells visualized for GFP and DAPI under upright microscope. (C) Boyden chamber migration assay was performed as described in materials and method section. The graph represents average number of migrated cells (stained with DAPI) ± SEM of three independent experiments done in triplicate. (D) MTT-based cell proliferation assay was performed for all five clones till 6 days. The relative proliferation was plotted for each of the clones. [Each bar graph data represents ± standard error mean (SEM) of three independent experiments]. (E) Model pathway summarizing possible molecular mechanism associated with K8 serine^{73} phosphorylation mediated regulation of cell proliferation, migration, and invasion.

at Serine[405] and Tyrosine[421]. Mutational analysis has shown that ERK-mediated Serine[405] phosphorylation of cortactin enhances its binding with N- WASP and WASP but this is inhibited by Src mediated Tyrosine[421] phosphorylation of cortactin [40]. This inhibits further activation of the Arp2/3 complex and in turn affects actin nucleation and dynamics. Similarly, GSK3 mediated phosphorylation of CAP1 at Serine[307] and Serine[309], which was increased in case of K8-S73A mutant, is known to inhibit its binding to cofilin and further accumulation of actin stress fibers [25]. Both of these molecules are important modulators of actin dynamics and in turn cell migration and invasion that also correlates with our phenotypic validations. All together our data suggest K8 phosphorylation at Serine[73] position can modulate intricate pathways and thereby migration and metastatic potential of the cells (Fig. 7E). Earlier reports have shown, aberrant accumulation of an important oncogenic transcription factor c-Jun upon dephosphorylation at Serine[243] leading to accelerated G1/S transition and thereby hyperproliferation [41] as observed in our K8-S73D phosphomimetic mutant dataset. In case of K8-S431 dataset, despite the significant phenotypic alterations, majority of the differentially regulated phopsphosites were novel/less characterized, hence we could not draw any phosphorylation-oriented model pathway. However, a protein level comprehensive model pathway generated by IPA, provides multiple impending start-points for further mechanistic studies for elucidating K8 Serine[431] phosphorylation-mediated oncogenic pathways.

In summary, to the best of our knowledge this study may represent the first report investigating regulatory role of site-specific K8 phosphorylation and could identify many phosphoproteins and signaling pathways to be altered upon K8 phosphorylation modulation. Altogether the bioinformatics analysis suggested that the K8 phosphorylation might be modifying cancer related phenotype by differentially regulating an imperative part of the cellular phosphoproteome. In concordance with our global phosphoproteome profiling, the biochemical, and phenotypic validations confirmed a potential role of K8 phosphorylation in neoplastic progression of skin- SCCs. In addition, our phosphoproteomic analysis not only recapitulates previous findings but also unravels many novel K8 phosphorylation-mediated functional networks and signaling mechanisms, elucidating its much broader regulatory role in cancer.

We would like to thank Dr. Hunain Alam (MD Anderson Cancer Centre, University of Texas, USA) for initiating the Keratin 8 phosphorylation based study in our lab. We thank Dr. Sorab N Dalal (ACTREC, TMC, India) for his generous gift (HEK293-FT and pTU6 PURO vector). We also thank Dr. Rita Mulherkar (ACTREC, TMC, India) for providing us A431 cell-line as a kind gift. We also thank Ankit Jain and Kiran Kumar (Institute of Bioinformatics, Bangalore) for their generous help during data analysis. This work was supported by grant from Department of Biotechnology (Grant no. BT/PR7860/BRB/10/1222/2013). Richa Tiwari was supported by fellowship from ACTREC, TMC, India.

The authors have declared that they have no potential conflicts of interest.

5 References

[1] Coulombe, P. A., Omary, M. B., 'Hard' and 'soft' principles defining the structure, function and regulation of keratin intermediate filaments. *Curr. Opin. Cell Biol.* 2002, *14*, 110–122.

[2] Fillies, T., Werkmeister, R., Packeisen, J., Brandt, B. et al., Cytokeratin 8/18 expression indicates a poor prognosis in squamous cell carcinomas of the oral cavity. *BMC Cancer* 2006, *6*, 10.

[3] Owens, D. W., Lane, E. B., The quest for the function of simple epithelial keratins. *Bioessays* 2003, *25*, 748–758.

[4] Omary, M. B., Ku, N. O., Tao, G. Z., Toivola, D. M., Liao, J., "Heads and tails" of intermediate filament phosphorylation: multiple sites and functional insights. *Trends Biochem. Sci.* 2006, *31*, 383–394.

[5] Kim, H. J., Choi, W. J., Lee, C. H., Phosphorylation and reorganization of keratin networks: implications for carcinogenesis and epithelial mesenchymal transition. *Biomol. Ther.* 2015, *23*, 301–312.

[6] Chinembiri, T. N., du Plessis, L. H., Gerber, M., Hamman, J. H., du Plessis, J., Review of natural compounds for potential skin cancer treatment. *Molecules* 2014, *19*, 11679–11721.

[7] Darwiche, N., Ryscavage, A., Perez-Lorenzo, R., Wright, L. et al., Expression profile of skin papillomas with high cancer risk displays a unique genetic signature that clusters with squamous cell carcinomas and predicts risk for malignant conversion. *Oncogene* 2007, *26*, 6885–6895.

[8] Alam, H., Gangadaran, P., Bhate, A. V., Chaukar, D. A. et al., Loss of keratin 8 phosphorylation leads to increased tumor progression and correlates with clinico-pathological parameters of OSCC patients. *PLoS One* 2011, *6*, e27767.

[9] Selvan, L. D., Renuse, S., Kaviyil, J. E., Sharma, J. et al., Phosphoproteome of *Cryptococcus neoformans*. *J. Proteomics* 2014, *97*, 287–295.

[10] Wisniewski, J. R., Zougman, A., Nagaraj, N., Mann, M., Universal sample preparation method for proteome analysis. *Nat. Methods* 2009, *6*, 359–362.

[11] Vizcaino, J. A., Cote, R. G., Csordas, A., Dianes, J. A. et al., The PRoteomics IDEntifications (PRIDE) database and associated tools: status in 2013. *Nucleic Acids Res.* 2013, *41*, D1063–D1069.

[12] Dinkel, H., Chica, C., Via, A., Gould, C. M. et al., Phospho.ELM: a database of phosphorylation sites—update 2011. *Nucleic Acids Res.* 2011, *39*, D261–D267.

[13] Chen, E. Y., Tan, C. M., Kou, Y., Duan, Q. et al., Enrichr: interactive and collaborative HTML5 gene list enrichment analysis tool. *BMC Bioinformatics* 2013, *14*, 128.

[14] Mi, H., Poudel, S., Muruganujan, A., Casagrande, J. T., Thomas, P. D., PANTHER version 10: expanded protein families and functions, and analysis tools. *Nucleic Acids Res.* 2016, *44*, D336–D342.

[15] Alam, H., Kundu, S. T., Dalal, S. N., Vaidya, M. M., Loss of keratins 8 and 18 leads to alterations in alpha6beta4-integrin-mediated signalling and decreased neoplastic progression in an oral-tumour-derived cell line. *J. Cell Sci.* 2011, *124*, 2096–2106.

[16] Iyer, S. V., Dange, P. P., Alam, H., Sawant, S. S. et al., Understanding the role of keratins 8 and 18 in neoplastic potential of breast cancer derived cell lines. *PLoS One* 2013, *8*, e53532.

[17] Kraus, S., Naor, Z., Seger, R., Intracellular signaling pathways mediated by the gonadotropin-releasing hormone (GnRH) receptor. *Arch. Med. Res.* 2001, *32*, 499–509.

[18] George, A. J., Thomas, W. G., Hannan, R. D., The renin-angiotensin system and cancer: old dog, new tricks. *Nat. Rev. Cancer* 2010, *10*, 745–759.

[19] Heinonen, H., Nieminen, A., Saarela, M., Kallioniemi, A. et al., Deciphering downstream gene targets of PI3K/mTOR/p70S6K pathway in breast cancer. *BMC Genomics* 2008, *9*, 348.

[20] Guertin, D. A., Sabatini, D. M., Defining the role of mTOR in cancer. *Cancer Cell* 2007, *12*, 9–22.

[21] Cremona, C. A., Behrens, A., ATM signalling and cancer. *Oncogene* 2014, *33*, 3351–3360.

[22] Sotgia, F., Martinez-Outschoorn, U. E., Howell, A., Pestell, R. G. et al., Caveolin-1 and cancer metabolism in the tumor microenvironment: markers, models, and mechanisms. *Annu. Rev. Pathol.* 2012, *7*, 423–467.

[23] Hirata, H., Tatsumi, H., Sokabe, M., Zyxin emerges as a key player in the mechanotransduction at cell adhesive structures. *Commun. Integr. Biol.* 2008, *1*, 192–195.

[24] Lua, B. L., Low, B. C., Cortactin phosphorylation as a switch for actin cytoskeletal network and cell dynamics control. *FEBS Lett.* 2005, *579*, 577–585.

[25] Zhou, G. L., Zhang, H., Wu, H., Ghai, P., Field, J., Phosphorylation of the cytoskeletal protein CAP1 controls its association with cofilin and actin. *J. Cell Sci.* 2014, *127*, 5052–5065.

[26] Elowe, S., Dulla, K., Uldschmid, A., Li, X. et al., Uncoupling of the spindle-checkpoint and chromosome-congression functions of BubR1. *J. Cell Sci.* 2010, *123*, 84–94.

[27] Daub, H., Olsen, J. V., Bairlein, M., Gnad, F. et al., Kinase-selective enrichment enables quantitative phosphoproteomics of the kinome across the cell cycle. *Mol. Cell* 2008, *31*, 438–448.

[28] Olsen, J. V., Blagoev, B., Gnad, F., Macek, B. et al., Global, in vivo, and site-specific phosphorylation dynamics in signaling networks. *Cell* 2006, *127*, 635–648.

[29] Tanaka, T., Iino, M., Sec 8 regulates cytokeratin8 phosphorylation and cell migration by controlling the ERK and p38 MAPK signalling pathways. *Cell Signal* 2015, *27*, 1110–1119.

[30] Mizuuchi, E., Semba, S., Kodama, Y., Yokozaki, H., Down-modulation of keratin 8 phosphorylation levels by PRL-3 contributes to colorectal carcinoma progression. *Int. J. Cancer* 2009, *124*, 1802–1810.

[31] Lew, D. J., Kornbluth, S., Regulatory roles of cyclin dependent kinase phosphorylation in cell cycle control. *Curr. Opin. Cell Biol.* 1996, *8*, 795–804.

[32] Lindqvist, A., Rodriguez-Bravo, V., Medema, R. H., The decision to enter mitosis: feedback and redundancy in the mitotic entry network. *J. Cell Biol.* 2009, *185*, 193–202.

[33] Gingras, A. C., Raught, B., Gygi, S. P., Niedzwiecka, A. et al., Hierarchical phosphorylation of the translation inhibitor 4E-BP1. *Genes Dev.* 2001, *15*, 2852–2864.

[34] Pyronnet, S., Dostie, J., Sonenberg, N., Suppression of cap-dependent translation in mitosis. *Genes Dev.* 2001, *15*, 2083–2093.

[35] Shuda, M., Velasquez, C., Cheng, E., Cordek, D. G. *et al.*, CDK1 substitutes for mTOR kinase to activate mitotic cap-dependent protein translation. *Proc. Natl. Acad. Sci. USA* 2015, *112*, 5875–5882.

[36] Choo, A. Y., Yoon, S. O., Kim, S. G., Roux, P. P., Blenis, J., Rapamycin differentially inhibits S6Ks and 4E-BP1 to mediate cell-type-specific repression of mRNA translation. *Proc. Natl. Acad. Sci. USA* 2008, *105*, 17414–17419.

[37] Livingstone, M., Bidinosti, M., Rapamycin-insensitive mTORC1 activity controls eIF4E:4E-BP1 binding. *F1000Res* 2012, *1*, 4.

[38] van Gorp, A. G., van der Vos, K. E., Brenkman, A. B., Bremer, A. et al., AGC kinases regulate phosphorylation and activation of eukaryotic translation initiation factor 4B. *Oncogene* 2009, *28*, 95–106.

[39] Gallie, D. R., The role of the initiation surveillance complex in promoting efficient protein synthesis. *Biochem. Soc. Trans.* 2004, *32*, 585–588.

[40] Martinez-Quiles, N., Ho, H. Y., Kirschner, M. W., Ramesh, N., Geha, R. S., Erk/Src phosphorylation of cortactin acts as a switch on-switch off mechanism that controls its ability to activate N-WASP. *Mol. Cell Biol.* 2004, *24*, 5269–5280.

[41] Taira, N., Mimoto, R., Kurata, M., Yamaguchi, T. et al., DYRK2 priming phosphorylation of c-Jun and c-Myc modulates cell cycle progression in human cancer cells. *J. Clin. Invest.* 2012, *122*, 859–872.

